UNIVERSITY OF CALIFORNIA,
IRVINE

Development and application of human microglia model to examine the influence of genetic risk factors on microglial function in Alzheimer's disease

DISSERTATION

Submitted in partial satisfaction of the requirements
For the degree of

DOCTOR OF PHILOSOPHY

in Biological Sciences

by

Amanda Katherine McQuade

Dissertation Committee:
Professor Mathew Blurton-Jones, Chair
Professor Leslie M. Thompson
Professor Marcelo Wood

2021

TABLE OF CONTENTS

LIST OF FIGURES

INTRODUCTION

CHAPTER 1

CHAPTER 2

CHAPTER 3

LIST OF TABLES

INTRODUCTION

ACKNOWLEDGEMENTS

I would like to thank my thesis mentor Dr. Mathew Blurton-Jones for allowing me to work with him during my PhD and helping me develop into an independent researcher. I am particularly grateful for the freedom you have given me to explore new ideas and projects which gave me confidence in my strengths as a scientist. I have also enjoyed being able to learn from your strengths as an amazing writer and incredible idea-man. Working with you has been an absolute pleasure and I'm excited for future collaborations we may have going forward. I will always look to you as a valued mentor and inspirational scientist.

I would also like to thank both my thesis committee, Dr. Leslie Thompson and Dr. Marcelo Wood, as well as my advancement committee, Dr, Mathew Inlay and Dr. Andrea Tenner. I feel so honored to have been able to work with all of you throughout my graduate career. Our annual meetings always led to leaps forward in my science and my ability as a researcher. Your support through my time at UCI has been integral to what I have been able to accomplish and prepared me to take my next steps with confidence.

I owe a tremendous amount of thanks to the entirety of the Blurton-Jones lab, Dr. Edsel Abud, Jaclyn Beck, Joia Capocchi, Jean Paul Chadarevian, Dr. Christel Claes, Morgan Coburn, Emma Danhash, Dr. Hayk Davtyan, Dr. Alberto Granzotto, Dr. Jonathan Hasselmann, Zahara Kreulen, Tau En Lim, Dr. Samuel Marsh, Jessica Sanchez, Sepideh Kiani Shabestari, Jorge Silva, Alexandra Sotelo, and Christina Tu. You all have offered critical advice with my work, helped out in many different ways, and have made coming into work every day fun!

I am grateful for my rotation mentor Dr. Craig Walsh for being a critical mentor early in my graduate work and to his student Dr. Laura McIntyre for her support, mentorship, and

close friendship throughout my graduate studies. I am grateful to have Laura as a guide and role model for success.

I would also like to particularly thank several collaborators that have made these projects possible including Dr. Amit Jairaman, Dr. Shiva Othy, and Dr. Michael Cahalan who were critical mentors in my understanding of calcium signaling and scientific writing, Dr. You Jung Kang and Dr. Hansang Cho who performed many directed chemotaxis assays, Dr. Gianna Fote and Dr. Joan Steffan who supplied APOE, as well as many collaborators at Merck, particularly Dr. Rebecca Mathew, and Denali Therapeutics, particularly Dr. Kathryn Monroe and Dr. Karthik Raju.

Furthermore, I am extremely grateful to my T32 mentors and role models Dr. Peter Donovan and Dr. Leslie Thompson. Taking part in the training grant and receiving guidance and support from you both has helped me grow as a scientist in more ways than I can explain. Your advice on everything from science to community has helped me forge the career path I want to follow.

Lastly I would like to thank my family and friends who have supported me through this process. Particularly, my interdisciplinary Tuesday crew Dr. Kate Jesse and Jared Goldberg, my cohort mates who have gone through this besides me, Albert Ta and Kristianna Sarkan, as well as my family Dr. Miriam McQuade, Dr. Vicki Darrow, and Dr. James McQuade. You all have given me tremendous strength and I am so lucky to have you in my life.

This work was funded by NINDS-T32-NS082174 (AM), ARCS Foundation (AM), NIH-R01-AG048099 AG-055524, 056303 (MBJ), CIRM RT3-07893, AG061895 (HD). It was supported by many core resources at UCI including the Alzheimer's Disease Resource

Center (ADRC), Memory Impairments and Neurological Disorders (MIND), Center for the Neurobiology of Learning and Memory (CNLM), Sue and Bill Gross Stem Cell Research Center (SCRC), and the Institute for Immunology (IFI). Finally, this work would not have been possible without generous donations from Alzheimer's disease patients and their families who value and support this research.

CURRICULUM VITAE

Amanda McQuade MS

Education

University of California, Irvine, CA — Defense: August 2021
PhD, Neurobiology and Behavior GPA: 4.0

Scripps College Claremont, CA — Graduation Date: May 2012
BA, Neuroscience: Cell, Molecular GPA: 3.6

Honors and Awards

- UCI School of Biological Sciences- James L. McGaugh Award ($1000)
- Center for the Neurobiology of Learning and Memory's (CNLM) Renée Harwick Advanced Graduate Student Award ($1000)
- Carl W. Cotman Scholar Award-UCI MIND ($250)
- Junior Faculty Award- ADPD 2021 ($300)
- Achievement Awards for College Students (ARCS) Foundation Scholar ($10000)
- 2021 ARCS Orange County People's Choice Award ($100)
- NIH-T32 Training grant in stem cell translational medicine for neurological disorders (graduate tuition)
- Graduate Deans Recruitment Fellowship ($5000)
- Francisco J. Ayala Fellowship ($10000)
- Moser Trust for Science Scholarship- B. Paul Moser Charitable Trust ($10000)
- W. M. Keck Summer Research Fellowship ($4000)
- Keck Science Department Neuroscience Summer Fellowship ($5000)
- 2nd place GPS-BIOMED Pitch Competition 2017 ($50)
- UCI finalist for Grad Slam Competition 2018, 2020
- SoCal Flow Summit Scholarship Winner ($300)
- Federal Work Study Scholarship ($5334)
- Certificates: *Mentoring Excellence Program*- UCI
  Scientific Writing and Publishing- Nature
  Effective Communication- UCI
  Quantitative Approaches and Statistical Concepts- UCI

Research Experience

Dr. Mathew Blurton-Jones Lab: University of California, Irvine, CA — Winter 2017-present
Doctoral Candidate
- Developed streamlined technique to differentiate human iPSCs into microglia
- Investigated function of microglial Alzheimer's risk genes: MS4A4A, MS4A6A, TREM2, PLCG2

Dr. Vanessa Peterson: Genome Sciences; Merck Pharmaceuticals, Boston, MA — Summer 2019
Future Talent Program
- Worked in target ID for Alzheimer's disease program
- Developed assays for Neuroscience therapeutic area

Dr. Craig Walsh Lab: University of California, Irvine, CA Fall 2016
Graduate Student Researcher
- Researched how neural precursor cells induce regulatory T cells in murine model of MS
- Co-culture of mouse splenocytes with iPSC derived neural precursor cells, FACS analysis

Dr. Julie Andersen Lab: Buck Institute for Research on Aging, Novato, CA Summer 2016
Research Intern
- Investigated connections between astrocyte senescence, neurodegeneration, and protein aggregation
- Optimized induction of senescence using amyloid-beta pre-formed fibrils
- Co-cultured neurons with senescent astrocytes and assayed neuronal health

Dr. Melissa Coleman Lab: Keck Science Department, Claremont, CA Spring 2013 - Summer 2016
Undergraduate Researcher
- Analyzed Zebra Finch song as a model for language acquisition and maintenance
- Performed brain lesioning surgeries and collected electrophysiological responses

Dr. Pierre Vanderhaeghen Lab: Universite Libre de Bruxelles, Brussels, Belgium Fall 2014
Research Intern
- Characterized transcriptional effects of an oncogene, Bcl6, that effects early corticogenesis
- Prepared *in situ* hybridizations on embryonic mouse brains

Dr. Martin Brand Lab: Buck Institute for Research on Aging, Novato, CA Summer 2013
Research Intern
- Characterized optimal growth conditions for pancreatic alpha cell lines
- Protein turnover assays for uncoupling proteins in the context of diabetes

Dr. Xiamin Zeng Lab: Buck Institute for Research on Aging, Novato CA Summer 2011
Summer Scholars Program: Seven week intensive culminating in poster competition
- Differentiated human neuronal stem cells into astrocytes
- Cultured and maintained embryonic stem cells

Publications

- Amit Jairaman*, **Amanda McQuade*,** You Jung Kang, Alberto Granzotto, Jean Paul Chadarevian, Sunil Gandhi, Ian Parker, Ian Smith, Shivashankar Othy, Hansang Cho, Mathew Blurton-Jones, Michael Cahalan. TREM2 regulates purinergic receptor-mediated calcium signaling and motility in human iPSC-derived microglia. (submitted) eLife.

- **Amanda McQuade,** You Jung Kang, Morgan Coburn, Amit Jairaman, Jonathan Hasselmann, Emma Danhash, Eric Martinez, Christina H. Tu, Jean Paul Chadarevian, Alexandra Sotelo, Jorge Silva, Sepideh Kiani Shabestari, G. Aleph Prieto, Ian Smith, Hayk Davtyan, Michael Cahalan, Hansang Cho, Mathew Blurton-Jones. Gene expression and functional deficits underlie TREM2-kockout microglia responses in human models of Alzheimer's disease. (2020) *Nature Communications*. 11(1) 5370. PMC: 7584603.

- **Amanda McQuade**, Morgan Coburn, Christina Tu, Jonathan Hasselmann, Hayk Davtyan, Mathew Blurton-Jones. Development and validation of a simplified and highly reproducible method to produce large numbers of iPSC-derived human microglia. (2018) *Molecular Neurodegeneration*. 13, 67. PMC6303871.

- **Amanda McQuade**, Mathew Blurton-Jones. Differentiation of iPS-Microglia. (Accepted 2021). *Methods in Molecular Biology.*

- **Amanda McQuade**, Mathew Blurton-Jones. Microglia in Alzheimer's disease: exploring how genetics and phenotypes influence risk. (2019). *Journal of Molecular Biology* 19, 30064-6. PMID:30738892.

- Sepideh Kiani Shabestari, Samuel Morabito, Emma Pascal Danhash, **Amanda McQuade,** Emily Elizabeth Miyoshi, Jean Paul Chadarevian, Christel Claes, Morgan Alexandra Coburn, Jonathan Hasselmann, Jorge Silva, Alessandra C. Martini, Jessica Ramirez Sanchez, Elizabeth Head, David A. Hume, Clare Pridans, Hayk Davtyan, Vivek Swarup, Mathew Blurton-Jones. Absence of microglia leads to diverse comorbidities and promotes lethality in Alzheimer's disease mice. (submitted) Nature Communications.

- Tongfei Liu, Bing Zhu, Yan Liu, Xiaoming Zhang, Jun Yin, Xiaoguang Li, LuLin Jiang, Andrew P. Hodges, Sara Brin Rosenthal, Lisa Zhou, Joel Yancey, **Amanda McQuade**, Mathew Blurton-Jones, Rudolph E. Tanzi, Timothy Y. Huang, Huaxi Xu. Multi-omic comparison of Alzheimer's variants in human ESC-derived microglia reveals convergence at APOE. (2020). *Journal of Experimental Medicine.* 217 (12). PMID: 32941599

- Yang You, Kathleen Borgmann, VenkataViswa Edara, Satomi Stacy, **Amanda McQuade,** Christina Muratore, Samuel Walter Hersh, Tracy young-Pearse, Mathew Blurton-Jones, Anuja Ghorpade, Tsuneya Ikezu. Proteomic Profiling of Human Neural Cells Derived Exosomes to Identify Cell-type Specific Surface Markers. (2019). *The Journal of the Alzheimer's Association.* 15, P969.

- Alessandra Cadete Martini, Angela Gomez-Arboledas, Stefania Forner, Carlos J Rodriguez-Ortiz, **Amanda McQuade**, Emma Danhash, Jimmy Phan, Dominic Javoillo, Jordan-Vu Ha, Laura Trujillo-Estrada, Celia de Cunha, Rahasson R Ager, Jose C Davila, Masashi Kitazawa, Mathew Blurton-Jones, Antonia Gutierrez, David Baglietto-Vargas, Rodrigo Medeiros, Frank M. LaFerla. Amyloid-beta impairs TOM1-mediated IL-1R1 signaling. (2019). *PNAS*.

- Jonathan Hasselmann, Morgan A. Coburn, Whitney England, Dario X. Figueroa Velez, Sepideh Kiani Shabestari, Christina H. Tu, **Amanda McQuade,** Mahshad Kolhdouzan, Karla Echeverria, Christel Claes, Talylot Nakayama, Ricardo Azevedo, Nicole G. Coufal, Claudia Z. Han, Brian J. Cummings, Hayk Davtyan, Christopher K. Glass, Luke M. Healy, Sunil P. Gandhi, Robert C. Spitale, Mathew Blurton-Jones. Development of a Chimeric Model to Study and Manipulate Human Microglia *in Vivo.* (2019) *Neuron*. 10.1016 PMID:31375314.

- Shankar Chinta, Georgia Woods, Marco Demaria, Anand Rane, Ying Zou, **Amanda McQuade**, Subramanian Rajagopalan, Chandani Limbad, David Madden, Judith Campisi, Julie Andersen. (2018). Cellular senescence is induced by the environmental neurotoxin paraquat and contributes to neuropathology associated with Parkinson's disease. (2018) *Cell Reports*. 22, 930-940. PMC5806534.

- Hannah Shoenhard, **Amanda McQuade,** Nancy Day, Zachary Burkett, Lisette Farve, Evelyn Ross Shapiro, Lillian Johnson, Rebecca Arnold, and Melissa Coleman. Song stability after perturbations of auditory pathways in the zebra finch. (In revisions) *Journal of Neurophysiology*.

Selected Graduate Presentations

- **15th International Conference on Alzheimer's and Parkinson's Diseases 'ADPD' (2021)**
  Invited talk; Junior Faculty Award: Interactions between Alzheimer's risk factors, TREM2 and MS4A6A, in human iPS-Microglia

- **Virtual Glia Symposium (2021)**
  Invited talk: TREM2-knockout microglia have impaired response to Alzheimer's pathology

- **STEMCELL Technologies (2021)**
  Invited talk: Modulating Alzheimer's risk using human TREM2-knockout microglia

- **Girls in STEAM Symposium - *St. Margaret's Episcopal School* (2020)**
  Invited talk: How the brain fights back against Alzheimer's disease

- **NeuroLaunchpad (2020)**
  Invited talk: Human TREM2-/- microglia fail to activate towards Alzheimer's disease pathology

- **International Symposium for Networking in Neuroscience-ISNN (2020)**
  Invited talk: Human TREM2-/- microglia fail to activate towards Alzheimer's disease pathology

- **Neurobiology and Behavior Department Retreat (2020)**
  Invited talk: Immune responses to Alzheimer's disease pathology reveal insight for therapeutic targets

- **UCI Alumni Fall Social (2019)**
  Invited talk: Human models of the immune system in Alzheimer's disease

- **Target ID and Validation meeting: Merck Pharmaceuticals (2019)**
  Invited talk: MS4A6A as a therapeutic target in neurodegenerative disease

- **14th International Conference on Alzheimer's and Parkinson's Diseases 'ADPD' (2019)**
  Invited talk: Human Isogenic TREM2 knockout microglia exhibit transcriptional and functional changes in vitro *as well as impaired directed migration towards beta-amyloid plaques* in vivo

- **International Conference on Learning and Memory (2018)**
  Using iPS-derived microglia to uncover the role of MS4A in Alzheimer's Disease

- **New Frontiers in Neuroinflammation, Keystone Colorado (2018)**
  Alzheimer's risk gene family, MS4A, changes microglial phagocytosis and Ca^{2+}

Outreach and Leadership

- **ReMIND Co-Chair - *Research and Education in Memory Impairments and Neurological Disease***
  Doctoral trainee-led group to promote outreach in the community as well as promoting collaboration within the next generation of pre-and post-doctoral students
  Taught local students the about the brain, memory, and disease through demonstrations
  Organize annual Emerging Scientists Symposium
  Planned and hosted the inaugural Beall Scholars Program for high school students

- **Tech Trek - *American Association of University Women***
  Week long camp to inspire 7th grade girls to remain in STEM fields
  Interviewing potential candidates, and taking the campers on lab tours and demonstrations
  Keynote speaker at fundraising events

- **CNLM Brain Explorer's Academy mentor - *Center for the Neurobiology of Learning and Memory***
  Three month program teaching 8-14 year olds about neuroscience, science communication, and ethics
  Culminates in review for *Frontiers for Young Minds*

- **Virtual Journal club in the Neuroscience of Learning and Memory**
  10-week program for high school students to learn about scientific publishing, peer review, and skills for reading scientific manuscripts
  Led groups of 5-10 students to understand Science manuscripts and basic neuroscience concepts

- **Reach Out Teach Out science fair mentor**
  Four month program aiding students from low income schools
  Training in scientific methods and over-seeing their science fair projects

- **Brews and Brains**
  Meet with community members around Orange County to discuss the groundbreaking research at UCI
  10 min talks about my own research aimed towards the lay audience
- **Committee for Inclusive Excellence Presentations**
  Neurobiology and Behavior Faculty Retreat, UCI faculty orientation, T32 training grant retreat
  Organized interactive presentation on implicit bias and power dynamics in the workplace

Professional Development

- **Guest Lecturer, Department of Neuroscience, Scripps College** 2020-2021
  NEUR 148L Cellular, Molecular Neuroscience
  Lecture on stem cell models of neurodegeneration and current research on Alzheimer's disease

- **NINDS Strategic planning evaluation for Training and Diversity (2021-2026)** 2020
  Discussion panel for National Institute of Neurological Disorders and Stroke to enhance training, mentorship, and diversity in the workforce (with Michelle Jones-London and Stephen Korn)

- **Teaching Assistant, Department of Neurobiology and Behavior, UCI** Winter 2018 - Spring 2020
  N113L Neurobiology Laboratory; Bio47 Stress
  Prepared Lectures, quizzes, practical lab exams to provide feedback to students
  Aided students in experimental techniques and science writing skills

- **Neurobiology and Behavior associate professor search committee** Winter 2019
  Developed search advertisement for new faculty in Neurobiology and Behavior department
  Participated in application review and interview process

- **Reviewer *Frontiers for Young Minds*** Summer 2018

- **Member GPS-BIOMED/ GPS-STEM** Fall 2017- Present
  Graduate Professional Success in Biomedical Sciences program funded by NIH-BEST initiative
  Attended workshops for professional development, participated in alumni mentorship program

- **Activate to Captivate – professional communication workshop** Summer 2017
  Attended 8-week program to develop and strengthen presentation skills
  Learned how to best craft a story for sharing research to a general or scientific audience

- **Teaching Assistant, Department of Neuroscience, Scripps College** Fall 2015
  NEUR 148L Cellular, Molecular Neuroscience; Supervised by Melissa Coleman
  Evaluated performance and provided feedback for 30 students

ABSTRACT OF THE DISSERTATION

Development and application of human microglia model to examine the influence of genetic risk factors on microglial function in Alzheimer's disease

By

Amanda Katherine McQuade

Doctor of Philosophy in Biological Sciences

University of California, Irvine, 2021

Professor Mathew Blurton-Jones, Chair

Alzheimer's disease (AD) is a progressive neurodegenerative disease for which there is no cure. Worldwide, AD is estimated to effect 50 million people with 10 million new cases each year. Developing therapeutics for Alzheimer's disease has been particularly difficult given the complex etiology of this disease. Alzheimer's disease is characterized by an accumulation of parenchymal beta-amyloid protein plaques, tau neurofibrillary tangles, and neuroinflammation. For sporadic AD, which accounts for around 95 % of AD cases, the direct trigger of neurodegeneration remains unclear. Understanding the mechanistic pathophysiology of this disease will allow for the development of more effective targeted therapeutics and biomarker studies to help patients.

In the last decade, genome-wide association studies (GWAS) have renewed interest in neuroinflammation as a potential disease-modifying mechanism. These large-scale genetic studies have uncovered a striking enrichment of immune-specific genes as risk-factors for Alzheimer's disease. However, the function of many of these GWAS loci are not well understood. Additionally, many of these genes have poor homology between human cells and traditional murine disease-models. Thus, there is a critical need to

develop a model of human microglia in order to understand how these immune risk factors influence human microglial function.

The focus of this dissertation is to develop and characterize a model of human microglia that can be readily studied without the need for isolation of human brain tissue surgically or post-mortem. Building on previous research in the lab, we have developed a model of human microglia differentiated from induced pluripotent stem cells (iPS-Microglia). This model follows developmental ontogeny with a primary differentiation into CD43+ hematopoietic progenitor cells before transition into a microglial differentiation medium containing neuron and astrocyte derived cytokines to educate our microglia in a homeostatic brain-like environment. The result is a highly pure population of iPS-Microglia which perform key microglial functions and cluster alongside human microglial transcriptomes **(Chapter 1)**.

Because this microglial model is fully defined beginning from iPS cells, it is possible to combine this approach with modern molecular biological manipulation such as CRISPR gene editing. This dissertation focuses on studies surrounding the AD-risk loci Triggering Receptor Expressed on Myeloid Cells II (TREM2). Predicted loss of function mutations in TREM2 increase Alzheimer's disease risk up to 2-3 fold making it the highest microglial-specific risk factor for AD. By performing CRISPR-mediated knockout of TREM2 in human iPSCs and differentiating into microglia, we find that TREM2-knockout locks microglia in a homeostatic state. Specifically, microglia lacking TREM2 are deficient in SYK-mediated phagocytosis, CXCR4-mediated migration, and are more sensitive to MCSF-mediated cell death.

In vivo, this translates to an inability to perform chemotaxis towards and compaction of beta-amyloid plaques leading to a build-up of pathology in the brain. We also characterize a distinct lack of transcriptional activation in TREM2 knockout cells suggesting that induction of the Disease Associated Microglia (DAM) profile may be an essential immune response in shielding the brain from dementia **(Chapter 2)**.

Because TREM2-knockout cells are locked in a homeostatic state, they express high levels of homeostatic microglia markers P2RY12 and P2RY13. These purinergic receptors are critical for microglial communication with neurons and clearance of dead cells. We show that purinergic signaling has a profound effect on microglial motility and process extension and that hyper-expression and response of purinergic signaling in TREM2-knockout microglia may render these cells unable to sense gradients and activate against disease pathology. Furthermore, we highlight that partial inhibition of purinergic receptors will rescue migratory deficits characterized in TREM2-knockout microglia suggesting a therapeutic mechanism **(Chapter 3)**.

Taken as a whole, the development of the iPS-Microglia model has yielded critical insight into the interaction of microglial function and the development of Alzheimer's disease. This model has been readily adapted by many academic labs as well as pharmaceutical companies with the aim of studying human microglial function or other disease risk loci. By further studying AD risk genes in this fashion, we may be able to converge on several mechanisms by which microglial functions are able to attenuate or drive neurodegeneration. Focusing therapeutic efforts on these pathways could lead to the development of immunotherapies for Alzheimer's disease.

INTRODUCTION

Microglia in Alzheimer's disease: Exploring how genetics and phenotype influence risk

Amanda McQuade, Mathew Blurton-Jones

Alzheimer's Disease and the Amyloid Cascade Hypothesis

Alzheimer's Disease (AD) is the most common form of dementia and the sixth leading cause of death in the Unites States (Alzheimer's Association). Unlike most other causes of death, the incidence of AD continues to rise, and cases are expected to double within the next 30 years as our population ages. Basic and translational science coupled with medical advances, have greatly increased human lifespan, but with this comes increased risk of developing age-related diseases, such as AD. Thus, it is critically important to focus our research efforts on increasing the healthy years of life in older individuals.

Alzheimer's disease was first identified in 1908 by a German Neurologist, Alois Alzheimer who described patients who exhibited disorientation, confusion, and progressive memory loss. His pathological examinations further revealed brain atrophy and the accumulation of key pathologies including intraneuronal neurofibrillary tangles, extracellular plaques, and morphological changes in microglia, the primary immune cells of the brain(Alzheimer et al., 1995). One hundred years past this original characterization, the diagnosis of AD remains largely similar, though somewhat more precise. Clinicians look for insidious onset of amnesic presentation, difficulties finding words, impaired facial recognition, and deficits in problem solving(McKhann et al., 2011). Researchers today are still searching for validated biomarkers through neuroimaging, cerebrospinal fluid (CSF), blood, or urine tests as well as genetic risk profiling, but none have yet proved to be reliably conclusive in large-scale clinical trials.

While the majority of AD occurs 'sporadically' in aged individuals, much can be learned from the rarer familial forms of AD (fAD). fAD accounts for around 2 % of all AD

cases, and often occurs earlier in life with onset in the 30s or 40s. Familial Alzheimer's disease occurs due to inherited genetic mutations within the genes presenilin-1, presenilin-2, or amyloid precursor protein (APP). Each of these mutations effects the production and processing of beta-amyloid (Aβ), which is the primary component of the extracellular plaques that were first described by Alois Alzheimer. The identification and subsequent understanding of the functional effects of these mutations, led to the proposal by Hardy and Higgins in 1992 of the 'amyloid cascade hypothesis' of AD (Hardy and Higgins, 1992). This hypothesis posits that Aβ accumulation is the initial cause of AD that in turn induces a series of downstream pathological cascades including neurofibrillary tangle formation, inflammatory responses, as well as synaptic and neuronal loss. In strong support of this hypothesis, imaging studies have now clearly shown that Aβ begins to accumulate some 10-15 years prior to diagnosis. As a response to this hypothesis and the evidence that Aβ pathology is one of the first recognizable signs of AD, many drugs have been developed to clear Aβ from the brain in an attempt to relieve the symptoms of AD and potentially halt disease progression. To date, many therapies targeting Aβ synthesis or clearance have been tested in clinical trials (bapineuzumab, solanezumab, tarenflurbil, phenserine, gammagard etc.) but unfortunately none have yet proved to be effective in reducing memory deficits or halting disease progression in late stage trials. Famously, one compound; PF-04494700 a drug licensed by Pfizer, actually caused AD patients to deteriorate faster than their placebo counterparts.

A likely issue with Aβ centered treatments may be that patients are treated too late in the disease process. Since Aβ has already been accumulating for ~10 years by the time patients are first diagnosed with AD or mild cognitive impairment (MCI), removal of

Aβ from the brain is unlikely to resolve the additional downstream consequences of AD neuropathology. In others words, once neuroinflammation, tau pathology, and neurodegeneration begin, it may make little difference in disease progression to remove the initial insult of Aβ plaques. Instead, therapies that better target these downstream processes may be far more effective at later stages of disease. Yet, Aβ therapies could still be useful if treatments can be begun during the prodromal phases of the disease. Thus, research into earlier diagnosis and accurate biomarkers remains critical.

Microglia in AD pathogenesis

As mentioned previously, signs of microglial activation in AD, as assessed by broad morphological analysis, was first described by Alois Alzheimer in 1908(Alzheimer et al., 1995). Since then, many groups have clearly demonstrated the close spatial-temporal relationship between Aβ plaques and activated microglia in both AD patients and mouse models (Figure 1.1). Several studies have also further visualized beta-amyloid itself within microglia cell bodies, suggesting an important role for microglia phagocytosis in the clearance of beta-amyloid (Wisniewski et al., 1981). Because microglia are preferentially activated in close proximity to Aβ plaques, many groups hypothesized that the plaques are responsible for activating microglia, further explaining the prominent hypothesis that beta-amyloid initiates the Alzheimer's disease cascade. Yet, we now have evidence that microgliosis occurs *prior* to visible Aβ plaque deposition (Boza-Serrano et al., 2018). Furthermore, recent evidence suggests that microglia may even contribute to the seeding of plaques as pharmacological depletion of microglia leads to a significant reduction in plaque pathology in 5xfAD transgenic mice (Sosna et al., 2018). The next big

questions are: what process leads to this microglial activation, and what are microglia doing to promote plaque formation or to inhibit plaque clearance?

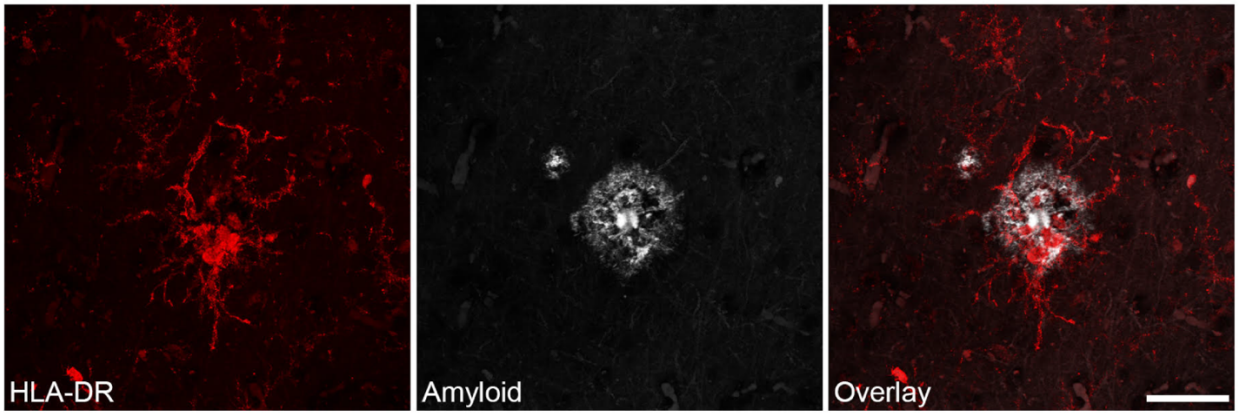

Figure 1. Disease-associated microglia surrounding Aβ plaques. Immunofluorescent stain of human Alzheimer's patient tissue demonstrates microglia (stained with DAM marker HLA-DR, red) surrounding Aβ plaques (gray). HLA is upregulated in microglia around plaques. The scale represents 50 μm.

Because microglia are highly sensitive to changes in their environment, these cells have proven difficult to study. Thus far, murine models have served as the primary tool to study microglial genetics and function. While these model systems have led to important discoveries of microglial ontogeny and function, it has also become clear that there are important differences between murine microglia and human microglia which are particularly evident in aging and disease (Friedman et al., 2018; Ueda et al., 2016). Thus, we must be careful not to simply conclude that findings in mouse models will necessarily translate to human microglia. In order to study human microglia, several labs have developed techniques to isolate human microglia from brain tissue removed during surgical resection of epileptic foci or brain tumors (Bennett et al., 2016; Durafourt et al., 2012; Gosselin et al., 2017). This approach provides one of the very few methods to study

viable human brain-derived microglia, but remains logistically very challenging. Another innovative technique to overcome the difficulty of studying human microglia has been to isolate microglia or their nuclei from postmortem brain tissue. These techniques have allowed researchers to discover important human-specific changes that occur as microglia age(Olah et al., 2018). Still, it is likely that the agonal state preceding death, co-morbid infectious or inflammatory conditions such as pneumonia, or post-mortem delay influence microglial gene expression and activation state which may may obscure and greatly complicate data interpretation. Given these complications, several groups including our own have developed protocols to differentiate human microglia from pluripotent stem cells (Abud et al., 2017; Douvaras et al., 2017; Haenseler et al., 2017; McQuade et al., 2018; Muffat et al., 2016; Pandya et al., 2017; Takata et al., 2017). Producing human microglia *in vitro* allows scientists to study these cells using better-controlled and more mechanistic approaches including the use of drug libraries and genetic manipulation such as CRISPR.

Although a fully defined microglia differentiation protocol is extremely useful for experiments that aim to study the mechanistic functions of human microglia, microglia in isolation may function quite differently than those in the brain environment. More comprehensive models of human microglia in a brain-like environment continue to be developed and include studies that involve engrafting human iPS-derived microglia into 3D neuronal cultures, brain organoids, or murine brains (Abud et al., 2017; Ormel et al., 2018; Park et al., 2018) In order to recapitulate how human microglia react to realistically complex disease environments such as beta-amyloid plaques, neurofibrillary tangles, or traumatic brain injury, etc., a chimeric xenotransplantation system is likely to best mimic

human disease and thus help narrow the focus of pre-clinical targets to ones which most accurately reflect what occurs in patients.

Genome-wide Association Studies

Some clues as to how microglia may be effecting the progression of Alzheimer's disease can be found by studying which microglia-specific gene variants cause risk for or protection from AD. In recent years, the power of genomics has allowed geneticists to uncover many single nucleotide polymorphisms (SNPs) that are correlated with differential AD risk. These studies have confirmed the previously established importance of Apolipoprotein E (APOE), while also uncovering many new risk-SNPs. SNP variants may occurr within gene coding regions, or influence disease risk through known promoters, enhancers. Additionally SNPs may be sign posts which are inherited alongside mutations which are in map linkage disequilibrium. For this review, we will only discuss SNPs which are correlated with actual changes in gene expression or protein function. Surprisingly, around two thirds of these new AD-risk SNPs are exclusively or most highly expressed in microglia. This data has been corroborated by many groups including a recent study of over 300,000 individuals that reported 48 AD-risk SNPs (FDR $< 10^{-5}$), 29 of which are most highly expressed by microglia (60.4%) (Figure 2) (Zhang et al., 2014). This data hints that changes in microglial function may influence differential risk for AD, suggesting that these brain-resident immune cells play a far greater role in disease development and progression than previously thought. While this review will not cover the role of every microglial specific risk gene, we provide a broad overview of all current AD-risk SNPs in Table 1.

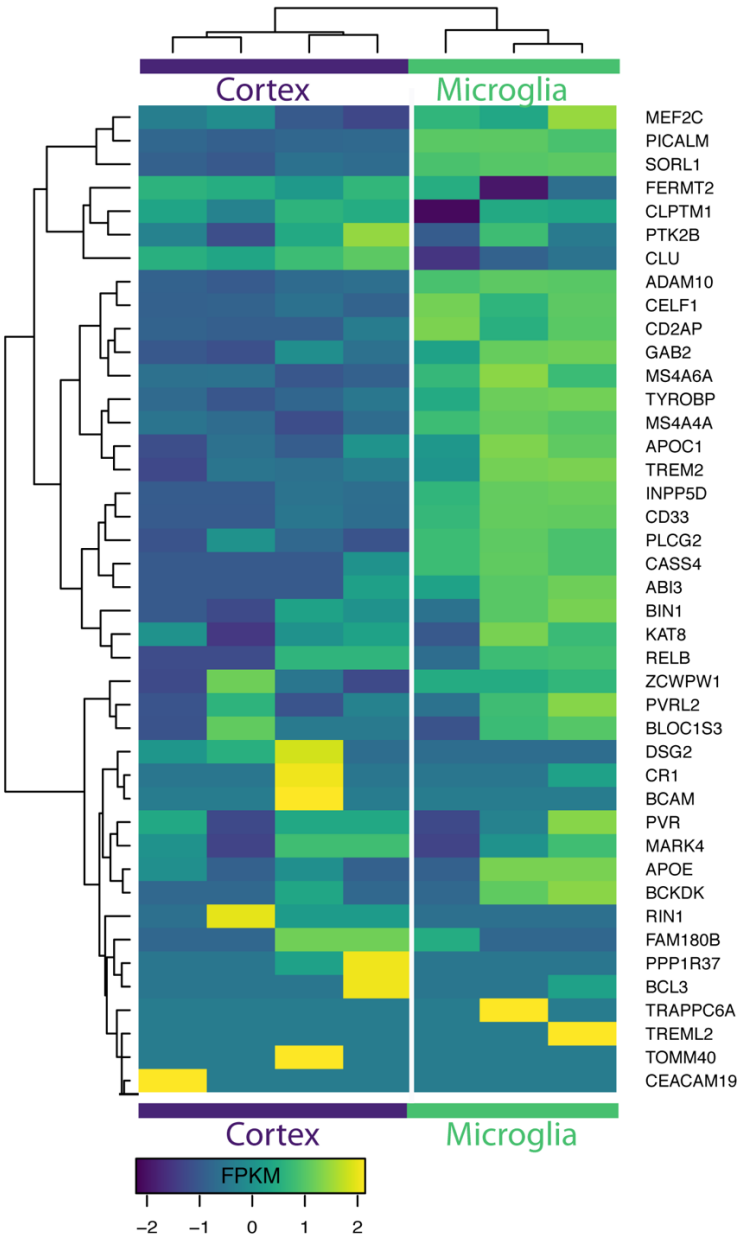

Figure 2. Alzheimer's risk genes are enriched in microglia over total cortex expression. Transcriptome data from Zhang et al. [24] was used to generate this heatmap of expression levels of each AD risk gene in the brain cortex (left) versus expression level in microglial cells (right). Data are displayed in frequency per kilobase million reads (FPKM).

SNP ID	Proposed gene affected	Function	Citation
rs3764650 rs3752246	ABCA7	lipid transport	Allen et al. Neurology 2012
rs616338	ABI3	actin polymerization	Sims et al. Nat Genet 2017
rs2305421	ADAM10	cleaved TNFa and E-cadherin	Akhter et al. Neurobio Aging 2018
rs4420638	APOC1	lipid metabolism	Lin et al. J Hu Genetics 2016
rs5167	APOC4	lipid metabolism	Allan et al. Genomics 1995
rs2075650	APOE	lipid metabolism	Lin et al. J Hu Genetics 2016
rs889555	BCKDK	unknown immune function	NA
rs2965101 rs2927438	BCL3	NF-kB immune regulation and survival	Poveda et al. Exp Mol Med 2017
rs744373 rs7561528	BIN1	endocytosis and phagocytosis	Prokic et al. J Mol Md 2014, Gold et al. J Exp Med 2004
rs597668	BLOC1S3	endosome and lysosome trafficking	Seshadri et al. JAMA 2010
rs7274581 rs6024870	CASS4	cell adhesion and axonal transport	Beck et al. Oncoscience 2014
rs9349407 rs9296559	CD2AP	cytoskeletal remodeling	Guimas et al. Cell Mol Life Sci 2018
rs3865444 rs3826656	CD33	phagocytosis	Griciuc et al Neuron 2013
rs2965109	CEACAM16	antigen cell adhesion	Kammerer et. Al J Biol Chem 2012
rs714948	CEACAM19	antigen cell adhesion	Kleita et al. Int J Oncol 2013
rs10838725	CELF1	transcription regulation	Dasgupta and Ladd Wiley Interdiscp Rev RNA 2013
rs35577563	CLPTM1	telomere regulation	Carkic et al. J Oral Sci 2016
rs11136000	CLU	complement, apoptosis, lipid transport	Karch and Goate Biol Psy 2015
rs679515 rs3818361	CR1	complement	Rogers et al. Neurobiol Aging 2006
rs8093731	DSG2	lysosomal function	Karch and Goate Biol Psy 2015
rs11767557 rs11771145	EPHA1	immune response, cell adhesion and motility	Misra et al. Indian J Med Res 2018, Aasheim et al. Blood 2005
rs10415983	EXOC3L2	exocytosis	Dayeh et al. PLoS Genet 2014
rs12287076	FAM180B	unknown	NA
rs17125944	FERMT2	actin polymerization	Yasuda-Yamahara et al. Matrix Biol 2018
rs1385600	GAB2	cell growth and apoptosis	Bagyinsky et al. Clin Interv Aging 2014

rs5848	GRN	lysosomal function	Paushter et al. Acta Neuropathol 2018
rs9271192	HLA-DRB5-DBR1	antigen presentation	Karch and Goate Biol Psy 2015
rs35349669	INPP5D	myeloid proliferation and survival	Efthymiou and Goate Mol Neurodegener 2017
rs7196161	KAT8	cell survival	Patillon et al. PLoS One 2012
rs8100183	MARK4	inflammasome	Li et al. Nat Commun 2017
rs190982	MEF2C	immune profliferation and antigen presentation	Sao et al. Phychiatry Clin Neurosci 2018
rs558678 rs554311	MS4A2	hematopoietic immune response	Keuk et al. Immuno Cell Bio 2015
rs610932 rs11824773	MS4A4A	signal transduction phagocytosis	Greer et al. Cell 2016 and unpublished data from our lab
rs10897011 rs7926729	MS4A4E	unknown immune function	Hollingworth et al. Nat Genetics 2011
rs610932 rs983392	MS4A6A	Phagocytosis, calcium homeostasis	unpublished data from our lab
rs17643262	NKPD1	lipid synthesis	Amin et al. Biol Psych 2017
rs2718058	NME8	cytoskeletal and axonal transport	Liu et al. Oncotarget 2016
rs3851179 rs541458	PICALM	endocytosis	Zhao et al. Nat Neurosci 2016
rs72824905	PLCG2	calcium signaling	Conway et al. Molecular Neurodegener 2018
rs145999145	PLD3	APP processing	Satoh et al. Alzheimers Res Ther
rs3848140	PPP1R37	phosphotase activity	Han er al. PLoS One 2017
rs2058716	PRKD3	inflammatory signaling	Baker et al. PLoS One 2018
rs28834970	PTK2B	inflammation	Beck et al. Oncoscience 2014
rs2301275	PVR	immune activation	Stamm et al. Oncogene 2018
rs10402271 rs1871047	PVRL2	chlosterol metabolism	Lin et al. J Hu Genetics 2016
rs2376866 rs117612135	RELB	immune migration	Dohler et al. Front Immunol 2017
rs10498633	SLC24H4-RIN3	cardiocascular function	Giri et al. Clin Interv Aging 2016
rs12285364	SORL1	lipoprotein receptor	Holstege et al. Eur J Hum Genet 2017
rs760136 rs10524523	TOMM40	chlosterol metabolism	Lin et al. J Hu Genetics 2016
rs28367893	TRAPPC6A	protein transport	Chang et al. Oncotarget 2015

rs75932628	TREM2	phagocytosis, migration, activation	Gratuze et al. Mol Neurodegen 2018
rs9381040	TREML2	immune activation, phagocytosis	Zheng et al. Neurobiol Aging 2017
rs1476679	ZCWPW1	histone modification	Gao et al. Oncotarget 2016

Of the GWAS-risk genes, SNPs within Triggering Receptor Expressed on Myeloid Cells 2 (TREM2) are associated with the highest risk of developing AD, increasing disease risk by 2-4 fold. As the name suggests, TREM2 is exclusively expressed on cells within the myeloid lineage. Thus, in the brain, TREM2 expression is dominated by microglia. Additionally, recent comparisons of human peripheral blood monocytes and both iPSC-derived and brain-derived microglia further suggest that TREM2 expression is greatly enriched in microglia versus other monocyte lineages (Abud et al., 2017). Several of the AD-associated SNPs occur within the Trem2 coding region, including R47H, R62H, and H157Y. R47H TREM2 mutations, in particular have been ardently studied, uncovering relationships between carriers of this variant and increased CSF biomarkers such as tau, p-tau181, and soluble Trem2 (sTrem2), each of which have been associated with worse disease progression(Deming et al., 2018; Jay et al., 2017; Lill et al., 2015). Research on the function of R47H and other TREM2 variants thus far suggests that AD-risk is incurred through a partial loss of function (Kober et al., 2016), however, the localization of the R47H and R62H mutations within the ligand binding domain of TREM2 suggest perhaps a more nuanced alteration in specific microglial responses.

Thus far, the majority of studies examining TREM2 in relation to AD have utilized TREM2 deletion that in general appears to reduce microglial activation in response to varying stimuli. For example, murine AD models with $TREM2^{-/-}$ exhibit decreased microglial activation resulting in less microglial migration to beta-amyloid plaques and

delayed plaque clearance (Kleinberger et al., 2014). In addition, plaques in TREM2$^{-/-}$ mice are less compacted, leading to increased plaque-associated neuritic dystrophy (Condello et al., 2015; Wang et al., 2016). These data collectively suggest that microglial activation is necessary for clearance of plaques, and that suppression of these activation programs may accelerate plaque accumulation. Interestingly, total microglial numbers are also decreased in TREM2$^{-/-}$ mice potentially due to their inability to initiate activation-related proliferation and/or impaired microglial survival. Indeed, Trem2 expression normally decreases with some forms of microglial activation such as LPS treatment, but is conversely elevated in microglia adjacent to beta-amyloid plaques. Furthermore, microglia that lack trem2 do not seem to activate normally in response to injury (Keren-Shaul et al., 2017; Krasemann et al., 2017). In addition, as a transmembrane protein, recent studies have demonstrated that TREM2 can be proteolytically cleaved, resulting in sTREM2 which may serve as a promising biomarker for AD and may also provide additional immunomodulatory functions (Suárez-Calvet et al., 2016a, 2016b; Zhong et al., 2017) .

In addition to specific mutations in Trem2, other microglial AD-risk genes, membrane spanning 4-domains subfamily A members 4A and 6A (MS4A4A, MS4A6A) have recently been associated with altered sTrem2 levels in patient CSF. The MS4A family is itself linked to altered AD risk; in autopsied AD brains and blood samples from AD-patients with MS4A risk SNPs, expression of both MS4A4A and MS4A6A is increased. Importantly, these elevated expression levels also parallel increasing Braak tangle and plaque scores (Allen et al., 2012; Karch et al., 2012a; Proitsi et al., 2014). Interestingly, an AD-risk SNP (rs6591561) associated with increased expression of both

MS4A genes, is also correlated with reduced levels of sTrem2. Conversely, rs1582763, a SNP associated with decreased MS4A4A and MS4A6A is linked to increased sTrem2 and protection from Alzheimer's disease (Deming et al., 2018). However, MS4A proteins likely also influence disease risk independently of their effect on sTrem2. For example, unpublished data from our lab suggests these proteins play a role in regulating phagocytosis. Furthermore, other members of the MS4A family such as CD20 (MS4A1) have previously been implicated in immune regulation independent of Trem2 signaling.

CD33 or Siglec-3, is another myeloid cell specific receptor that has been significantly associated with Alzheimer's disease(Hollingworth et al., 2011; Jiang et al., 2014). Sialic acid binding triggers Immunoreceptor Tyrosine-based Inhibitory Motif (ITIM) signaling through Siglec proteins such as CD33, which has previously been shown to induce SYK-mediated signaling cascades that lead to changes in phagocytosis that are similar to those triggered by TREM2/DAP12 signaling (Linnartz and Neumann, 2013). CD33 expression is also increased in human AD brains and correlates with increased plaque burden as well as swifter disease progression (Jiang et al., 2014). Within BV2 immortalized microglia and murine CD33 knockout models of AD reduced expression of CD33 is associated with impaired clearance of beta-amyloid (Griciuc et al., 2013). Extrapolation from these data may seem confusing given that they suggest increased expression of CD33 in microglia would be predicted to increase beta-amyloid phagocytosis while also leading to increased plaque burden. However, this combination can be resolved if we again consider the microglial seeding hypothesis whereby increased phagocytosis of beta-amyloid would lead to higher levels of plaque seeding leading to increased plaque load.

In addition, an elegant recent study of monocyte-derived microglia-like (MDMi) cells recently demonstrated that the CD33 AD risk SNP rs3865444 is associated with increased expression and membrane localization of full-length CD33 and decreased expression of a shorter splicing variant that lacks the immunoglobulin V-set domain, which together lead to reduced phagocytic activity (Ryan et al., 2017). In parallel, it was discovered that a protective SNP (rs12459419) leads to increased splicing of exon 2 leading to a shorter length protein (Malik et al., 2013). While our understanding of CD33 biology continues to improve, additional research is still needed to determine whether the main role of CD33 in AD is through modulation of Aβ phagocytosis or whether additional immune regulatory aspects of altered CD33 signaling play a more important role in disease pathogenesis.

Of additional interest, ATP-binding cassette transporter A7 (ABCA7) is a membrane transporter expressed highly by neurons, microglia, oligodendrocytes, and endothelial cells, but still seems to have the largest effect on disease risk through microglia (Zhang et al., 2014). In AD, SNPs in ABCA7 seem to be associated with a gain of function that may enhance phagocytosis of apoptotic cells and beta-amyloid (Allen et al., 2012; Jehle et al., 2006; Kim et al., 2013; Ramirez et al., 2016; Tanaka et al., 2011). On a broader scale, human post-mortem tissue analysis has shown that SNPs in ABCA7, which increase ABCA7 expression, correlate with increased hippocampal atrophy. Inversely, when ABCA7 was deleted from the J20 amyloid model of AD, a decrease in plaque deposition was observed. These data again suggest that changes in microglial phagocytosis of beta-amyloid may underlie the effects of microglial risk genes on disease. On the other hand, our studies to date have been guided by the existing knowledge in the

field and the somewhat biased expectation that any studies of AD-associated microglial function should by definition examine beta-amyloid phagocytosis. Yet, a growing number of studies suggest that phagocytosis of other CNS-derived substrates such as synapses or myelin could be at least as important to disease progression and we and others are finding that microglial genes can differentially effect phagocytosis of differing substrates. Likewise, many other less studied functions of microglia, could also be critically involved in this disease. Thus, it seems a more comprehensive, unbiased analysis of the effects of AD risk genes on human microglial function and gene expression are desperately needed to improve our understanding of these cells and their role in AD.

Now that it has become clear that microglia are crucial in AD pathogenesis, the field needs to better understand *how* these cells influence disease risk and whether the normal function of microglia in disease is generally protective or pathogenic. Though many of these risk genes eventually effect production or clearance of Aβ plaques, it is not known whether this is the mechanism that confers altered disease risk or whether this is merely a byproduct of a more important pathway or our somewhat biased experimental designs. By understanding the broader role of microglia and the immune system in AD we will be able to gain insight into the elusive causes of late onset Alzheimer's disease in order to better target disease-modifying therapies that can prove to be effective in clinical trials.

Microglia in Homeostasis and Disease

In homeostatic conditions, microglia are responsible for promoting neuronal health through secretion of trophic factors and synaptic remodeling as well as clearing

pathogens, protein aggregates, myelin, and dead cell debris. These immune cells tile to form a grid through the brain, ensuring that no section goes unsurveiled. Homeostatic microglia are highly ramified and each of their processes is appreciably motile, constantly probing their environment for potential pathogens (Davalos et al., 2005). When a threat arises, microglia quickly become activated in order to address the insult. Activated microglia can secrete pro-inflammatory cytokines, clear pathogenic materials through phagocytosis and lysosomal degradation, and may also induce astrogliosis and astrocyte-associated changes to the blood brain barrier. After the pathogen has been cleared, microglia will typically return to a homeostatic state.

In some cases, however, microglia activation fails to resolve. In these circumstances, the constitutively active microglia often become detrimental to brain health. They may aberrantly over-prune synapses, kill neurons through phagoptosis, or induce unnecessary astrogliosis through pro-inflammatory cytokine secretion. Through prolonged, unnecessary microglial activation, severe neurodegeneration may occur. For example, aberrant inflammation in traumatic brain re-injury results in an inability for lesions to heal (Donat et al., 2017). Chronic microglial activation has also been strongly implicated in many neurodegenerative diseases, playing a role in multiple sclerosis, amyotrophic lateral sclerosis, Huntington's disease and Alzheimer's disease (Allen et al., 2012; Lill et al., 2015; Mammana et al., 2018).

As mentioned previously, problems can also arise if, conversely, microglia are unable to become appropriately activated in response to an insult, such as in Trem2 knockout models. When microglia are constitutively homeostatic, they may not be able to properly remove pathogens, debris, or dead cells. In this case, these hazardous materials

may build up creating further imbalances in brain homeostasis. Because microglia are responsible for supporting brain health and homeostasis through many avenues, microglia may influence the onset of AD in various ways, some of which are explored below.

Migration, phagocytosis, and lysosomal degradation

Many of the Alzheimer's risk genes highly expressed in microglia effect microglial phagocytosis of beta-amyloid. Given the widespread interest in and adoption of the amyloid cascade hypothesis (Hardy and Higgins, 1992), it follows that the majority of research on microglia in AD has often begun with examinations of this question. However, amyloid targeted therapeutics have thus far failed to improve or delay cognition in late stage clinical trials, leading some to speculate that beta-amyloid deposition could be a sign post of other more detrimental issues rather than a pathogen directly. If therapies can be developed that can reset and enhance microglial-mediated clearance of beta-amyloid, many would predict that this might stop or delay disease progression. Yet, as with other amyloid targeting therapies such an approach would likely only be useful if initiated during very early prodromal phases of the disease.

Phagocytosis of beta-amyloid is a complex system which includes migration towards the beta-amyloid plaques, endocytosis of beta-amyloid and lysosomal degradation into its constituent amino acids. The accumulation of beta-amyloid plaques observed in AD brains may be occurring from deficits in any or all of these components. These dysfunctions may be beta-amyloid specific or may also effect a broader range of phagocytosis of other substrates including apoptotic cells, myelin, or debris.

The ability of a microglia to migrate is crucial to its immune surveillance activity. In order to clear something from the brain, microglia must first follow chemotactic cues towards the debris or pathogens. This process is complex to study given that there are many chemokines, but often the mechanisms can be extrapolated from macrophage biology. When neurons die, for example, ADP and nucleotides released from the dying cell form a chemoattractive gradient sensed by the purinergic receptor P2RY12 on microglia (Corriden and Insel, 2012; De Simone et al., 2010; Moore et al., 2015). When P2YR12 is chemically blocked, microglia are unable to activate in response to ADP/ATP and additionally do not migrate along their concentration gradient. *In vivo*, blockade of P2YR12 would likely inhibit microglial activation in response to dead neurons leading to a build up of apoptotic debris in the brain (Eyo et al., 2018). This is similar to what occurs with trem2 responses to beta-amyloid in which knockout of trem2 inhibits microglial migration toward amyloid plaques leading to increased beta-amyloid accumulation in AD mouse models. Correspondingly, it has been suggested that trem2 and its' co-receptor dap12 may act as an actual phagocytic receptor for beta-amyloid. However, a large number of receptors on microglia have been posited to bind beta-amyloid and thus additional research is needed to tease out which receptors are necessary for directed migration and which are more important for beta-amyloid internalization.

If a microglia cell is able to properly migrate towards its target, the cell will still need to express the receptors and machinery to complete phagocytosis of this substrate. We still do not fully understand all the components involved in microglial phagocytosis, but much has been learned from assuming homology with other myeloid cells. In terms of neural phagocytosis, one of the major signals for a microglia cell to engulf its target is

exposed phosphatidylserine. This phospholipid becomes exposed on the cell surface during the early stages of apoptosis and in response to oxidative stress, ATP depletion, or increased calcium ion levels all of which are signs of cellular stress and increase with age(Brown and Neher, 2014; Suzuki et al., 2013; Tyurina et al., 2007). Interestingly tau-laden neurons have also been shown to aberrantly expose phosphatidylserine(Asai et al., 2015; Brelstaff et al., 2018). Microglial recruitment to these neurons may be a partial mechanism for how tau causes neurotoxicity. Indeed, PET imaging in mice has shown tau accumulation to precede microglial activation which strongly correlated with a reduction in brain volume(Ishikawa et al., 2018). Other groups however cite microglia as the mediators of tau spreading though phagocytosis remains important in either case (Asai et al., 2015).

Protein aggregates, on the other hand, often must become opsonized before they can be recognized by a microglia cell. The most well-studied opsonins are IgG antibodies and the complement system both of which have been associated with AD(Fu et al., 2012; Hong et al., 2016a; Marsh et al., 2016). Though, for beta-amyloid proteins, it has also been suggested that opsonization is not necessary. Many toll-like receptors, g-protein coupled receptors, and several AD-risk genes (trem2, abca7) have been proposed to serve as beta-amyloid receptors. For some of these receptors, it is likely that beta-amyloid does indeed bind, but rather than triggering phagocytosis of Aβ, this ligand may trigger downstream pro-inflammatory signaling cascades. It is difficult to distinguish receptors necessary for activation from those necessary for engulfment since removal of the former may still inhibit beta-amyloid phagocytosis by causing the cells to remain in a homeostatic state. This may be the case with AD-risk genes such as TREM2 and ABCA7. However,

cell culture based studies have begun to provide initial evidence that beta-amyloid can indeed be recognized by TREM2, albeit only when bound to Apolipoprotein E(Yeh et al., 2016).

After a microglia cell has successfully sensed, migrated to, and engulfed a particle. It must still degrade the particle. For most substrates that have been engulfed, the phagocytic vesicle containing the cargo will merge with early and late endosomes to load digestive enzymes and acidify the pH before finally merging with a lysosome to form a phagolysosome(Desjardins et al., 1994). Within the phagolysosome, particles are broken up by hydrolytic enzymes suitable for the low pH of the lysosome and can then be released from the cell. The specific proteins involved in this pathway differ depending on the cell type and the substrate being engulfed. Currently, the downstream signaling pathways involving specific processing of apoptotic cells(Zhou and Yu, 2008) or beta-amyloid(Tam et al., 2014, 2016) have not been found to be linked to disease progression directly. However, more research into microglia-specific responses to phagocytic substrates in homeostatic or activated states will be required to better understand how these immune cells are able to respond to pathogenic stimuli in both early and later stages of disease progression. General knowledge from other immune cell types demonstrates that when phagolysosome formation or function is disrupted, this results in a build up of debris within enlarged phagolysosomes and can even result in cell death through necrosis(Turk and Turk, 2009).

Several groups have showed that activating microglia not only boosts the migration to and engulfment of Aβ, but microglia treated with pro-inflammatory cytokines or LPS can actually degrade Aβ more efficiently. This is in part because activation induces

acidification of the lysosomes which encourages faster and more complete degradation of proteins and cellular debris. If a microglia is unable to properly activate in response to neuroinflammatory stimuli, lysosomal efficiency would not increase, resulting in further reduction of the ability of microglia to process pathogenic debris. It is possible that a cascade like this may be the multifactorial trigger promoting disease progression, however, there is also significant data suggesting that many other important microglia functions are also altered in Alzheimer's disease as discussed below.

Cytokine secretion, astrogliosis, and blood-brain barrier breakdown

Cytokines and chemokines are important mediators of neuroinflammation. Somewhat contradictory to the story surrounding Trem2 which concludes that hindering microglial activation increases AD risk, pro-inflammatory cytokines such as CCL2 and TNFα are increased in human AD brains. In addition, homeostatic cytokines such as CX3CL1 are dramatically decreased. CX3CL1 is secreted from neurons and acts as a homeostatic signal for the microglia receptor CX3CR1. In studies of AD models deficient for CX3CR1, AD brains displayed decreased beta-amyloid plaque deposition and substantially less neurodegeneration(Chen et al., 2016; Lee et al., 2010; Liu et al., 2010). Not surprisingly, $CX3CR1^{-/-}$ mice showed increased levels of CCL2 and TNFα further confirming their activated state as a result of the absence of homeostatic signaling. Yet in stark contrast to this, deletion of CX3CR1 in tau transgenic models leads to increased neurofibrillary tangle pathology and behavioral deficits(Bhaskar et al., 2010). Thus, the effects of microglia activation can be diametrically opposite between the two hallmark AD pathologies. A similar relationship has also been described following treatment of AD

mice with LPS, which leads to increased microglial activation and reduced beta-amyloid plaques, but enhanced tangle pathology(Zuroff et al., 2017). Effects from pro-inflammatory cytokines can of course be pleiotropic as cytokines may have autocrine and paracrine effects signaling both back to microglia as well as to astrocytes furthering the spread of neuroinflammation, perhaps providing a partial explanation for these findings. Alternatively, perhaps the key role of microglia in AD is as an intermediary that transduces the proinflammatory-inducing effects of beta-amyloid plaques into increased neuritic dystrophy and tau pathology. In support of this are recent findings regarding the influence of TREM2 deletion and mutations on plaque barrier formation(Condello et al., 2015).

In terms of pro-inflammatory cytokines, CCL2 levels are increased in patients with Alzheimer's disease and may potentially provide a reasonable biomarker for disease progression(Westin et al., 2012). The mechanism of CCL2 in disease progression is still unclear though there is evidence that CCL2 expression alters phagocytosis of beta-amyloid plaques and effects disease progression through this axis(Kiyota et al., 2009). Others propose that CCL2 is mainly effective through recruitment of peripheral mononuclear phagocytes though it remains unclear and controversial whether these cells actually migrate into the brain during human disease(Guedes et al., 2018). TNFα, is similarly increased in Alzheimer's patient brains as well as model systems and seems to also increase phagocytosis of beta-amyloid(Ma et al., 2015). Though the effect of TNFα may be broader in that it is secreted by neurons as well and has independent effects on neuronal survival and proliferation(Bhaskar et al., 2014).

Many important microglial-derived pro-inflammatory cytokines such as CCL2, TNFα, Il1□, IL-6 and others also influence astrocyte activation or astrogliosis(Benveniste

and Benos, 1995; Hanisch, 2002). Even in injury models, removal of microglial cytokines inhibits astrogliosis from occurring further proving that microglia are often responsible for induction of astrocyte reactivity(Balasingam et al., 1994; Selmaj et al., 1990). Like microgliosis, astrogliosis is particularly prevalent near plaques suggesting they play a role either in barrier formation to protect neurons and/or in the chemoattractive recruitment of microglia to the plaque environment(Kamphuis et al., 2014; Osborn et al., 2016). Conversely there is also evidence that astrogliosis is detrimental in that increased astrocyte derived IL-1β, iNOS, and ROS secretion acts as a positive feedback mechanism to increase neuroinflammation and may even harm the blood brain barrier(Balasingam et al., 1994; Osborn et al., 2016) which would allow for further recruitment of peripheral phagocytes into the brain via CCL2/CCR2 signaling.

Damage Associated Microglia

Since the direct pathways through which microglia influence Alzheimer's disease remain unclear, several groups have begun to study microglial biology using broader unbiased approaches. For example, Keren-Shaul et al. used single-cell RNA-sequencing to uncover a specific population of microglia whose temporal appearance mirrored the progression of plaque pathology in the 5x-fAD mouse model (Keren-Shaul et al., 2017). These Damage Associated Microglia (DAM) are formed via a two-step process the second of which appears to be TREM2 dependent since in $TREM2^{-/-}$ mice, microglia remain in the intermediate activation phase throughout disease progression. Therefore, DAM have been hypothesized to be beneficial in the context of AD knowing that Trem2 loss of function mutations are known to exacerbate disease severity and age of onset.

Interestingly, Krasemann et al. have discovered a similar set of genes which they have denoted the microglia neurodegenerative phenotype or MGnD (Krasemann et al., 2017). Here, the authors have described a more generalized phenotypic change associated with several neurodegenerative diseases and demonstrate that this activation state is influenced by APOE. Using mouse models of amyotrophic lateral sclerosis (ALS), multiple sclerosis (MS), and Alzheimer's disease, the authors highlight genes that are induced or repressed commonly across disease type. This list includes many of the same genes discovered in Keren-Shaul et al. including increased apoe, hla, clec7a, and cd11c expression as well as decreased p2ry12, cx3cr1 and tmem119 expression. Although the gene sets discovered in each paper are not identical, it seems likely that each group has independently discovered a similar set of cells. Indeed DAM microglia have been shown to be similarly occurring in ALS as well. Interestingly, MGnDs and the corresponding loss of more homeostatic microglia have been proposed to be detrimental in contrast to the subsequent conclusions of Keren-Shaul et al. Whether the MgnD and DAM phenotype is equivalent and more importantly whether they are detrimental or beneficial will likely depend on the nature of the disease process and timing. For example, one might predict that DAM phenotypes are protective against beta-amyloid given the effects of TREM2 deletion on DAMs and plaque load whereas DAM cells might conversely by detrimental in the context of tau pathology or synaptic pruning. Continued validation of these unbiased approaches and extension of these studies to include examination of human microglia are critically needed and will hopefully help narrow down the true roles of microglia in neurodegenerative disease.

Microglia as a therapeutic target

Since microglia effect so many crucial pathways in the brain, therapies which effect this cell type may have unexpected off-target effects. Fortunately some of the most important microglial functions, such as synaptic pruning, occur predominantly early in life and thus it may not be detrimental to dampen these processes in Alzheimer's patients. Another concern is that microglia share many transcriptional and functional pathways with peripheral monocytes and macrophages. For this reason, small molecule therapies may produce unwanted side effects on these peripheral targets. Currently, in AD, is not yet clear whether immune activation or suppression will be therapeutic as examples in this review have been presented in support of both possibilities. In either case, broad activation or suppression of myeloid cells would likely be detrimental for patients. Sustaining myeloid activation globally may cause chronic inflammation similar to macrophage activation syndrome(Grom et al., 2016; Lull and Block, 2010). On the other hand, general suppression of immune activation in aged patients who already experience an increased risk of infection and immune impairment would leave patients increasingly vulnerable to infectious disease. For these reasons, the most successful microglial therapies will need to be precisely targeted towards microglia but not other monocytes and thus need to capitalize on our growing understanding of the genetic and functional differences between these closely related cells.

If cell-specificity can be sufficiently achieved, it is possible that broad activation or suppression of microglia may be effective although the timing of these approaches will likely be critical. Recent data from mouse studies in which microglia are ablated using a CSF-1 blockade demonstrated no cognitive detriments from complete removal of

microglia in otherwise normal WT mice(Sosna et al., 2018). While behavioral studies in mice are much less nuanced than human cognition, this research suggests that therapeutic microglia suppression, perhaps via more subtle means such as reduced proliferation(Olmos-Alonso et al., 2016), may be therapeutically tractable. Although ideally a specific pathway of microglia activity such as migration, phagocytosis, or cytokine signaling pathways could be isolated and specifically modulated, the effect of microglia on AD pathogenesis does not seem to be that simple. Indeed, this review has provided evidence for disruption in all three of those pathways in AD and likely further study of microglia enriched risk genes will uncover additional microglia functions that influence disease progression.

Perspectives

This review presents a broad overview of the current data positing that the immune system, primarily microglia, plays a much larger role in disease development and progression than previously understood. With the rapid growth of research focusing on microglia in AD, many different functional pathways have been proposed to alter disease risk. Of these, most pathways can be broadly altered by changing microglial activation state. In order to separate these individual pathways from the pleiotropic effects of broad microglia activation, more research towards understanding the spectrum of human microglial activation states will be required. We have learned a great deal from studying peripheral macrophages, but given the key transcriptome and functional differences between peripheral macrophages and microglia, we must assume that microglial activation is likewise quite different. Furthermore, even murine microglia *in vivo* have been

shown to significantly differ from human microglia and these differences are enhanced in aging, making it particularly difficult to study age-related human disease in traditional murine models. While mouse models are extremely useful for studying microglia in their natural environment, they are inherently biased based on what we currently understand to cause Alzheimer's disease and thus will always produce data related to those original assumptions. In order to create a more accurate model of microglia in Alzheimer's disease using patient derived iPS-microglia, one potential promising approach will be to utilze brain organoid models or generate chimeric mouse models to study the complex interactions between human microglia, neurons, astrocytes, and AD neuropathology.

CHAPTER 1

Development and Validation of a Simplified Method to Generate Human Microglia from Pluripotent Stem Cells

Amanda McQuade, Morgan Coburn, Christina H. Tu,
Jonathan Hasselmann, Hayk Davtyan, Mathew Blurton-Jones

Introduction

Microglia are highly specialized tissue resident macrophages within the brain. Their homeostatic functions include shaping neural circuits through promotion of neuronal growth and differentiation as well as synaptic pruning. Microglia have also been strongly implicated in a number of neurological diseases and injuries. Most recently, genetic studies have identified many genes that are highly expressed in microglia which are associated with altered risk of developing Alzheimer's disease (AD), Parkinson's disease, Frontotemporal Dementia, or Amyolateral Sclerosis(Endo et al., 2015; Heneka et al., 2015; Radford et al., 2015; Schapansky et al., 2015). These new discoveries have placed microglia and neuroinflammation at the forefront of disease progression emphasizing the need for new model systems to enable the study of human microglia. Yet, microglia have proven to be difficult cells to study given that many differences exist between human and murine microglia(Bennett et al., 2016). Additionally, there are significant challenges in isolating and culturing these cells(Durafourt et al., 2012; Ueda et al., 2016). Primary human microglia can be isolated in relatively limited numbers from postmortem brain tissue or following surgical resection of brain tumors or epileptic foci. However, given the considerable sensitivity of microglia to environmental changes, samples isolated from patients with neurological disease or following the agonal state prior to death, are likely to be activated and may differ depending on disease state, comorbidities, or cause of death. In order to study a more homeostatic human microglia and to utilize modern experimental manipulations such as CRISPR gene editing, many scientists have instead turned to induced pluripotent stem cells (iPSCs).

In the past three years, several labs, including our own, have developed various protocols for differentiating microglia-like cells from pluripotent stem cells(Abud et al., 2017; Douvaras et al., 2017; Haenseler et al., 2017; Muffat et al., 2016; Pandya et al., 2017; Takata et al., 2017). While the purity, yield, and reproducibility of these different approaches varies considerably, each of these methods produces myeloid cells that exhibit transcriptional profiles and many key functional or morphological characteristics of human microglia. However, the relatively complex nature of these protocols has made it challenging for labs new to stem cell culture or those lacking fluorescence-associated cell-sorting (FACS) core facilities to quickly adopt these approaches. We have therefore developed an appreciably simplified method (iPS-microglia 2.0) to produce both large numbers and highly purified cultures of human microglia. The resulting cells exhibit RNA transcript profiles that are nearly identical to iPS-microglia generated using our previously published protocol(Abud et al., 2017), but provide a significantly increased yield at a reduced cost and omit the prior need for a hypoxic incubator and FACS capabilities, making the protocol more readily accessible for a wider variety of labs.

Materials and Methods

Ethics Statement: All experiments were carried out according to human stem cell (hSCRO) and animal use (IACUC) protocols that were approved by the University of California, Irvine.

Find the complete catalog of materials and catalog numbers in Supplementary Table 5

Simplified Differentiation of iPSCs to HPCs

Improved and simplified differentiation of iPSCs to $CD43^{+}$ primitive hematopoietic progenitor cells (HPCs) is achieved using Stem Cell Technologies STEMdiff™

Hematopoietic Kit (Catalog # 05310). On day -1, feeder-free iPSCs that have been expanded in TeSR-E8 media are passaged with ReLeaSR (STEMCELL technologies) into mTeSR E8 medium with 0.5 μM Thiazovivin onto matrigel coated (1 mg/mL) 6-well plates (Corning Costar). Small aggregates of ~100 cells each are plated at 10-20 aggregates per cm^2. The initial plating density is critical as higher density impairs mesoderm differentiation and lower density decreases yield. Thus one can plate iPSCs at 2-3 different densities and select the wells on day 0 that have optimal density to proceed with. When approximately two 100 cell colonies per cm^2 have been achieved, replace TeSR-E8 medium with medium A (Basal medium plus Supplement A at 1:200 dilution, 2 mL per well of a 6-well). On day 2 (48 hours after original media change), do not fully change media, but rather replace 50% medium A, 1 mL per well of a 6-well. On day 3, carefully remove all media by tilting the plate to one side and aspirating from the edge. Then add 2 mL/well medium B (Basal medium plus supplement B at 1:200). Without removing media, supplement with 1 mL/well of medium B on days 5, 7, 9. On day 10 and again on day and 12, non-adherent cells may be collected. Remove medium with non-adherent cells carefully and centrifuge 300 x G 5 min. After centrifugation, replace conditioned medium back to each well and add 1 mL fresh medium B if further collection on day 12 will be completed.

FACS analysis has confirmed that these non-adherent cells represent highly pure populations (>93%) of $CD43^+$ hematopoietic progenitor cells (Supplementary Figure 2). Importantly, simply collecting the floating cells is all that is required to isolate large numbers of highly purified $CD43^+$ cells. No FACS or MACS isolation is required as

identical microglia are produced using any of these three methods (Supplementary Figure 1). However, because the cells are not being sorted for purity, the collection of non-adherent cells must be carefully completed. Do not spray medium over adherent cells to wash as this will loosen cells which are not $CD43^+$ and decrease culture purity.

At this point, HPCs may be frozen at 2-8 million cells per mL in BamBanker (Wako). HPCs should be thawed directly into microglial differentiation medium with cytokines (below) and plated onto Matrigel-coated plates at 10,000 cells per cm^2. We typically find that viability post-thaw is between 50-85%, with improved viability when greater densities of HPCs are thawed together.

Updated Differentiation of $CD43^+$ HPCs to iPS-microglia 2.0

Volumes specified for 35 mm well (1 well of a 6-well plate).

On day 0 of iPS-microglia differentiation, plate HPCs at 10,000 cells per cm^2 onto 1 mg/mL Matrigel-coated plates (100,000 per 35 mm well). Plate cells into iPS-microglia medium at 2 mL per 35 mm well: DMEM/F12, 2X insulin-transferrin-selenite, 2X B27, 0.5X N2, 1X glutamax, 1X non-essential amino acids, 400 µM monothioglycerol, 5 µg/mL insulin. Immediately before use, microglial medium should be supplemented with 100 ng/mL IL-34, 50 ng/mL TGFβ1, and 25 ng/mL M-CSF (Peprotech) taken from single-use frozen aliquots (important: do not freeze/thaw these cytokines as it will significantly impair differentiation and yield as well as induce activation. It is crucial to thaw cytokines immediately before use). Throughout the differentiation of HPCs to microglia, these cells will predominantly grow non-adherently. On days 2, 4, 6, 8, and 10, add 1 mL fresh media

plus freshly thawed tri-cytokine cocktail. Cytokines are diluted to the concentrations listed above before adding to conditioned medium. Do not fully remove media during the microglial differentiation as the cells secrete paracrine cytokine signals and will not properly differentiate upon removal of those. On day 12, collect 6 mL media from each 35 mm well leaving 1 mL conditioned medium on the plate. Centrifuge non-adherent cells in removed medium for 5 min at 300 x G. Aspirate medium and resuspend non-adherent cells in 1 mL fresh medium plus tri-cytokine cocktail per 35 mm well and add back to the same well which contains the 1 mL conditioned medium. Continue to supplement media (1 mL) on days 14, 16, 18, 20, 22, and 24. On day 25, centrifuge cells leaving 1 mL conditioned media per 35 mm well as on day 12. On day 25, cells should be resuspended in microglia media plus 100 ng/mL IL-34, 50 ng/mL TGFβ1, 25 ng/mL M-CSF, 100 ng/mL CD200 and 100 ng/mL CX3CR1 to further mature microglia and ensure homeostasis. On day 27, feed cells with microglia media with five cytokine cocktail (1 mL per well). On day 28 cells collected for RNA sequencing or use for transplantation or functional assays. If necessary, cells can be maintained for 1-2 additional weeks via media supplementation as above, although longer-term culture is not advised.

Isolating RNA

Total RNA was isolated from cells using RNeasy Mini kit (Qiagen). Approximately 1 million iPS-microglia cells were lysed in RLT buffer and RNA was isolated per manufacturer's instructions with DNAse treatment (10 minutes) and increased spin times to maximize yield (16000 x G for 1.5 min). RNA integrity was measured using the Bioanalyzer Agilent 2100. All libraries were prepared from samples with RNA integrity values ≥ 9.7. 500 ng

RNA per sample was used to create RNA-seq libraries through the Illumina TruSeq mRNA stranded protocol. Each sample was then sequenced in the Illumina HiSeq 4000 platform.

RNA sequencing Analysis

RNA sequencing read integrity was verified using FastQC. BBDuk was used to trim adapters and filter out poor quality reads([CSL STYLE ERROR: reference with no printed form.]). Reads were aligned to the GRCh.38.12 human transcriptome using Kallisto(Bray et al., 2016a). Lowly expressed genes (expression count summed over all samples < 10) were removed before differential expression analysis. Differential Expression of TPM was calculated using DESeq2(Love et al., 2014). An FDR cutoff of 0.001 and fold change of at least 2 was used to determine differentially expressed genes (Supplemental Table 1, 2, 3, 4). Visualizations were constructed in part using R in addition to the Genialis visual informatics platform (app.genialis.com) ([CSL STYLE ERROR: reference with no printed form.]). Gene ontology analysis was performed using EnrichR.

Phagocytosis Assay

Phagocytic activity of iPS-microglia was examined using the the Amnis Imagestream (Millipore) to combine immunofluorescence and flow cytometry. iPS-Microglia or iPS-Microglia 2.0 were treated with either 1 µg/mL pHrodo tagged zymosan A beads, 20 µg/mL S. aureus, or 2 ug/mL fluorescent beta-amyloid (Anaspec). After allowing 1 hour at 37 degrees for phagocytosis, microglia were resuspended in cold FACS buffer (DPBS, 1% BSA, 0.5 mM EDTA) and stained for 30 min at 4 degrees with 1:100 anti-CD45

(Biolegend, clone HI30) and Zombie-violet live/dead stain. 10,000 events were captured for each sample which were gated for in focus live cells before analysis. IDEAS software was used to generate masks of internalized signal (substrate within CD45) and percent of cells with internalized substrates were calculated as well as mean fluorescent intensity which remained constant for each cell type.

Animals

All animal procedures were conducted in accordance with the guidelines set forth by the National Institutes of Health and the University of California, Irvine Institutional Animal Care and Use Committee. The MITRG mouse was purchased from Jackson Laboratories (stock #017711); briefly, this strain was developed on a BALB/c background containing two knockouts alleles: $Rag2^{-}$ ($Rag2^{tm1.1Flv}$) and $il2\gamma c^{-}$ ($Il2rg^{tm1.1Flv}$); and three humanized knock-in alleles: hCSF-1 ($Csf1^{tm1(CSF1)Flv}$), h-IL-3/GM-CSF ($Csf2/Il3^{tm1.1(CSF2,IL3)Flv}$) , and hTPO ($Thpo^{tm1.1(TPO)Flv}$). All mice were age and sex matched and group housed on a 12h/12h light/dark cycle with food and water *ad libitum*.

Adult Intracranial Transplants

All mouse surgeries and use were performed in strict accordance with approved NIH and AALAC-certified institutional guidelines. Direct intracranial injections of iPS-microglia into the cortex and hippocampus were performed on adult MITRG mice. Briefly, adult mice (2-3 months old) were anesthetized under continuous isoflurane and secured to a stereotaxic frame (Kopf). Using a 30-guage needle affixed to a 10 µL Hamilton syringe, mice received 2 µL of mature iPS-microglia suspended in sterile 1X DPBS at 50,000

cells/μL at each injection site. Transplantation was conducted bilaterally in the cortex and hippocampus at the following coordinates relative to bregma: anteroposterior, −2.06 mm; dorsoventral, −1.75 mm (hippocampus), -0.95 mm; mediolateral, ±1.75 mm. Cells were injected at a rate of 50,000/30sec with 4 minutes in between injections. The needle was cleaned with consecutive washes of PBS, 70% (vol/vol) ethanol, and PBS in between hemispheres and animals. Animals were allowed to recover on heating pads before being placed in their home cages and received 2 mg/mL Acetaminophen (Mapap) diluted in water for five days. Animals were perfused 2 months following surgery with 1X PBS followed by 4% paraformaldehyde, entire brains were removed for immunohistochemistry and confocal microscopy.

Immunohistochemistry and Confocal Microscopy

Fixed half brains were first cryoprotected in a 30% sucrose and 0.05% NaN_3 solution in 1X PBS for 72 hours. Tissue was then sectioned into 40 μm thick slices on a freezing microtome (Leica SM 2010R), and stored in 0.05% NaN_3 solution in 1X PBS as free floating wells. For staining, tissue was blocked for 1 hour in 1X PBS, 0.2% Triton X-100, and 10% goat serum. Immediately following blocking, sections were placed in primary antibodies diluted in 1X PBS and 1% goat serum and incubated overnight on a shaker at 4°C. Sections were labeled with combinations of anti-Ku80 (1:250; Abcam ab79220), anti-Iba1 (1:200; Wako 019-19741), anti-P2RY12 (1:200; Sigma HPA014518) and mounted with DAPI Fluoromount (SouthernBiotech). Immunofluorescent sections were then visualized and captured using an Olympus FX1200 confocal microscope. Images represent confocal Z-stack taken with equivalent laser and detection settings.

Results

The transcriptome of iPS-microglia 2.0 differentiated without hypoxia or cell sorting are almost identical to those generated using our prior approach

Our new differentiation protocol still mimics *in vivo* microglia ontogeny by first differentiating iPSCs into hematopoietic progenitor cells (HPCs), followed by passage into microglial differentiation medium, and concludes with a final maturation step by adding neural and astrocytic factors, thereby educating the microglia in a brain-like environment while maintaining a pure, homeostatic population of microglia (Figure 1).

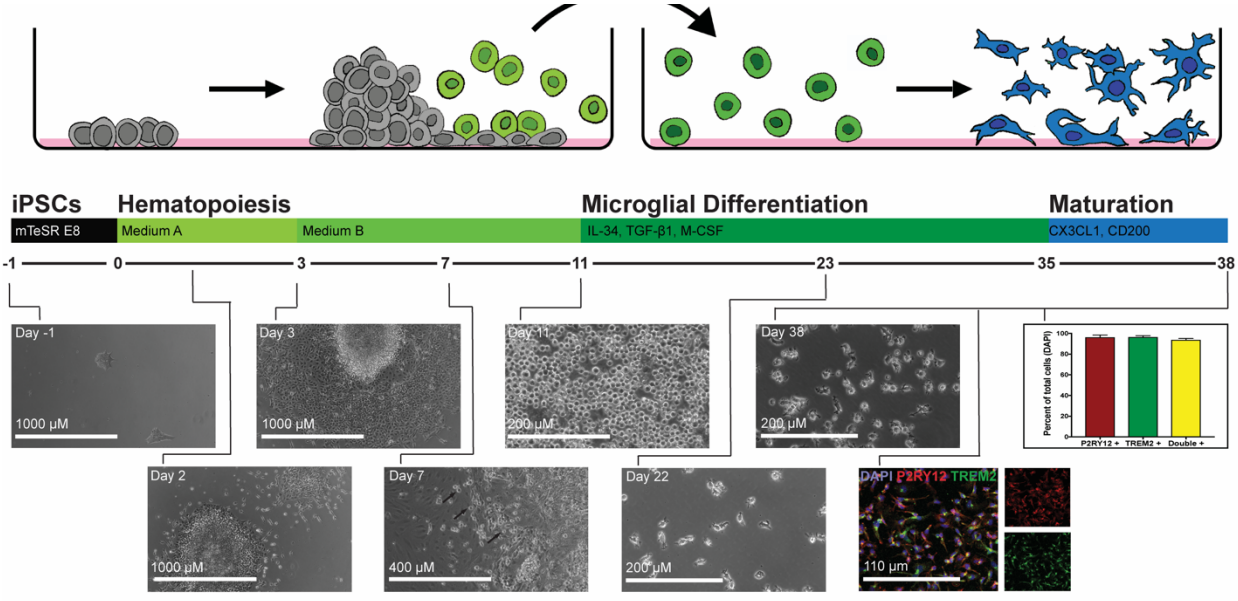

Figure 1.1. A simplified microglial differentiation protocol can be used to produce large numbers of highly pure human microglia. Schematic showing the process of differentiation from iPSCs through the mesoderm lineage (days 0–3) and further promoting hematopoiesis (days 3–11). Primitive hematopoietic progenitor cells begin to appear on day 7 (black arrows) and by day 11 large numbers of round non-adherent HPCs are observed. Floating HPCs are then transferred into new medium to induce microglial differentiation for 27 days. The last 3 days of microglial differentiation include additional neuronal and astrocytic ligands to further educate microglia toward a brain-like, homeostatic environment. By day 38, large numbers of highly pure microglia that stain positively for both P2RY12 and TREM2 (> 94%) have been produced and are ready for experimentation

In order to test whether or not an extensively simplified and commercially available hematopoietic stem cell differentiation protocol could be used to generate equivalent homeostatic microglia, we differentiated four independent iPSC lines, and one ESC line (H9) in parallel using our previously published protocol (Abud et. al., 2017, iPS-microglia) and the simplified iPS-microglia 2.0 protocol described here. Our prior protocol required FACS to isolate $CD43^+$ hematopoietic progenitors before transitioning to microglial differentiation medium. To determine whether FACS sorting was also necessary for our newer approach, we compared three different sorting methods on the same iPSC background. On day 11 when HPCs were ready to be transitioned into microglial medium, we isolated $CD43^+$ HPCs using either FACS, magnetic-activated cell sorting (MACS), or by simply collecting all non-adherent cells. After analyzing RNA-sequencing on these samples, we performed unbiased clustering and found that FACS and MACS sorted iPS-microglia 2.0 intercluster with unsorted samples demonstrating that these isolation procedures are not necessary for this updated protocol (Supplementary Figure 1). Notably, one of the first results we observed with this simplified protocol was that the number of $CD43^+$ HPCs produced using this novel commercially available method was substantially increased, while also maintaining the high degree of purity (90-94%) for the HPC marker CD43 (Supplementary Figure 2). From one million starting iPS cells, 125 million $CD43^+$ cells can be produced, representing an approximately 60-fold increase over our prior method. Following transition to microglial medium, the four lines of unsorted HPCs were further differentiated and matured in parallel. At the final day of microglial

maturation, iPS-microglia or iPS-microglia 2.0 were harvested for RNA isolation and analyzed via RNA sequencing.

At a transcriptome level, our new protocol produced homeostatic human microglia that were virtually identical to microglia generated using our prior methods. Principal component analysis of the full transcriptome explained 73% of variation in all samples within PC1 (44%) and PC2 (29%) and revealed that our new microglia (iPS-microglia 2.0) closely cluster and are interspersed with microglia differentiated using our previously published protocol, yet are highly distinct from human $CD14^+$ or $CD14/CD16^+$ blood monocytes and dendritic cells (Figure 2A, B, Figure 3, Supplemental Table 1). Consistent with our previous findings, both iPS-microglia and iPS-microglia 2.0 exhibit very similar gene expression profiles to brain-derived cultured human microglia, although some differences between these groups remain. In order to highlight important microglial and monocyte enriched genes, we performed a secondary principal component analysis with a previously-identified microglial/monocyte focused gene set which revealed a developmental component (PC1, 48% of variance) and again shows interclustering of iPS-microglia 2.0 with microglia generated using our previously published approach (Figure 2B, D). Importantly, this developmental trajectory remains quite distinct from monocytes and dendritic cells (Figure 2B).

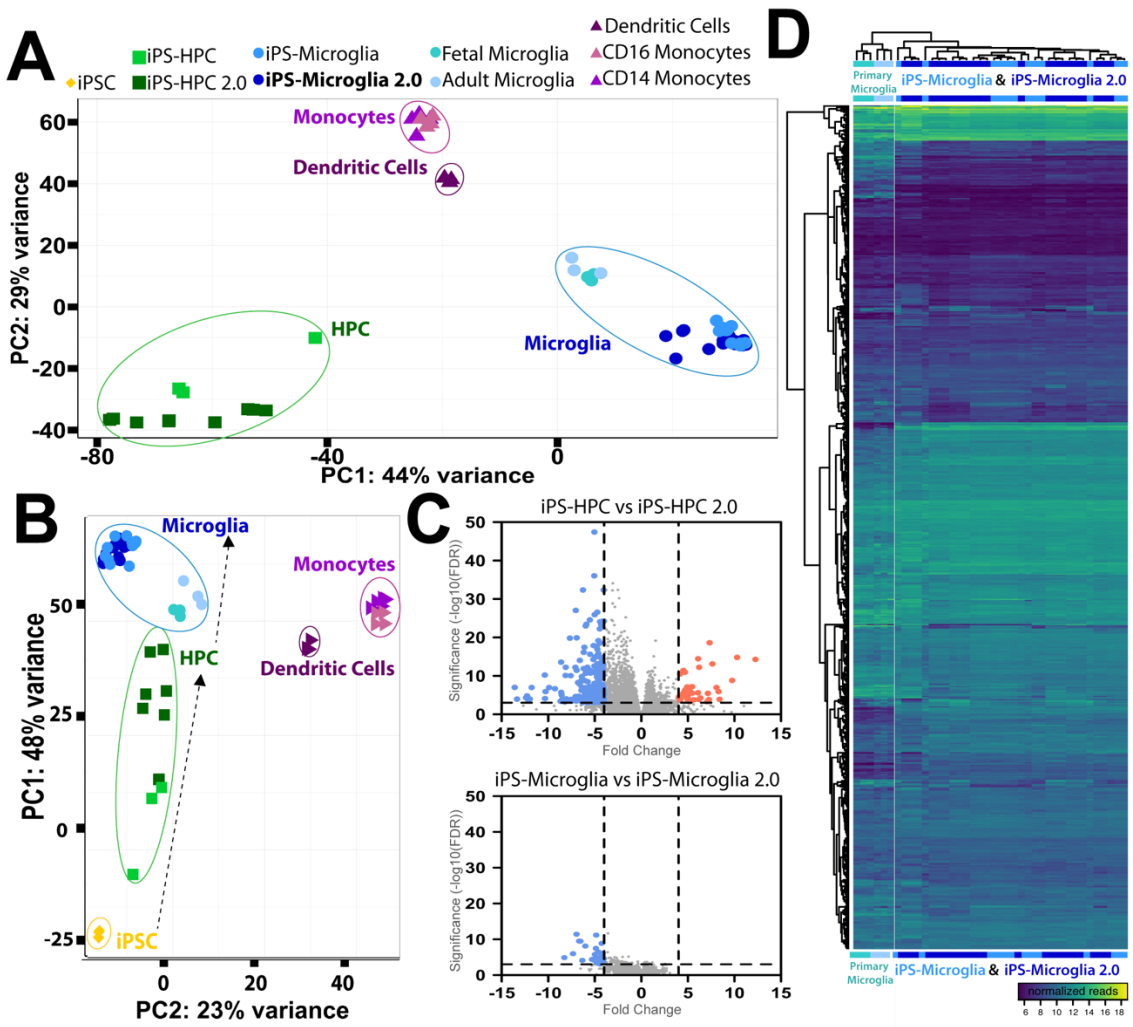

Figure 1.2. iPS-microglia 2.0 are virtually identical to iPS-microglia generated using a more complex protocol. a Principle component analysis demonstrates that iPS-microglia 2.0 (dark blue) and iPS-microglia differentiated using our previously published protocol (blue) exhibit highly equivalent gene expression profiles that cluster closely with cultured human fetal and adult microglia (light blue and teal). Additionally, these cells are distinct from human CD14+ monocytes (purple) and CD16+ inflammatory monocytes (pink), and dendritic cells (maroon). **b** Principal component analysis using a gene list enriched for 882 microglial genes from (Gosselin et al., 2017), further demonstrates the equivalent gene expression between iPS-microglia and fetal and adult microglia. This analysis also highlights the trajectory of differentiation from iPSCs to Microglia and shows the separation between our protocol and monocytic and dendritic cell populations. **c** Volcano plot of differential expression analysis ($p < 0.001$, log2(FC) > 2) between iPS-HPC and iPS-HPC 2.0 samples (top) as well as iPS-microglia and iPS-microglia 2.0 (bottom). Significantly increased or decreased genes are shown in coral or blue respectively. **d** Heatmap using 882 microglial-enriched genes further demonstrates the highly similar gene expression profiles between iPS-microglia and iPS-microglia 2.0 and the close similarity of both cell populations to fetal and adult cultured microglia

Interestingly, RNA sequencing analysis of HPCs generated using our previously published approach versus HPC 2.0 revealed some intriguing differences between these two populations. Based on the developmental trajectory shown in Figure 2B, these data suggest that HPC 2.0 samples are closer to microglia on the primary principle component showing the developmental trajectory than HPCs from our previously described protocol. Indeed HPC 2.0 populations include lower percentages of cells expressing the primitive HPC marker CD235a, although both populations express equivalently high levels of another primitive HPC marker; CD43 which is typically absent in definitive HPCs(Ditadi and Sturgeon, 2016) (Supplemental Figure 2, Supplementary Table 3). Importantly, although some differences do exist in gene expression between these two HPC populations, very few differences in gene expression persist once HPCs are matured into microglia (Figure 1, Figure 2C,D, Supplementary Table 2). For example, expression analysis comparing iPS-microglia and iPS-microglia 2.0 revealed only 55 differentially expressed genes. To determine whether these differences occur in a uniform pathway or are indicative of important functional effects that need to be considered, we next used Reactome 2016 gene ontology analysis to examine these 55 genes. This analysis revealed only three significant gene ontology pathways (*Platelet activation, signaling and aggregation_Homo sapiens_R-HAS-76002*, FDR=0.03665; *Chemokine receptors bind chemokines_Homo sapiens_R0HSA-380108*, FDR= 0.03665; *Tryptophan catabolism_Homo sapiens_HSA-72140*, FDR= 0.03665). The chemokine receptor pathway is of course important for microglial function, although this pathway was implicated by only 3 differentially expressed genes: CXCL10, CCL5, and PF4. Thus, we

expect that microglial functional activity will be largely equivalent between iPS-microglia and iPS-microglia 2.0.

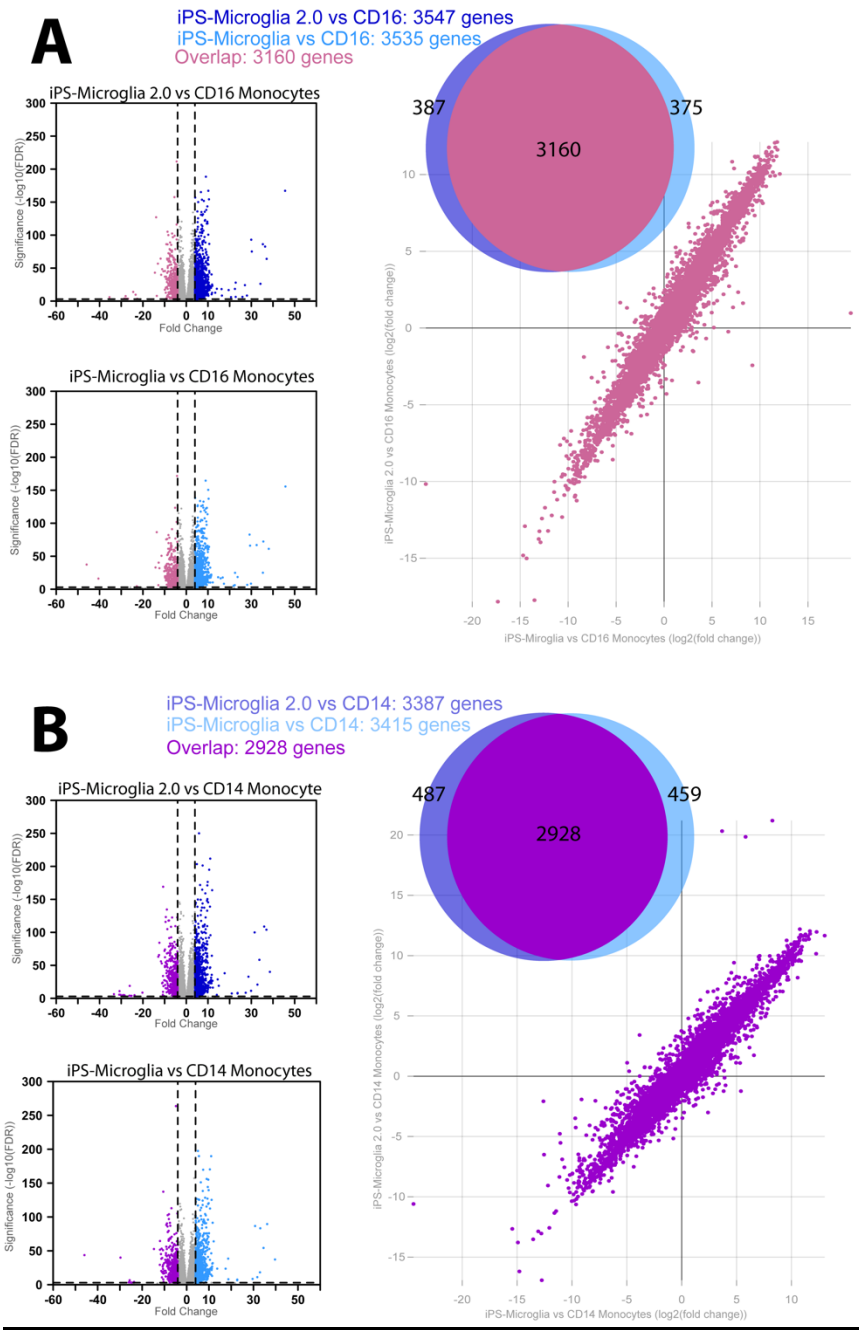

Figure 1.3. iPS-microglia 2.0 are distinct from CD14⁺ and CD16⁺ monocytes. Microglia differentiated using our published protocol are distinct from CD14⁺ monocytes and CD16⁺ inflammatory monocytes. In order to ensure our iPS-microglia 2.0 are similarly distinct from monocytes, differential expression analysis was computed with DEseq2. **A**

Volcano plots of differentially expressed genes comparing genes enriched in $CD16^+$monocytes (pink) with genes enriched in iPSmicroglia 2.0 (dark blue) or iPS-microglia (light blue) show many significant differences between monocytes and microglia. Venn diagrams and comparative fold change plots of differentially expressed genes show that the vast majority of differences are identical between iPS-microglia and iPS-microglia 2.0 when compared to $CD16^+$ monocytes. Direct comparisons of the fold change expression level (TPM) of every gene are shown in comparative fold change plots which demonstrate the striking similarity of differential expression when iPS-microglia and iPS-microglia 2.0 are each compared to $CD16^+$ monocytes. **b** The same is true for comparisons of iPS-microglia and iPS-microglia 2.0 with $CD14^+$ monocytes (purple).

Functional validation of iPS-microglia 2.0

To determine whether the functional activity of iPS-microglia 2.0 is indeed equivalent to microglia generated using our prior approach, we next compared phagocytic activity of cells generated using both methods (Abud et al., 2017). Since the ability of microglia to clear pathogens and extracellular aggregates via phagocytosis is an important aspect of microglial function, we exposed microglia to several different substrates and measured the percentage of cells which phagocytose each substrate using an Amnis Imagestreamer which combines flow cytometry and high throughput immunofluorescence (Figure 4). As expected, the levels of phagocytosis differed between the three varying substrates with beta-amyloid fibrils producing the highest response. *S. aureus* bioparticles, a TLR 1,2,6 agonist produced an intermediate degree of phagocytosis and Zymosan, a TLR 2/Dectin 1 agonist from *S. cerevisia* induced the lowest level of phagocytosis (Figure 4). Importantly, regardless of the differential response to these three phagocytic substrates, iPS-microglia and iPS-microglia 2.0 exhibited identical rates of phagocytosis for each of the substrates, demonstrating that this simplified differentiation method does not alter this important microglial function (Figure 4).

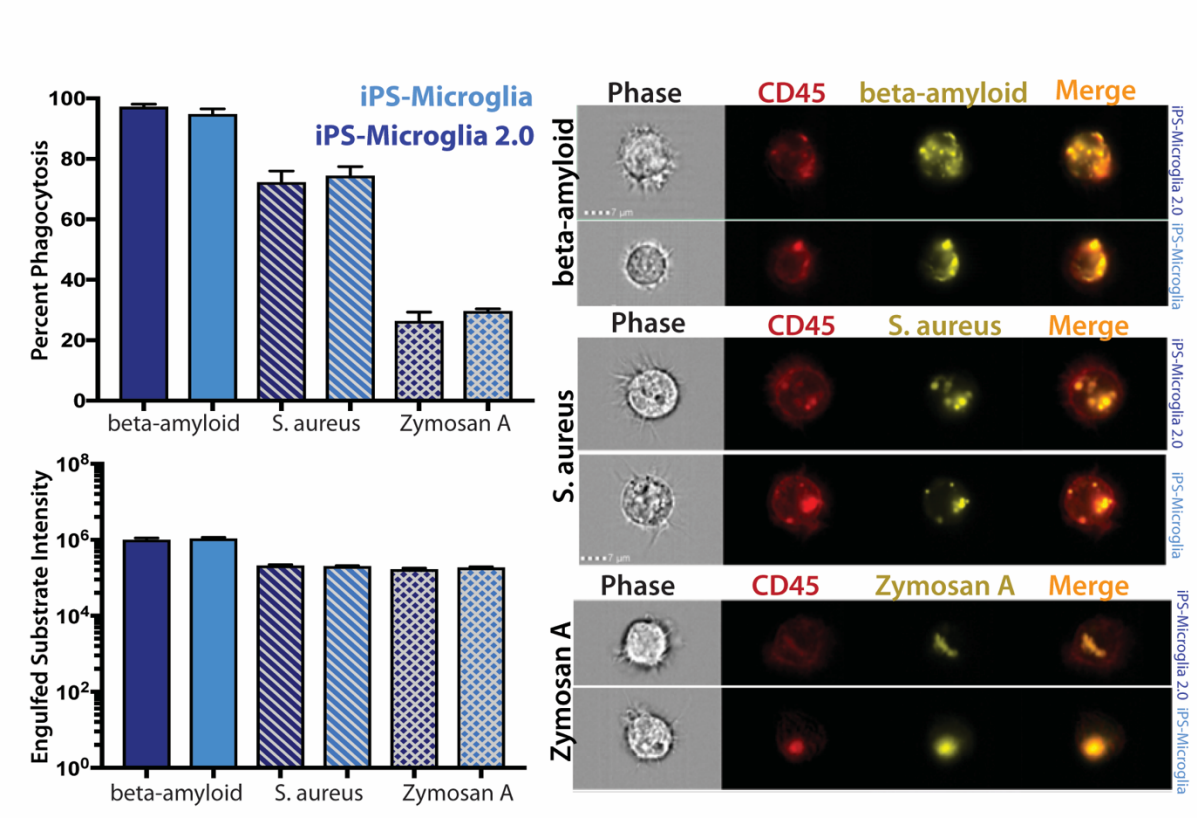

Figure 1.4 iPS-microglia 2.0 exhibit equivalent substrate-dependent phagocytosis. iPS-microglia and iPS-microglia 2.0 were exposed to fluorescent beta-amyloid fibrils, pHrodo tagged *S. aureus*, or pHrodo tagged Zymosan A bioparticles from *S. cerevisiae*. Quantification of the percent of total cells with positive fluorescent signal and the mean fluorescence intensity of that signal is shown on the left. No significance differences were found between each differentiation type, demonstrating the equivalent functional activity of microglia generated by these two differentiation paradigms. Representative images of phase, CD45 staining, and the fluorescent signal of beta-amyloid (top), *S. aureus* (middle), and Zymosan A (bottom) are shown on the right. One representative image of 10,000 quantified images is shown for iPS-microglia 2.0 (top of each set) and iPS-microglia (bottom of each set).

iPS microglia 2.0 engraft well into xenotransplantation-compatible MITRG mice

We previously demonstrated that iPS-microglia can engraft and ramify, fulfilling characteristic microglia morphology and marker expression in the brains of xenotransplantation-compatible MITRG mice(Abud et al., 2017). Thus, we aimed to further validate the identity of our iPS-microglia 2.0 through intracranial transplantation of

iPS-microglia 2.0 into MITRG mice (Knock-out: Rag2; Il2rg; Knock-in: M-CSF^{h}; IL-3/GM-CSF^{h}; TPO^{h}), and to compare this engraftment to equivalently transplanted iPS-microglia that were generated using our previously described differentiation method. In each case, fully mature microglia were transplanted into the hippocampus and overlaying cortex of adult mice which were sacrificed after 2 months for histological examination of morphology and key marker expression. Both iPS-microglia and iPS-microglia 2.0 can be identified within the mouse brain via expression of the human-specific nuclear marker, Ku80 (Figure 5, green). Importantly, regardless of the differentiation method, transplanted human microglia display typical microglial morphology, extending complex branching processes. Both iPS-microglia and iPS-microglia 2.0 also express the microglial/monocyte marker Iba1 (Figure 5, Overlay images C, G, K, & O, red) and the homeostatic microglial marker P2RY12 (Figure 5 Overlay images, D, H, L, & P, red) in both cortex and hippocampus, indicating that these cells engraft well and remain homeostatic. Transplanted iPS-microglia 2.0 also exhibit the tiling and distinct niches typical of *in vivo* microglia, and can be seen interspersed with the endogenous population of mouse microglia (Figure 5, arrows indicate Iba1^{+}/Ku80^{-} mouse cells). Taken together, these findings further demonstrate that iPS-microglia 2.0 are equivalent to microglia generated using our previously published protocol and can be readily transplanted into MITRG mice to enable *in vivo* studies of human microglia.

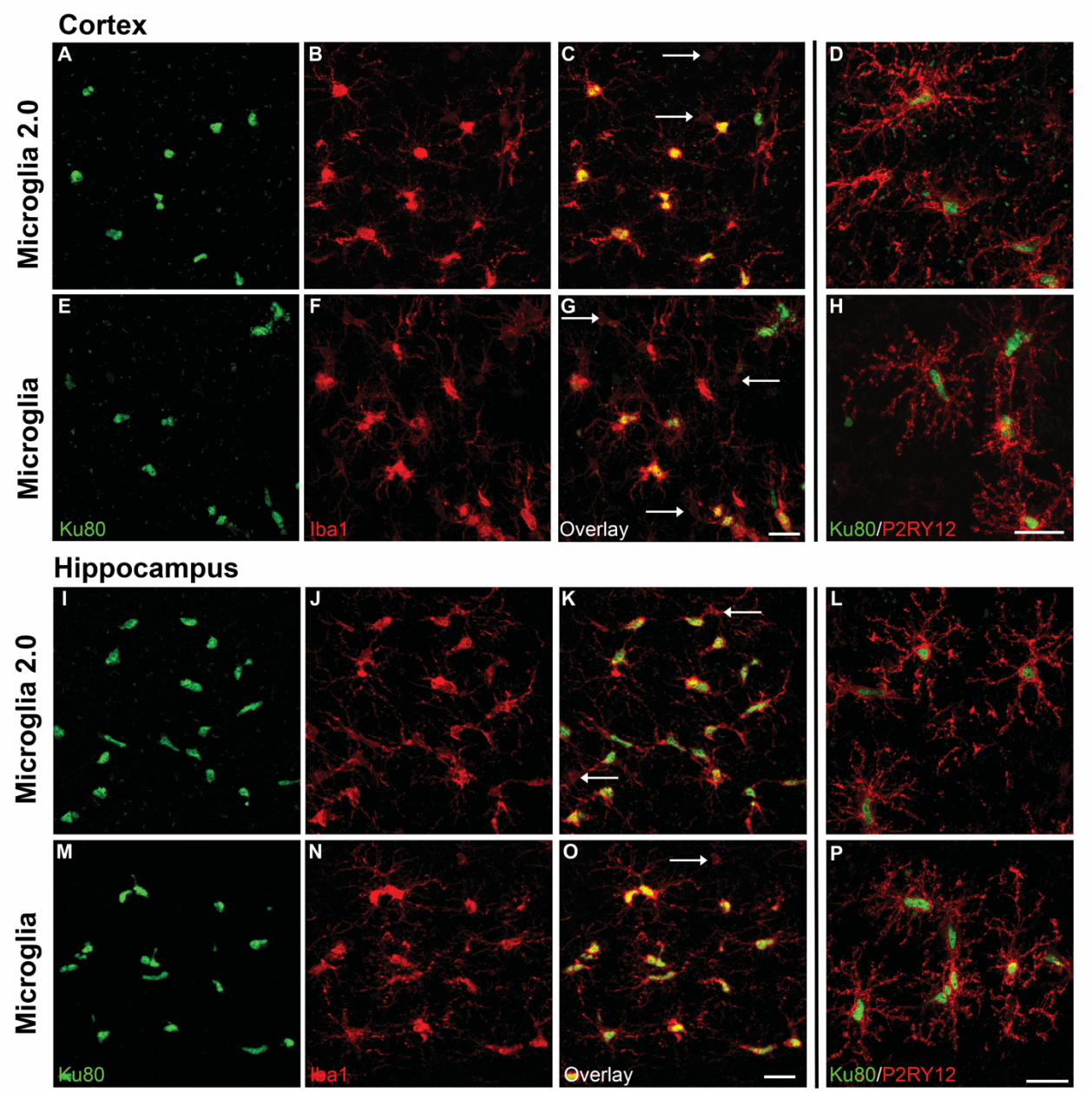

Figure 1.5 Transplanted iPS-microglia 2.0 display typical microglial markers and morphology comparable to our previously described iPS-microglia. Adult 2 month old MITRG mice were transplanted with (**a-d** & **i-j**, top rows) iPS-microglia 2.0 or (**e-h** & **m-p**, bottom rows) iPS-microglia. Brains were harvested 2 months post-transplant. Representative images of cortical (**a-h**) and hippocampal (**i-p**) transplanted cells demonstrate complex process ramification and typical tiling. Transplanted iPS-microglia and iPS-microglia 2.0 both express Iba-1 (Overlay images **c**, **g**, **k**, & **o**, red) and the microglia specific marker, P2RY12 (Overlay images **d**, **h**, **l**, & **p**, red) and demonstrate human nuclear staining (Ku80, green). Additionally, transplanted human microglia can be seen integrating and tiling with the endogenous mouse microglia population (Arrows indicate Iba1+/Ku80- cells).

Small molecule activation of TGFβ signaling produces microglia-like cells that are similar, but transcriptionally distinct from iPS-microglia 2.0

TGFβ1 is a crucial astrocyte-derived cytokine that promotes microglial homeostasis (Abutbul et al., 2012; Butovsky et al., 2014). TGFβ1 signaling results in phosphorylation of smad2/3 and ultimately up-regulates expression of CX3CR1, an important receptor for microglial function and survival (Chen et al., 2002; Elmore et al., 2014). Indeed, removal of either TGFβ1 or CX3CR1 greatly decreases microglia populations in murine models(Butovsky et al., 2014; Elmore et al., 2014). As we have previously shown, removal of TGFβ1 from iPS-microglia for even 24 hours also results in dramatic changes in the microglial transcriptome, including down-regulation of homeostatic signatures (Abud et al., 2017).

In order to increase cost-efficiency during iPS-microglia 2.0 differentiation, we attempted to replace recombinant TGFβ1 with Inducer of Definitive Endoderm 1 or 2 (IDE1, IDE2). As its name suggests, IDE has been used to differentiate iPS cells into definitive endoderm through activation of TGFβ signaling(Borowiak et al., 2009). More specifically, IDE1/2 have been shown to induce phosphorylation of the downstream TGFβ signaling molecule smad2(Borowiak et al., 2009). This led us to hypothesize that IDE1 or IDE2 could induce expression of microglial genes in an equivalent fashion to recombinant TGFβ if added after mesoderm formation and hematopoiesis.

To determine whether IDE1 or IDE2 could replace recombinant TGFβ in our differentiation protocol, HPCs harvested on day 10 were placed into microglia differentiation media and varying concentrations of IDE1 or IDE2 (1 μM, 10 μM, 100 μM, 1000 μM) were added in place of TGFβ (Figure 6A). During the first 4 days of microglia differentiation we used an Incucyte live imaging system to examine the growth kinetics of each group to provide an initial assessment of the effects of varying IDE concentrations. Surprisingly, this analysis demonstrated that IDE2, regardless of concentration, impaired normal microglial proliferation and thus was not studied further. In contrast, IDE1 was able to mimic the typical growth kinetics observed in control cells differentiated in parallel and maintained in normal TGFβ-containing medium. Because the control TGFβ microglial growth curve fell between the 10 μM and 1 μM IDE1 curves, we next adjusted the IDE1 concentrations to include a 5 μM dose. In addition, two higher concentrations of IDE1 (50 μM, and 500 μM) were also included as the growth kinetic measurements suggested that these concentrations might further increase the yield of microglia.

All groups were differentiated in parallel for the complete 38 day paradigm before RNA-sequencing was performed. To compare these new samples with our iPS-microglia, fetal and adult microglia, and other cell types, we generated a correlation matrix (Figure 6B) which demonstrated that IDE1 iPS-microglia remain distinct from monocytes and dendritic cells and cluster closely with our other iPS-microglia. IDE-treated cells also exhibited strong expression of key microglial genes including CSF1R, P2YR12, TREM2, OLFML3, HEXB, and C1Q (Supplementary Table 4). Based on the hierarchical clustering within our correlation matrix (Figure 6B), we find that microglia differentiated in IDE1 have

transcriptomic profiles that are more similar to primary cultured microglia (fetal and adult microglia). One possible explanation for this finding is that IDE1 may have greater stability within the culture media than TGFβ1 and thus provide a more uniform and consistent activation of TGFβ signaling pathways. Alternatively, IDE1 could potentially provide increased specificity by only targeting smad2 signaling. To further understand the comparative effects of IDE1 versus TGFβ1 we further compared these groups of iPS-microglia using DEseq2 to highlight any differentially expressed genes (Supplementary Table 4). Interestingly, gene ontology analysis of these differentially expressed genes revealed only five pathways that were significantly enriched between these two populations of microglia (Figure 6C), again showing their strong similarity. Taken together these data suggest that IDE1 can indeed be used in place of TGFβ1, although researchers should also consider these differentially altered pathways and genes in there decision whether or not to use this further modified approach.

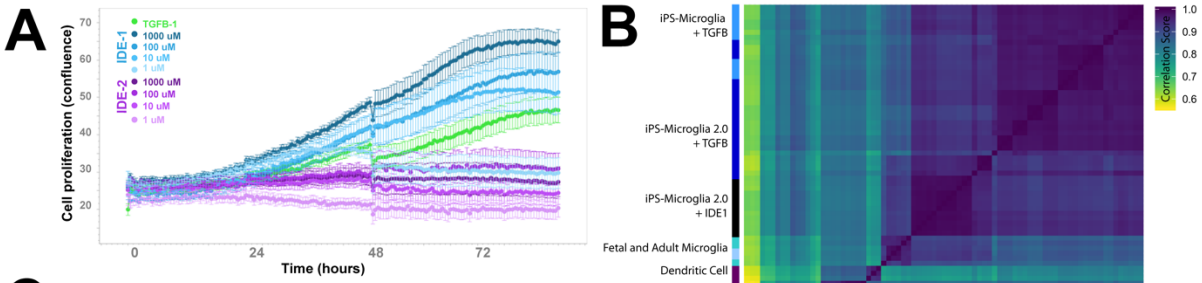

C

FDR	Reactome Gene Ontology	Enriched In
0.0000413	Extracellular matrix organization_Homo sapiens_R-HSA-1474244	IDE samples
0.001008	O-linked glycosylation_Homo sapiens_R-HSA-5173105	IDE samples
0.007454	Chemokine receptors bind chemokines_Homo sapiens_R-HSa-380108	IDE samples
0.02760	Class A/1 (Rhodopsin-like receptors)_Homo spaiens_R-HSA-373076	TGFB samples
0.01863	GPCR ligand binding_Homo sapiens_R-HSA-500792	TGFB samples

Figure 1.6. The small molecule compound IDE1 can be used in place of TGFβ-1 to produce iPS-microglia. IDE1 and IDE2 were added to microglia cultures in place of TGFβ-1 at the indicated concentrations. **a** Growth curves from the first 3.5 days of microglial differentiation show that IDE2 is insufficient to allow proliferation of these cells. In contrast, IDE1 (blue) at lower concentrations shows similar growth kinetics to TGFβ control cells (green). **b** Correlation matrix displaying all samples analyzed in this manuscript shows cells differentiated with IDE1 cluster closely with iPS-microglia 2.0 and

are actually more similar to fetal and adult microglia than TGFβ control microglia. **c** Gene ontology analysis using the Reactome database displays differences between IDE1 treated cells and TGFβ (FDR < 0.001, FC > 2). Enrichment in IDE samples reflects an increased expression of genes within this GO family in IDE1 treated cells.

Discussion

In recent years, the importance of microglia in brain development, homeostasis, and disease has become increasingly clear. Because microglia have been implicated in many neurological diseases and injuries including neurodegeneration, traumatic brain injury, and developmental disorders, several groups have developed methods to try to make these cells more accessible for neurological research. Until recently, microglia could only be studied through brain biopsies, postmortem analysis, or in animal models. Although mouse models of neuroinflammation have been extremely useful in uncovering important new findings, many differences exist between human and murine microglia. For example, one recent study identified several co-regulated myeloid gene expression modules that occur in human AD, but do not occur in AD mouse models(Friedman et al., 2018). Likewise, many differences exist between the murine and human complement system that is closely linked to neurodegenerative diseases including AD(Ueda et al., 2016). At least two microglial-expressed AD risk genes, CR1 and MS4A4A, have no murine ortholog, further highlighting the challenges of studying the role of microglia in human disease with mouse models alone.

To study human microglia, some highly skilled groups have turned to human biopsy material. Working closely with neurosurgeons, these researchers have developed methods to isolate human microglia from brain tissue removed during a surgical resection

of a brain tumor or intractable epileptic foci(Bennett et al., 2016; Durafourt et al., 2012; Gosselin et al., 2017). Using this approach, researchers have uncovered exciting data and greatly advanced our understanding of the human microglial transcriptome. However, epileptic foci and tumor tissue induce neuroinflammation and despite best efforts to avoid isolating microglia from 'diseased-effected tissue' it is likely that microglia isolated from these patients exhibit considerable variation and alterations in activation state(Garofalo et al., 2017; Kan et al., 2012).

Another strategy for studying human microglia involves the isolation of microglia or their nuclei from postmortem brain tissue. Using this approach, researchers have uncovered important age-related differences in the human microglial transcriptome(Olah et al., 2018). Still, it remains unclear whether the agonal state that precedes death, inflammatory co-morbidities, or post-mortem delay might influence microglial gene expression. In the case of Alzheimer's disease, most patients die from an accompanying infectious disease such as Pneumonia(Burns et al., 1990; Kukull et al., 1994). Interestingly, animal models of Pneumonia exhibit significant changes in brain microglial activation state(Ji et al., 2016; Wang et al., 2018). Thus, it is likely that this and other common infectious co-morbidities can complicate the interpretation and analysis of postmortem-isolated human microglia.

Given the considerable challenges with isolation and study of postmortem or biopsied human microglia, several groups, including our own, developed protocols which utilize the power of stem cells to produce human microglia *in vitro*(Abud et al., 2017; Douvaras et al., 2017; Haenseler et al., 2017; Muffat et al., 2016; Pandya et al., 2017; Takata et al.,

2017). These methods have begun to enable more detailed mechanistic studies of human microglia by allowing controlled experimental treatments, drug testing, and genetic manipulation. However, the currently existing protocols are relatively complicated and can be challenging to adopt, especially for groups with little prior stem cell experience. Thus, to address this challenge we developed and validated the greatly simplified and refined method presented here. In comparing this new method to our previously published differentiation protocol, we confirm that iPS-microglia 2.0 show highly similar RNA transcript profiles to iPS-microglia as well as primary fetal and adult primary microglia. In addition, iPS-microglia 2.0 remain distinct from blood monocytes and importantly display largely the same differentially expressed genes between microglia and monocytes as our previously published iPS-microglia.

To further investigate and characterize iPS-microglia 2.0 we functionally validated these cells by examining phagocytosis of three different substrates; Staphylococcus Aureus, Zymosan A, and fibrillar beta-amyloid. While each substrate exhibited differential degrees of phagocytosis, these levels were equivalent between our previously described iPS-microglia and iPS-microglia 2.0. Lastly, to determine whether iPS-microglia 2.0 can also be used for in vivo studies, we transplanted microglia derived via both methods into xenotransplantation-compatible MITRG mice, confirming that engraftment, *in vivo* morphology, and marker expression was equivalent between iPS-microglia and iPS-microglia 2.0. Taken together, these functional and in vivo experiments further support the conclusion that microglia generated via these two methods are virtually identical.

In addition, we tested IDE1 as a small molecule agonist of TGFβ signaling cascades. To this end, we confirmed that TGFβ1 substitution with IDE1 produced cells that are similar to iPS-microglia 2.0, and additionally highly similar to adult and fetal primary microglia. We have provided differential gene expression analysis to highlight the important differences between IDE- and TGFβ1-treated iPS-microglia 2.0, which researchers should consider when deciding whether to use TGFβ or cost-saving IDE1 for iPS-microglia generation.

In summary, we provide detailed methods and validation of a greatly simplified protocol to produce significantly increased numbers of pure human microglia. The RNA-sequencing, functional validation, and transplantation studies presented here clearly demonstrate that highly pure populations of human iPS-microglia can be generated via this greatly simplified protocol. We anticipate that this streamlined and highly reproducible protocol will enable many more interested researchers to now study human microglia, leading to further breakthroughs in this field.

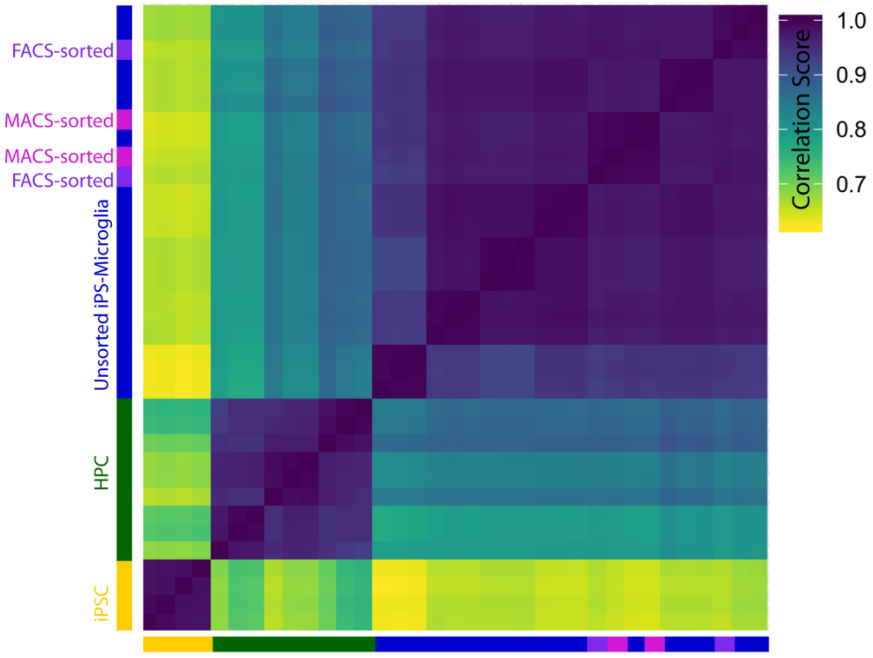

Figure S1.1. FACS and MACS sorted HPCs differentiate into equivalent microglia as unsorted HPCs. Hierarchical clustering of all iPS-microglia 2.0 samples show that MACS (fuchsia) and FACS (purple) sorting at the HPC stage has no effect on the final differentiated microglia as these samples intercluster with iPS-microglia 2.0 produced from floating unsorted HPCs (blue).

	CD43+	CD43+ CD41+	CD43+ CD41+ CD235a+
iPS-HPC	90.95 ± 2.8	77.9 ± 9.6	10.5 ± 13.2
iPS-HPC 2.0	93.76 ± 2.3	61.3 ± 15.1	2.44 ± 2.8

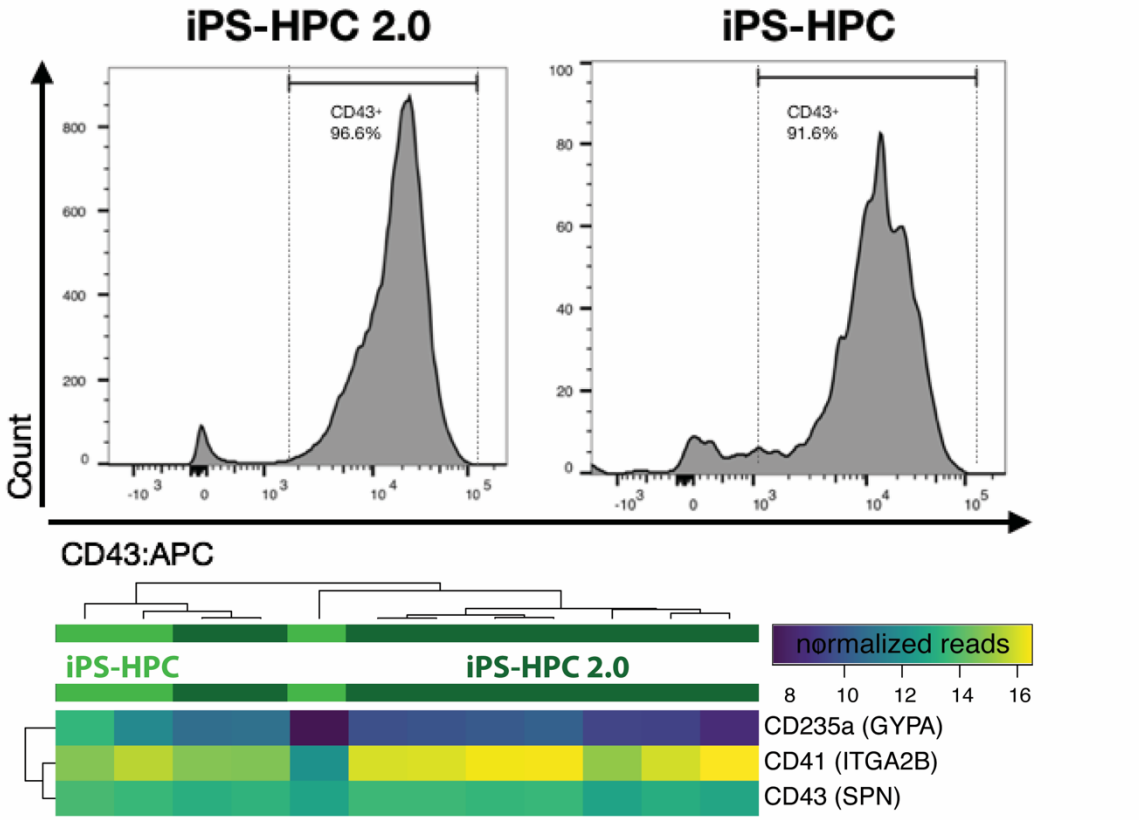

Figure S1.2. **Both HPC and HPC 2.0 methods produce cells with consistently high expression of the primitive HPC marker CD43.** (Top) Quantification of flow cytometry analysis from four independent iPSC lines per method ($n = 3$ wells/line) reveal a similarly high proportion of cells (> 90%) that express the primitive HPC marker CD43 following differentiation with either our previous or currently described approach. In contrast, two other primitive HPC markers, CD41 and CD235a, exhibit relatively low and heterogeneous expression within this CD43+ population (Middle). Representative FACS plots demonstrating typical CD43+ histograms (pre gated for live, single cells). Gates were drawn based on FMO (fluorescence minus one) controls. (Bottom) Heatmap from RNA sequencing of iPS-HPC samples shows similar gene expression levels for CD43, CD41, and CD235a.

CHAPTER 2

Gene expression and functional deficits underlie TREM2-knockout microglia responses in human models of Alzheimer's disease

Amanda McQuade, You Jung Kang, Jonathan Hasselmann, Amit Jairaman, Alexandra Sotelo, Morgan Coburn, Sepideh Kiani Shabestari, Jean Paul Chadarevian, Gianna Fote, Christina H. Tu, Emma Danhash, Jorge Silva, Eric Martinez, Carl Cotman, G. Aleph Prieto, Leslie M. Thompson, Joan S. Steffan, Ian Smith, Hayk Davtyan, Michael Cahalan, Hansang Cho, Mathew Blurton-Jones

Introduction

Microglia and neuroinflammation are strongly implicated in the genetics and neuropathology of late-onset Alzheimer's Disease (AD) (Jansen et al., 2019; Lambert et al., 2013). As the primary immune cell of the brain, microglia perform key macrophage-functions such as phagocytosis of dead cell debris and protein aggregates, cytokine/chemokine signaling, and immune surveillance and response (Reviewed in (McQuade and Blurton-Jones, 2019)). Yet, microglia also exhibit important neuroprotective functions that include providing trophic support for neurons, promoting oligodendrocyte differentiation, and modulating synaptic pruning and plasticity(McQuade and Blurton-Jones, 2019). With the recent identification of several AD-risk loci near immune genes, combined with the development of pluripotent stem cell-derived microglia and chimeric mouse models, it is increasingly possible to examine the mechanisms that underlie the influence of human microglia on AD-risk.

Among these microglial-specific AD risk loci, variants in triggering receptor expressed on myeloid cells 2 (TREM2) confer the largest effect on disease risk, causing a similar increase in risk as one APOE ε4 allele (Jonsson et al., 2013; Shi and Holtzman, 2018). Within the central nervous system, TREM2 is predominantly expressed by microglia, raising fundamental questions about its role in driving microglia-specific functions associated with neurodegenerative diseases. TREM2 is part of the immunoglobulin superfamily and acts on the plasma membrane as a key member of the microglia sensome, mediating responses to phospholipids, APOE, and several other potential stimuli(Daws et al., 2003; N'Diaye et al., 2009; Wang et al., 2015; Zhao et al., 2018). To transduce intracellular responses, TREM2 requires an adaptor protein, Tyro

Protein Kinase Binding Protein (TYROBP/DAP12), which activates downstream signaling cascades including SYK, ERK, PLCG2, and NFAT.

Although complete loss-of-function mutations in TREM2 are most strongly linked to Nasu-Hakola disease and frontotemporal dementia, AD-associated TREM2 mutations such as R47H and R62H occur within the ligand binding domain and are thought to confer a partial loss of function(Bouchon et al., 2001; Cheng et al., 2018; Parhizkar et al., 2019; Zheng et al., 2016). Some reports suggest that two loss-of-function TREM2 mutations, Q33X and W191X, may also influence AD risk(Borroni et al., 2014; Song et al., 2017), although this association remains unclear(Cuyvers et al., 2014; Jin et al., 2015). Nevertheless, studies of TREM2 deletion have greatly enriched our overall understanding of the normal function of TREM2 and have revealed important differences between murine and human cells in late versus early disease time-points(Bemiller et al., 2017; Cheng-Hathaway et al., 2018; Xiang et al., 2018).

For example, variable results have been reported regarding the impact of TREM2 deletion on tau pathology and neurodegeneration (Bemiller et al., 2017; Kang et al., 2018; Leyns et al., 2017). While the response of TREM2 knockout microglia to beta-amyloid is more consistent, in that murine microglia reliably show decreased clustering around plaques, the signals that underlie differential response remain unknown (reviewed in Hammond et al., 2018(Hammond et al., 2018)). Murine TREM2 has been shown to influence the accumulation of beta-amyloid in transgenic mice, although the magnitude and direction of this effect is variable and appears to be highly dependent on the stage of disease(Bemiller et al., 2017; Cheng-Hathaway et al., 2018; Leyns et al., 2017; Ulrich et al., 2014). TREM2 has also been shown to influence microglial survival, although whether

this function plays a role in human AD remains unknown(Cheng et al., 2018; Zhong et al., 2017). To further understand these phenotypes and their impact on human disease, studies that examine the function of TREM2 in human microglia are critically needed.

In this study, we generated three isogenic TREM2 knockout induced pluripotent stem cell (iPSC) lines, differentiated these cells into microglia, and examined the transcriptional and functional effects of TREM2 deletion in human microglia. We have uncovered increased susceptibility to M-CSF-dependent survival in TREM2 KO microglia, decreased levels of phagocytosis of disease-relevant substrates, interactions between TREM2 and an allelic series of APOE, and CXCR4-dependent migration deficits. To further understand the impact of TREM2 deletion on human microglial function *in vivo*, we have combined this isogenic approach with a chimeric mouse model of AD(Hasselmann et al., 2019), performing single cell sequencing, flow cytometry, and neuropathological analysis to examine the interactions between microglia and beta-amyloid pathology *in vivo*, leading to a further understanding of the effect of TREM2 on human disease-associated microglia (DAM). Taken together, these studies provide insight into the normal and disease-associated functions of TREM2 in human microglia.

Materials and Methods

Animals. All animal procedures were conducted in accordance with the guidelines set forth by the National Institutes of Health and the University of California, Irvine Institutional Animal Care and Use Committee who approved the study protocol. The MITRG mouse was purchased from Jackson Laboratories (stock #017711); this BALB/c/129 model includes two knockouts alleles, Rag2- (Rag2tm1.1Flv), γc- (Il2rgtm1.1Flv), and three

humanized knock-in alleles, M-CSFh (Csf1tm1(CSF1)Flv), IL-3/GM-CSFh (Csf2/Il3tm1.1(CSF2,IL3)Flv), TPOh (Thpotm1.1(TPO)Flv). The related and parental M-CSFh mouse line was also purchased form Jackson Laboratories (stock # 017708) and contains Rag2 and Il2rg deletions and humanized M-CSFh. The 5xFAD-MITRG model was created by backcrossing the MITRG mouse with 5xFAD mice which overexpress co-integrated transgenes for Familial Alzheimer's Disease (FAD) mutant APP (Swedish, Florida, and London) and mutant FAD PS1 (M146L and L286V). Progeny of these pairings were then genotyped (Primers are provided in Supplementary Table 2) and backcrossed with MITRG mice to return the 5 MITRG genes to homozygosity and maintain the APP/PS1 transgenic loci in the hemizygous state, resulting in the 5xfAD-MITRG model (Rag2-; γc-; M-CSFh; IL-3/GM-CSFh; TPOh; Tg(APPSwFlLon,PSEN1*M146L*L286V)6799Vas). All mice were age and sex matched and group housed on a 12h/12h light/dark cycle with food and water ad libitum. Mice are housed with ambient temperature and humidity.

Generation of iPSC cell lines from human Fibroblasts. Human iPSC cell lines were generated by the University of California, Irvine Alzheimer's Disease Research Center (UCI ADRC) Induced Pluripotent Stem Cell Core from subject fibroblasts under approved Institutional Review Boards (IRB) and human Stem Cell Research Oversight (hSCRO) committee protocols. Informed consent was received by each of the participants who donated fibroblasts. Non-integrating Sendai virus was used to perform reprogramming thereby avoiding any integration-induced effects (Cytotune 2.0). iPSCs were confirmed to be karyotype normal by G-banding, sterile, and pluripotent via Pluritest Array Analysis

and trilineage *in vitro* differentiation. The Pluritest is a microarray-based assessment of pluripotency based on iPS whole transcriptome analysis referenced to a library of functionally validated iPSCs (https://www.pluritest.org/). Additional GFP- and RFP-αtubulin expressing iPSC lines (AICS-0036 and AICS-0031-035) were purchased from Corriel and originally generated by Dr. Bruce Conklin. To avoid the potential selection of latent or hidden infections all iPSC culturing and microglia differentiation and experimentation is performed without the use of antibiotics. In addition, all lines are routinely tested for sterility including mycoplasma testing. iPSCs were maintained feeder-free on matrigel in complete TeSR-E8 medium (Stemcell Technologies) in a humidified incubator (5% CO2, 37°C). All lines will be available upon request to corresponding author.

Differentiation of iPS-microglia from iPSCs (McQuade et al., 2018)**.** iPS-microglia were differentiated as detailed in McQuade et al. 2018. Briefly, iPSCs are differentiated to hematopoetic progenitor cells using the STEMdiff Hematopoetic kit for 10-12 days before passage into microglia differentiation medium(Abud et al., 2017; McQuade et al., 2018) including DMEM/F12, 2X insulin-transferrin-selenite, 2X B27, 0.5X N2, 1X glutamax, 1X non-essential amino acids, 400 µM monothioglycerol, and 5 µg/mL human insulin. Cultures were maintained in this basal medium supplemented with 100 ng/mL IL-34, 50 ng/mL TGF-β1, and 25 ng/mL M-CSF (Peprotech) for 28 days. For the last three days in culture, two additional cytokines were added (100 ng/mL CD200 (Novoprotein) and 100 ng/mL CX3CL1 (Peprotech)) to mature the microglia in a homeostatic brain-like environment(Abud et al., 2017).

CRISPR-mediated knockout of Trem2 in iPSCs. This manuscript uses four independent isogenic sets of TREM2 knockout iPSCs. These lines were each made on different patient iPSC backgrounds (two male, one female; all lines APOE3/3). 2 x 10^5 induced pluripotent stem cells were isolated following Accutase enzymatic digestion for 3 min at 37 ^{o}C. Cells were resuspended in 60 µL nucleofection buffer from Human Stem Cell Nucleofector™ Kit 2 (Lonza). The suspension was combined with 50 µg of RNP complex formed by incubating Alt-R® S.p. HiFi Cas9 Nuclease V3 (IDTDNA) with fused crRNA:tracrRNA (IDTDNA) duplex for 15 min at 23 ^{o}C. The suspension was transferred to the Amaxa Nucleofector cuvette and transfected using program B-016. Cells were plated in TeSR™-E8™ (STEMCELL Technologies) media with 0.25 µM Thiazovivin (STEMCELL Technologies) overnight to recover. Cells were digested the following day with Accutase and single-cell plated to 96-well plates in TeSR™-E8™ media with 0.25 µM Thiazovivin and CloneR™ (STEMCELL Technologies) supplement for clonal isolation and expansion. Genomic DNA was extracted using Extracta DNA prep for PCR (Quantabio) from a sample of each clone upon passage and amplified for sequencing using Taq PCR Master Mix (ThermoFisher Scientific) at the cut site (Primers are provided in Supplementary Table 2). PCR product from promising clones was transformed using TOPO™ TA Cloning™ Kit for Subcloning, with One Shot™ TOP10 (ThermoFisher Scientific) for allele-specific sequencing. The top three off-target sites as identified by IDTDNA were amplified and sequenced per clone of interest to confirm absence of off-targeting before banking for future experiments.

Immunoblotting. SDS/PAGE Western blot was performed according to previously established protocols (S. Marsh et al. PNAS 2016). Two human anti-TREM2 antibodies were used to confirm knockdown and knockout (R&D AF1828, Sigma HPA012571). Anti-P-SYK was probed with Cell signaling 2710 (1:1,000); anti-SYK was probed with Cell Signaling 13198 (1:2,000). Following initial labeling, blots were stripped in 0.2 N NaOH for 15 min. anti-GAPDH (47724 Santa Cruz 1:5,000) was probed to control for protein loading. Blots were visualized with Goat Anti-Mouse (Millipore, AP308P; 1:10,000) or -Rabbit (Millipore, 12-348; 1:10,000) HRP conjugate and on a Bio-Rad ChemiDoc Gel Imaging System. Images were quantified in ImageJ (version 2.0.0) and statistical analyses were carried out in GraphPad Prism 7.

Homogenous time-resolved fluorescence (HTRF). Cisbio human TREM2 HTRF kit was used as per manufacturer's instructions. 100,000 iPS-microglia were plated in a 96-well format overnight in 200 uL microglia maintenance medium. Conditioned medium was collected and cells were lysed in Lysis Buffer 3. After antibody addition, plates were incubated overnight at room temperature and read on CLARIOstar imager (BMG Labtech).

RNA isolation and sequencing preparation. Total RNA was isolated using RNeasy Mini kit (Qiagen). One million iPS-microglia were lysed in 700 μL RLT buffer and RNA was isolated per manufacturer's instructions with DNAse treatment (10 minutes, RT). Centrifugation times were increased to 16000 x G for 1.5 min to maximize yield. RNA integrity was measured using the Bioanalyzer Agilent 2100. All libraries were prepared

from samples with RNA integrity values ≥ 9.5. 500 ng RNA per sample was used to create RNA-seq libraries through the Illumina TruSeq mRNA stranded protocol. Samples were sequenced on the NovoSeq S4 chip (WT vs KO Fig. 1C and neuron treatment Supplemental Fig. 1) or Illumina HiSeq 4000 platform (antibody treatment Fig. 1J).

Cell death assay. iPS-microglia were plated at 30 % confluence into a 96-well plate (4 wells per line per condition). At time 0, all microglia were treated with IncuCyte Caspase-3/7 Green Apoptosis Assay Reagent 1:1000. Cells were maintained in the described medium: fresh complete medium, fresh basal medium + 100 ng/μL IL-34 + 25 ng/μL M-CSF, fresh basal medium + 50 ng/μL TGF-B1, or basal medium with no cytokines for 3 days. Four 20X images per well were collected every hour. Using IncuCyte 2018B software, image masks for phase confluence (visually gated out apoptotic cells) as well as caspase 3/7 signal (green) were generated. Graphs display caspase normalized to phase confluence. Completed with 2 lines.

Collection and pHrodo labeling of human AD synaptosomes. Human brain tissue samples were obtained from the UCI ADRC from patients who have given informed consent. These samples were from deceased AD patients upon autopsy (PMI< 3 hours) and slowly frozen and stored in isotonic 0.32 M sucrose, 10 mM HEPES, pH 7.4 at -80°C. Synaptosome preparation was adapted from *Prieto et al. (*J Neuroscience, 2017*)* Samples were thawed at 37°C and homogenized using a pre-cooled glass/Teflon homogenizer (clearance 0.1-0.15 mm) with addition of protease inhibitors, phosphatase inhibitors (Thermo Scientific), and an antioxidant cocktail (Sigma- Aldrich; #A1345). Brain

homogenate was centrifuged at 1200 x *g* for 10 minutes at 4°C and the resulting supernatant fraction (S1) was collected. The S1 fraction was centrifuged at 12,000 x G for 20 min at 4°C and the resulting supernatant (S2) was aspirated. The crude synaptosome pellet (P2) (containing synaptosomes and mitochondria) was labeled for 45 min at RT with amine reactive pHrodo™ Red SE or pHrodo™ Green STP ester (Thermo), a lipophilic, fluorogenic dye that increases in fluorescence as the surrounding environment acidifies. Labeled synaptosomes were washed twice with excess ice-cold 1X HBSS. For each washing step and experimental procedure, synaptosomes were resuspended by gently pipetting up and down using Finntip pipette tips (Thermo) to minimize shear force stress and preserve synaptosome integrity.

Fluorescent APOE collection and validation. Hek293T cells were cultured at 37 °C, 5% CO_2 in DMEM supplemented with 10% (vol/vol) FBS. Cells were plated at 250,000 cells/mL and transfected 24 hours later with Lipofectamine 2000 and 1 µg of DNA for APOE2, 3, or 4 tagged with mCherry-SepHluorin. Media was changed 24 hours after transfection, washed once with PBS, and incubated for 48 hours in microglial basal medium. Media was collected and centrifuged at 750 x G for 5 minutes and transferred to a new tube to eliminate dead cell debris.

To assess APOE concentration across isoforms, 20 µL of media was analyzed by SDS/PAGE on a NuPage Novex 4-12% Bis-Tris precast gel with MOPS running buffer (Invitrogen) and transferred onto an Immobilon-FL PVDF (LI-COR) membrane. Whole protein was quantified using the revert assay, and the membrane was blocked with Intercept (TBS) Blocking Buffer (LI-COR) for 1 hour. The membrane was then incubated

in primary antibody overnight, washed three times with TBS-0.1% Tween-20, and incubated for 1 hour in Intercept block supplemented with 0.1% Tween-20 and near-infrared conjugated secondary antibody. Membranes were imaged on a LI-COR scanner and quantified using Empiria Software.

To assess the lipidation state of APOE in the media, 20 µL of conditioned media from APOE transfected Hek293T cells or 2 µL of HA-tagged APOE protein purified from bacteria (construct cloned in-house) was added to 6.25 µL NativePAGE 4X Sample Buffer (Invitrogen BN2008) and run on a NativePAGE mini gel (Invitrogen BN2112BX10). NativePAGE Running Buffer (Invitrogen BN20001) was used to make light and dark cathode buffer and anode buffer. Gel was transferred onto an Immobilon-P PVDF membrane (Millipore IPVH00010). The membrane was blocked with Pierce StartingBlock Buffer (Fisher Scientific EN37543) for 30 minutes and incubated overnight with primary antibody (803301, Biolegend, 1:1000), washed three times with TBS-0.1% Tween-20, and incubated for 1 hour in StartingBlock Buffer with HRP-conjugated secondary antibody (115-035-146 Jackson Immunoresearch, 1:10,000). HRP was detected using SuperSignal West Dura Chemiluminescent reagents (Fisher Scientific PI34076) and imaged using an Azure c600 system.

Phagocytosis assay. Phagocytic activity of isogenic iPS-microglia was examined using the IncuCyte S3 Live-Cell Analysis System (Sartorius). Microglia were plated at 50% confluence on Matrigel-coated 96-well plates. Four fields of view in each of four wells were captured for each condition. 15 min after plating, 50 µL APOE containing medium, 50 µg/mL pHrodo tagged human AD synaptosomes, 100 ng/mL pHrodo tagged zymosan

A beads, or 2 µg/mL fluorescent beta-amyloid was added to cells. Images of phase and fluorescence were captured in the IncuCyte S3 live cell imager. Using IncuCyte 2019B software, image masks for fluorescent signal (phagocytosis of each substrate) were normalized to cell body area. APOE phagocytosis completed with two lines.

Ratiometric Ca^{2+} imaging using Fluo-4 and Fura-Red. iPSC-derived microglia were plated on fibronectin-coated 35 mm, No. 1.5 thickness glass bottom dishes (1:100, MatTek Corporation). After 24 hours of culture, cells were loaded with 3 µM Fluo-4 AM and 3 µM Fura-Red AM (Molecular Probes) in the presence of Pluronic Acid F-127 (Molecular Probes) for 30 minutes at room temperature (RT). Ca^{2+} dyes were then washed off 3 times using microglial cell culture media and cells were resuspended in Ca^{2+} Ringer's solution for 10 minutes to allow de-esterification of the dyes. Time-lapse images were acquired at RT in a single z-plane at 20 frames/ minute using Olympus Fluoview FV3000i confocal laser scanning microscope equipped with high speed resonance scanner, IX3-ZDC2 Z-drift compensator and a 40x silicone oil objective (NA 1.25). Fluo-4 and Fura-red were both excited using a 488 nm diode laser (0.05 % laser transmissivity, 10 % laser ND filter) and two high-sensitivity cooled GaAsP PMTs set to wavelengths 494-544 nm and 580-680 nm were used for detection in the green and red channels respectively. Images were exported to Image J, background subtracted and single-cell analysis was done by drawing ROIs around each cell in the field. Average intensities in the green and red channels were calculated for each ROI at each time-point. Fluo-4/Fura-Red ratio was then obtained to further generate traces showing single-cell and average changes in cytosolic Ca^{2+} over time. Completed with 2 lines.

Creation and culture of human neural progenitor cells (NPCs). ReN cell VM human neural progenitor cells (hNPCs, EMD Millipore, Billerica, MA, USA) were transfected with commercially available APPSL-GFP Alzheimer's lentiviruses (EMD Millipore) to develop ReN cells producing high levels of Aβ (AD hNPCs) through overexpression of a variant of the human amyloid precursor protein (APP) containing K670N/M671L (Swedish) and V717I (London) FAD mutations (APPSL). As previously published,(Choi et al., 2014) cells were transfected with 50-100 µL vital solution (1 x 10^6 TU/mL) and incubated for 24 hrs. After, cells were washed 3X to stop infection. Expression of infected genes is confirmed by fluorescence. For the control counterpart, ReN cells were transfected with the control GFP construct (LentiBrite™ GFP Control, EMD Millipore) to develop control hNPCs. After 3 days of incubation, the transgene positive cells were enriched by FACS sorting (BD FACS Aria II, BD Biosciences). The either of hNPCs or AD hNPCs was plated onto the culture flask coated with 1% Matrigel (BD Biosciences, San Jose, CA, USA) in DMEM/F12 (Life Technologies, Grand Island, NY, USA) media supplemented with 2 mg heparin (StemCell Technologies, Vancouver, Canada), 2% (v/v) B27 neural supplement (Life Technologies, Grand Island, NY, USA), 20 mg EGF (Sigma-Aldrich, St Louis, MO, USA), 20 mg bFGF (Stemgent, Cambridge, MA, USA), and 1% (v/v) penicillin/streptomycin/amphotericin-B solution (Lonza, Hopkinton, MA, USA) and incubated at 37 °C supplied with 5% CO_2. Cell culture media were changed every 3 days until cells were confluent.

Preparation of 3D human AD models in the microfluidic device. We employed our 3D organotypic microfluidic model mimicking pathological signatures of human AD brains, developed by Park et al.(Park et al., 2018), to compare chemotaxis of iPS-microglia in response to AD cues. Briefly, ReN cells were 3D cultured in the central chamber of microfluidic device at the cell density of 2 x 10^6 cells/mL in the 10% of Matrigel diluted with DMEM/F12 differentiation media supplemented with 2 mg heparin, 2% (v/v) B27 neural supplement, and 1% (v/v) penicillin/streptomycin/amphotericin-B solution without growth factors. The microfluidic devices were incubated at 37 °C supplied with 5% CO_2 and replaced one half volume of the differentiation media every 3.5 days until the cells were fully differentiated into neurons and astrocytes (approximately 2.5 weeks). To develop early AD and late AD models, the cells were further incubated in the device for 0.5 weeks (3-week AD model) and 7.5 weeks (9-week AD model).

Migration study of iPS-microglia in response to beta-amyloid. iPS-microglia (2000 cells/device) were loaded in the angular chamber to test the activation and chemotaxis of microglia to the central chamber containing either $A\beta_{40}$ (100 ng/mL), $A\beta_{42}$ (1 ng/mL), 3-week AD model, 9-week healthy model, or 9-week AD model. To characterize motility, we monitored the number of recruited microglia in the central chamber for 4 days under the fully automated Nikon TiE microscope (10× magnification; Micro Device Instruments, Avon, MA, USA).

Scratch Wound Assay. Motility was observed using Essen Incucyte WoundMaker Assay. 100,000 iPS-microglia were plated per well on fibronectin-coated 96-well plate

(n=3 wells) for 1 hr for cells to become adherent. Scratches were repeated 4X. Cells were imaged at 24 hours post-scratch. Wound confluence (confluence of cells within original wound ROI) was calculated using Incucyte 2019B Software.

Flow cytometry. Microglia were treated with FC block (1:100; BD Biosciences 553142) 5 min in FACS buffer (DPBS, 2% BSA, 50 μM EGTA) before adding live/dead stain (1:100; Biolegend 423113), CD9-APC (1:100; Biolegend 312108) or CXCR4-APC (1:50; Biolegend 306510) for 30 min at 4 C in the dark. Samples were washed 3X in FACS buffer. 100,000 events per sample were collected on BD LSRFortessa with FACSDiva 9.0 and analyzed in FlowJo 10.7.1. Gates were drawn on fluorescence minus one (FMO) controls.

Immunohistochemistry. Half brains were drop fixed in 4% (w/v) PFA for 48h. The brains were cryoprotected in a 30% sucrose. Brains were sectioned coronally into 40 μm-thick slices on a freezing microtome (Leica SM 2010R) and stored in a solution of 0.05% NaN3 in 1X PBS as free-floating slices. For staining, tissue was blocked for 1 h in 1X PBS, 0.2% Triton X-100, and 10% goat serum. Immediately following blocking, brain sections were placed in primary antibodies diluted in 1X PBS and 1% goat serum and incubated overnight on a shaker at 4 °C. Samples were then incubated in conjugated secondary antibodies for 1 hr followed by mounting on microscope slides. Sections were labeled with combinations of Amylo-Glo RTD Amyloid Plaque Stain Reagent (1:100; Biosensis TR-300-AG) (incubation for 20 minutes was needed before the addition of the primary antibodies), anti-GFP (1:500; Millipore Ab16901), anti-TagRFP (1:10,000; Kerafast

EMU113), anti-Ku80 (1:250; Abcam ab79220), mounted with Fluoromount-G (SouthernBiotech). Additional samples were stained in anti-CXCR4 (1:100; MAB172 Clone 44716, R&D Systems), anti-CD9 (1:200; 312102, Biolegend), or anti-HLA-DRB1 (1:200; 14-9956-82, Invitrogen).

Early Postnatal Intracerebroventricular Transplantations. Postnatal day 2-3 5xfAD-MITRG or WT-MITRG mice were placed in a clean cage over a heating pad with a nestlet from the home cage to maintain the mother's scent. Pups were then placed on ice for 2-3 minutes to induce hypothermic anesthesia. Free-hand transplantation was performed using a 30-gauge needle affixed to a 10 µL Hamilton syringe, mice received 1 µL of iHPCs suspended in sterile 1X DPBS at 62.5 total cells/µL at each injection site (see Hasselmann et al. 2019.) Equal numbers of pups received mixed lines of GFP WT and RFP TREM2 KO HPCs (or the opposite combination). HPCs were thawed and plated into complete microglia medium and allowed to recover for 2 days prior to transplantation. Bilateral injections were performed at 2/5th of the distance from the lambda suture to each eye, injecting into the lateral ventricles at 3 mm and into the overlying anterior cortex at 1 mm, and into the posterior cortex in line with the forebrain injection sites, and perpendicular to lambda at a 45° angle. Transplanted pups were then returned to their home cages and weaned at P21. All mice were then sacrificed at 6 months of age as detailed below.

Tissue dissociation for scRNA-seq and flow cytometry. Following perfusion with ice cold 1X DPBS containing 5 µg/ml actinomycin D, half brains were dissected, and the

cerebellum was removed. Tissue was briefly stored on ice in RPMI 1640 containing 5 µg/mL actinomycin D, 10 uM triptolide, and 27.1 ug/mL anisomycin until subsequent perfusions were completed. Tissue dissociation was then performed utilizing the Tumor Dissociation kit, human (Miltenyi) and the gentleMACS Octo Dissociator with Heaters (Miltenyi) according to manufacturer guidelines with modifications. Briefly, tissue was cut into ~1 mm^3 pieces and placed into the C-tubes with the kit's enzymes, 5 µg/mL actinomycin D, 10 µM triptolide, and 27.1 µg/mL anisomycin and samples were dissociated using the preprogrammed protocol. Following enzymatic digestion, samples were strained through a 70 um filter and pelleted by centrifugation. Myelin and debris were removed by resuspending the pellet in 8mL 23% Percoll, overlaid with 2 mL of 1X DPBS, spinning at 400 x G for 25 minutes at 4°C, with acceleration and brake set to 0, and discarding the myelin band and supernatant.

Magnetic Isolation and FACS sorting of WT and TREM2 KO ex vivo microglia. Dissociated cell pellets were resuspended in 160 µL FACS buffer (0.5% BSA in 1X DPBS) + 40 µL Mouse cell removal beads (Miltenyi) and incubated at 4°C for 15 minutes. Magnetically labelled cells were then separated using LS columns and the MidiMACs separator (Miltenyi) while the unlabeled human cells were collected in the flow through. Isolated human cells were pelleted via centrifugation and prepared for cell sorting by resuspending in 400 µL of FACS buffer containing Hoescht 33342 (1:400) as a viability marker. For separation of human microglia expressing either endogenous GFP or RFP, samples were sorted on a FACS ARIA Fusion II (BD Biosciences) using the 70 um nozzle at the lowest flow rate. After removing doublets, by both forward and side scatter

parameters, and selecting for live cells (Hoescht 33342^{-}), both GFP (GFP^{+}RFP^{-}) and RFP (GFP^{-}RFP^{+}) cells were gated on and sorted into individual tubes. For each cell type, 15,000 cells were sorted into collection tubes containing 5uL of FACS buffer, resulting in a final volume of ~20 µL.

Single-cell sequencing. scRNA-seq library preparation was performed according to the 10X Chromium Single Cell 3' Reagents kit v3 user guide and loading the full sample volume onto the Chromium chip (20 uL containing ~15,000 cells). The workflow was then followed according to the 10X protocol and samples were pooled at equimolar concentrations for sequencing on an Illumina HiSeq 4000. FASTQ files were aligned to both the human GRCh38.p12 transcriptome (Ensembl release 95) and the mouse mm10 transcriptome (Ensembl release 95)(Cunningham et al., 2019) using the CellRanger V3 count command, with the expected cells set to 5,000 and no secondary analysis performed. Following alignment, all reads that aligned to the mouse transcriptome were removed from the dataset before additional processing.

Quantification and Statistical Analysis

In vitro experiments. Data are presented as SEM and n represents the number of technical replicates of cell culture experiments. Unless specified, all experiments were carried out with all three isogenic knockout sets. Most statistical comparisons were conducted by ANOVA for Bonferroni's post hoc test in GraphPad Prism 7. For all experiments excluding RNA-sequencing and phagocytosis a statistically significant difference was defined as $p < 0.05$. For phagocytosis experiments, $p < 0.001$ was used.

Image processing and plaque quantification. Immunofluorescent sections were visualized and captured using an Olympus FV3000RS confocal microscope. Images represent confocal Z-stack taken with identical laser and detection settings. For human microglial proximity to plaque quantification, Z-stack images were taken at 40X magnification (10 slices taken with a Z thickness of 1 um), 4 images per hemisphere (n=3 GFP WT & RFP TREM2 KO, n=3 GFP TREM2 KO & RFP WT). Human microglia numbers and locations were detected and quantified through Ku80 (GFP/RFP positive) immunofluorescence using the Olympus cellSense imaging software. Cells located within the 50 μm radius from the center of the closest Amylo-Glo positive aggregate were detected. The distance of the center of the detected cells from the closest edge of the aggregate was then measured. Expression of HLA-DR or CD9 in GFP versus RFP cells in the same region were also quantified in Olympus CellSens 2.3. T-test run on Graphpad Prism 7.

Bulk RNA-sequencing analysis. RNA-sequencing data was processed and interpreted using either the Genialis visual informatics platform or in-house bioinformatic analysis pipelines. RNA-sequencing read integrity was verified using FastQC. BBDuk was used to trim adapters and filter out poor quality reads. Remaining reads were then mapped to the hg19 reference genome using the HISAT aligner or the GRCh38 reference genome (Ensembl release 97(Cunningham et al., 2019)) using Kallisto v0.46.0(Bray et al., 2016b). Complete clustering linkage was measured by pearson coefficient. Lowly expressed genes (expression count summed over all samples < 10) were removed before differential expression analysis. Differentially expressed genes were calculated using DESeq2(Love

et al., 2014) by applying FDR cutoffs between 0.01 and 0.001 and log fold change of at least 0.5. Geneset enrichment analysis was performed using EnrichR GO Biological Processes 2018. Volcano plots were generated using the 'ggplot2' R package(Wickham, 2009) and heatmaps were generated using the 'pheatmap' R package(Kolde, 2019).

Single Cell RNA Data Visualization and Differential Gene Analysis. UMI count tables were read into Seurat (v3)(Stuart et al., 2019) for preprocessing and clustering analysis. Initial QC was performed by log normalizing and scaling (default settings) each dataset followed by PCA performed using all genes in the dataset. Seurat's ElbowPlot function was used to select principal components (PCs) to be used for clustering along with a resolution parameter of 0.5 and clusters identified as being doublets, gene poor, or dividing were removed from the dataset prior to downstream analysis. Secondary QC cutoffs were then applied to retain only cells with less than 30% ribosomal genes, 15% mitochondrial genes, greater than 600 genes but less than double the median gene count, and greater than 500 UMI but less than double the median UMI count.

Cells passing QC were then merged according to mouse of origin (e.g. TREM2 WT and KO microglia from the same 5x-MITRG mouse) using Seurat's 'merge' function and data were processed using Seurat's wrapper for the 'sctransform' R package(Hafemeister, 2019), while regressing out library size differences, percent ribosomal genes, and percent mitochondrial genes. PCA was then performed using the top 1,000 variable genes after removing ribosomal and mitochondrial genes from the lists (WT: 930 genes; 5X: 968 genes). For xMGs isolated from MITRG mice, a shared nearest neighbor (SNN) plot was generated using Seurat's 'FindNeighbors' function using PCs

1:20 as input, clustering was performed using the 'FindClusters' function and a resolution parameter of 0.5, and dimension reduction was performed using the 'RunUMAP' function with the same PCs used for generating the SNN plot. xMGs isolated from the 5X-MITRG mouse were processed similarly, using PCs 1:14 and a resolution parameter of 0.3. Differentially expressed genes were determined between clusters using the 'FindAllMarkers' function, which employs a Wilcoxon Rank Sum Test, with and FDR cutoff of 0.01, an LFC cutoff of 0.25, and the requirement that the gene be expressed in at least 10% of the cluster.

Information regarding the QC cutoffs and clustering parameters used in this analysis can be found in Supplemental Data 4.

Data Availability. The datasets generated and analyzed in this study are available through GEO (bulk sequencing: GSE157652; single-cell sequencing: GSE158234). Source data are provided in a Source Data File for all western blots ((McQuade et al., 2020) Figure 1a, 1g). Flow cytometry gating schema are provided in Source Data File Figure 5b, 6c (McQuade et al., 2020). Any additional data presented in this paper is available from the corresponding author upon request.

Code Availability. Base codes are open-source following citations linked in the methods section. Standard parameters were used unless otherwise noted in the methods section.

Results

Differential transcriptomic effects of TREM2 stimulation versus deletion in human iPSC-microglia. Because preliminary data on TREM2 function suggests that AD-

associated TREM2 mutations result in a partial loss of function(Cheng-Hathaway et al., 2018), we sought to mimic this effect by generating three isogenic sets of CRISPR-modified TREM2 knockout (KO) induced pluripotent stem cell (iPSC) lines. Following microglial differentiation(McQuade et al., 2018), we verified the loss of TREM2 expression at the protein level in all knockout lines by Western blot and Homogeneous Time Resolved Fluorescence (HTRF) analysis (Fig. 1a). HTRF analysis of conditioned culture medium further demonstrated secretion of soluble TREM2 exclusively in WT and not in TREM2 knockout cell lines (Fig. 1b). This strongly suggests that WT iPS-microglia exhibit normal trafficking and localization of TREM2, and further confirms lack of TREM2 expression in KO lines.

Next, we performed RNA sequencing to determine the genes and pathways that are disrupted in TREM2 KO human microglia. Two independent sets of TREM2 isogenic microglia generated from two distinct patients were sequenced to account for any cell line-dependent effects (Fig. 1c-e). Although some differences were noted between the two isogenic sets, many transcripts exhibited equivalent changes in both KO lines. Using a cutoff of +/- 1 log fold change and an FDR < 0.05, this dataset identified 390 differentially expressed genes (DEG) which were enriched for several important pathways including ‘regulation of calcium-mediated signaling’ and ‘ERK1 and ERK2 cascades, and cell migration’ (GO Biological Process 2018 adjusted $p < 0.05$; Fig. 1c-e, Supplemental Data 1). As expected, the most significantly down-regulated gene in knockout microglia was TREM2 itself, followed closely by glycoprotein NMB (GPNMB) which was recently shown to be up-regulated in plaque-associate microglia(M et al., 2018) (Fig. 1d, Supplemental Data 1). Interestingly, loss of GPNMB expression causes primary cutaneous

amyloidosis(Cf et al., 2018), suggesting that GPNMB may play an important role in the clearance of amyloidogenic proteins. In line with recent AD mouse studies, TREM2 deletion also led to a significant reduction of APOE and APOC1 gene expression(Krasemann et al., 2017; Parhizkar et al., 2019).

As some of the key downstream consequences of TREM2 expression in microglia may only manifest when TREM2 signaling is activated, we next sought to identify an optimal method to drive TREM2 signaling in wild type cells using TREM2 KO microglia as a negative control to further validate the specificity of this approach. A variety of ligands have been proposed to activate TREM2 downstream signaling including APOE, beta-amyloid, phosphatidyl serine, and several other lipids(Daws et al., 2003; N'Diaye et al., 2009; Wang et al., 2015; Zhao et al., 2018), however, each of these ligands produces pleotropic effects, binding to and signaling through multiple receptors and pathways. Indeed, when TREM2 WT and KO cells are stimulated with dead iPSC-derived neuron fragments, both genotypes responded similarly (Supplemental Fig. 1, Supplemental Data 2), suggesting that TREM2-specific responses to neuronal debris may be masked by signaling mediated via other microglia receptors such as the TAM receptor tyrosine kinase family(L et al., 2016). Because we found that TREM2 expression does not substantively alter the microglial transcriptional response to dead neurons, we concluded that a more specific method of TREM2 activation would be needed to further interrogate TREM2 function.

Therefore, we opted to stimulate TREM2 signaling by using a commercially available polyclonal TREM2 antibody (R&D; AF1828). Similar protocols have proved useful for the activation of various immune receptors (e.g., antibody-based crosslinking

of CD3 for T cell receptor activation), and this particular antibody has been successfully used to quantify TREM2/DAP12 signaling with a split-luciferase reporter system(Mm et al., 2017). Given the growing interest in development of TREM2 activating antibodies as a potential therapy for AD, this approach could also provide data that would further inform translational studies(Wang et al., 2020a). Since microglia express Fc receptors, an equivalent concentration of preimmune IgG was used as an additional isotype control. Using this approach, we confirmed that AF1828 exposure produces rapid phosphorylation of spleen tyrosine kinase (SYK), a known signaling molecule downstream of TREM2/DAP12 activation (Fig. 1f,g). In contrast, treatment of WT cells with control IgG or treatment of TREM2 knockout microglia with AF1828 produced no phosphorylation of SYK (Fig. 1g).

Next, we coupled this stimulation approach with RNA sequencing to identify genes for which expression was altered both after knockout and, in the opposing direction, 24 hours after antibody stimulation of WT microglia (Fig. 1h-j, Supplemental Data 3, log(FC) ≥ 0.5 and FDR < 0.001). These reciprocally changed genes are indicative of transcripts that, for example, decrease expression in the absence of TREM2 and increase expression in WT cells stimulated with anti-TREM2 antibody, but are not altered with control IgG or vehicle (DPBS) treatments. Geneset enrichment analysis on this highly specific reciprocally changed gene set showed similarity to enrichment seen with just knockout of TREM2 (Fig. 1e,j). The 72 reciprocally changed genes also highlighted key differences in chemotaxis (positive regulation of leukocyte chemotaxis), specific immune response families (cellular response to tumor necrosis factor), and cell survival pathways (positive regulation of ERK1 and ERK2 cascade) (Fig. 1i).

To functionally validate these findings, we next examined whether TREM2 expression and signaling alters microglial survival, phagocytosis, and chemotaxis as predicted by this geneset enrichment analysis.

TREM2 knockout microglia are hypersensitive to stress-induced cell death. From our previous geneset enrichment analysis, we found that MAPK and ERK pathways are strongly enriched (Fig. 1e,i). These pathways are involved in regulating cell survival and apoptosis. Additionally, previous data from murine microglia has indicated that TREM2 deficiency leads to increased cell death, a process that was hypothesized to rely on macrophage colony-stimulating factor (M-CSF)(Zheng et al., 2017). It has been suggested that TREM2 works cooperatively with CSF1R signaling which is necessary for microglial survival(Otero et al., 2009, 2012; Sosna et al., 2018). Therefore, we induced cell death in human iPS-microglia by cytokine starvation for 3 days and tested the importance of three key cytokines (M-CSF, IL-34, and TGF-β1) in microglial apoptosis (Fig. 2a).

Microglial apoptosis was visualized using a fluorogenic Caspase 3/7 detector and time-lapse imaging. At baseline, we found TREM2 knockout microglia already showed increased caspase signal compared to their WT isogenic pairs which was not surprising given that MAPK and ERK pathways were enriched even when comparing WT and KO lines without stimulation (Fig. 1e, 2b).

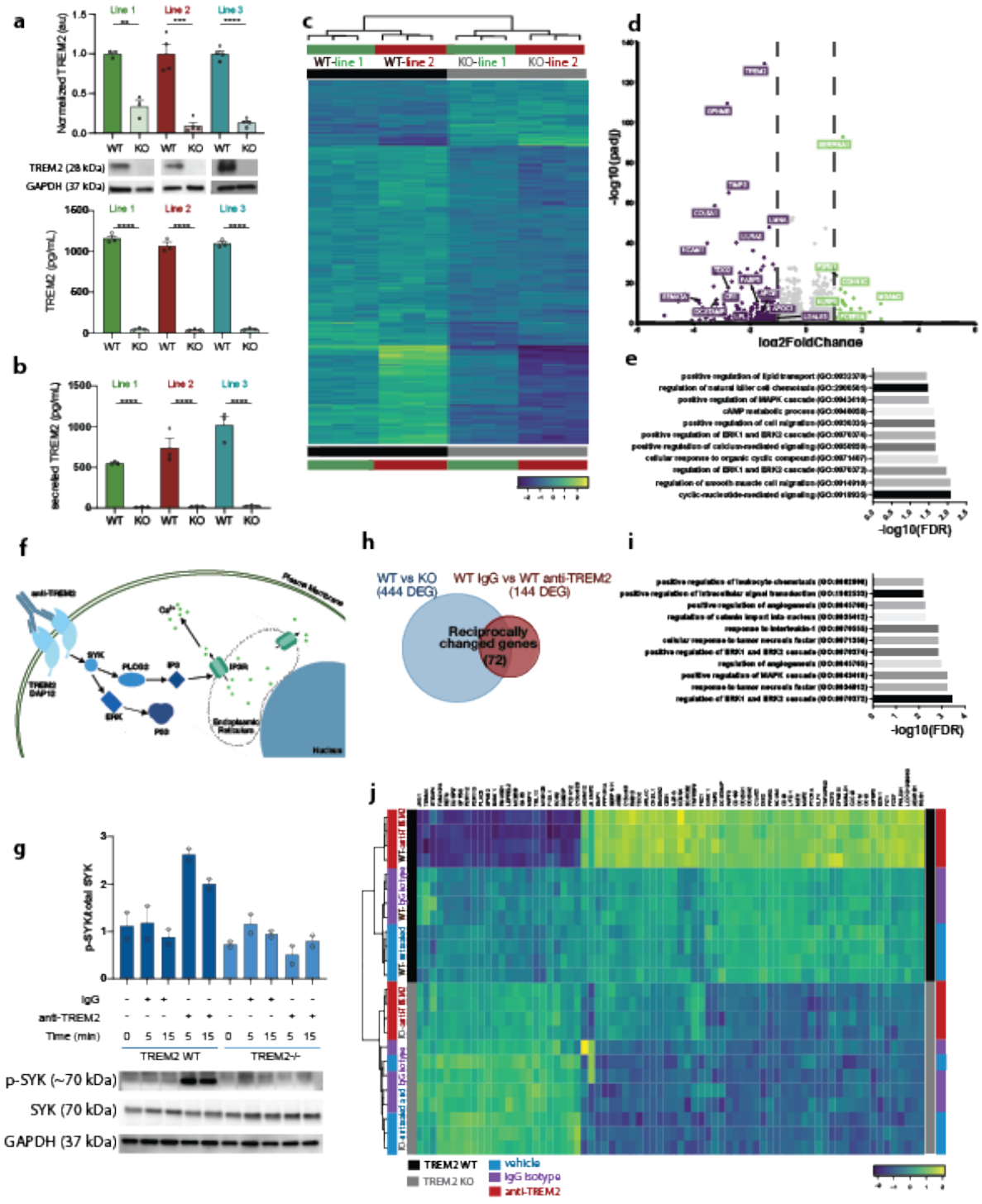

Figure 2.1. TREM2 knockout and stimulation elicit transcriptional changes in iPS-derived microglia. a Confirmation of isogenic TREM2 knockout lines by western blot ($n = 3$ or 4 lanes for each of 3 lines; t-test $^{**}p < 0.01$, Line 1 $p = 0.0024$, Line 2 $p = 0.0098$, Line 3 $p = 0.0094$), homogeneous time resolved fluorescence (HTRF; $n = 3$ independent wells for each of 3 lines; t-test $^{****}p < 0.0001$), and **b** sTREM2 secretion by HTRF; $n = 3$

independent wells for each of 3 *t*-test ****$p < 0.0001$). Different colors represent individual patient lines. Lighter shades represent KO lines. Data are represented as mean values ± SEM. **c**Heatmap of DEG for TREM2 WT versus KO ($n = 2$ independent lines; $n = 3$/line). Scale represents median-centered VST transformed counts from DESeq2. **d** Volcano plot showing DEG for TREM2 WT versus KO in 2 independent lines (green—increased expression in KO; purple—decreased expression in KO). **e** Geneset enrichment analysis of WT vs KO (EnrichR; adj $p < 0.05$ determined by EnrichR algorithm). Genes in these families were mainly increased in WT cells. **f** Schematic of TREM2 antibody stimulation paradigm. **g** Western blot showing phosphorylation of SYK in WT (dark blue) and KO (light blue) microglia within 5–15 min of exposure to the polyclonal TREM2 antibody (AF1828) or control IgG. (20 µg/mL32 $n = 2$ independent samples). Data are represented as mean. **h** Venn diagram of differentially expressed genes in WT vs KO microglia (444 DEGs) compared to WT microglia 24 h after treatment with IgG versus anti-TREM2 antibody (144 DEGs). Venn diagram reveals 72 reciprocally changed DEGs. **i** Geneset enrichment analysis of reciprocally changed genes (EnrichR; adj $p < 0.05$ determined by EnrichR algorithm). **j** Heatmap of the resulting 72 reciprocally changed genes. Scale represents median-centered counts (TPM).

Time-lapse imaging of WT microglia in complete medium (no cytokine starvation) revealed minimal caspase activation as expected (Fig. 2a,c; dark blue). However, in TREM2 KO lines, increased apoptosis was quantified even in complete medium suggesting they may have a higher dependency on cytokines than WT lines (Fig. 2a,c; light blue). As expected, cytokine starvation (removal of M-CSF, IL-34, and TGF-β1) induced microglial death in both WT and KO lines. However, TREM2 KO lines still demonstrated elevated caspase 3/7 signal compared to WT lines (Fig. 2a,c; red), highlighting that TREM2 KO microglia exhibit increased sensitivity to stress conditions and respond through apoptosis.

In order to determine whether this apoptotic response is specifically through M-CSF/CSF-1R signaling, iPS-microglia were grown in medium lacking *only* the CSF1R ligands (IL-34 and M-CSF). Indeed, this alone was sufficient to induce the same levels of apoptosis seen with full cytokine starvation (Fig. 2a,c; orange). In contrast, removal of TGF-β1 alone, an important regulator of microglial homeostasis, did *not* alter caspase

activation (Fig. 2a,c; grey). Therefore, we conclude that human TREM2 modulates CSF1R signaling leading to higher levels of cell death in TREM2 knockout lines.

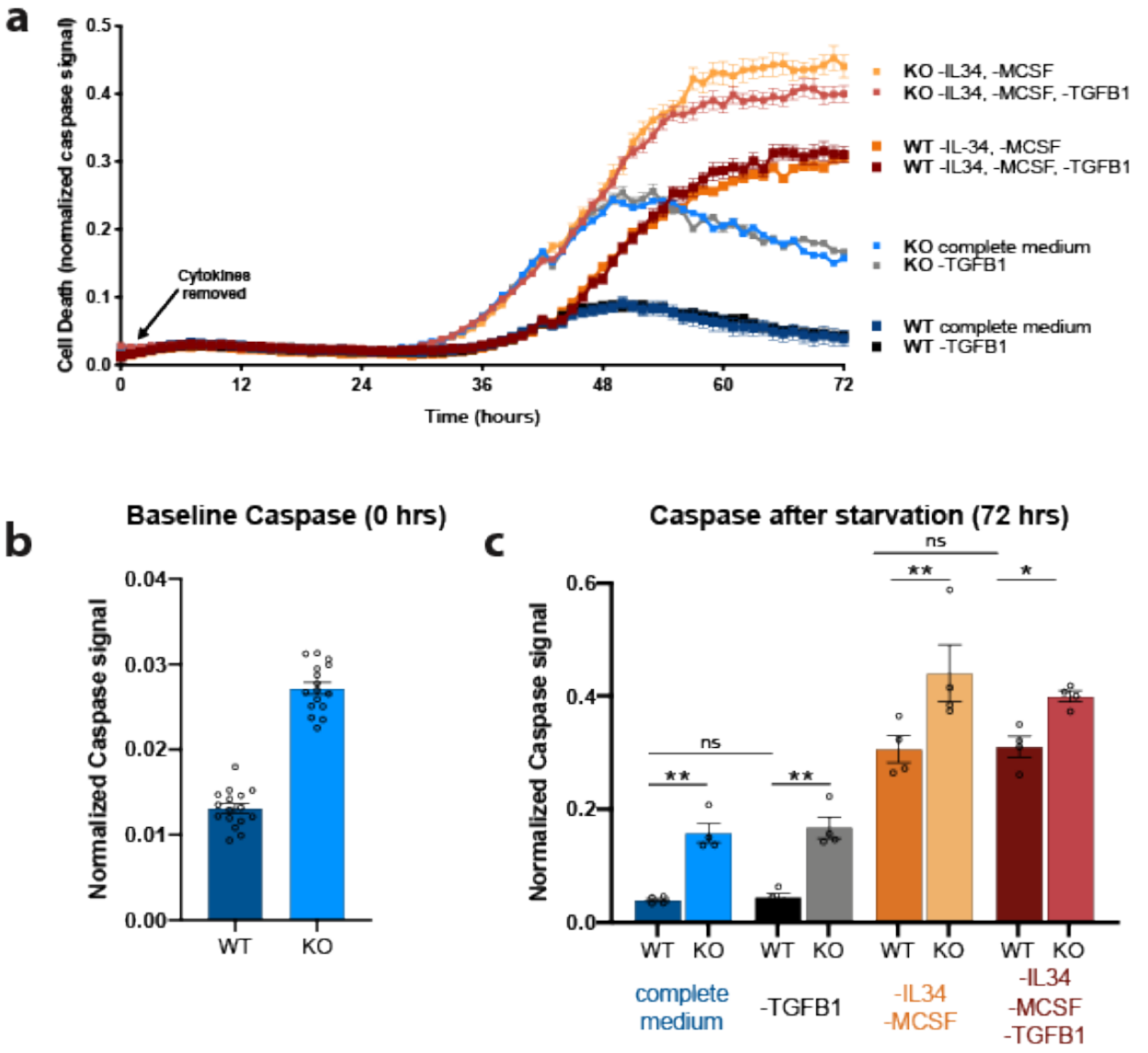

Figure 2.2. TREM2 knockout microglia exhibit decreased caspase activation at baseline and after cytokine starvation. a Caspase 3/7 levels imaged over 3 days in culture with complete medium (blue), no TGFB1 (gray), no IL-34, no MCSF (orange)or no IL-34, no MCSF, no TGFB1 (red). Images captured on Incucyte S3 live-cell imager. Darker shades represent TREM2 WT. Data are represented as mean values ± SEM. **b** Quantification of caspase 3/7 after 0 h in culture. (*t*-test ****$p < 0.0001$). Data are represented as mean values ± SEM. **c** Quantification of caspase 3/7 after 72 h in culture. (ANOVA, Tukey post hoc test. WT vs KO complete medium: $p = 0.0052$, WT vs KO -TGFB1: $p = 0.0035$, WT vs KO -IL34/MCSF: $p = 0.0014$, WT vs KO -

IL34/MCSF/TGFB1: $p = 0.045$, ns: $p > 0.9999$). For all panels, $n = 4$ images in four independent wells. Data are represented as mean values ± SEM. Experiment was reproduced with two independent lines.

TREM2 is necessary for phagocytosis of APOE by human microglia. Apolipoprotein E, the largest genetic risk factor for AD, has been proposed as an important TREM2 ligand(Parhizkar et al., 2019; Shi and Holtzman, 2018; Yeh et al., 2016). However, it remains unclear whether APOE-mediated disease risk is specifically related to its interactions with TREM2. Additionally, our sequencing data highlighted differences in lipid transport (Fig. 1e), prompting us to further examine the potential interactions between TREM2 and APOE. Therefore, we exposed TREM2 isogenic lines to an allelic series of recombinant, lipidated APOE (Fig. 3a; Supplemental Fig. 2).

Interestingly, we found that microglial phagocytosis of APOE in WT cells is dependent on APOE genotype, with APOE4 being internalized at a significantly higher rate than APOE3 which is taken up at higher levels than the AD protective allele; APOE2 (Fig. 3a). Importantly, these differences in phagocytosis were based on the APOE genotype of the exogenously added protein, not the APOE genotype of the microglia (all APOE 3/3). Further investigation is needed to determine if this recognition is crucial to AD development, but this data highlights that APOE genotypes are differentially recognized by microglia.

Next, we investigated the importance of TREM2 expression on phagocytosis of APOE. When TREM2 expression is lost, we detected no significant uptake of APOE fluorescence above the vehicle control (Fig. 3a). This stark difference was surprising given that TREM2 knockout microglia still express other canonical APOE receptors. Indeed, our RNA sequencing revealed no changes in expression of canonical APOE

receptors between lines including LDL2, LRP1, and HSPG2 (adj p-values 0.85, 0.98, 0.15 respectively) (Supplemental Data 1). Thus, even in the presence of other APOE receptors, TREM2 knockout microglia do not phagocytose detectable lipidated APOE protein suggesting that TREM2 is necessary for phagocytosis of APOE by human microglia.

To gain further mechanistic understanding on the role of TREM2 signaling in APOE phagocytosis, we also pre-treated iPS-microglia with a SYK inhibitor (see signaling schematic Fig. 1f), R406 to block TREM2 signaling transduction. For these experiments APOE3 was utilized as it represents the most common variant of APOE. Pre-treatment of microglia with R406 was able to partially, but significantly, block APOE phagocytosis in WT cells suggesting this phagocytosis does occur through TREM2/DAP12 signaling (Fig. 3b, right).

TREM2 is critical for phagocytosis of fibrillar beta-amyloid and human synaptosomes but not Zymosan A. As TREM2 has been proposed to act as a receptor for many ligands which are engulfed by microglia *in vivo*, we tested whether exposure of TREM2 isogenic lines to several other substrates would reveal corresponding functional differences. First, we exposed TREM2 isogenic lines to fibrillar beta-amyloid. As expected, phagocytosis of beta-amyloid was significantly decreased in KO lines (Fig. 1c). We further confirmed the requirement of TREM2/DAP12 downstream signaling by blocking SYK with R406 which proved sufficient to block phagocytosis in WT lines. Importantly, blocking SYK in TREM2 KO lines had no effect (Fig 1c).

To address previous studies that suggest TREM2 may play a role in synaptic pruning(Filipello et al., 2018), we next exposed microglia to pHrodo-labeled human synaptosome fractions isolated from AD brain tissue(Abud et al., 2017). Interestingly, TREM2 knockout microglia exhibited impaired phagocytosis of synaptosomes, suggesting that TREM2 may play an important role in synaptic pruning (Fig. 3d). Again, blocking downstream TREM2 signaling through SYK with R406 was able to partially block phagocytosis of synaptosomes in WT lines highlighting the importance of TREM2/DAP12 signaling in phagocytosis of this ligand.

To investigate whether the observed decrease in phagocytosis is specific to disease-relevant substrates or instead due to a more global down-regulation of phagocytic activity, we also tested phagocytosis of zymosan A, a dectin 1/2 agonist (Fig. 3e). This control ligand was taken up equally well by WT and TREM2 knockout cells, and phagocytosis of zymosan A was not altered by SYK inhibition, demonstrating that loss of TREM2 signaling results in substrate-specific deficits in phagocytosis (Fig. 3e).

TREM2 antibody stimulation partially alters phagocytosis. To further explore phagocytic deficits in TREM2 KO lines, we pre-stimulated isogenic microglia with anti-TREM2 antibody or an isogenic IgG control before exposing cells to APOE3, beta-amyloid, synaptosomes, or Zymosan A (Supplemental Fig. 3). As expected, anti-TREM2 antibody treatment on TREM2 knockout lines did not have any effect. For phagocytosis of APOE3 and human synaptosomes, treatment of WT cells with anti-TREM2 antibody decreased phagocytosis. This decrease may be due to internalization of TREM2 following antibody stimulation that could in turn temporarily mimic a loss of function phenotype in

response to secondary stimulation. With beta-amyloid and zymosan A, anti-TREM2 antibody had no effect, suggesting the TREM2 receptor itself may not be directly responsible for initiating phagocytosis of these substrates. However, in the case of beta-amyloid, we do show SYK signaling is important (Fig. 3c). This finding fits with the prior identification of several other microglial receptors that have been implicated in beta-amyloid internalization by microglia(Frenkel et al., 2013; Koenigsknecht and Landreth, 2004). Additionally, this may suggest that the reduction of beta-amyloid phagocytosis in TREM2 knockouts may be more strongly influenced by changes in SYK activation state than by direct binding between TREM2 and beta-amyloid.

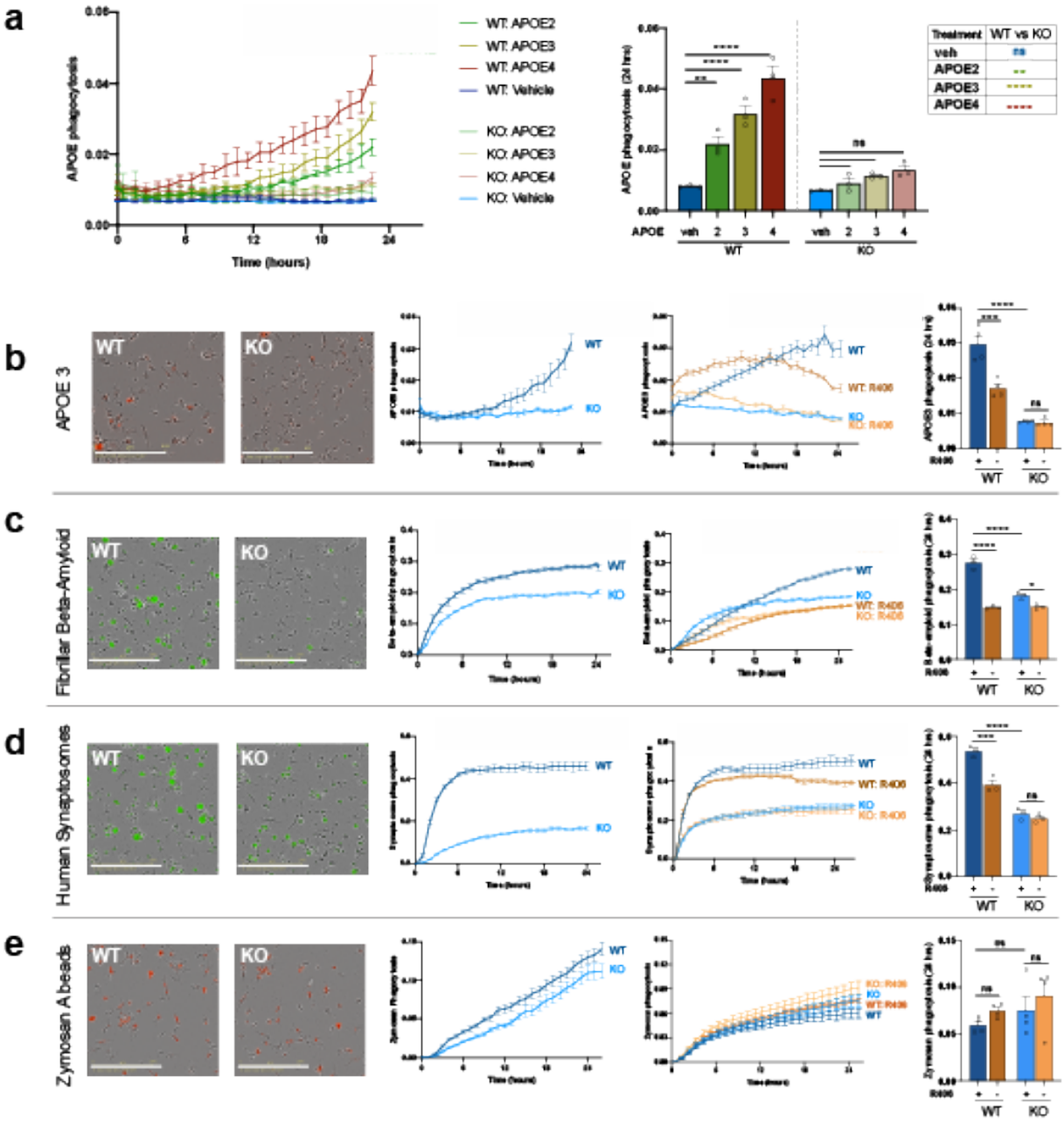

Figure 2.3. TREM2 knockout decreases phagocytosis of disease-relevant stimuli. **a** Isogenic TREM2 WT and KO microglia were exposed to recombinant APOE 2 (green), APOE 3 (yellow), APOE4 (red), or a vehicle control (blue). Images were taken every hour for 24 h with IncuCyte S3 live imaging system. Scale bar: 200 µm. Statistical differences were quantified at 24 h (right, $n = 3$ independent wells with 4 images per well. Table (right) shows difference between WT and KO lines for each APOE genotype replicated in 2 isogenic backgrounds; two-way ANOVA, Tukey post hoc test, multiple comparisons. WT(veh) vs WT(APOE2): $p = 0.0052$, WT (APOE2) vs KO (APOE2): $p = 0.0075$, ****$p < 0.0001$, ns: $p > 0.8$.) Data are represented as mean values ± SEM. Microglia were exposed to **b** recombinant APOE3 (red), **c** fibrillar fluorescent beta-amyloid

(green), **d** pHrodo-labeled human synaptosomes (green), or **e** pHrodo-labeled Zymosan A (red). Left shows representative images at 24 h. Inner graphs show untreated cells and the relative effects of TREM2 deletion alone on phagocytosis, or with addition of a SYK inhibitor (5 μM R406). Statistical differences were quantified at 24 h (right). For all panels, $n = 3–4$ independent wells with 4 images per well; two-way ANOVA, Tukey post hoc test, multiple comparisons. **b** ***$p = 0.0002$, ****$p < 0.0001$, ns $p = 0.998$ **c** *$p = 0.0393$, ****$p < 0.0001$ **d** ***$p = 0.0008$, ****$p < 0.0001$, ns $p = 0.7912$ **e**WT vs WT + R406 $p = 0.301$, KO vs KO + R406 $p = 0.320$, WT vs KO $p = 0.344$. Data are represented as mean values ± SEM. Experiments were replicated in three isogenic lines with equivalent results.

TREM2 deletion reduced clustering around amyloid plaques and impairs migration towards beta-amyloid producing cultures. Several groups have previously shown that TREM2 deficient mouse microglia exhibit decreased clustering around beta-amyloid plaques(Ulrich et al., 2014; Wang et al., 2016). To determine whether human TREM2 knockout microglia exhibit a similar impairment, we transplanted GFP or RFP-expressing isogenic human microglia into the brains of 5x-MITRG mice (Fig. 4a). These transgenic mice, obtained by backcrossing the 5x-fAD mouse model of AD with MITRG xenotransplantation-compatible mice (hCSF1, hCSF2, hTPO, Rag2 knockout, il2rγ knockout), were specifically developed to examine the functional behavior of transplanted human microglia *in vivo*(Abud et al., 2017). Using this approach, we co-transplanted combinations of WT and TREM2 knockout human microglia (either GFP:WT, RFP:TREM2 KO or vice versa) into post-natal day 2-3 mice which were allowed to age for 6 months. Brain sections were stained with Amylo-Glo, a Thioflavin S analog, to detect fibrillar beta-amyloid plaques. As expected, WT human microglia exhibited a robust response to beta-amyloid plaque pathology, surrounding the plaques in a manner highly similar to that observed in human AD tissue(Wang et al., 2016). In stark contrast, TREM2 knockout human microglia appeared unresponsive to plaque pathology, exhibiting little to

no association with plaques and lacking the characteristic morphological changes observed in isogenic wild type microglia (Fig. 4a). These data are highly consistent with the response of murine TREM2 knockout microglia to plaque pathology and with observations in human TREM2 R47H cases, (Condello et al., 2015; Ulrich et al., 2014; Yuan et al., 2016) but also represent the first report to our knowledge that examines the impact of TREM2 deletion on human microglial plaque association.

Since, *in vivo,* beta-amyloid plaques are quite complex consisting of not only beta-amyloid itself but many other proteins, dystrophic neurites, and reactive astrocytes, we next performed *in vitro* migration assays to determine if TREM2 knockout cells exhibit impaired migration towards beta-amyloid alone or whether additional signals derived from AD neurons might further influence the association between microglia and plaque pathology. To this end, we used two-chamber microfluidic migration devices(Park et al., 2018) to measure the migration of WT and KO microglia toward soluble beta-amyloid or toward beta-amyloid producing human neuronal/glial mixed cultures. Whereas no significant differences were observed between WT and KO microglia in migration towards $A\beta_{1-40}$ or $A\beta_{1-42}$ alone, the more physiological combination of $A\beta_{1-40}$ and $A\beta_{1-42}$ revealed a significant impairment in the migration of TREM2 knockout microglia (Fig. 4b).

To determine whether additional neurally-derived cues may influence TREM2-mediated chemotaxis, we also analyzed microglial migration towards Aβ producing human neurons and astrocytes plated within the central chamber. With co-culture of young (3-week old) neurons and astrocytes we observed minimal microglial recruitment, although an impairment in TREM2 knockout migration was already evident (Fig. 4c). However, when neurons and astrocytes were aged to 9-weeks, a timepoint that was

previously shown to correspond to increasing amyloid pathology and cell death in this system(Park et al., 2018), we observed significant migration of WT microglia to the central chamber, whereas TREM2 knockout microglia remained completely unresponsive to these cell-derived chemotactic signals (Fig. 4c).

An outstanding question is whether the observed lack of migration is due to an inability of TREM2-deficient cells to sense and respond to chemoattractive cues or merely an inability of TREM2 knockout cells to move. To address this issue, we performed a scratch wound assay to observe general motility of TREM2 WT and KO microglia. This experiment showed no significant differences in baseline motility for WT and TREM2 knockout microglia suggesting that the differences quantified above are specific to chemoattractive migration (Fig. 4d).

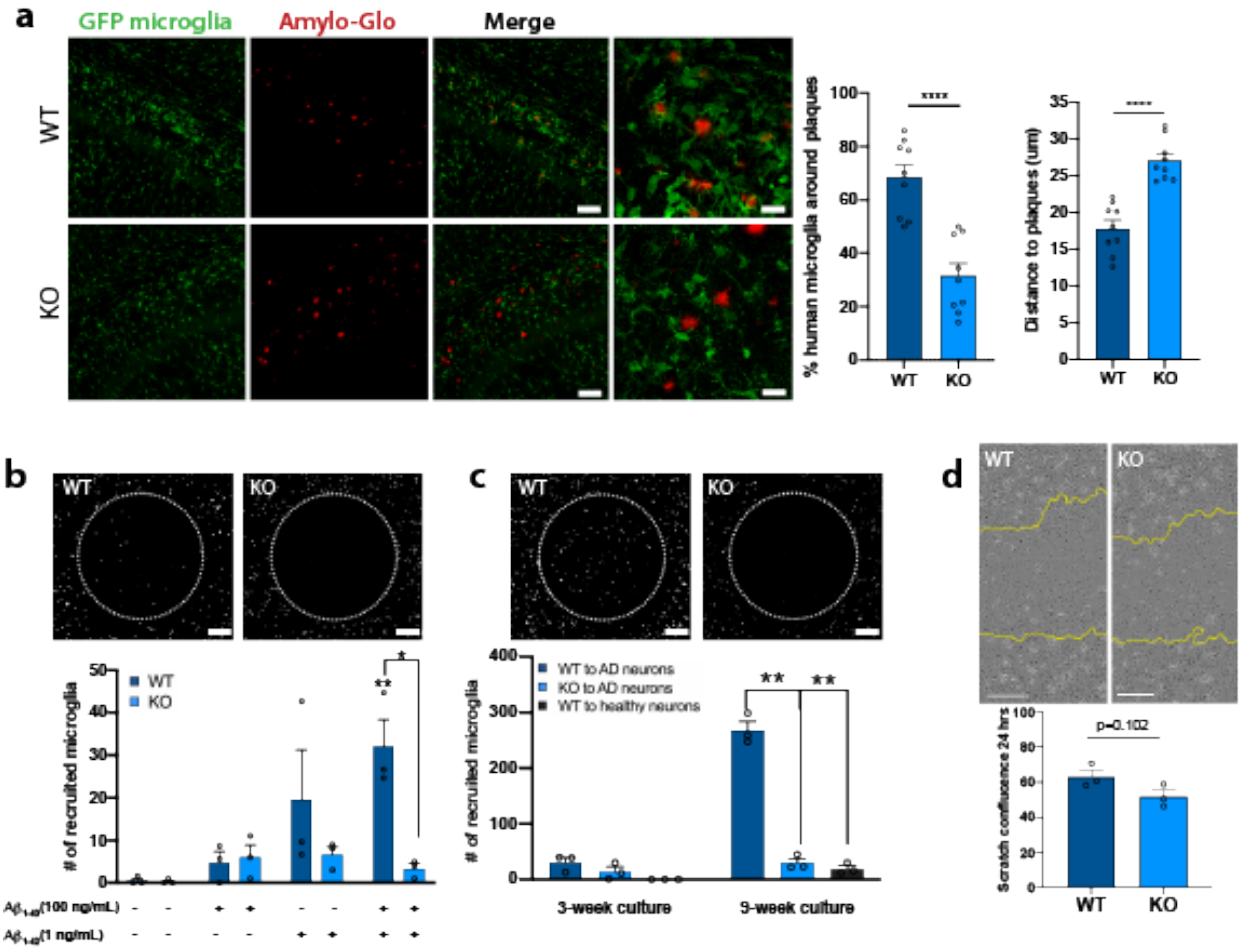

Figure 2.4. Deletion of TREM2 reduces the association of microglia with amyloid plaques and impairs migration toward amyloid and AD model cultures. a GFP-expressing TREM2 WT (top) or KO (bottom) microglia xenotransplanted into 5x-MITRG mice and aged 6 mo. were examined to assess the proximity between beta-amyloid plaques (red, Amylo-glo) and microglia (green). Scale bar low power: 40 µm; high power: 20 µm. Percent of each genotype within 50 µm of a plaque and raw distance to closest plaque was quantified (*t*-test ****$p < 0.0001$, $n = 9$ individual mice, 4 images per mouse). Darker blue represents TREM2 WT. Data are represented as mean values ± SEM. Experiment was run with two individual patient backgrounds. **b** In vitro migration of microglia toward soluble recombinant beta-amyloid. Images show microglia plated in outer chambers and allowed to migrate for 4 days through microfluidic channels toward beta-amyloid ($A\beta_{1–40}$ and $A\beta_{1–42}$) within the inner chamber (delineated by the dashed circle). Scale bar: 500 µm. ($n = 3$ independent devices, unpaired *t*-test *$p = 0.0114$; WT vs WT + $A\beta_{1–40}$ and $A\beta_{1–42}$ $p = 0.0076$). Data are represented as mean values ± SEM. **c** WT and TREM2 knockout microglial migration toward 3-week old Aβ-producing human neural and astrocyte mixed cultures or toward 9-week old wild type cultures. Scale bar: 500 µm. ($n = 3$ independent devices unpaired *t*-test **$p < 0.001$; WT vs KO $p = 0.0078$; WT vs WT(AD) vs WT (healthy) $p = 0.0063$). Data are represented as mean values ± SEM. Experiments from b,c were reproduced with equivalent results in two independent

lines. **d** Scratch wound assay imaged and quantified 24 h post scratch with IncuCyte WoundMaker revealed no significant differences in general motility ($n = 3$ independent wells with 4 images per well, t-test $p = 0.102$). Yellow line demarcates original scratch. Data are represented as mean values ± SEM. Experiment was reproduced in three independent lines. Scale bar: 200 µm.

CXCR4 mediates migration deficits in TREM2 knockout microglia. To further investigate the mechanism of impaired migration in TREM2 KO microglia, we returned to our RNA-sequencing data which revealed that expression of CXCR4, an important chemo-attractive receptor, was reduced in the TREM2 knockout cells (Supplemental Data 1,3). Immunofluorescent and flow cytometry analysis of isogenic WT and TREM2 knockout microglia further confirmed that this receptor is decreased at the protein level in TREM2 knockout lines (Fig. 5a,b). Of further interest, CXCR4 expression has been shown to increase in murine disease associated microglia (DAMs)(Keren-Shaul et al., 2017; Krasemann et al., 2017) and in our own recent study of plaque-associated human microglia(Hasselmann et al., 2019), further supporting the potential role of this receptor in microglial migration toward plaques. CXCR4 has also been well characterized as a chemokine receptor in the peripheral immune system(Guo et al., 2017), responding to the ligand SDF-1α (CXCL12). CXCR4 is a canonical G-protein coupled receptor (GPCR) and its engagement results in the activation of $G_{q/11}$ and subsequent elevation of cytosolic Ca^{2+} via IP_3 mediated ER-store release, a downstream response that is also implicated in TREM2 signaling. In the brain, SDF-1α is highly expressed in neurons and astrocytes particularly in the hippocampus(Luo et al., 2008; Zhang et al., 2014) and increasing SDF-1α promotes the recruitment of microglia to plaques in AD mice(Wang et al., 2012).

To examine the potential role of CXCR4 signaling in iPS-microglia, cells were loaded with Fluo-4 and Fura-Red for ratiometric Ca^{2+} imaging and treated with SDF-1α in

Ca^{2+}-free buffer to unambiguously isolate Ca^{2+} signals downstream of CXCR4 activation. Using this approach, we found that WT microglia showed significantly greater responses to SDF-1α than TREM2 knockout microglia (Fig. 5c, left and middle panels). Analysis of individual-cell responses further revealed that only a subset of cells were activated by SDF-1α in both WT and TREM2 knockout microglia (Fig. 5c right, Supplemental Fig. 4, Supplemental Movie 1, 2), suggesting that only a subset of microglia were primed to respond to SDF-1α signaling, and this percent was significantly lower in TREM2 knockout microglia (WT; 39% responded, KO: 11.5% responded). Single-cell quantification showed that the average peak Ca^{2+} response to SDF-1α was lower in TREM2 knockout microglia (Fig. 5c, Supplemental Fig. 4). These results strongly suggest that TREM2 knockout microglia have lower sensitivity to SDF-1α, likely due to the observed lower expression of CXCR4 mRNA and membrane-localized CXCR4 protein, which could in turn explain their migratory defect.

Next, to determine if CXCR4 signaling is necessary for migration, we used AMD3100 to block CXCR4 receptor activity during migration towards astrocyte and neural cultures(Donzella et al., 1998). Previous data highlights that this mixed model of neurons and glia does indeed express SDF-1α, and additionally, SDF-1α was shown to be increased when using Aβ-producing neurons and astrocytes compared to healthy controls(Park et al., 2018). We observed migration of WT microglia only in cultures in which SDF-1α was induced (AD neurons) and CXCR4 signaling was functional (no AMD3100, Fig. 5d). These data strongly suggest that CXCR4 is necessary for migration of human microglia towards human beta-amyloid expressing neural and astrocyte cultures. Thus, these data support the possibility that activating CXCR4 in TREM2

deficient microglia may be a useful approach in AD to rescue microglial migration towards dying cells and/or amyloid plaques.

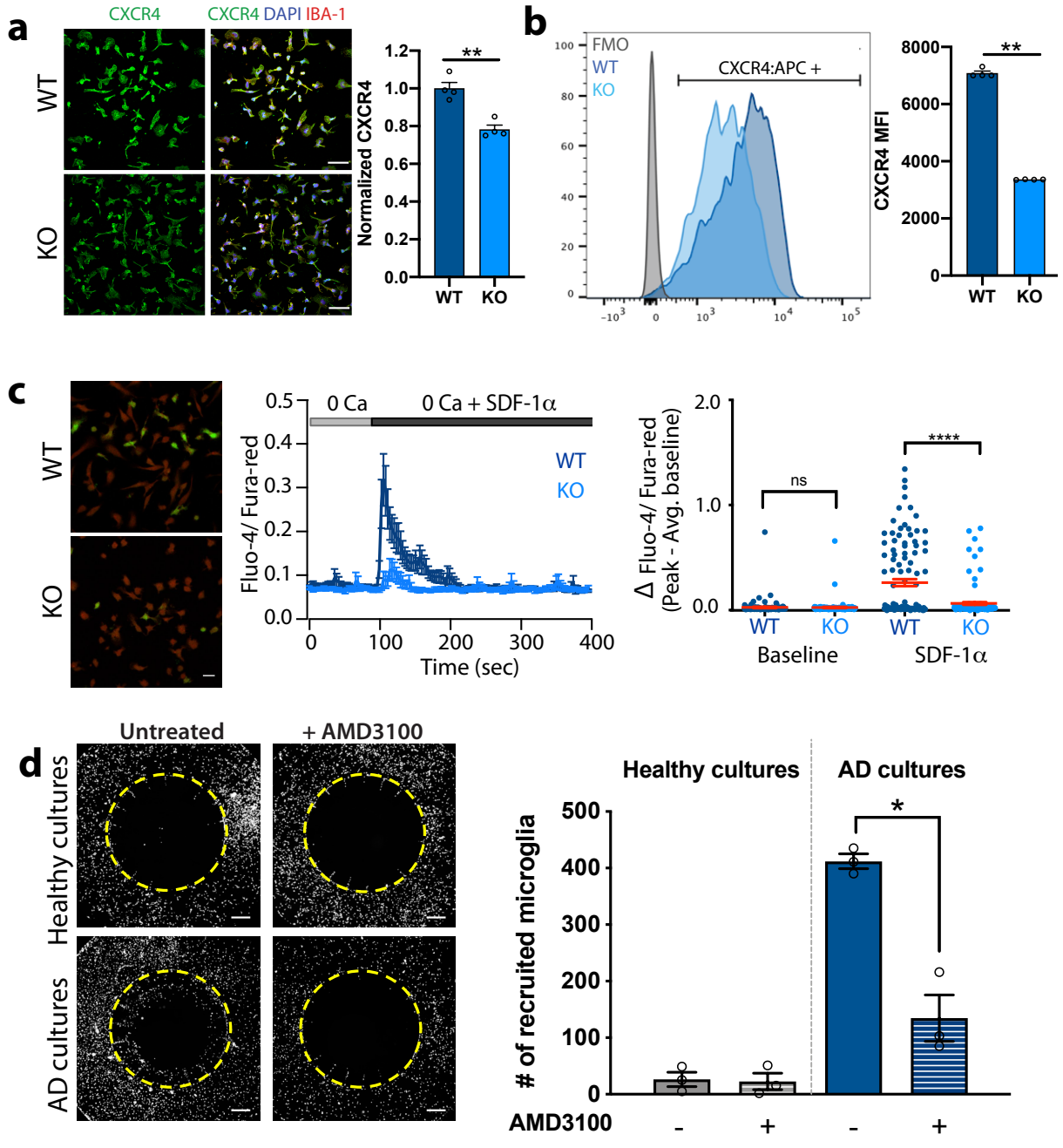

Figure 2.5. TREM2 knockout microglia are deficient in CXCR4 which is required for migration. a Expression of CXCR4 (green), IBA-1 (red) in in vitro TREM2 isogenic lines. CXCR4 signal was normalized to DAPI (blue) intensity. Scale bar: 40 µm. In quantification, darker shades represent TREM2 WT. ($n = 4$ independent wells, 4 images per well, Experiment replicated in three independent lines; unpaired t-test $p = 0.0015$).

Data are represented as mean values ± SEM. **b** Flow cytometry of CXCR4:APC (gated on fluorescence minus one (FMO) control (gray)) and quantification of mean fluorescence intensity (MFI) ($n = 3$ independent samples (100,000 events each), unpaired *t*-test $p = 0.0017$). Data are represented as mean values ± SEM. Gating strategy in Source data file. Reproduced with all three isogenic sets with similar results. **c** Overlay of maximum intensity projection images over time of Fluo-4 (green) and Fura-Red (red) loaded WT and TREM2 KO cells after activation with SDF-1α (left panel, Scale bar: 20 μm). Time-lapse run showing average cytosolic Ca^{2+} response to 250 ng/mL SDF-1α measured by ratiometric Fluo-4 and Fura-Red signal (middle panel, Data are mean ± SEM; $n = 51–61$ cells). Summary of single cell baseline and maximal SDF-1α induced Ca^{2+} elevation in WT and KO microglia (right panel, Data are mean ± SEM, $n = 111–120$ cells, 2 experiments). *Y*-axis denotes either peak baseline or peak SDF-1α response subtracted from the average baseline for each cell (****$p < 0.0001$, n.s not significant, as measured by One-way ANOVA; Post-hoc Tukey's multiple comparisons test). **d** WT microglia were allowed to migrate to 9-week old healthy or beta-amyloid producing (AD) neural/glial cultures plated within the central chamber (white dashed circle). Microglia pseudocolored gray. AMD3100 was used at 10 ng/mL. Scale bar: 50 μm (unpaired *t*-test, $p = 0.003$) Experiment was reproduced in two lines (total $n = 5$). Data are represented as mean values ± SEM.

TREM2 knockout microglia fail to respond appropriately to amyloid plaque pathology *in vivo*. It has been shown that expression of TREM2 is increased in the DAM sub-population found in AD mice(Keren-Shaul et al., 2017), and is required for transition towards this phenotype(Keren-Shaul et al., 2017; Krasemann et al., 2017). However, recent data from our lab and others(Hasselmann et al., 2019; Mancuso et al., 2019) suggests that the genes associated with human DAM formation have limited overlap with previously defined mouse datasets(Mathys et al., 2019). To determine if TREM2 KO effects DAM formation in *human* microglia, we co-transplanted iPS-derived hematopoietic progenitor cells into post-natal day 2-3 MITRG mouse pups allowing for the direct comparison of WT and KO human microglia within the same mouse. In order to identify which microglia were derived from TREM2 WT versus knockout iPSCs, we mixed RFP-expressing WT cells with GFP-expressing KO cells and vice versa. Using this technique, we find long-term engraftment of human microglia within the mouse

forebrain(Hasselmann et al., 2019). When crossed to the 5xfAD mouse (5x-MITRG) we also find that these cells respond to the onset and progression of disease with characteristic morphological and transcriptional changes.

After isolating human microglia from MITRG or 5x-MITRG mouse brains at 6 months of age, we performed single cell RNA sequencing to visualize the sub-populations of human microglia. In non-diseased MITRG mice we found four transcriptionally distinct sub-populations of microglia (Fig. 6a, Supplemental Data 4, 5, Supplemental Table 1). By analyzing the top genes in each population which significantly differ from the entire dataset, we determined that these 4 sub-populations were differentiated by genes involved in Major Histocompatibility Complex (MHCII) and Human Leukocyte Antigen (HLA) presentation (34.2%), the type 1 interferon response (10.8%), a small vaguely defined cluster which we termed “degranulation” (1.9%) and a “homeostatic” cluster that expressed high levels of canonical and homeostatic microglia genes while lacking expression of genes defining the other clusters (53.1%) (Fig. 6a, Supplemental Data 5) (clustering heatmaps and key gene expression UMAPs are included in Supplemental Fig. 5). However, when looking at TREM2 knockout microglia transplanted into the same mouse, we saw these population percentages shift toward a more homeostatic profile even in the non-diseased mouse (Fig. 6a, Supplemental Table 1; 61% homeostatic, 23.5% HLA, 12.6% interferon, and 2.9% degranulation), consistent with the notion that TREM2 deletion may trap microglia in a homeostatic state(Krasemann et al., 2017) not only in disease but also in response to normal aging as well. This suggests that TREM2 knockout microglia are intrinsically hypo-reactive.

Next, we examined WT and TREM2 knockout microglia that had been co-transplanted into littermate 5x-MITRG mouse pups and allowed to age for 6 months. When WT microglia transplanted into this AD model were examined, we uncovered five transcriptionally distinct sub-populations (Fig. 6b). The four populations seen in non-AD mice were still present as well as an additional population (13% of WT cells) that matches the human DAM population that we recently described(Hasselmann et al., 2019). As expected, exposure to beta-amyloid pathology, shifted WT microglia away from homeostatic and interferon high phenotypes, towards DAM phenotypes (Fig. 6a,b bar and pie graphs, Supplemental Table 1, WT and 5x analyzed together in Supplemental Data 5).

However, when TREM2 knockout microglia transplanted into the AD model were examined, we found that these cells fail to properly activate with 77% of TREM2 knockout microglia in the AD mice remaining homeostatic and only 1.8% transitioning toward the DAM subtype (~7 fold less than seen in WT cells, Supplemental Data 5, Supplemental Table 1). We additionally note that TREM2 KO microglia show ~2 fold less enrichment of the HLA high cluster. Thus, human TREM2 knockout microglia exhibit a similar impairment in the response to beta-amyloid pathology as murine microglia, although the precise gene set of this lost 'DAM' population only partially overlaps (~12%) with that of the murine counterpart(Hasselmann et al., 2019).

TREM2 knockout microglia do not form DAMs *in vivo.* Because our single-cell sequencing was performed with only one animal per genotype to provide a discovery-based approach and because RNA does not always directly correlate with protein

expression(De Jager et al., 2018), next we sought to corroborate our results by examining protein expression in a larger cohort of mice. To validate our findings that CD9 expression (marker of the DAM cluster(Hasselmann et al., 2019)) primarily increased in WT cells (not TREM2 KO) in the AD model brain (not WT) we performed flow cytometry for CD9 in all 4 sets of animals (MITRG + WT, MITRG + KO, 5x-MITRG + WT, 5x-MITRG + KO). Again, we used co-transplanted animals and thus cells from the same brain could be separated by GFP or RFP expression to denote TREM2 genotype (Fig. 6c, left). This analysis confirmed that non-diseased animals (MITRG) express very low levels of CD9 protein. We also confirm that CD9 levels are significantly higher for WT cells in an AD-model brain (5x-MITRG) than KO cells from the same brain. Indeed, there is no significant difference in the number of CD9 positive “DAMs” for KO cells in the non-diseased and AD-model brains (Fig. 6c). This, again, suggests that TREM2 KO cells are locked in a homeostatic state despite exposure to beta-amyloid pathology. Since these cells are isolated from co-transplanted brains of WT and KO cells, these results suggest that the presence of activated WT cells is not sufficient to induce a DAM phenotype in nearby KO cells.

To further validate and confirm our single cell sequencing and flow cytometry results at the anatomical level, brain slices from the cortex of the same co-transplanted mice were examined. Expression of HLA and DAM markers increase specifically around beta-amyloid plaques, consistent with our recent publication(Hasselmann et al., 2019). We highlight that TREM2 knockout microglia (GFP) do not exhibit the typical plaque-associated increase in expression of HLA markers (Fig. 6d, HLA-DRB1) or DAM markers (Fig. 6e, CD9) as seen with WT cells (RFP), consistent with the notion that TREM2 knockout cells are locked into a more homeostatic phenotype. Importantly, mice

transplanted with the opposite combination of GFP/RFP cells show an equivalent loss of CD9 and HLA-DRB1 in TREM2 KO (RFP) microglia (Supplemental Fig. 6). Together, these data robustly show that human TREM2 knockout microglia fail to activate in response to beta-amyloid plaques *in vivo.*

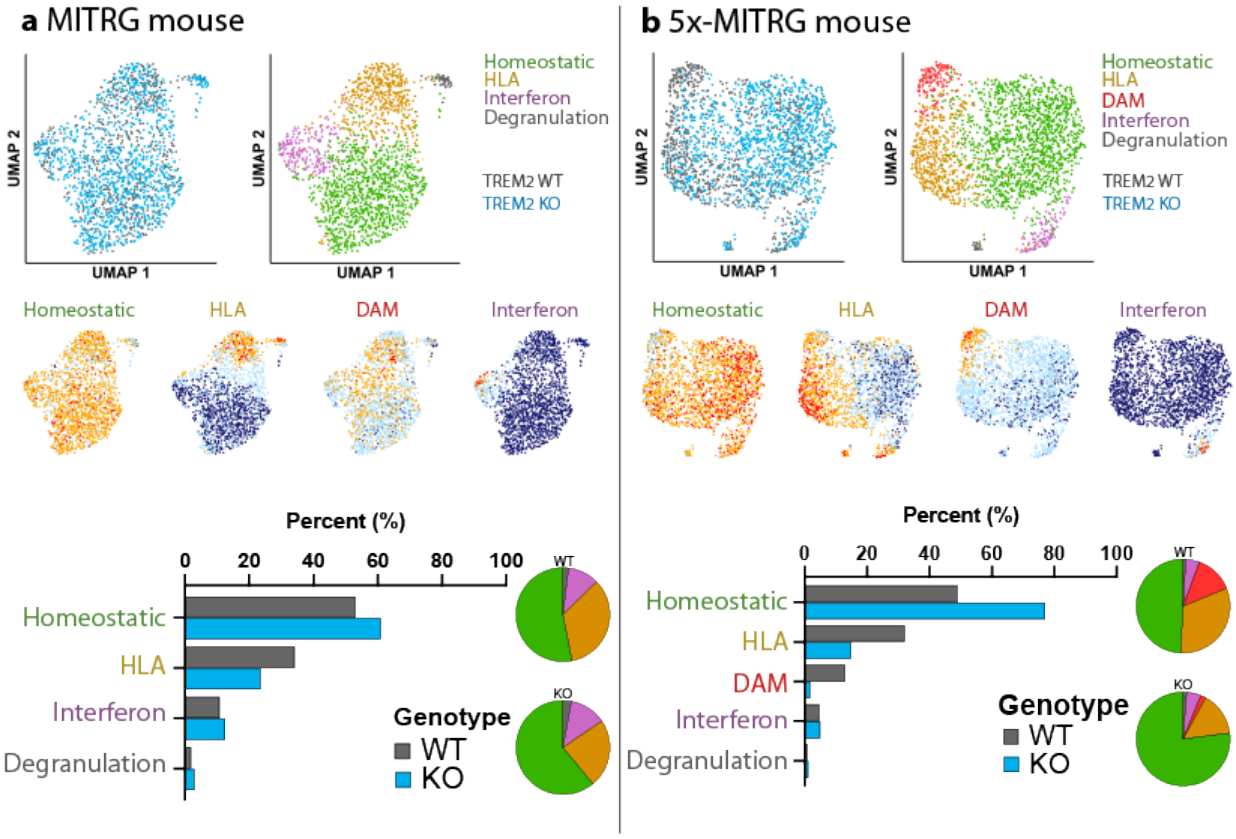
a MITRG mouse
b 5x-MITRG mouse
UMAP 1
UMAP 2
Homeostatic
HLA
DAM
Interferon
Degranulation
TREM2 WT
TREM2 KO
Percent (%)
0
20
40
60
80
100
WT
KO
Genotype

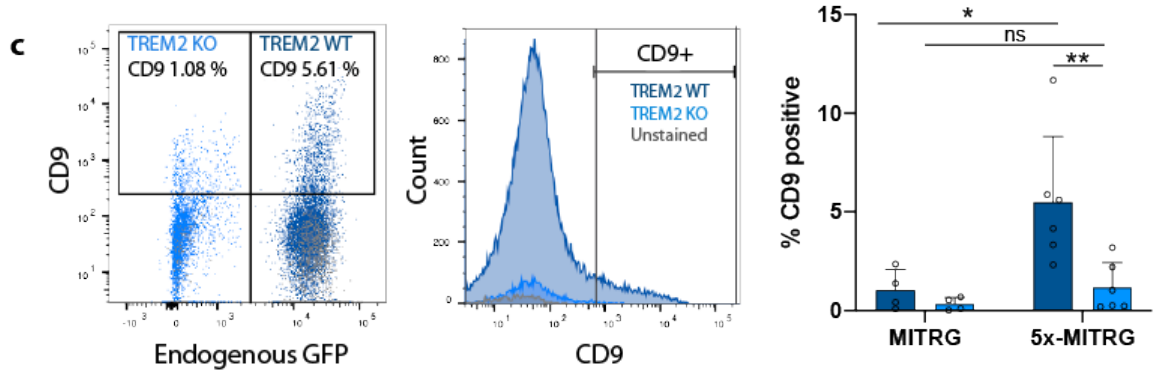
c
TREM2 KO
CD9 1.08 %
TREM2 WT
CD9 5.61 %
CD9
Endogenous GFP
CD9+
TREM2 WT
TREM2 KO
Unstained
Count
CD9
% CD9 positive
*
ns
**
MITRG
5x-MITRG

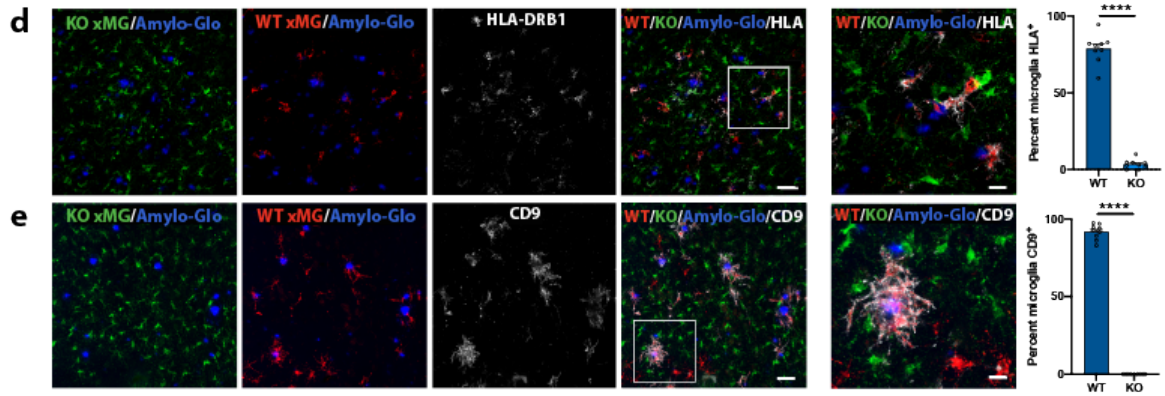
d
KO xMG/Amylo-Glo
WT xMG/Amylo-Glo
HLA-DRB1
WT/KO/Amylo-Glo/HLA
Percent microglia HLA+
****
WT
KO
e
CD9
WT/KO/Amylo-Glo/CD9
Percent microglia CD9+

Figure 2.6. Deletion of TREM2 suppresses the development of disease-associated microglia (DAMs) in vivo. UMAP plots from WT and TREM2 knockout microglia transplanted into a **a** MITRG or **b** 5x-MITRG mouse. Top left shows the TREM2 genotype of each cell in the plot (gray = WT, blue = TREM2 KO) and the adjacent UMAP shows the clustering of human microglia sub-populations in non-diseased mice. Pie charts highlight the relative distribution of each TREM2 genotype within each cluster. The lower four UMAP plots demonstrate the relative expression of known homeostatic (green), human leukocyte antigen (HLA, yellow), interferon (pink), and DAM (red) markers. Homeostatic:CX3CR1, P2RY12, P2RY13, TMEM119, SALL1. HLA: HLA-DRA, HLA-DRB1, HLA-DRB5, HLA-DPA1, HLA-DPB1, HLA-DMA, HLA-DQA1, HLA-DQA2, HLA-DQB1, CD74. Interferon:IFIT1, IFIT2, ISG15, IFI6, IFITM3, MX1, MX2, STAT1. DAM: CD9, TREM2, SPP1, ITGAX, CD83, APOC1, LGALS3. Bar graphs show relative cluster percentages for each cell type. **c** Flow cytometry of co-transplanted TREM2 WT and KO microglia. Left dot plot shows GFP positive WT microglia (and GFP negative KO microglia) expression of CD9. Middle plot shows the same data as a histogram pre-split on RFP/GFP expression. As in (**a**), expected % CD9+ cells is around 5–10%. Right plot shows the quantification of all animals $n = 6$ independent 5x-MITRG mice and 4 MITRG mice. (two way ANOVA with Tukey post hoc test, $*p = 0.018$; $**p = 0.0099$, ns $p = 0.916$). Data are represented as mean values±SEM. Gating strategy in Source data file. **d** Histological analysis of human microglia within the 5x-MITRG mouse confirms TREM2 WT microglia (RFP+) express higher levels of the activation markers **d** HLA-DRB1 (gray) and **e** CD9 than TREM2 knockout microglia (GFP+). Reverse permutation of WT/KO shown in Supplementary Fig. 6. Scale bar low power: 40μm high power: 10μm (n=9 individual mice per genotype with 4 images per mouse. unpaired t-test two-tailed $****p < 0.0001$). Transplants were completed with one isogenic set. Data are represented as mean values±SEM.

Discussion

By combining TREM2 stimulation and RNA sequencing we were able to improve our understanding of the downstream genetic targets of TREM2 signaling (Fig. 1). By using an anti-human TREM2 antibody to specifically stimulate TREM2 downstream signaling cascades. With this stimulus, we have uncovered TREM2-specific transcript alterations that were enriched for gene sets related to cellular migration and survival. Because these experiments were carried out using human cells and stimulation of human TREM2, our RNA-sequencing data may also prove useful to investigators seeking to better understand

the potential therapeutic application of TREM2 stimulating antibodies that have recently began testing in early stage clinical trials.

Consistent with our sequencing results with functional experiments, we have further highlighted viability differences in our TREM2 isogenic microglia. Even without any stimulation or stress, TREM2 knockout microglia show lower viability (Fig. 2b). When additional stressors such as loss of growth factors are added, this phenotype is exacerbated (Fig. 2a,c). Furthermore we confirm that depletion of CSF1R signaling alone is sufficient to replicate this response.

Guided by our sequencing results, we also examined the microglial phagocytosis of APOE (Fig. 3a,b). Previous studies examining how APOE isoforms interact with TREM2 have been inconsistent. For example, Atagi et al. found that TREM2 binds all APOE isoforms with similar affinity, whereas Bailey et al. found that TREM2 showed the highest affinity for APOE4 above APOE3 or APOE2(Atagi et al., 2015; Bailey et al., 2015). Here, we were able to demonstrate that APOE variants are recognized and engulfed by human microglia at different rates with APOE4 > APOE3 > APOE2. However, whether or not this result contributes to the known effect of APOE on disease risk remains unclear. Of further interest, we find that microglia lacking TREM2 do not internalize any APOE. This occurs despite normal expression of canonical APOE receptors (no difference from WT lines by RNA-sequencing). Together, this data suggests that TREM2 is necessary for microglial responses to APOE and may even be the only functional APOE receptor on human microglia.

We have also investigated microglial responses to other disease-relevant stimuli through phagocytosis. We show that TREM2 knockout microglia perform less

phagocytosis of human synaptosomes and beta-amyloid but not zymosan A and that this phenotype occurs partially via decreased signaling through SYK in KO cells (Fig. 1,3). While dectin-1 stimulation (by zymosan A) does induce phosphorylation of SYK, it has been shown that the resulting phagocytosis is independent of SYK(Schorey and Lawrence, 2008; Underhill et al., 2005). We corroborate this data by showing that phagocytosis of zymosan A is unchanged by the presence of SYK inhibitor R406 (Fig. 3e). Thus, we conclude that TREM2 knockout lines are deficient only in SYK-dependent phagocytosis. This pathway makes intuitive sense given that TREM2 signal transduction includes phosphorylation of SYK (Fig. 1f,g) which we suggest is necessary for a normal phagocytic response in these disease-relevant conditions.

While decreased synaptic phagocytosis in TREM2 knockout microglia (modeled here with synaptosomes) may be surprising given that synaptic over-pruning is hypothesized to worsen AD progression, similar results have been shown in murine microglia(Filipello et al., 2018; Hong et al., 2016b). Additionally, it is possible that the ligand binding domain TREM2 mutations most strongly associated with AD, may not alter the recognition of this specific phagocytic substrate in the same way as a loss-of function deletion. Additionally, TREM2 function in synaptic pruning may be isolated to developmental stages *in vivo.* It has recently been shown in mice that TREM2 knockout results in hyper-connectivity in the brain and indeed lower expression of TREM2 is correlated with increased prevalence of autism spectrum disorder(Filipello et al., 2018).

Based on our RNA sequencing results and previous research in the field, we next investigated the role of TREM2 in motility and directed migration. By combining studies of human microglia both *in vitro* and *in vivo,* we conclude that TREM2 knockout microglia

fail to migrate towards beta-amyloid as well as beta-amyloid producing neurons and astrocytes (Fig. 4). We also report, that expression of the chemoattractive receptor, CXCR4, is diminished in TREM2 knockout microglia and exposure to its ligand, SDF-1α, uncovers a significant deficit in the calcium response to this ligand, suggesting that loss of CXCR4 signaling likely contributes to the impaired migration of TREM2 knockout microglia to beta-amyloid plaques (Fig. 5). To corroborate these data, we show that blocking CXCR4 signaling with AMD3100 is sufficient to prevent migration of WT microglia towards beta-amyloid producing neurons and astrocytes (Fig. 5d). This suggests that CXCR4 signaling may offer a potentially useful therapeutic target to re-mobilize microglia towards amyloid plaques and degenerating neurons.

Of interest, SDF-1α as well as other endogenous CXCR4 ligands including Ubiquitin and macrophage migration inhibitory factor (MIF) have been shown to be increased in AD brain tissue particularly around plaques, co-localizing with dystrophic neurons and within murine DAM populations(Harris et al., 2020; Lee et al., 2011; Saini et al., 2010; Zhang et al., 2019). This further highlights the need for exploration of the role of CXCR4 in microglial migration in disease particularly as a potential therapeutic for patients with mutations in TREM2.

Lastly, because microglial function and gene expression are greatly influenced by other cell types and environmental factors in the brain, we performed xenotransplantation of human microglia into the murine brain. Previous studies have shown that activation of microglia with a strong pro-inflammatory stimuli (eg. LPS) decreases TREM2 expression hinting that levels of TREM2 may be a crucial indicator of microglial activation(Zhou et al., 2019). Conversely, TREM2 expression increases in the DAM sub-population found in

AD mice(Keren-Shaul et al., 2017). This microglial profile was delineated by Keren-Shaul et al., 2017 as well as Krasemann et al., 2017 who showed that TREM2 expression is required for transition to this disease-responsive transcriptome signature. However, recent data from our lab shows that the DAM prolife in human microglia is distinct from those shown in Keren-Shaul and Krasemann's murine DAMs(Hasselmann et al., 2019), thus bringing into question whether human TREM2 similarly prevents human DAM formation *in vivo.* We therefore performed *xeno*transplantation of human TREM2 isogenic microglia and were able to examine responses of WT and TREM2 KO microglia in both AD-model and non-diseased mice. This investigation allowed us to demonstrate that TREM2 knockout microglia are generally locked in a homeostatic state and unable to adopt a DAM transcriptomic state. Interestingly, we note that this is the case not only in AD model mice but also in non-diseased states as well, suggesting that deficits in TREM2 signaling intrinsically affect human microglia responses, though this effect is greatly exacerbated in disease.

These experiments replicated the same human microglial clusters published in Hasslemann and Coburn et al. 2019 and reveal that TREM2 is partially required for transition into the HLA and DAM clusters in disease. Loss of TREM2 significantly increases the percentage of microglia present in the homeostatic cluster at the expense of these clusters (Fig. 6) which we confirmed by both flow cytometry and immunohistochemistry. Whether or not this result causes the migration deficit (lack of DAM activation produces a lack of migration) or occurs as a result of this deficit (lack of migration to plaques results in fewer DAMs) is not yet understood. However, we do see CXCR4 expression highly expressed in the human DAM population and decreased in

TREM2 KO microglia (Fig. 5, Supplemental Data 4), suggesting that TREM2 is required to elicit CXCR4-dependent migration toward plaques and the subsequent adoption of a DAM state.

Of further interest, depending on how we set clustering of the single cell sequencing data, we uncovered an additional TREM2-dependent shift in a cluster of p53 apoptotic/senescent microglia (65% of genes associated with p53 including 40.5% of the population known to be direct targets of p53). These cells are likely either senescent or at the earliest stages of cell death, since fully dead cells are removed within the sequencing analysis pipeline (see methods). This senescent cluster was only observed in 5x-MITRG samples and was enriched almost 10-fold in TREM2 knockout microglia (0.6% of WT cells, 5.8% of TREM2 knockout cells) (Supplemental Fig. 7). This finding closely parallels our *in vitro* data (Fig. 1e,i, Fig. 2) which has also implicated p53 signaling and showed that TREM2 knockout microglia are hyper-sensitive to stress, inducing apoptosis at a much higher rate than WT cells. However, we were unable to identify human-specific antibodies to confirm this population by histology and thus re-clustered our data to include only verified clusters. It is also possible that we do not see this cluster *in vivo* because it is an artifact of the isolation protocol, though that does not seem to be the entire explanation given that this cluster appears only in 5x-MITRG samples and not the non-diseased animals which were isolated in parallel. Thus, we posit that human TREM2 deficient cells exposed to Alzheimer's pathology may be more sensitive to isolation.

Together, the data in this manuscript highlight the utility of combining *in vitro* and *in vivo* analysis to produce complementary datasets in order to better understand the complex mechanisms of microglial biology. We present evidence of TREM2 involvement in CSF1R-dependent survival, SYK-dependent phagocytosis of synaptosomes, beta-amyloid, and APOE, CXCR4-dependent migration, and formation of the human DAM response. These molecular studies have elucidated microglial processes and receptors that may be important in the progression of AD. Future studies will be needed to understand which of these mechanisms underlie the risk incurred by loss of TREM2 function before they can be studied as potential therapeutic targets for the treatment of neurodegenerative diseases.

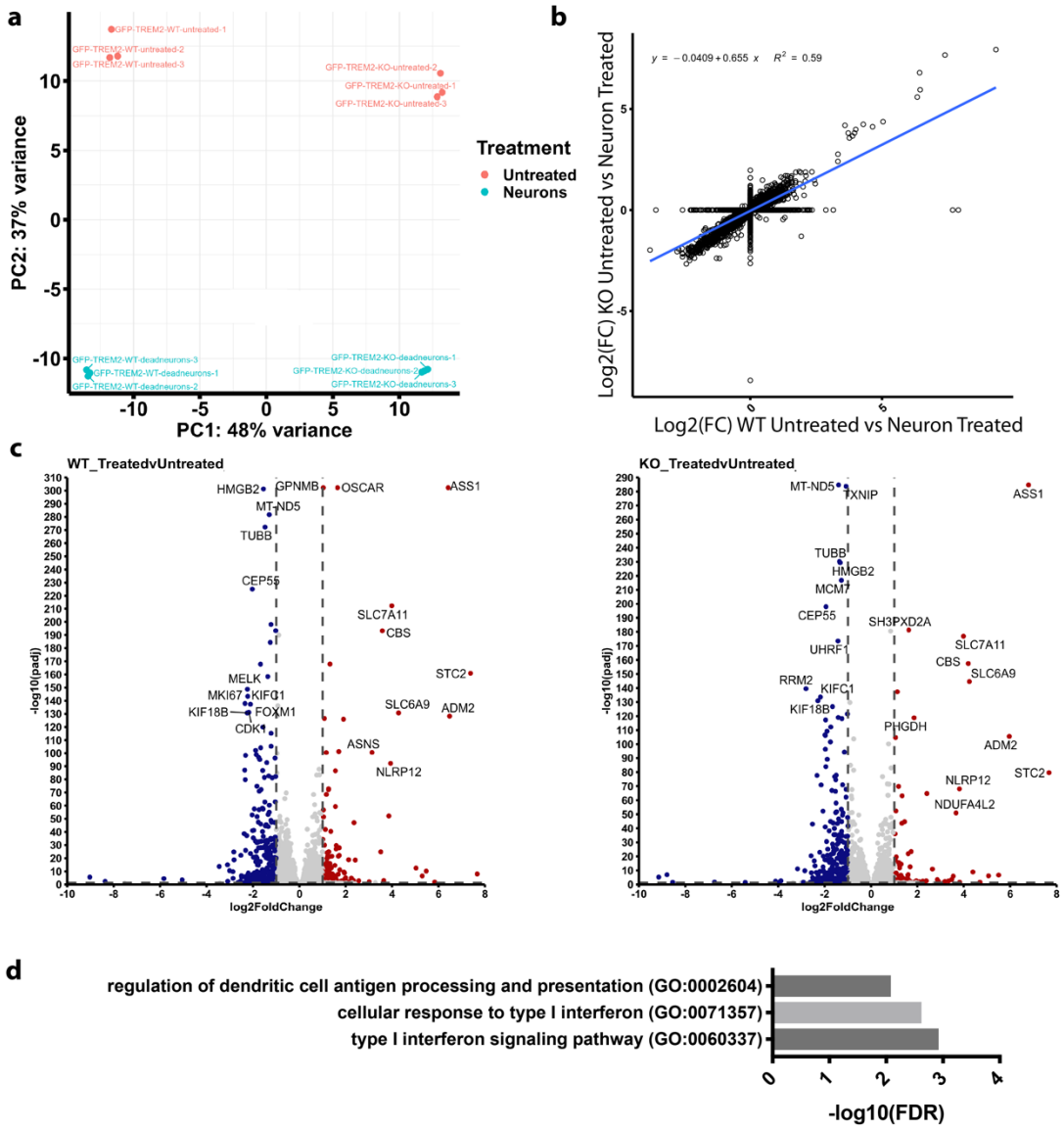

Figure S2.1. Neuron treatment of isogenic microglia. **a** In iPS-Microglia treated with dead neurons, both WT and TREM2KO lines respond with similar magnitudes. The first two principal components (PC) are split on WT vs KO and treated vs untreated. Note that TREM2 knockout lines appear to respond with equal magnitude as their WT counterparts. **b** Linear regression on WT cells treated with neurons vs KO cells treated with neurons reveals alignment of the transcriptome response (R-squared 0.59). **c** Volcano plots of differentially expressed genes between untreated vs treated TREM2 WT cells (left) and TREM2 KO cells (right) show majorly the same transcript alterations. **D** Reciprocally changed genes between KO and treatment with neurons show only three significantly altered gene ontology groups.

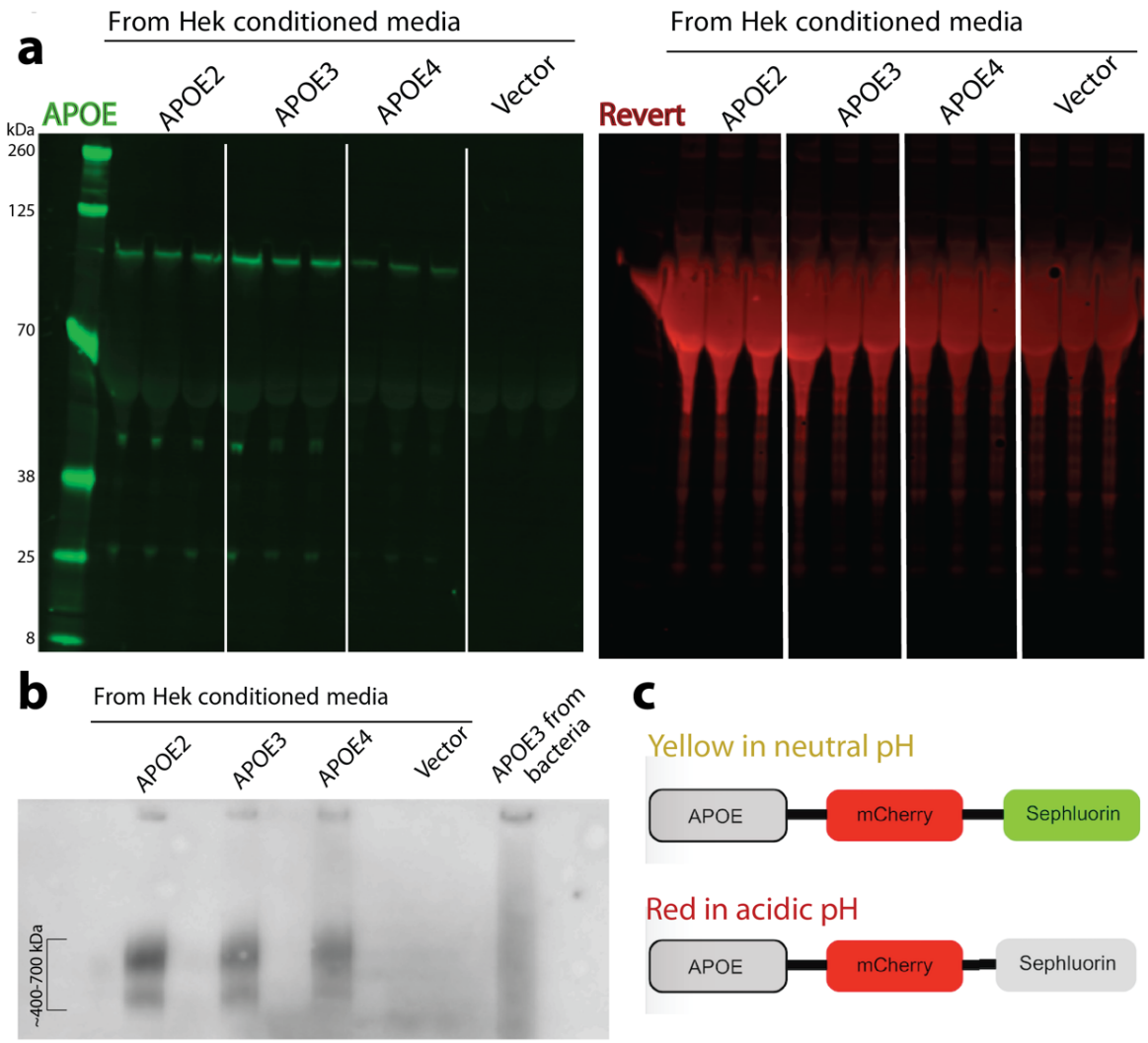

Figure S2.2. APOE from HEK293T cells. Conditioned medium from transfected HEK293T cells was isolated and analyzed by **a** western blot (APOE-green; Revert total protein dye-red) and **b** native gel (Biolegend D6E10). Consistently, APOE4 is secreted at lower levels than APOE 2 and APOE3 as published previously. Microggram amounts of APOE were normalized for experimentation. By native gel, APOE shows the expected double band which suggests proper lipidiation state. Non-lipidated APOE from bacteria is shown as a smear negative control). **C** Schematic of construct used. In neutral pH both mCherry and SEpHlourin are expressed simultaneously resulting in yellow color. In acidic pH, SEpHlourin is quenched and only red signal remains.

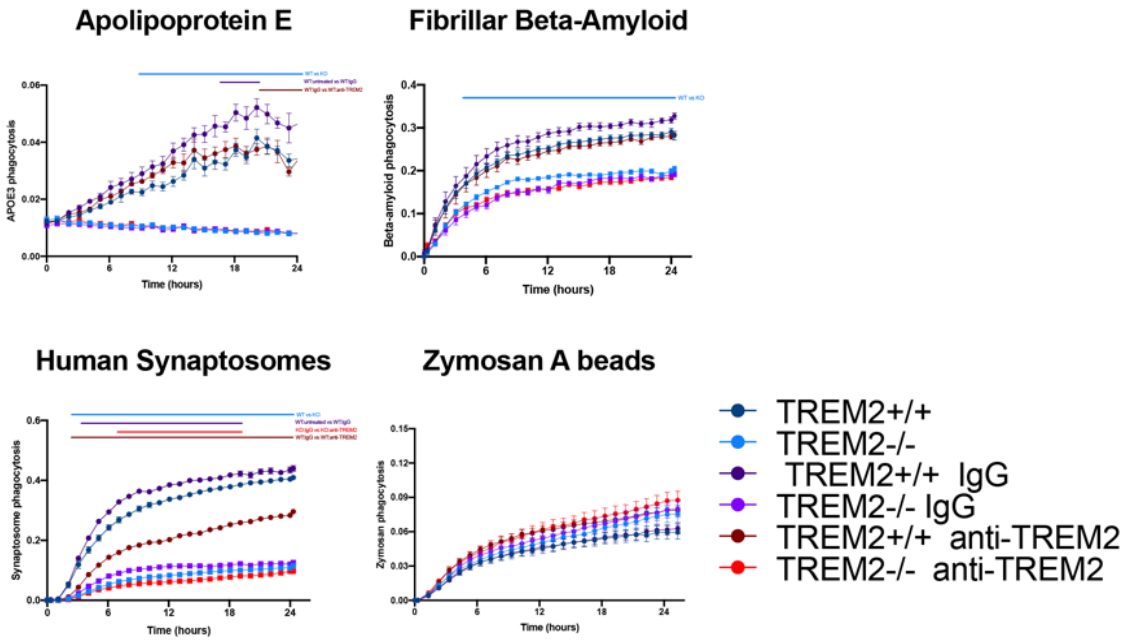

Figure S2.3 Phagocytosis of all substrates after pre-treatment with anti-TREM2 antibody. TREM2 WT (dark colors) and KO (light colors) were pre-treated with 20 ng/mL IgG (purple) or anti-TREM2 (AF1828, red) for 15 min before addition of fluorescent substrates. Bars above data represent significance (p 0.0001; 2-way ANOVA multiple comparisons at each time point). Data are represented as values +/- SEM (n=4 images each from 4 independent wells, experiments were replicated in all three isogenic backgrounds).

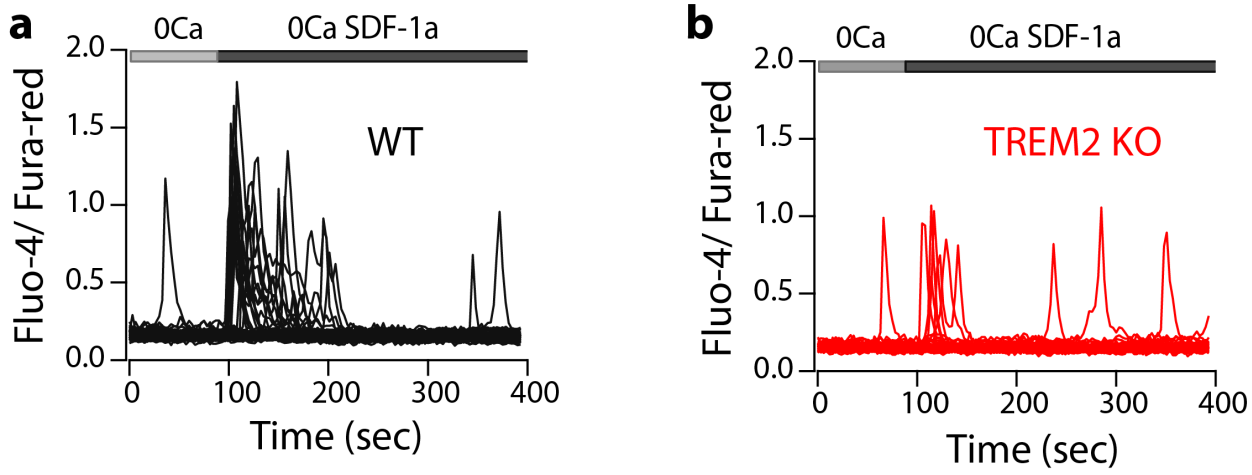

Figure S2.4. Individual cell traces of ratiometric calcium responses to SDF-1a. Representative single-cell traces showing responses to SDF-1a in **a** WT and **b** TREM2 KO microglia. Cells were imaged with Fluo-4 and Fura-Red. (n=111-116; 2 runs).

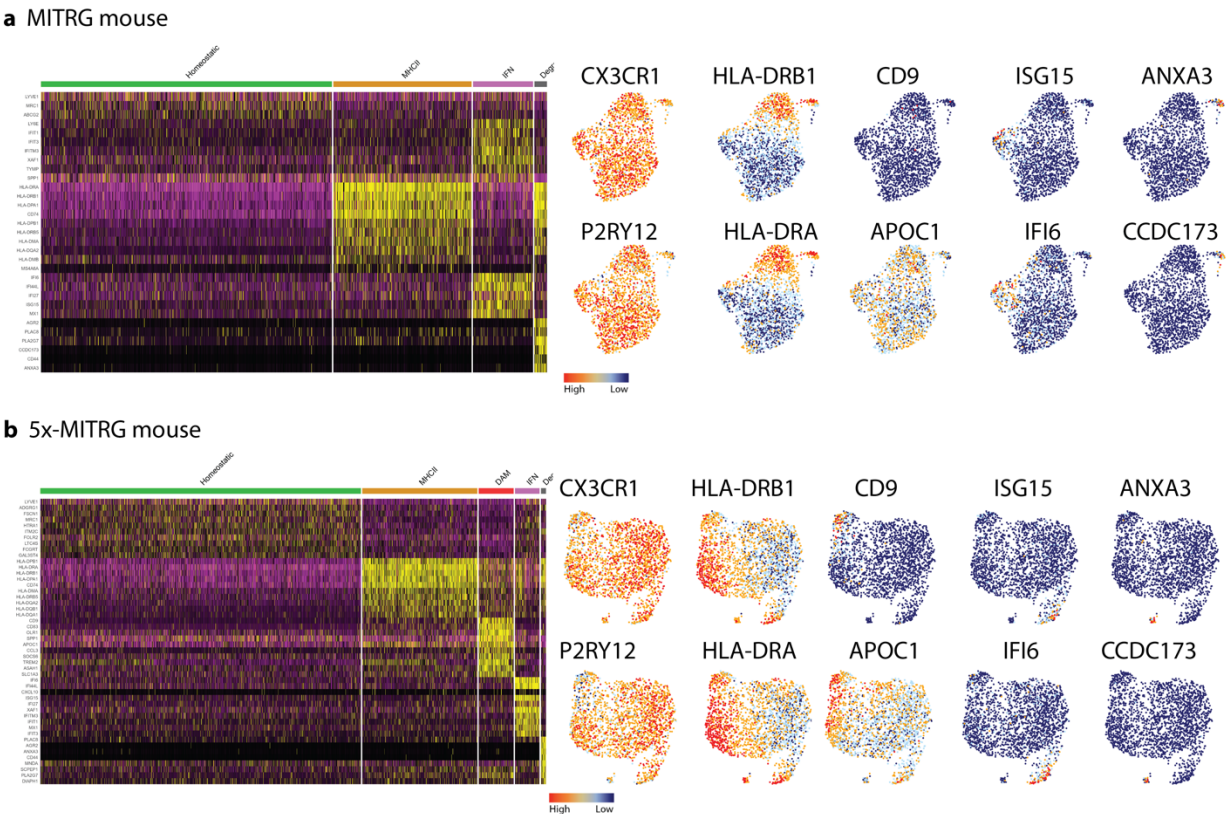

Figure S2.5. Clustering and key gene expression for single-cell sequencing. Heatmaps for **a** MITRG and **b** 5x-MITRG mouse highlight key genes driving differences in clusters. These genes were used to define the naming scheme for each cluster. UMAP expression plots of key genes in each cluster are shown to the left. CX3CR1 and P2RY12 are high for homeostatic clusters. HLA-DRB1 and HLA-DRA are highly expressed in the HLA (MHCII) cluster. CD9 and APOC1 are highly expressed in DAMs. ISG15 and IFI6 are key interferon regulatory genes which are found in the interferon cluster. ANXA3 and CCDC173 demarcate the degranulation cluster.

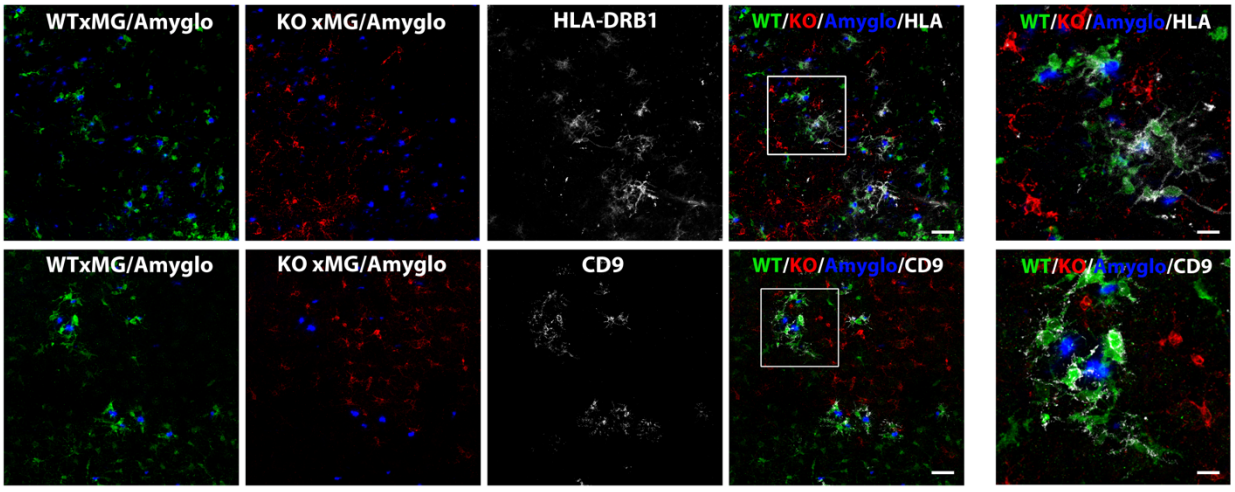

Figure S2.6. CD9 and HLA expression in GFP-WT and RFP-KO lines. Histological analysis of human microglia within the 5x-MITRG mouse confirms TREM2 WT microglia (GFP+) express higher levels of the activation markers HLA-DRB1 (top) and CD9 (bottom) than the TREM2 knockout microglia (RFP+). Scale bar = 40 um for low power images and 10 um for high power images.

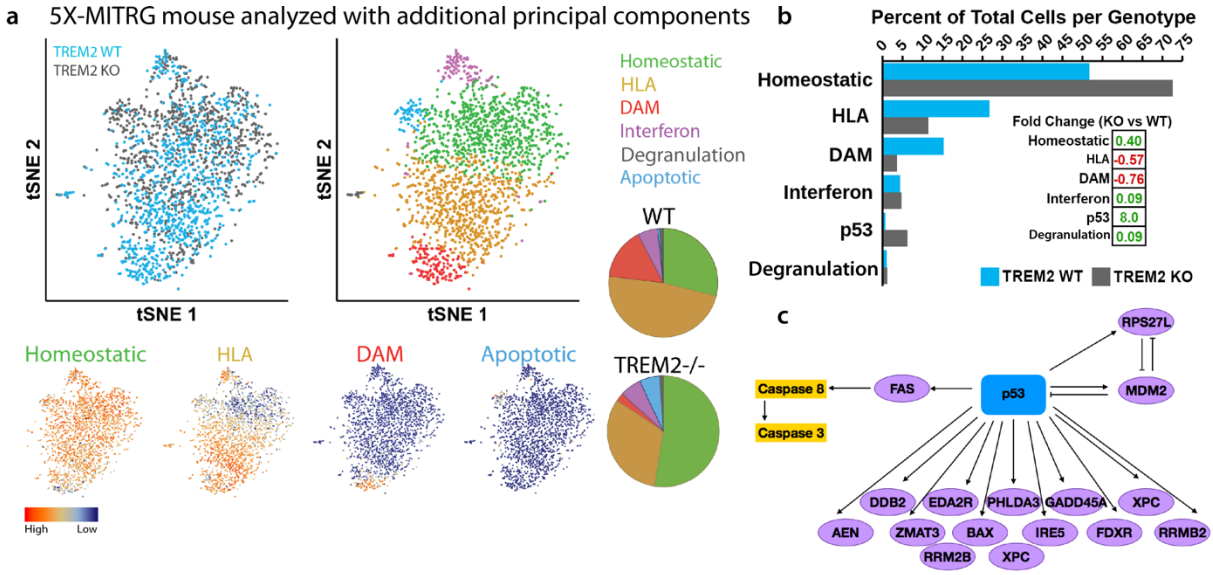

Supplemental Figure 7. Appearance of apoptotic cluster in sequencing analysis. **a** Analysis of single-cell sequencing data with additonal principal components reveals apoptotic cluster. **b** Same data as shown in pie charts in **a** visualized as bar graph and fold-change table Green values are increased in WT cells. Red values are decreased in WT cells compared to TREM2-/- cells. **c** Schematic of genes significantly enriched in the apoptotic cluster (purple) support this cluster as being p53 dependent.

Figure S2.7. Appearance of apoptotic cluster in sequencing analysis. a Analysis of single-cell sequencing data with additional principal components reveals apoptotic cluster. **b** Same data as shown in pie charts visualized as bar graph and fold-change table. Green values are increased in. WT cells. Red values are decreased in WT cells compared to TREM2 KO cells. **c** Schematic of genes significantly enriched in the apoptotic cluster (purple) support this cluster as being p53 dependent.

CHAPTER 3

TREM2 deletion enhances purinergic signaling and regulates calcium-mediated motility and chemotaxis in human microglia

Amanda McQuade, Amit Jairaman, You Jung Kang, Alberto Granzotto, Jean Paul Chadarevian, Sunil Gandhi, Ian Parker, Ian Smitch, Shiva Othy, Mathew Blurton-Jones, Mike Cahalan,

Introduction

As the primary immune cells of the central nervous system, microglia survey their local environment to maintain brain homeostasis and respond to local brain injury or abnormal neuronal activity. Microglia are strongly implicated in several neurodevelopmental and neurodegenerative diseases (Andersen et al., 2021; Crotti et al., 2014; Fahira et al., 2019; Jansen et al., 2019; McQuade and Blurton-Jones, 2019; Pimenova et al., 2020; Tan et al., 2013), warranting further study of human microglial dynamics. Purinergic metabolites (ATP, ADP, UTP, UDP) in the brain constitute key signals driving microglial activation and chemotaxis (Davalos et al., 2005; De Simone et al., 2010; Honda et al., 2001; Koizumi et al., 2007). ATP released from both homeostatic and damaged cells is hydrolyzed locally by nucleosidases such as the ectonucleotidase NTPDase1 (CD39) or pyrophosphatase NPP1 to produce ADP (Dissing-Olesen et al., 2014; Madry and Attwell, 2015; Zhang et al., 2014). ADP is then detected by P2Y purinergic receptors on microglia, causing PLC-mediated Ca^{2+} release from the endoplasmic reticulum (ER) lumen. Ca^{2+} depletion from the ER in turn activates ER STIM1 proteins to translocate proximally to puncta where closely apposed plasma membrane Orai1 channels are activated. This mechanism underlies store-operated Ca^{2+} entry (SOCE) in many cell types (Prakriya and Lewis, 2015), including microglia (Gilbert et al., 2016; McLarnon, 2020; Mizuma et al., 2019).

Purinergic signaling is central to microglial communication with other brain cell types and has been negatively correlated with the onset of Disease Associated Microglia (DAM) transcriptional states (Hasselmann et al., 2019; Keren-Shaul et al., 2017; Krasemann et al., 2017; Olah et al., 2020; Sala Frigerio et al., 2019). P2Y12 and P2Y13 receptors are highly expressed by microglia and are activated predominantly by ADP

(Weisman et al., 2012; Zhang et al., 2014). P2Y12 receptors are essential for microglial chemotaxis and have been implicated in the microglial response to cortical injury (Cserép et al., 2020; Haynes et al., 2006), NLRP3 inflammasome activation (Suzuki et al., 2020; Wu et al., 2019), neuronal hyperactivity and protection(Cserép et al., 2020; Eyo et al., 2014), and blood brain barrier maintenance (Lou et al., 2016). While purinergic receptors have been broadly identified as markers of microglial homeostasis, mechanisms by which receptor expression may drive or maintain homeostatic microglial states remain incompletely understood.

Neuroinflammatory pathologies are often associated with altered Ca^{2+} signaling (Leissring et al., 2000). Microglia, in particular, show altered Ca^{2+} responses in mouse models of Alzheimer's Disease (AD) by mechanisms that are not fully understood (Brawek et al., 2014; Demuro et al., 2010; Mustaly et al., 2018). Ca^{2+} responses to purinergic metabolites have been extensively studied in cultured murine microglia, acute brain slices, and more recently in anesthetized mice (Brawek et al., 2014; Davalos et al., 2005; Eichhoff et al., 2011; Honda et al., 2001; Irino et al., 2008; Milior et al., 2020). However, our understanding of how specific patterns of Ca^{2+} signals in microglia correlate with and tune downstream microglial responses such as cell motility or process extension remains incomplete. There is also a paucity of knowledge on how regulators of purinergic Ca^{2+} signals in microglia might play a role in the dysregulation of Ca^{2+} signaling associated with aging and neuroinflammation.

TREM2 encodes a cell surface receptor that binds a variety of ligands including various lipids, apolipoprotein E (ApoE), and amyloid-beta peptides and signals through its adaptor protein DAP12 to activate a host of downstream pathways (Cheng-Hathaway

et al., 2018; Krasemann et al., 2017; McQuade et al., 2020; Ulrich et al., 2014). Loss of TREM2 function is thought to lock microglia in a more homeostatic-like state (Andrews et al., 2020; Karch et al., 2012b; Krasemann et al., 2017). Indeed, microglia lacking TREM2 expression fail to activate against disease pathology correlating with increased risk of AD (Cheng et al., 2018; Krasemann et al., 2017; McQuade et al., 2020). Purinergic receptor hyperexpression has been reported at the transcriptome level across multiple TREM2 loss of function models including human patient mutations (Gratuze et al., 2020; Hasselmann et al., 2019; Keren-Shaul et al., 2017; Krasemann et al., 2017; McQuade et al., 2020; Sala Frigerio et al., 2019), although the mechanistic link between purinergic receptor expression and TREM2 function remains poorly understood.

We previously developed methods to generate human iPSC-derived microglia (iPSC-microglia) (Abud et al., 2017; McQuade et al., 2018), which can be used to model human microglial behavior *in vitro*. While iPSC-derived microglia are proving increasingly useful to investigate neurodegenerative disorders (Andreone et al., 2020; Cosker et al., 2021; Konttinen et al., 2019; Piers et al., 2019; Reich et al., 2021), Ca^{2+} signaling has not yet been extensively profiled in these models. In this study, we examined purinergic Ca^{2+} signaling in human iPSC-microglia and found that sustained Ca^{2+} influx in response to ADP regulates microglial process extension, motility speed, and turning behavior. We show that microglia lacking TREM2 are hyperresponsive to purinergic signaling. As a result, TREM2 KO microglia travel in straighter paths though they also exhibit a defect in directional chemotaxis, potentially due to their inability to sense gradients. Using novel iPSC-microglia lines that express a ratiometric genetically encoded Ca^{2+} probe, Salsa6f (Dong et al., 2017), we found that motility of wild-type (WT)

and TREM2 knockout (KO) human microglia is differentially tuned by Ca^{2+} signaling. Informed by these discoveries, we were able to rescue chemotactic deficiencies in TREM2 KO microglia by manipulating purinergic receptor signaling.

Materials and Methods

Generation of iPSCs from human fibroblasts

Human induced pluripotent stem cell lines were generated by the University of California, Irvine Alzheimer's Disease Research Center (UCI ADRC) Induced Pluripotent Stem Cell Core from subject fibroblasts under approved Institutional Review Boards (IRB) and human Stem Cell Research Oversight (hSCRO) committee protocols. Informed consent was received from all participants who donated fibroblasts. Reprogramming was performed with non-integrating sendai virus in order to avoid integration effects. To validate new iPSC lines, cells were karyotyped by G-banding and tested for sterility. Pluripotency was verified by Pluritest Array Analysis and trilineage in vitro differentiation. Additional GFP- and RFP-αtubulin expressing iPSC lines (AICS-0036 and AICS-0031-035) were purchased from Corriel and originally generated by Dr. Bruce Conklin. iPSCs were grown antibiotic free on Matrigel (Corning) in complete mTeSR1 or TeSR-E8 medium (StemCell Technologies) in a humidified incubator (5% CO_2, 37° C). All lines will be available upon request to the corresponding author.

CRISPR-mediated knockout of TREM2

Genome editing was performed as in (McQuade et al., 2020). Briefly, iPSCs were nucleofected with RNP complex targeting the second exon of TREM2 and allowed to

recover overnight. Transfected cells were dissociated with pre-warmed Accutase then mechanically plated to 96-well plates for clonal expansion. Genomic DNA from each colony was amplified and sequenced at the cut site. The amplification from promising clones was transformed via TOPO cloning for allelic sequencing. Knockout of TREM2 was validated by western blotting (AF1828, R&D) and HTRF (Cisbio) (McQuade et al., 2020).

iPSC-microglia differentiation

iPSC-microglia were generated as described in (McQuade et al., 2018). Briefly, iPSCs were directed down a hematopoetic lineage using the STEMdiff Hematopoesis kit (StemCell Technologies). After 10-12 days in culture, CD43+ hematopoteic progenitor cells are transferred into a microglia differentiation medium containing DMEM/F12, 2× insulin-transferrin-selenite, 2× B27, 0.5× N2, 1× glutamax, 1× non-essential amino acids, 400 µM monothioglycerol, and 5 µg/mL human insulin. Media was added to cultures every other day and supplemented with 100 ng/mL IL-34, 50 ng/mL TGF-β1, and 25 ng/mL M-CSF (Peprotech) for 28 days. In the final 3 days of differentiation 100 ng/mL CD200 (Novoprotein) and 100 ng/mL CX3CL1 (Peprotech) were added to culture.

Confocal Laser Scanning Microscopy

Unless otherwise stated, cells were imaged on an Olympus FV3000 confocal laser scanning inverted microscope equipped with high speed resonance scanner, IX3-ZDC2 Z-drift compensator, 40x silicone oil objective (NA 1.25) and a Tokai-HIT stage top incubation chamber (STXG) to maintain cells at 37°C. To visualize Salsa6f, 488 nm and

561 nm diode lasers were used for sequential excitation of GCaMP6f (0.3% laser power, 450V channel voltage, 494-544nm detector width) and TdTomato (0.05% laser power, 450V channel voltage, 580-680nm detector width), respectively. Fluo-4 and Fura-red were both excited using a 488 nm diode laser (0.07% laser power, 500V channel voltage, 494-544nm detector width for Fluo-4; 0.07% laser power, 550V channel voltage, 580-680nm detector for Fura-Red). Two high-sensitivity cooled GaAsP PMTs were used for detection in the green and red channels respectively. GFP was excited using the same settings as GCaMP6f. Other image acquisition parameters unique to Ca^{2+} imaging, microglia process and cell motility analysis are indicated in the respective sections.

Measurement of intracellular Ca^{2+}

Cell preparation: iPSC-microglia were plated on fibronectin-coated (5 µg/mL) glass-bottom 35 mm dishes (MatTek, P35G-1.5-14-C) overnight at 60 % confluence. Ratiometric Ca^{2+} imaging was done using Fluo-4 AM and Fura-Red AM dyes as described previously(McQuade et al., 2020). Briefly, cells were loaded in microglia differentiation medium with 3 µM Fluo-4 AM and 3 µM Fura-Red AM (Molecular Probes) in the presence of Pluronic Acid F-127 (Molecular Probes) for 30 min at room temperature (RT). Cells were washed with medium to remove excess dye and 1 mM Ca^{2+} Ringer's solution was added to the 35 mm dish before being mounted on the microscope for live cell imaging. We note that iPSC-microglia are sensitive to shear forces and produce brief Ca^{2+} signals in response to solution exchange that are dependent on extracellular Ca^{2+}, and that these are more prominent at 37^{o} C. To minimize these confounding effects, cells were imaged at RT and perfusion was performed gently. Salsa6f-expressing iPSC-microglia were

prepared for Ca^{2+} imaging in the same way as conventional microglia, but without the dye loading steps. The following buffers were used for Ca^{2+} imaging: (1) 1 or 2 mM Ca^{2+} Ringer solution comprising 155 mM NaCl, 4.5 mM KCl, 1 mM $CaCl_2$, 0.5 mM $MgCl_2$, 10 mM glucose, and 10 mM HEPES (pH adjusted to 7.4 with NaOH), (2) Ca^{2+}-free Ringer solution containing: 155 mM NaCl, 4.5 mM KCl, 1.5 mM $MgCl_2$, 10 mM glucose, 1 mM EGTA, 10 mM HEPES, pH 7.4. Live cell imaging was performed as described earlier. Cells were treated with ADP as indicated in the results section.

Data acquisition: Time-lapse images were acquired in a single Z-plane at 512 x 512 pixels (X = 318.2 µm and Y = 318.2 µm) and at 2-3 sec time intervals using Olympus FV3000 software. Images were time averaged over 3 frames to generate a rolling average and saved as .OIR files.

Data analysis: Time-lapse videos were exported to Fiji- ImageJ (https://imagej.net/Fiji), converted to tiff files (16-bit) and background subtracted. Single-cell analysis was performed by drawing ROIs around individual cells in the field and average pixel intensities in the green and red channels were calculated for each ROI at each time-point. GCaMP6f/ TdTomato (G/R Ratio) and Fluo-4/Fura-Red ratio was then obtained to further generate traces showing single-cell and average changes in cytosolic Ca^{2+} over time. Single-cell ratio values was used to calculate Peak Ca^{2+} signal and responses at specific time points after agonist application. Peak Ca^{2+} signal for each cell was baseline subtracted, which was calculated as an average of 10 minimum ratio values before application of agonist.

Microglia process extension analysis

Data acquisition: GFP-expressing iPSC-microglia were plated overnight on 35 mm glass bottom dishes at 40-50% confluence. Cells were imaged by excitation of GFP on the confocal microscope at 37^{o} C as described earlier. To study process extension in response to ADP, two sets of GFP images were obtained for each field of view across multiple dishes: before addition of ADP (baseline) and 30 min after application of ADP. Images were acquired as a Z-stack using the Galvo scanner at Nyquist sampling. Adjacent fields of view were combined using the Stitching function of the Olympus FV3000 Software and saved as .OIR files.

Process Analysis: The basic workflow for microglia process analysis was adapted from Morrison et al, Sci. Rep, 2017 (Morrison et al., 2017). Image stacks (.OIR files) were exported to Fiji- Image J and converted into 16-bit Tiff files using the Olympus Viewer Plugin (https://imagej.net/OlympusImageJPlugin). Maximum intensity projection (MIP) image from each Z-stack was used for further processing and analysis. MIP images were converted to 8-bit grey scale images, to which a threshold was applied to obtain 8-bit binary images. The same threshold was used for all sets of images, both before and after ADP application. Noise reduction was performed on the binary images using the Process -> Noise -> Unspeckle function. Outlier pixels were eliminated using Process -> Noise -> Outliers function. The binary images were then skeletonized using the Skeletonize2D/3D Plugin for Image J (https://imagej.net/plugins/skeletonize3d). Sparingly, manual segmentation was used to separate a single skeleton that was part of two cells touching each other. The Analyze Skeleton Plugin (https://imagej.net/plugins/analyze-skeleton/) was then applied to the skeletonized images to obtain parameters related to process

length and number of branches for each cell in the imaging field. Processes were considered to be skeletons > 8 µm. The data was summarized as average process length and number of branches, before and after ADP application for a specific imaging field, normalized to the number of cells in the field which allowed for pairwise comparison. Additionally, single cell data from all cell across all experiments was compared in some instances.

IP_3 uncaging

Whole-field i-IP_3 uncaging and mechanical stimulation were performed as previously described (Lock et al., 2016) with minor modifications. Briefly, iPSC-microglia were loaded for 20 min at 37° C with either Cal520 AM or Cal590 AM (5 µM, AAT Bioquest), and the caged i-IP_3 analog ci-IP_3/PM (1 µM, SiChem) plus 0.1% Pluronic F-127 in Microglia Basal Medium. Cells were washed and incubated in the dark for further 30 min in a HEPES-buffered salt solution (HBSS) whose composition was (in mM): 135 NaCl, 5.4 KCl, 1.0 MgCl2, 10 HEPES, 10 glucose, 2.0 $CaCl_2$, and pH 7.4. Intracellular Ca^{2+} ($[Ca^{2+}]_i$) changes were imaged by employing a Nikon Eclipse T*i* microscope system (Nikon) equipped with a 40x oil immersion objective (N.A.: 1.3; Nikon) and an Orca Flash 4.0LT CMOS camera (Hamamatsu). Cal520 or Cal590 were excited by a 488 or a 560 nm laser light source (Vortran Laser Technologies), respectively. i-IP3 uncaging was achieved by uniformly exposing the imaged cells to a single flash of ultraviolet (UV) light (350-400 nm) from a Xenon arc lamp. UV flash duration, and thus the amount of released i-IP_3, was set by an electronically controlled shutter.

Image acquisition and analysis were performed by using Metamorph (Molecular Devices) or Nikon NIS (Nikon) software. After conversion to stack tiff files, image sequences were analyzed with Flika, a custom-written Python-based imaging analysis software (https://flika-org.github.io/; (Ellefsen et al., 2014)). After background subtraction, either Cal520 and Cal590 fluorescence changes of each cell were expressed as $\Delta F/F_0$, where F_0 is the basal fluorescence intensity and ΔF the relative fluorescence change ($F_x - F_0$). Data are reported as superplots (Lord et al., 2020) of at least three independent replicates. Experiments were reproduced with two independent lines.

Comparisons were performed by unpaired non-parametric t-test (for experiments testing a single UV flash stimulus), two-way ANOVA followed by Tukey's post-hoc test (assuming normal distribution of data; for experiments testing multiple UV flash durations), and the "N-1" Chi-squared test (for the experiments comparing the % of responding cells to single cell i-IP3 uncaging or mechanical stimulation; https://www.medcalc.org/calc/comparison_of_proportions.php).

Immunocytochemistry

Cells were fixed with 4 % paraformaldehyde for 7 min and washed 3x with 1X PBS. For P2RY12, plates were pre-treated with citrate buffer (pH 6.0) for 20 min 95° C. Blocking was performed at room temp for 1 hr in 5 % Goat Serum, 0.1 % Triton5 X-100. Primary antibodies were added at 1:200 overnight 4° C (P2RY12; HPA014518 Sigma) (P2RY13; APR-017, Alomone). Plates were washed 3x before addition of secondary antibodies (Goat anti-Rabbit 488/555, ThermoFisher Scientific) and Hoeschst (ThermoFisher

Scientific). Images were captured on an Olympus FV3000RS confocal microscope with identical laser and detection settings. Images were analyzed with IMARIS 9.7.0 software.

Scratch wound assay

Nondirectional motility was analyzed using Essen Incucyte WoundMaker. iPSC-microglia were plated on fibronectin (StemCell Technologies) at 90% confluence. Scratches were repeated 4x to remove all cells from the wound area. Scratch wound confluency was imaged every hour until scratch wound was closed (15 hrs). Confluence of cells within the original wound ROI was calculated using IncuCyte 2020C software.

IMARIS Cell Tracking

For motility assays, iPSC-microglia were tracked using IMARIS 9.7.0 software. For videos of GFP lines, cells were tracked using spot identification. For videos of Salsa6f lines, surface tracking was used to determine ratiometric Ca^{2+} fluorescence and motility per cell. In both conditions, tracks were defined by Brownian motion with the maximum distance jump of 4 microns and 10 frame disturbance with no gap filling. Tracks shorter than 3 minutes in length were eliminated from analysis. After automated track formation, tracks underwent manual quality control to eliminate extraneous tracks, merge falsely distinct tracks, and add missed tracks. After export, data was plotted in Prism 9.1.0 or analyzed in excel using DiPer macros for Plot_At_Origin and mean squared distance (Gorelik and Gautreau, 2014).

Generation of Salsa6f-expressing iPSC lines

iPSCs were collected following Accutase enzymatic digestion for 3 min at 37° C. 20,000 cells were resuspended in 100 µL nucleofection buffer from Human Stem Cell Nucleofector™ Kit 2 (Lonza). Salsa6f-AAVS1 SHL plasmid Template (2 µg; Vector Builder) and RNP complex formed by incubating Alt-R® S.p. HiFi Cas9 Nuclease V3 (50 µg; IDTDNA) was fused with crRNA:tracrRNA (IDTDNA) duplex for 15 min at 23° C. This complex was combined with the cellular suspension and nucleofected using the Amaxa Nucleofector program B-016. To recover, cells were plated in TeSR™-E8™ (StemCell Technologies) media with 0.25 µM Thiazovivin (STEMCELL Technologies) and CloneR™ (StemmCell Technologies) overnight. The following day, cells were mechanically replated to 96-well plates in TeSR™-E8™ media with 0.25 µM Thiazovivin and CloneR™ supplement for clonal isolation and expansion. Plates were screened visually with a fluorescence microscope to identify TdTomato^{+} clones. Genomic DNA was extracted from positive clones using Extracta DNA prep for PCR (Quantabio) and amplified using Taq PCR Master Mix (ThermoFisher Scientific) to confirm diallelic integration of the Salsa6f cassette. A clone confirmed with diallelic Salsa6f integration in the AAVS1 SHL was then retargeted as previously described(McQuade et al., 2020) to knock-out Trem2.

Phagocytosis assay

Phagocytosis of transgenic iPSC-microglia was validated using IncuCyte S3 Live-Cell Analysis System (Sartorius) as in McQuade et al. 2020(McQuade et al., 2020). Microglia were plated 50% confluency 24 hours before substrates were added. Cells were treated with 50 µg/mL pHrodo tagged human AD synaptosomes (isolated as described in

McQuade et al. 2020), 100 ng/mL pHrodo tagged zymosan A beads (Thermo Fisher), 100 ng/mL pHrodo tagged S. Aureus (ThermoFisher), or 2 µg/mL fluorescent beta-amyloid (Anaspec). Image masks for fluorescence area and phase were generated using IncuCyte 2020C software.

Chemotaxis assay

iPSC-microglia were loaded into the angular chamber (2-5K cells/device) to test activation and chemotaxis towards the central chamber containing either ADP (100 ng/mL) or vehicle. When noted, PSB 0739 (10 µM) was added to both the central and angular chamber to inhibit P2RY12. To characterize motility, we monitored the number of recruited microglia in the central chamber for 4 days under the fully automated Nikon TiE microscope (10× magnification; Micro Device Instruments, Avon, MA, USA).

Results

TREM2 knockout microglia show exaggerated Ca^{2+} response to purinergic stimuli

To determine if TREM2 plays a role in microglial Ca^{2+} signaling, we compared cytosolic Ca^{2+} responses to the purinergic agonist ADP in isogenic, CRISPR-modified WT and TREM2 knockout (TREM2 KO) induced pluripotent stem cell-derived microglia (iPSC-microglia). ADP stimulation induced a biphasic Ca^{2+} response – a rapid initial peak followed by sustained Ca^{2+} elevation lasting several minutes, in line with previous observations in mouse microglia (Michaelis et al., 2015; Visentin et al., 2006). Both phases of the Ca^{2+} response were significantly elevated in TREM2 KO microglia (**Figure 1A, B**). TREM2-deficient microglia also showed exaggerated Ca^{2+} responses to other

purinergic agonists; ATP and UTP (**Figure 1C, D**). Notably, responses to ATP and UTP decayed faster than responses to ADP in both WT and TREM2 KO cells, indicating that purinergic stimulation by ADP is more effective in generating sustained Ca^{2+} signals in both WT and TREM2 KO cells (**Figure 1E and Figure 1-figure supplement 1A**).

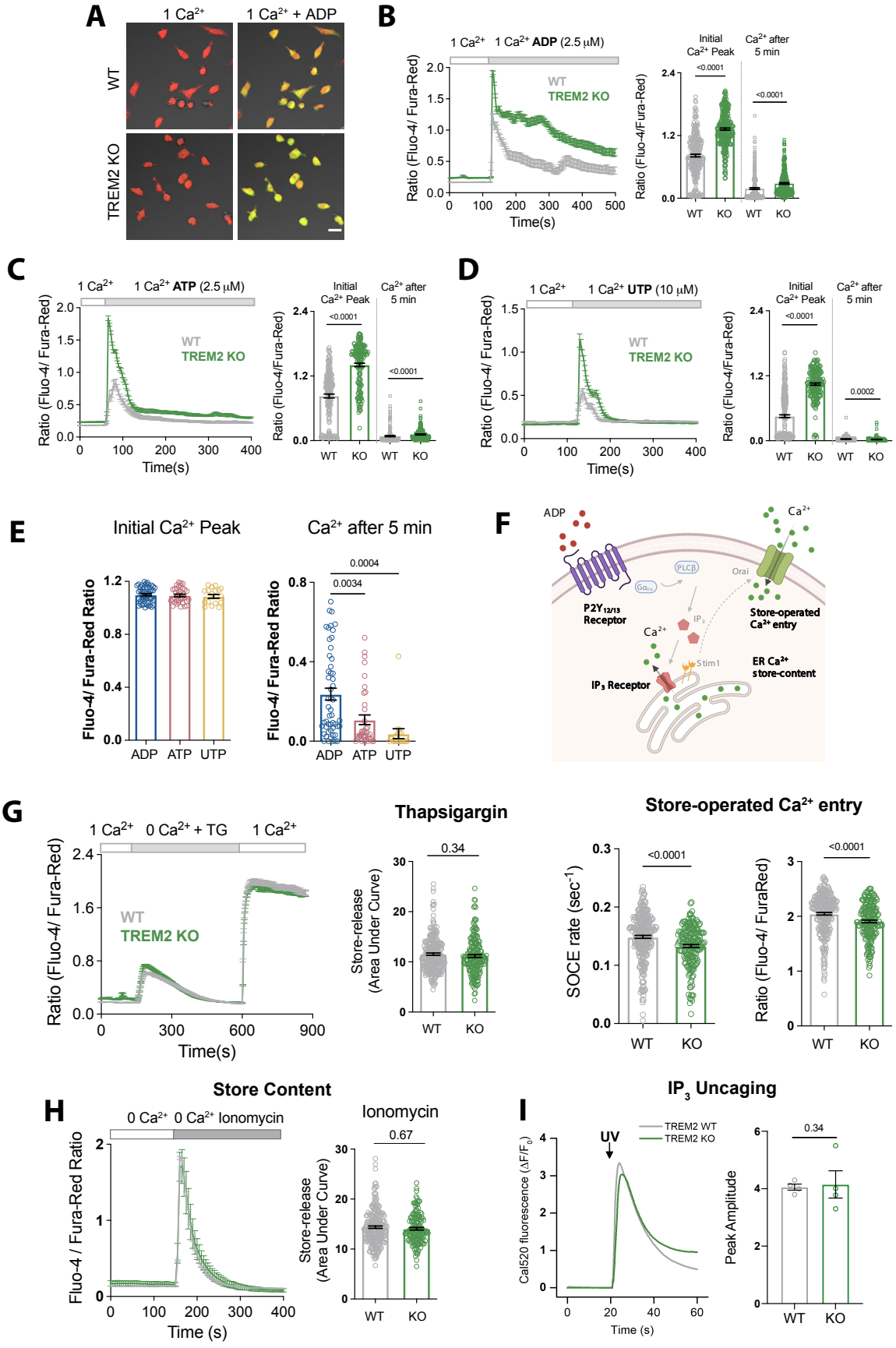
A
1 Ca2+
1 Ca2+ + ADP
WT
TREM2 KO
B
1 Ca2+ 1 Ca2+ ADP (2.5 μM)
WT
TREM2 KO
Ratio (Fluo-4/ Fura-Red)
Time(s)
Initial Ca2+ Peak
Ca2+ after 5 min
<0.0001
<0.0001
Ratio (Fluo-4/Fura-Red)
WT KO WT KO
C
1 Ca2+ 1 Ca2+ ATP (2.5 μM)
WT
TREM2 KO
Ratio (Fluo-4/ Fura-Red)
Time(s)
Initial Ca2+ Peak
Ca2+ after 5 min
<0.0001
<0.0001
Ratio (Fluo-4/Fura-Red)
WT KO WT KO
D
1 Ca2+ 1 Ca2+ UTP (10 μM)
WT
TREM2 KO
Ratio (Fluo-4/ Fura-Red)
Time(s)
Initial Ca2+ Peak
Ca2+ after 5 min
<0.0001
0.0002
Ratio (Fluo-4/Fura-Red)
WT KO WT KO
E
Initial Ca2+ Peak
Ca2+ after 5 min
Fluo-4/ Fura-Red Ratio
ADP ATP UTP
0.0004
0.0034
Fluo-4/ Fura-Red Ratio
ADP ATP UTP
F
ADP
Ca2+
PLCβ
Orai
P2Y12/13 Receptor
IP3
Store-operated Ca2+ entry
Ca2+
Stim1
ER Ca2+ store-content
IP3 Receptor
G
1 Ca2+ 0 Ca2+ + TG 1 Ca2+
WT
TREM2 KO
Ratio (Fluo-4/ Fura-Red)
Time(s)
Thapsigargin
0.34
Store-release (Area Under Curve)
WT KO
Store-operated Ca2+ entry
<0.0001
SOCE rate (sec-1)
WT KO
<0.0001
Ratio (Fluo-4/ FuraRed)
WT KO
H
Store Content
0 Ca2+ 0 Ca2+ Ionomycin
Fluo-4 / Fura-Red Ratio
Time (s)
Ionomycin
0.67
Store-release (Area Under Curve)
WT KO
I
IP3 Uncaging
UV
TREM2 WT
TREM2 KO
Cal520 fluorescence (ΔF/F0)
Time (s)
0.34
Peak Amplitude
WT KO

Figure 3.1. Microglia lacking TREM2 show exaggerated Ca^{2+} responses to purinergic stimulation. (**A**) Representative images of WT (top) and TREM2 KO (bottom) iPSC-Microglia loaded with Fluo-4 (green) and Fura-red (red) showing resting cytosolic Ca^{2+} and peak Ca^{2+} after ADP addition. Bright-field image overlaid, scale bar= 20 μm. (**B-D**) Average ratiometric traces (left panels) showing changes in cytosolic Ca^{2+} over time in response to 2.5 μM ADP (**B**), 2.5 μM ATP (**C**), and 10 μM UTP (**D**) in 1 mM Ca^{2+} containing buffer (n=39-44 cells, **B**; 63-71 cells, **C**; 45-55 cells, **D**). Quantification of baseline subtracted peak Ca^{2+} response and cytosolic Ca^{2+} levels 5 min after agonist application shown on the right (250-274 cells, **B**; 165-179 cells, **C**; 175-269 cells, **D**; 3-5 experiments; Mann-Whitney test). (**E**) Ca^{2+} levels in WT iPSC-Microglia 5 min after addition of ADP, ATP, and UTP (right, n=17-52 cells from 2-3 experiments). Cells were gated for similar initial peak Ca^{2+} response to agonists (left). (**F**) Schematic highlighting key downstream Ca^{2+} signaling events in response to ADP. (**G**) Average trace showing SOCE engaged via emptying ER Ca^{2+} stores with Thapsigargin (TG, 2 μM) in Ca^{2+}-free buffer followed by re-addition of 1 mM Ca^{2+} (90-129 cells). Bar-graph summaries of ER store-release quantified as area under the curve, rate of store-operated Ca^{2+} entry and peak SOCE (187-266 cells, 2 experiments, Mann-Whitney test). (**H**) Average trace (left, 71-117 cells) and summary of ER store-release after 2 μM Ionomycin treatment in Ca^{2+} free buffer (right, 146-234 cells, 2 experiments; Mann-Whitney test) (**I**) Same as H but in response to UV IP_3 uncaging (167-200 cells, nonparametric t-test). Data shown as mean ± SEM for traces and bar-graphs.

Sustained Ca^{2+} elevation in TREM2 KO microglia is not due to SOCE enhancement

To determine the mechanism driving higher Ca^{2+} elevations observed in TREM2 KO cells, we investigated specific steps in the purinergic Ca^{2+} signaling pathway. The initial Ca^{2+} response to P2Y receptor stimulation occurs through IP_3-mediated ER store-release which triggers sustained cytosolic Ca^{2+} elevations through SOCE (**Figure 1F**). Consistent with this, the sustained Ca^{2+} phase in TREM2 KO iPSC-microglia was blocked by Gd^{3+} and 2-APB, non-specific inhibitors of SOCE (**Figure 1-figure supplement 1B**). To determine if SOCE is more readily activated in TREM2 KO microglia, we directly measured the rate of Ca^{2+} influx following Ca^{2+} re-addition after maximal store-depletion with thapsigargin (TG). Instead, we find the rate and amplitude of SOCE were both modestly reduced in TREM2 KO cells (**Figure 1G**) and thus do not account for the elevated response of TREM2 KO microglia to ADP. Moreover, STIM1 and Orai1 mRNA

expression, and Orai1 protein expression remain similar in WT and TREM2 KO microglia (**Figure 1-figure supplement 2**).

We therefore hypothesized that the exaggerated secondary Ca^{2+} phase in TREM2 KO microglia may be driven by increased Ca^{2+} store-release resulting in increased SOCE. We plotted Ca^{2+} responses in individual cells, using Ca^{2+} levels 5 min after ADP as a surrogate for SOCE engagement and the initial peak Ca^{2+} as a readout of ER store-release (**Figure 1-figure supplement 3**). Both WT and TREM2 KO microglia showed a similar relationship between SOCE and store-release, suggesting that SOCE is engaged by similar mechanisms in the two cell types, but is recruited to a greater extent in TREM2 KO cells due to increased ER store-release. To examine whether a larger ER store content contributes to increased Ca^{2+} responses in TREM2 KO microglia, we measured Ca^{2+} levels after maximally depleting ER stores with thapsigargin (TG), ionomycin, or by IP_3 uncaging in Ca^{2+}-free solution buffered with EGTA. In all instances, quantification of peak or cumulative cytosolic Ca^{2+} increase suggested that ER store-content and IP_3 receptor activity is not altered in microglia lacking TREM2 (**Figure 1G-I**). Based on these results, we conclude that the effects of TREM2 on ADP-driven Ca^{2+} signals manifest upstream of IP_3 receptors, ER store Ca^{2+} levels, and SOCE.

Up-regulated P2Y12 and P2Y13 receptor expression drives increased ER Ca^{2+} release in TREM2 KO microglia

To isolate the early events of Ca^{2+} signaling upstream of SOCE, we monitored Ca^{2+} release in Ca^{2+}-free buffer and found that TREM2 KO cells still showed significantly higher Ca^{2+} response to ADP, compared to WT (**Figure 2A, B**). Dose-response curves for peak

Ca^{2+} response showed a steep leftward shift in TREM2 KO cells (**Figure 2C**). The EC_{50} value for WT microglia was 650 nM, whereas TREM2 KO microglia reached their EC_{50} by 15 nM. This stark difference was driven at least in part by a diminished percentage of WT cells responding to ADP at low μM doses (**Figure 2D**). However, limiting the analysis to only those cells that show a Ca^{2+} rise revealed that "responding" TREM2 KO cells still exhibited higher Ca^{2+} responses to ADP than "responding" WT cells (**Figure 2E**). TREM2 KO microglia are thus significantly more sensitive to ADP than WT cells and exhibit a strong shift in dose-dependent response which may be critical in sensing ADP and in detecting ADP gradients.

In principle, signal amplification in microglia lacking TREM2 could occur at the level of P2Y receptors or IP_3 receptors. Our results with IP_3 uncaging (Figure 1H) rule out any major differences in IP_3 receptor expression or activity. This was further corroborated at the transcriptome level, which showed similar expression of IP_3 receptor type 2 (the major IP_3R subtype expressed in iPSC-microglia) mRNA in WT and TREM2 KO cells (**Figure 1-figure supplement 2**)(Abud et al., 2017; McQuade et al., 2020). We therefore focused on P2Y12 and P2Y13 receptors, the main P2Y receptor subtypes in microglia that bind ADP(Abud et al., 2017; McQuade et al., 2018). RNA sequencing further showed that expression of P2Y12 and P2Y13 receptors was significantly increased in TREM2 KO cells (**Figure 2F**). To confirm up-regulation at the protein level, we performed immunostaining and found significantly higher expression of both these receptors on the plasma membrane of TREM2 KO cells (**Figure 2G, H**). Consistent with this, Ca^{2+} responses in TREM2 KO microglia were significantly inhibited by P2Y12 and P2Y13 receptor antagonists (PSB 0739 and MRS 2211) (**Figure 2I, J**), implicating involvement of both

receptor subtypes. In summary, deletion of TREM2 in iPSC-derived microglia leads to up-regulation of P2Y12 and P2Y13 receptors, rendering the cells hypersensitive to ADP signaling.

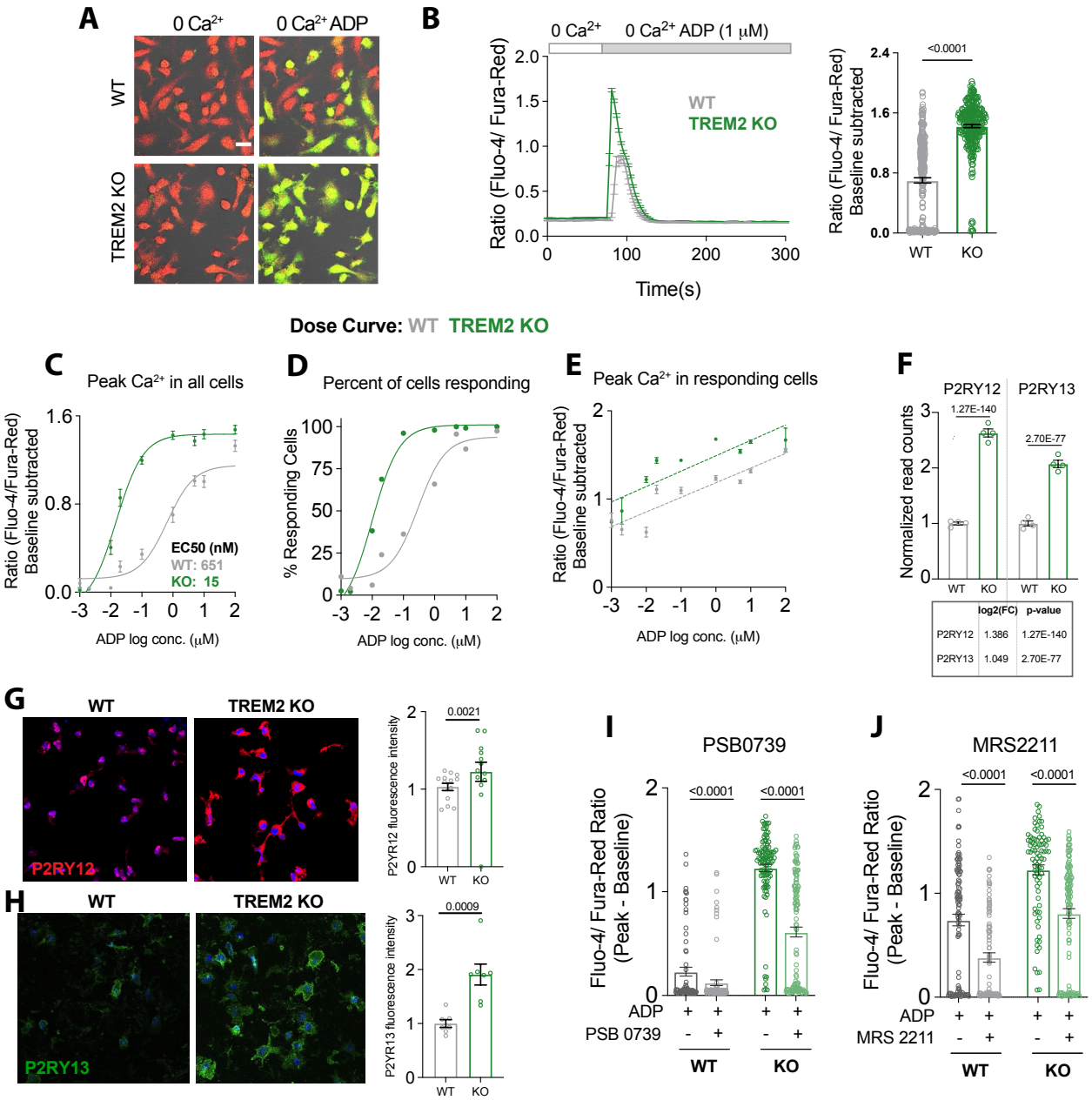

Figure 3.2. Higher sensitivity of TREM2 KO microglia to ADP is driven by increased purinergic receptor expression (**A**) Representative images of WT (top) and TREM2 KO (bottom) iPSC-Microglia before and peak Ca^{2+} response after ADP addition in Ca^{2+} free buffer. Overlay of Fluo-4 (green), Fura-red (red) and Brightfield (grey) images. Scale bar= 20 μm. (**B**) Average trace showing Ca^{2+} response to ADP in Ca^{2+}-free buffer (left, 64-83

cells). Quantification of peak signal (right, 264-289 cells, 4 experiments, Mann-Whitney test). (**C-E**) Dose-response curve showing baseline subtracted Peak Ca^{2+} responses to ADP (**C**), percent of "responding" cells (**D)** and peak Ca^{2+} responses only in "responding" cells (**E**). (Each data-point is average of 84-474 cells, WT; 70-468 cells, 2-5 experiments). (**F**) RNA normalized read counts of P2RY12/13 expression from bulk RNA-sequencing of WT and TREM2 KO iPSC-microglia (n=4, adjusted p-values from DESeq2). (**G-H**) Immunofluorescence and quantification of P2RY12 (**G**) and P2RY13 (**H**) in iPSC-microglia (n=4 independent wells, 3 images per well, student's t-test). (**I-J**) Peak Ca^{2+} response in Ca^{2+} free buffer after treatment with ADP in the presence of P2RY12 antagonist PSB 0739 (**I**) and P2RY13 antagonist MRS 2211 (**J**). (72-128 cells, **I**; 83-117 cells, **J**; representative of 3 experiments, Mann-Whitney Test). Data shown as mean ± SEM for traces and bar-graphs.

ADP promotes WT iPSC microglial motility in the absence of gradient

ADP is a potent chemoattractant for microglia (Honda et al, 2001). Analogous to a previous study in fibroblasts (Borges et al., 2021), we found that ADP treatment alters cell motility and leads to increased rates of scratch wound closure in WT iPSC-microglia (**Figure 3A**). To investigate this finding and test whether accelerated wound closure results from increased microglial speed or decreased turning behavior, we used time-lapse imaging to track microglial motility and analyze speed, displacement, and track straightness for individual cells (**Figure 3B**). Mean cell speed and displacement both increased after application of ADP, whereas track straightness was not significantly altered (**Figure 3C**). These data strongly suggest that ADP-driven motility in iPSC-microglia primarily arises from increases in microglial speed, not altered turning behavior. Additionally, we note that only a subset of cells increased their speed after ADP treatment, accounting for the significant spread in the distribution of cell motility. ADP-dependent increases in cell motility are reversed in the presence of P2Y12 (PSB 0739) and P2Y13 (MRS 2211) receptor antagonists, suggesting that both of these receptors participate in ADP-mediated migration responses (**Figure 3D**). To determine if Ca^{2+} influx is directly

involved, we measured cell migration in Ca^{2+}-free buffer; a transient Ca^{2+} signal would result from ADP-induced release of Ca^{2+} from internal stores, but without Ca^{2+} entry across the plasma membrane. We found that removing extracellular Ca^{2+} significantly decreased cell speed, displacement, and track straightness (**Figure 3E**). Based on these findings, we conclude that Ca^{2+} influx across the plasma membrane, and potentially engagement of SOCE, is required for ADP-induced migration in WT iPSC-microglia.

ADP promotes process extension in WT iPSC-microglia

In observing time-lapse videos of ADP-treated iPSC-microglia, we found that a subset of cells responded by extending processes and altering their morphology rather than increasing their motility. These observations mirror studies that have demonstrated microglial process extension in response to injury and purinergic stimulation in brain slices (Davalos et al., 2005; Haynes et al., 2006). To quantify this behavior, we compared process complexity before and 30 min after ADP exposure in WT microglia and found significant increases in both the number of branches per process and total length of these processes (**Figure 3F, Figure 3-figure supplement 1**). As with motility, process extension in response to ADP was inhibited by P2Y12 (PSB 0739) and P2Y13 (MRS 2211) receptor antagonists. Furthermore, even before process extension was activated with ADP, cells treated with P2Y antagonists showed significantly fewer and shorter processes.

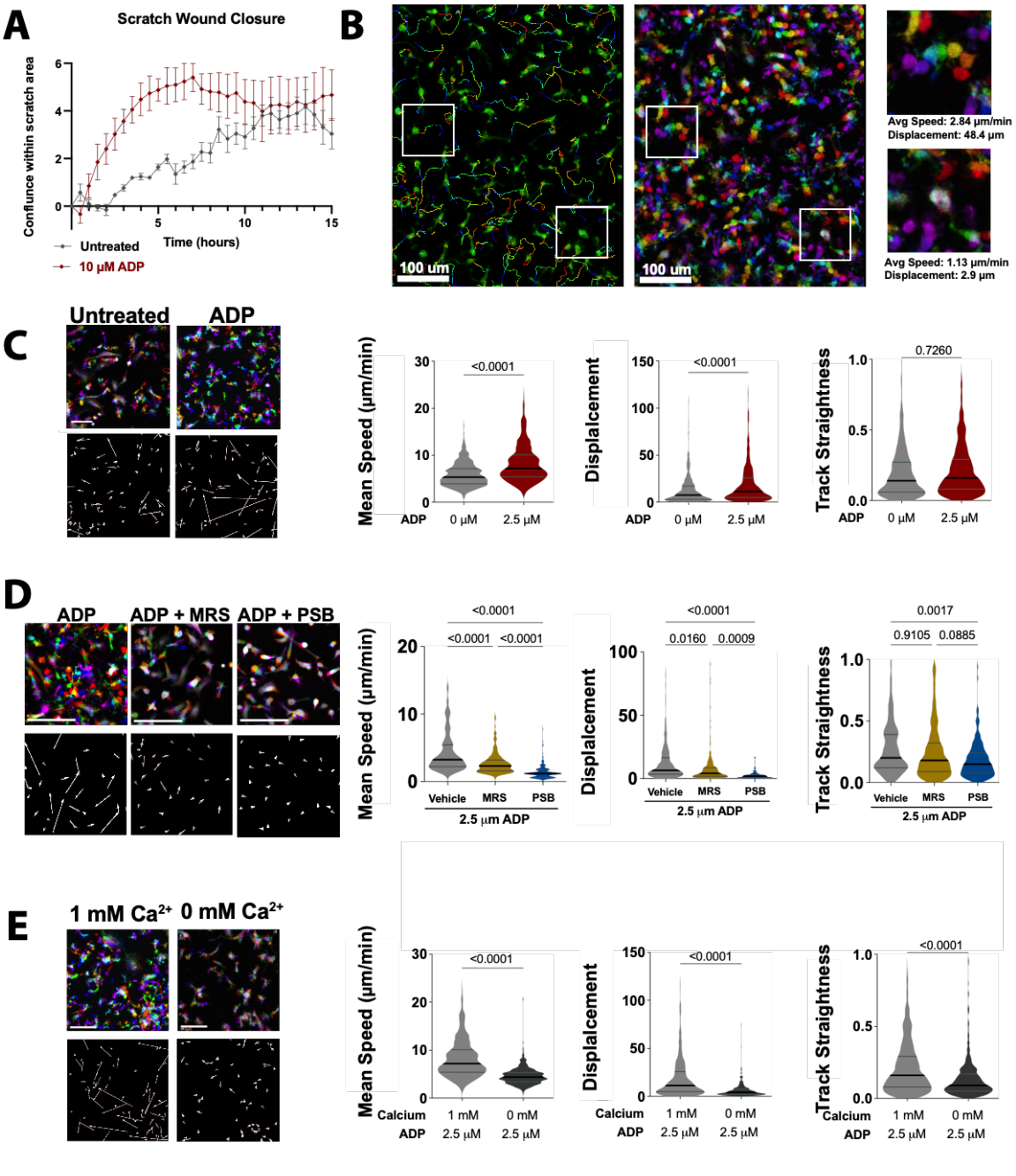
A
Scratch Wound Closure
Confluence within scratch area
Time (hours)
Untreated
10 µM ADP
B
100 um
100 um
Avg Speed: 2.84 µm/min
Displacement: 48.4 µm
Avg Speed: 1.13 µm/min
Displacement: 2.9 µm
C
Untreated
ADP
Mean Speed (µm/min)
Displacement
Track Straightness
<0.0001
<0.0001
0.7260
ADP
0 µM
2.5 µM
D
ADP
ADP + MRS
ADP + PSB
<0.0001
<0.0001
<0.0001
0.0160
0.0009
0.0017
0.9105
0.0885
Vehicle
MRS
PSB
2.5 µm ADP
E
1 mM Ca2+
0 mM Ca2+
<0.0001
<0.0001
<0.0001
Calcium
1 mM
0 mM
ADP
2.5 µM
F
ADP
ADP + MRS
ADP + PSB
Pre
Post
Process Length (µm)
<0.0001
0.9750
0.9810
No. of branches after ADP
0.0004
0.9752
0.9806
pre post
Vehicle
MRS
PSB

Figure 3.3. Nondirectional ADP exposure increases WT microglial speed and process extension. (**A**) Average trace showing closure of scratch wound produced with IncuCyte S3 WoundMaker. iPSC-microglia imaged every 30 min after scratch wound with or without ADP stimulation (n=4 wells; 2 images per well). (**B**) Representative image of WT iPSC-microglia motility 30 min after ADP exposure with cell tracks overlain (left). Pseudocolored images (center) across time: 0 min (red), 4 min (orange), 8 min (yellow), 12 min (green), 16 min (cyan), 20 min (blue), 24 min (purple), 28 min (magenta). Scale bar= 100 μm. White boxes zoomed in at right to demonstrate motile (top) and non-motile (bottom) cells. (**C**) Representative color images (top left) and displacement vectors (bottom left) of WT iPSC-microglia at baseline (no ADP, grey) and after 2.5 μM ADP treatment (red). Summary of Mean Speed (μm/min), Displacement over 10 min (μm/10 min) and Track straightness (track length/track displacement) (414-602 cells, 2 experiments). (**D**) Representative images, displacement vectors, and quantification of WT iPSC-microglia motility for 20 min following ADP addition. Cells were pre-treated with vehicle (grey), MRS 2211 (10 μM, gold), or PBS 0739 (10 μM, blue) (180-187 cells, 2 experiments). (**E**) Representative images, displacement vectors, and quantification of WT iPSC-microglia motility after ADP in 1 mM Ca^{2+} (light grey) or Ca^{2+}-free buffer (dark grey) (401-602 cells, 3 experiments). (**F**) Representative images (left) and process extension (right) of iPSC-microglia (cytoplasmic GFP, grey) before or 30 min after ADP addition. Cells were pre-treated with vehicle (grey), MRS 2211 (10 μM, gold), or PBS 0739 (10 □M, blue) (52-163 cells, 3-4 experiments). (**C-F**) One way ANOVA with Tukey post hoc test. Data shown as mean ± SEM for traces and bar-graphs.

Process extension is enhanced in TREM2 KO microglia

We next asked if deletion of TREM2 affects cell motility characteristics and process extension. Compared to WT cells, TREM2 KO iPSC-microglia showed a more dramatic increase in the number of branches and length of processes extended in response to ADP (**Figure 4 A-C, Figure 4-figure supplement 1A, B**). Some of these differences can be attributed to the reduced morphological complexity of TREM2 KO cells prior to stimulation, consistent with a recent report(Hall-Roberts et al., 2020). We found that TREM2 KO microglia still showed some increase in the number and length of processes, whereas in WT cells ADP application in Ca^{2+}-free buffer was insufficient to induce process extension. (**Figure 4-figure supplement 1C, D**). Thus, transient ADP-mediated Ca^{2+}

signals regulate microglial process extension differentially in WT and TREM2 KO microglia.

Calcium-dependent displacement is enhanced in ADP-stimulated TREM2 KO microglia

To further characterize differences in motility characteristics between WT and TREM2 KO microglia responding to ADP, we plotted mean square displacement (MSD vs. time) and cell track overlays (flower plots) which showed that motility in WT microglia is constrained relative to TREM2 KO cells (**Figure 4D-E**). Baseline motility characteristics in unstimulated cells, however, were similar in WT and KO lines (**Figure 4-figure supplement 2**), consistent with our previously published findings showing no difference in scratch wound closure rates (McQuade et al., 2020). To further understand the basis of differences in ADP-induced motility between WT and TREM2 KO cells, we analyzed mean speed, displacement and track straightness. While mean speeds were similar, TREM2 KO microglia showed greater displacement than WT cells raising the possibility that KO cells may turn with lower frequency (**Figure 4F, G**). Indeed, an analysis of track straightness revealed that TREM2 KO microglia move farther from their origin for the same total distance traveled (**Figure 4H**). Vector autocorrelation, an analysis of directional persistence(Gorelik and Gautreau, 2014), further confirmed that WT cells turn more frequently than TREM2 KO microglia (**Figure 4-figure supplement 3**). To assess if these differences require sustained Ca^{2+} influx in KO cells, we analyzed microglial motility in response to ADP stimulation in the absence of extracellular Ca^{2+} (**Figure 4I-M**). Mean-square displacement and cell-track overlay plots showed that motility is constrained

when Ca^{2+} is removed from the external bath in both WT and TREM2 KO cells (**Figure 4D-E vs. I-J**). Importantly, in the absence of extracellular Ca^{2+}, TREM2 KO microglia showed similar mean speed, displacement, and track-straightness as WT cells (**Figure 4K-M**). Based on this, we conclude that TREM2-dependent changes in microglial motility require sustained Ca^{2+} influx.

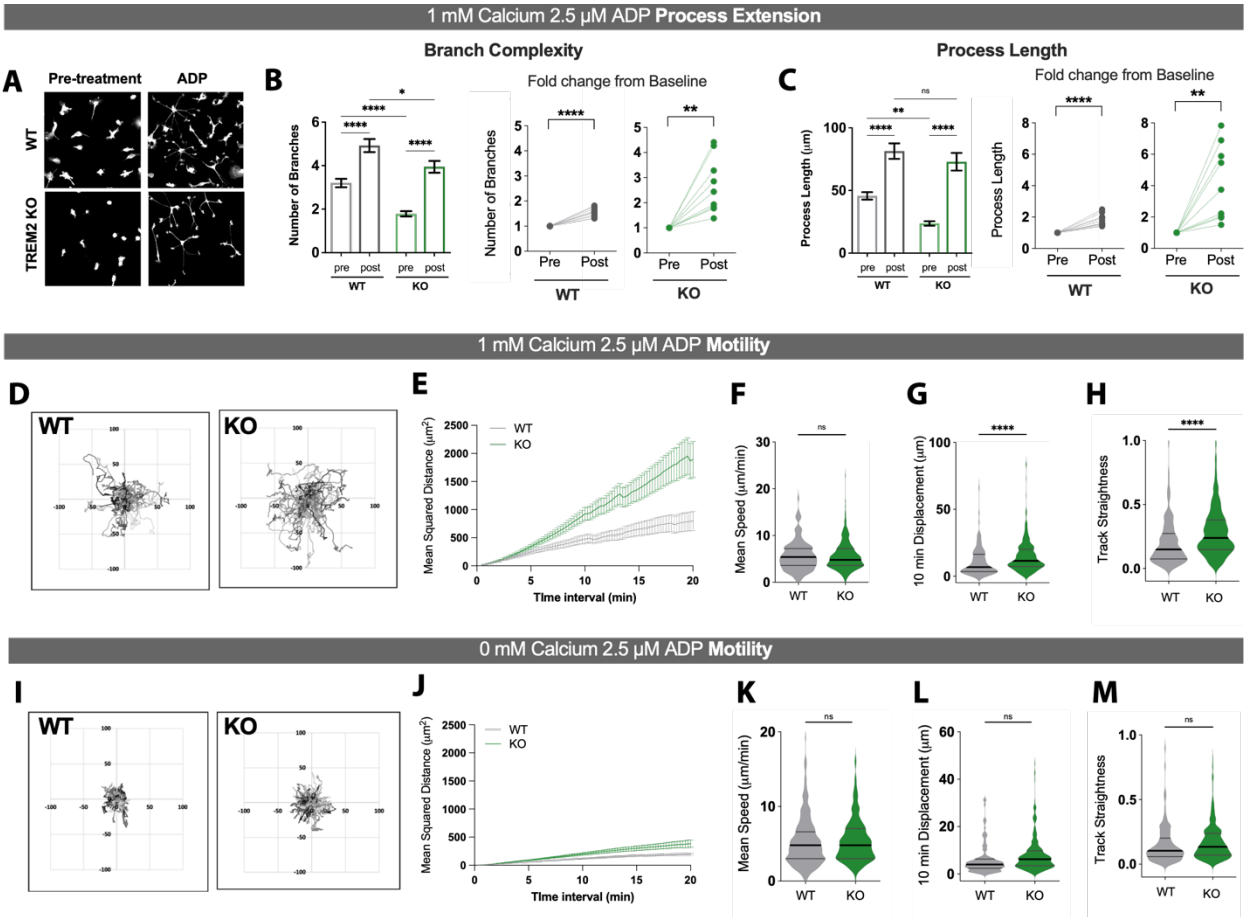

Figure 3.4. ADP-driven process extension and cell displacement are increased in TREM2 KO iPSC-microglia. (**A**) Representative images of GFP-expressing WT (top) and KO (bottom) iPSC-microglia, before and 30 min after 2.5 µM ADP addition. (**B**) Quantification of total number of branches per cell before and after ADP treatment (left) and paired dot-plots showing fold change in branch number from pre-ADP levels (right). Each data-point represents an imaging field in the paired-plots. (**C**) Total process length before and after ADP treatment displayed as raw values per cell (left) and as fold change from baseline conditions per imaging field (right) (n=151-158 cells, WT; 133-167 cells, KO; 9-10 imaging fields, 3-4 experiments for **B** and **C,** One-way ANOVA with multiple

comparisons for single-cell data, two-tailed paired t-test for the paired-plots). (**D-H**) Motility of WT (grey) and TREM2 KO (green) iPSC-microglia over 20 min following ADP addition in 1 mM Ca^{2+}-containing buffer summarized as mean-square distance vs time (**D**), flower plots of track displacement centered from point of origin at (0,0) (**E**). Statistics describe (**F**) mean-cell speed, (**G**) total track displacement, and track straightness (**H**) (130-327 cells, 7 experiments, student's t-test). (**I-M**) Same as (**D-G**) but in Ca^{2+}-free buffer (125-279 cells, 2 experiments, student's t-test).

Salsa6f expression in iPSC-microglia does not affect cell function

Our findings suggest that patterns of Ca^{2+} signaling in iPSC-microglia regulate cell motility and process extension. To directly monitor Ca^{2+} signaling and motility simultaneously in individual cells, we developed a novel iPSC line that expresses a genetically encoded, ratiometric Ca^{2+} indicator, Salsa6f (Dong et al., 2017). Salsa6f relies on GCaMP6f to detect Ca^{2+}, and is fused to tdTomato in order to provide a stable Ca^{2+}-independent red fluorescence, allowing cells to be tracked consistently even when Ca^{2+} levels are low. Salsa6f WT iPSC-microglia showed the expected increase in the GCaMP6f fluorescence in response to Ca^{2+} elevation without affecting tdTomato signal, permitting determination of ratiometric Ca^{2+} levels (G/R ratio), and confirming that the probe was functional (**Figure 5A-C and Figure 5-figure supplement 1**). Compared to non-transgenic iPSC-microglia, Salsa6f-expressing cells show similar expression of microglial identity markers P2RY13 and IBA1, retain their ability for phagocytosis across several substrates, and have similar differentiation yields, indicating that Salsa6f expression does not alter microglial function or activation (**Figure 5D-G**). Isogenic Salsa6f-lines lacking TREM2 were more responsive to ADP than WT cells, consistent with our data in Figures 1 and 2 (**Figure 5H**). Using this model, we are able to simultaneously track Ca^{2+} signals and cell-motility in response to ADP (**Figure 5I**).

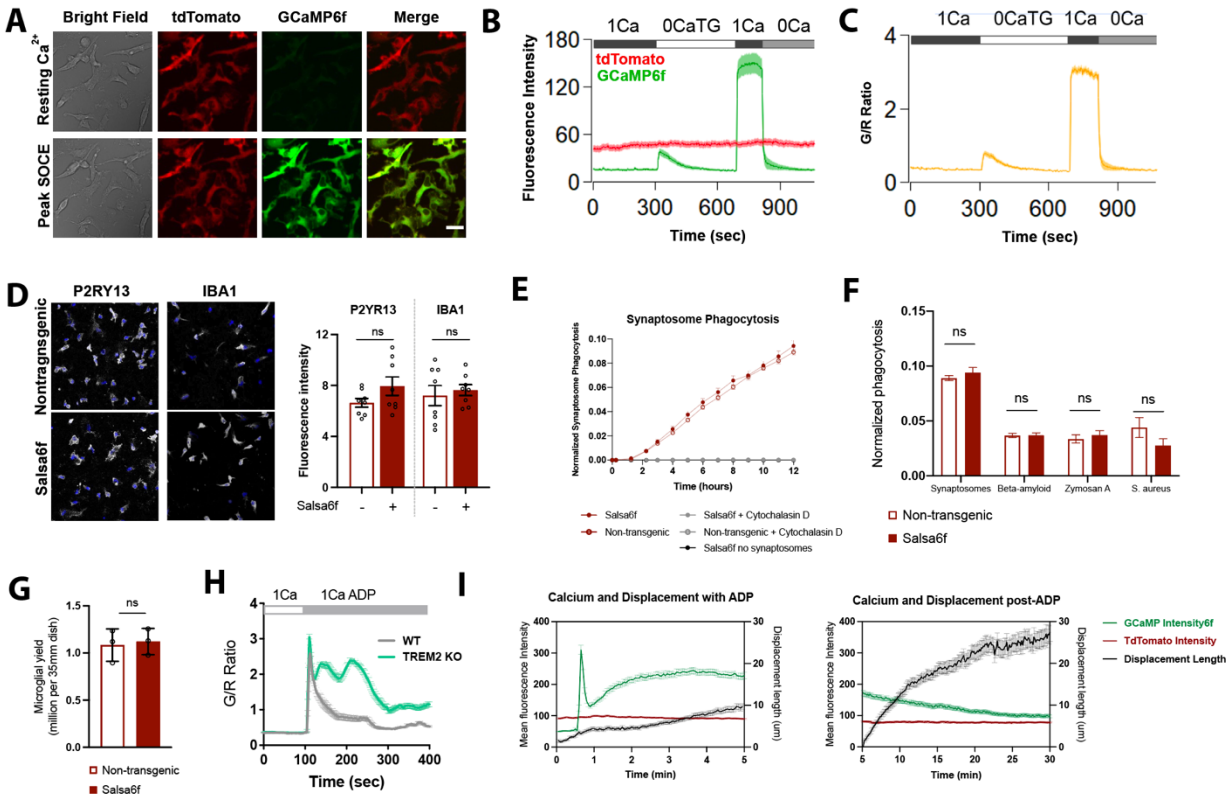

Figure 3.5. Validation of Salsa6f transgenic iPSC-microglia. (**A**) Representative green (GCaMP6f), red (tdTomato) and Green/Red channel overlay images of transgenic Salsa6f expressing iPSC-microglia at low (resting Ca^{2+}, top row) and high (Peak SOCE, bottom row) cytosolic Ca^{2+} levels. Bright-field image shown for comparison. Cells were treated with TG to evoke SOCE. Scale bar = 5 µm. (**B**) Trace of average change in fluorescence intensity of tdTomato (red) and GCamp6f (green) over time (n=32 cells). (**C**) Ratiometric GCaMP6f/ tdTomato signal (Green/ Red or G/R Ratio) over time calculated from (**B**). (**D**) Immunofluorescence images of P2RY13 and IBA1 in WT or Salsa6f-transgenic iPSC-microglia (left). Right panel shows quantification of P2RY13 and IBA1 protein expression (n=4 wells, 2 independent images per well, t-test). (**E**) Phagocytosis of Synaptosomes in WT non-transgenic (open circle) and Salsa6f-expressing (closed circle) iPSC-microglia. Cytochalasin D (grey, 10 µM) used as negative control to inhibit phagocytosis. Live cultures imaged on IncuCyte S3 (n=4 wells; 4 images per well). (**F**) Phagocytic load at 24 hrs for synaptosomes, beta-amyloid, zymosan A, and *S. aureus* (n=4 wells; 4 images per well; one way ANOVA with tukey post-hoc test). (**G**) Microglia cell counts at final day of differentiation (n=3 wells, t-test). (**H**) Ca^{2+} response to 2.5 µM ADP in WT vs TREM2 KO Salsa6f-expressing iPSC-microglia (n=41-53 cells). (**I**) Fluorescence intensity of tdTomato (red) and GCaMP6f (green) (left axis) simultaneously measured alongside cell displacement (black) (right axis).

Ca^{2+} levels tune motility in TREM2 KO iPSC-microglia

To further characterize the specific effects of long-lasting Ca^{2+} elevations on microglia motility without the confounding signaling effects of Ca^{2+}-independent pathways that are triggered by ADP (Das and Chinnathambi, 2020), we used the Salsa6f reporter line and developed a "Ca^{2+} clamp" assay to stabilize microglial cytosolic Ca^{2+} at "high" or "low" levels (**Figure 6A, B**), similar to studies that have previously been performed in T lymphocytes (Dolmetsch et al., 1997; Negulescu et al., 1996) . In WT cells, lowering extracellular Ca^{2+} from 2 to 0.2 mM predictably decreased the G/R ratio but did not influence mean speed, cell displacement, or track straightness (**Figure 6C top**). However, in TREM2 KO microglia, clamping Ca^{2+} to a lower level significantly increased speed, displacement, and track straightness (**Figure 6C bottom**). These observations suggest that motility characteristics (speed, displacement, and straightness) of TREM2 KO microglia are more sensitive to changes in cytoplasmic Ca^{2+} levels than in WT cells. Addition of ADP in this "clamp" paradigm to activate Ca^{2+}-independent signaling pathways that promote cell motility did not alter the potential for Ca^{2+} to tune cell motility in TREM2 KO microglia (**Figure 6-figure supplement 1**).

To further analyze the Ca^{2+} dependence of motility, we plotted Salsa6f ratios at every time point against the instantaneous speeds for each individual cell. This analysis did not reveal a significant relationship between instantaneous speed and instantaneous G/R Ca^{2+} ratio (**Figure 6D**). However, in TREM2 KO microglia, cells with higher instantaneous Ca^{2+} levels tended to show reduced instantaneous speed (**Figure 6D, E**). Furthermore, when stratifying cell speed as "fast" (> 10 μm/min) or "slow" (> 10 μm /min), we observe a marked reduction in percentages of "fast" cells when Ca^{2+} levels are high

(**Figure 6F**). We conclude that TREM2 KO human microglia are more sensitive to tuning of motility by Ca^{2+} influx than WT cells. Interestingly, cell displacement was found to correlate with Ca^{2+} to the same degree in both WT and KO cells (**Figure 6-figure supplement 2**). Together, these “calcium clamp” experiments revealed that motility is more readily tuned by modulating Ca^{2+} in TREM2 KO cells than in WT microglia.

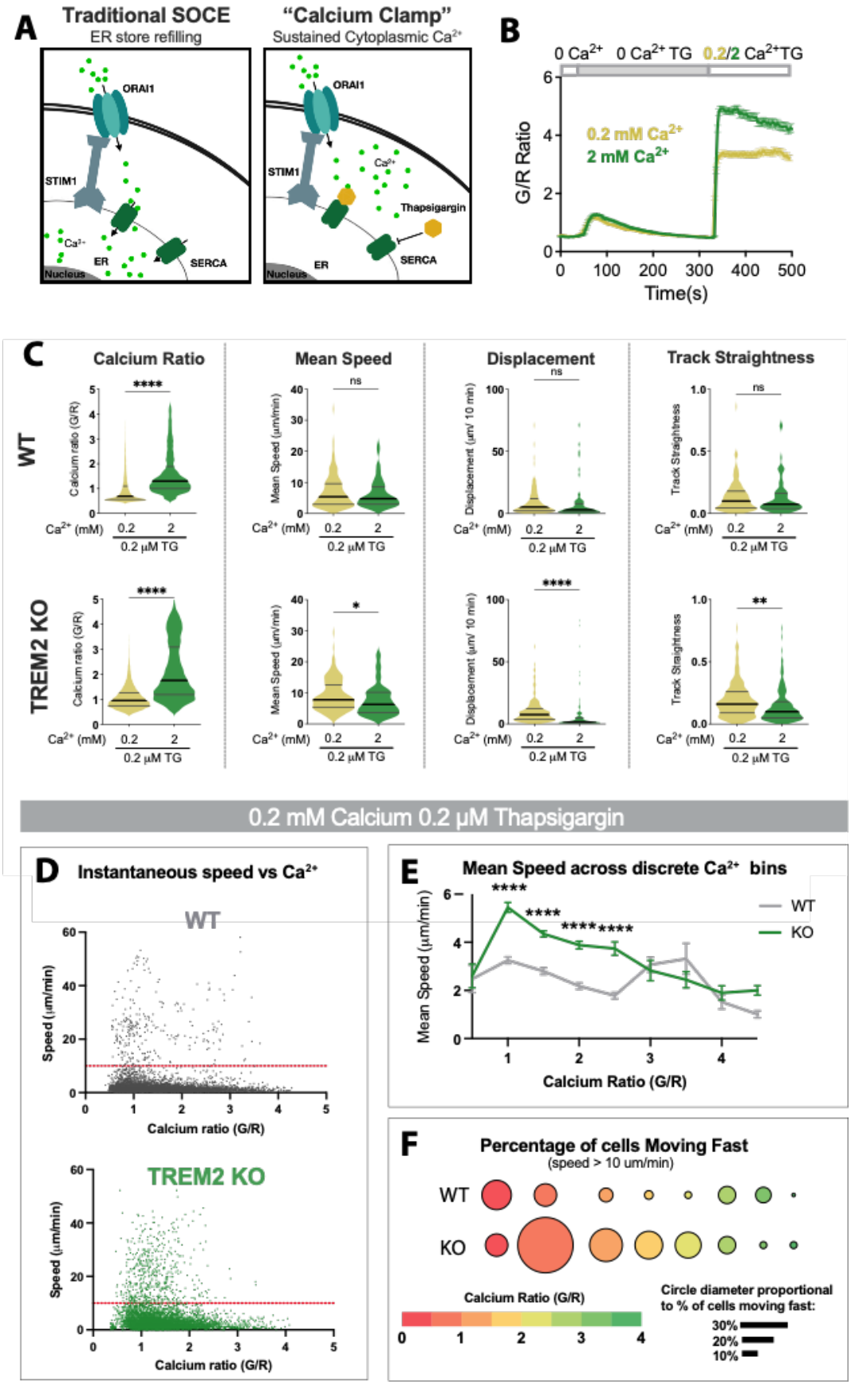
A
Traditional SOCE
ER store refilling
"Calcium Clamp"
Sustained Cytoplasmic Ca2+
ORAI1
STIM1
Ca2+
ER
SERCA
Nucleus
Thapsigargin
B
0 Ca2+
0 Ca2+ TG
0.2/2 Ca2+TG
0.2 mM Ca2+
2 mM Ca2+
G/R Ratio
Time(s)
C
Calcium Ratio
Mean Speed
Displacement
Track Straightness
WT
TREM2 KO
Calcium ratio (G/R)
Mean Speed (µm/min)
Displacement (µm/ 10 min)
Track Straightness
Ca2+ (mM)
0.2 µM TG
****
*
**
ns
0.2 mM Calcium 0.2 µM Thapsigargin
D
Instantaneous speed vs Ca2+
WT
TREM2 KO
Speed (µm/min)
Calcium ratio (G/R)
E
Mean Speed across discrete Ca2+ bins
WT
KO
Mean Speed (µm/min)
Calcium Ratio (G/R)
F
Percentage of cells Moving Fast
(speed > 10 um/min)
WT
KO
Calcium Ratio (G/R)
Circle diameter proportional to % of cells moving fast:
30%
20%
10%

Figure 3.6. Ca^{2+} levels tune microglial motility in TREM2 KO cells. (**A**) Schematic of traditional SOCE pathway with store-refilling (left) and a "Ca^{2+}– clamp" mechanism of sustaining cytoplasmic Ca^{2+} levels using TG to inhibit store-refilling (right). (**B**) Average SOCE traces in WT Salsa6f^{+} iPSC-microglia showing cytoplasmic Ca^{2+} 'clamped' at different levels after addition of 0.2 or 2 mM extracellular Ca^{2+}(n=78-110 cells). (**C**) Comparison of Ca^{2+} levels and microglia motility in WT (top) and TREM2 KO (bottom) microglia. Cytosolic Ca^{2+} summarized as instantaneous single-cell G/R Ratio (n=74-158). Mean-speed, displacement and track straightness calculated as before in Figure 3 and 4. Yellow (0.2 mM Ca, TG), green (2 mM Ca, TG). Students t-test **** $p < 0.0001$; ** $p = 0.0062$; * $p = 0.432$; ns > 0.9999. (**D**) Correlation of instantaneous Ca^{2+} and instantaneous speed in WT and KO cells. Red line denotes 10 μm/sec (cells above this threshold considered "fast moving"). (**E**) Mean speed of cells binned by instantaneous G/R Ca^{2+} ratio (1-way ANOVA **** $p < 0.0001$). (**F**) Percentage of fast moving cells quantified as a function of Salsa6f Ca^{2+} ratio. Circle color represents G/R Ca^{2+} ratio (red is lower Ca^{2+} ratio; green is higher Ca^{2+}). Circle diameter denotes the proportion of cells moving fast (larger circles represent a higher proportion of fast cells). (**D-F** n=78-100 cells).

Chemotactic defects in TREM2 KO microglia are rescued by dampening purinergic receptor activity

In vivo, directed migration of microglia is driven by gradients of ADP from dying or injured cells (Eyo et al., 2014; Haynes et al., 2006). To study chemotaxis toward ADP over a stable gradient, we exposed iPSC-microglia to ADP in two-chamber microfluidic devices. Consistent with previous findings, WT iPSC-microglia directionally migrated up the concentration gradient of ADP resulting in higher numbers of cells within the central chamber (McQuade et al., 2020; Park et al., 2018). In the absence of a chemoattractive cue, this directional migration was lost (**Figure 7A**). This assay revealed a deficit of chemotaxis in TREM2 KO microglia (**Figure 7A**), mirroring reports that TREM2 KO microglia are unable to migrate towards pathology *in vivo* (Cheng-Hathaway et al., 2018; McQuade et al., 2020; Meilandt et al., 2020). Given that ADP hypersensitivity in TREM2 KO cells is driven by increased expression of P2Y receptors, we examined the effects of dampening P2Y signaling to WT levels. Treatment with the P2Y12 antagonist, PSB 0739,

reduced Ca^{2+} responses in TREM2 KO cells and rescued the migration deficit in the chemotaxis assay (**Figure 7B-C)**. These results link the increased Ca^{2+} signals and altered motility characteristics evoked by ADP in TREM2 KO cells to a vital functional response in microglia.

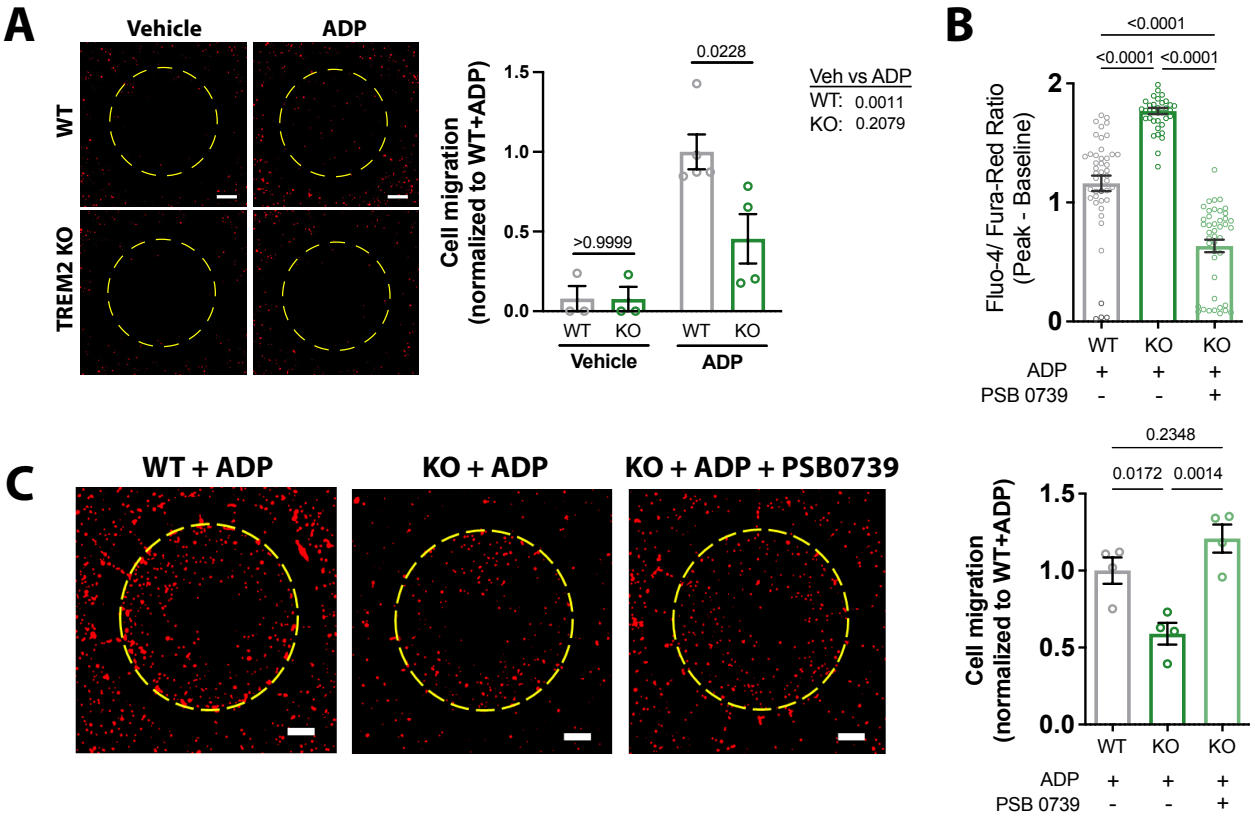

Figure 3.7. Migration deficits in TREM2 KO microglia are rescued by inhibition of purinergic signaling. (**A**) Migration towards ADP in a two-chamber microfluidic device. Representative images of RFP expressing microglia that migrated into the central chamber 3 days after 100 ng/mL ADP addition. Dotted circle delineates separation of inner and outer chamber. Scale bar = 500 μm. Quantification of microglial migration (right panel). Values are normalized to WT cells treated with ADP (n=3-4 experiments; One-way ANOVA with multiple comparisons). (**B**) Baseline subtracted peak ratiometric Ca^{2+} signal in response to 2.5mM ADP in 1 mM extracellular Ca^{2+}, and in the presence or absence of 10 μM PSB 0739 (44 cells, WT; 39-43 cells, KO; representative of 3 independent experiments; Students t-test). (**C**) Two-chamber migration to 100 ng/mL ADP with or without 10 μM PSB 0739. Values are normalized to WT cells with ADP (n=3-4 experiments; One-way ANOVA with multiple comparisons). Representative images shown on the left. Scale bar = 500 μm.

Discussion

This study focuses on two aims: understanding the roles of purinergic signaling in regulating human microglial motility behavior; and elucidating the impact of TREM2 loss of function on this pathway. We find that the high level of purinergic receptor expression in TREM2 KO iPSC-microglia renders them highly sensitive to ADP-mediated signaling and leads to exaggerated cytoplasmic Ca^{2+} responses. Mechanistically, this increase in Ca^{2+} signals is driven by enhanced IP_3-mediated store-release coupled to SOCE. Indeed, based on the dose-response curves for peak ADP-Ca^{2+} responses in Ca^{2+} free buffer, TREM2 KO cells have an EC_{50} at least 10-fold lower than WT cells. As a functional consequence, TREM2 KO microglia exhibit a defect in turning behavior, leading to greater displacement in response to ADP. Despite moving in straighter paths, TREM2 KO cells are unable to migrate towards a gradient of ADP as efficiently as WT cells, in line with previous studies showing reduced migration of TREM2 KO cells towards A□ plaques(McQuade et al., 2020). We propose a model (**Figure 8**) whereby enhanced ADP signaling abolishes the ability of TREM2 KO cells to distinguish gradations of agonist (here, ADP). The loss of gradient sensing results in an inability to perform directed chemotaxis. We hypothesize that increased ADP signaling and exaggerated Ca^{2+} responses in TREM2 KO cells result in local Ca^{2+} signals that are no longer restricted to the cell region near to the highest ADP concentrations, thereby disrupting the polarity of key signaling molecules that drive directed cell motility. Interestingly, a recent study showed that TREM2 KO iPS-microglia show increased migration towards a gradient of the complement product C5a *in vitro*(Reich et al., 2021). Specific signaling pathways may thus exert different effects on migratory behavior in the absence of TREM2.

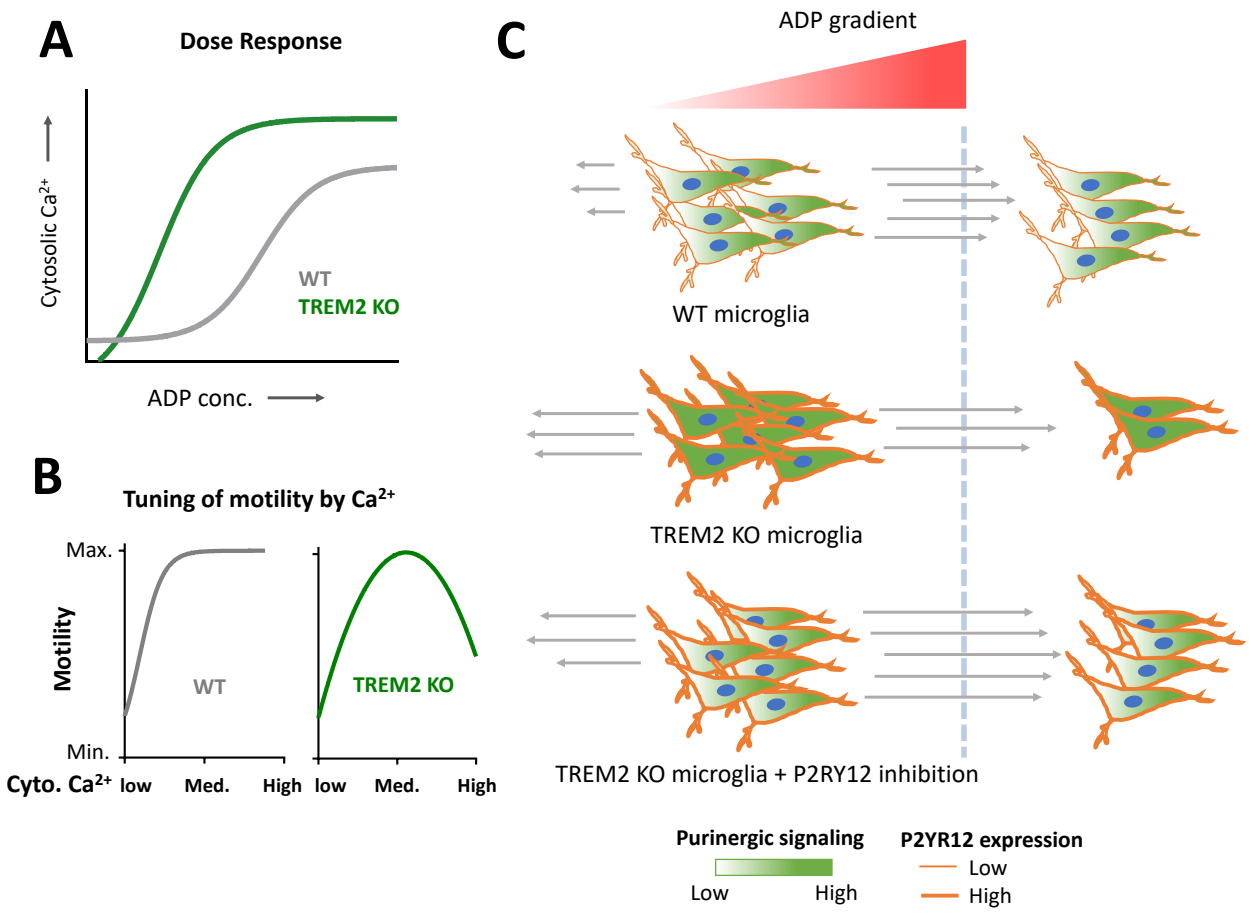

Figure 3.8. A Model for Ca^{2+} regulation of ADP-mediated chemotaxis in microglia lacking TREM2. (**A**) Dose-response curve comparing ADP-mediated peak-Ca^{2+} response in WT and TREM2 KO microglia. EC50 for KO cells is more than 10-fold lower than WT microglia. P2RY12 and 13 receptor expression is higher in cells lacking TREM2 rendering them hypersensitive to ADP signaling. (**B**) Elevations in Ca^{2+} regulate motility (mean speed, displacement and turning behavior) differentially in WT and TREM2 KO cells. Motility in KO microglia is more amenable to tuning by changing extracellular Ca^{2+} concentration. (**C**) Due to exaggerated purinergic ADP signaling, microglia lacking TREM2 exhibit a deficit in moving towards ADP gradients. Despite moving in straighter tracks, TREM2 KO cells migrate in all directions contributing to their chemotactic inefficiency. Partially suppressing P2RY12 signaling and lowering cytosolic Ca^{2+} in TREM2 KO cells rescues the chemotactic defect by restoring their ability to move towards the ADP gradient, in line with findings that Ca^{2+} signals tune TREM2 KO cell motility behavior.

The amplitude and duration of Ca^{2+} signals shape specificity of downstream cell responses. Our experiments with ADP in Ca^{2+} free buffer revealed that transient Ca^{2+}

signals are insufficient to induce microglial motility in either WT or TREM2 KO cells. Previous studies have shown that mouse microglia with genetic deletion of STIM1 or Orai1 also show defects in cell migration to ATP(Lim et al., 2017; Michaelis et al., 2015), likely because diminished SOCE renders them unable to sustain Ca^{2+} signals in response to ATP. The dependence of motility on prolonged purinergic Ca^{2+} signals may thus be a general feature of microglia. In contrast, shorter Ca^{2+} transients can initiate some process extension in TREM2 KO but not in WT microglia, suggesting a threshold for ADP signaling that is reached in KO but not WT cells, and highlighting subtle differences in the Ca^{2+} requirement for motility and process extension in TREM2 KO microglia.

To directly monitor Ca^{2+} signaling and motility simultaneously in individual cells, we developed a novel iPSC-microglia cell-line expressing a genetically encoded, ratiometric Ca^{2+} indicator Salsa6f, a GCaMP6f-tdTomato fusion protein. Because Salsa6f allows simultaneous measurement of Ca^{2+} signal and tracking of processes, this novel iPSC line is likely to be a useful tool to dissect the relationship between Ca^{2+} signaling and the function of various iPSC-derived human cell types including neurons, astrocytes, and microglia. In addition, this line may be readily xenotransplanted for use with human/microglia chimeric models to examine functional Ca^{2+} responses to injury and pathology *in vivo*. Using Salsa6f-expressing microglia, we uncovered critical differences in how Ca^{2+} levels tune motility in WT and TREM2 KO microglia. By tracking instantaneous velocity at the same time as Ca^{2+} ratios in individual cells, we found that TREM2 KO cells with high Ca^{2+} levels show decreased speed whereas WT cells do not show any significant correlation between velocity and cytoplasmic Ca^{2+}. Reducing extracellular Ca^{2+} concentration in a Ca^{2+} clamp assay resulted in increased mean speed,

displacement, and straighter paths for TREM2 KO iPSC-microglia, but had no effect on these motility metrics in WT cells. Consistent with this observation, chemotaxis in TREM2 KO cells was restored by partially inhibiting P2RY12 receptors. The ability to regulate purinergic receptor activity may be required to decrease motility when nearby the damage site. TREM2 KO microglia may lack this ability and continue to move away from damage. Understanding why TREM2 KO cells do not or cannot decrease purinergic receptor expression after an insult may prove useful for therapeutic modulation of microglial activation states.

The studies presented here provide evidence that reducing purinergic receptor activity may be clinically applicable in Alzheimer's patients with TREM2 loss of function mutations. Pharmacologically targeting P2Y12 receptors to dampen both the Ca^{2+} dependent (PLC) and independent (DAG) arms of the GPCR signaling pathway may be useful to control microglial activation and motility. However, our results suggest that altering downstream Ca^{2+} flux may be sufficient, and thus CRAC (Orai1) channel blockers that would specifically inhibit the sustained Ca^{2+} signals without affecting the initial Ca^{2+} transient or the activation of DAG may be a more targeted approach.

Currently, TREM2 activating antibodies are being examined in early stage clinical trials (Alector Inc., 2021a; Wang et al., 2020b), making it critically important to understand the broad consequences of TREM2 signaling. Therefore, an understanding of how TREM2 influences responses to purinergic signals, and regulates Ca^{2+} signals more generally, is important in translationally relevant iPSC-microglia. Beyond TREM2, we have found that protective variants in MS4A6A and PLCG2 gene expression also

decrease P2RY12 and P2RY13 expression (unpublished data), suggesting this mechanism of microglial activation could be common to several microglial AD risk loci.

In summary, deletion of TREM2 renders iPSC-microglia highly sensitive to ADP, leading to prolonged Ca^{2+} influx which increases cell displacement by decreasing cell turning. Despite this, TREM2 KO microglia show a defect in chemotaxis that is likely due to their inability to sense ADP gradients. Decreasing purinergic signaling in TREM2 KO microglia is able to rescue directional migration by chemotaxis. We suggest that purinergic modulation or direct modulation of Ca^{2+} signaling could provide a novel therapeutic strategy in many AD patient populations, not solely those with reduced TREM2 function.

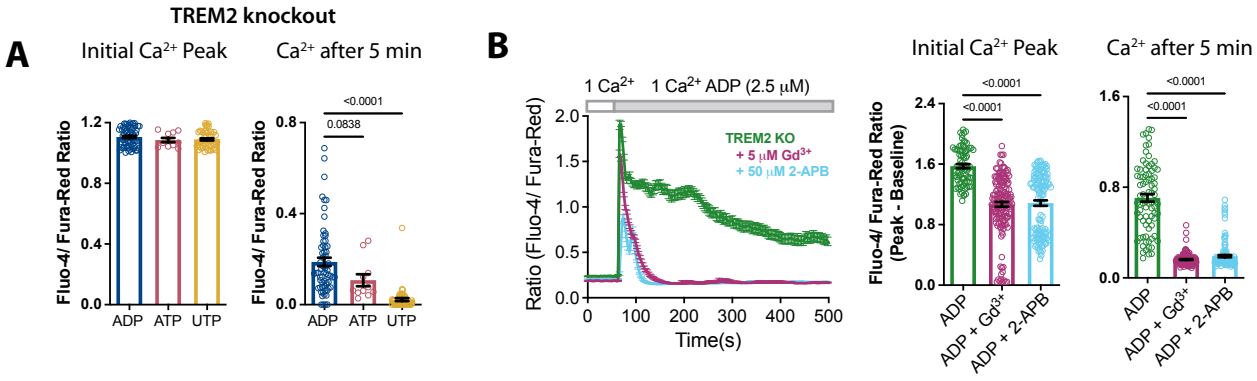

Figure 3.1- figure supplement 1. Differential engagement of SOCE by purinergic agonists. (**A**) Ca^{2+} responses in TREM2 KO iPSC-microglia 5 min after application of 2.5 μM ADP (blue), 2.5 μM ATP (red), and 10 μM UTP (yellow) that are gated for similar initial peak Ca^{2+} response to the agonists shown in the left panel (n=11-65 cells, pooled from 2 experiments). (**B**) Ratiometric Ca^{2+} responses in WT iPSC-microglia treated with 2-APB (50 μM) or Gd^{3+} (5 μM) to block store-operated Ca^{2+} entry (SOCE) (n= 80-148 cells). P-value calculated for **A** and **B** using ordinary one-way ANOVA with multiple comparisons.

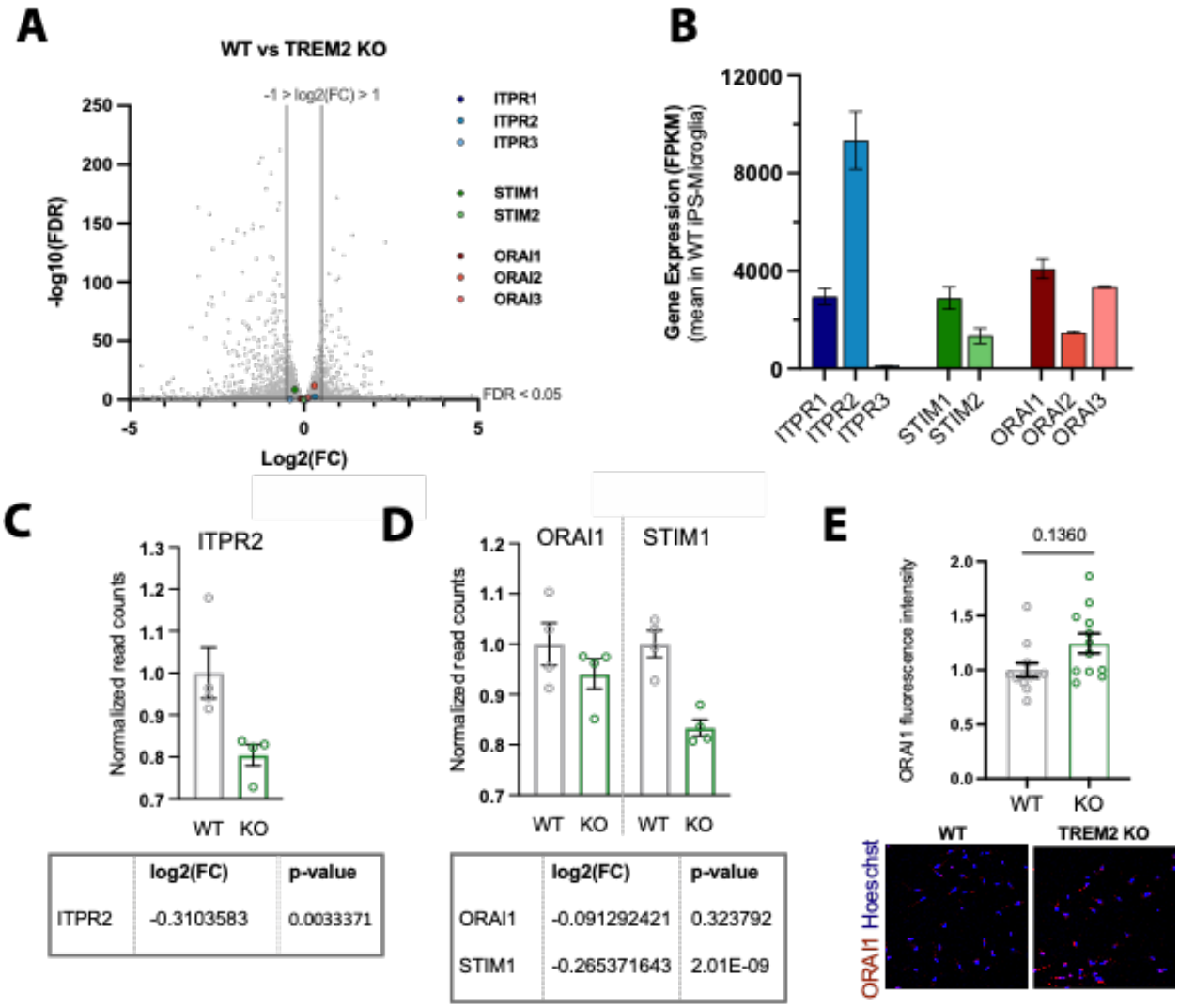

	log2(FC)	p-value
ITPR2	-0.3103583	0.0033371

	log2(FC)	p-value
ORAI1	-0.091292421	0.323792
STIM1	-0.265371643	2.01E-09

Figure 3.1- figure supplement 2. CRAC channel and IP3R not altered after knockdown of TREM2. (**A**) Volcano plot of differentially expressed genes from bulk RNA-sequencing of WT and TREM2 KO iPSC-microglia (n=4). Genes for IP3R, STIM1, and ORAI1 are highlighted. (**B**) Raw frequency per kilobase million reads (FPKM) in iPSC-microglia. (**C**) RNA normalized read counts of highly expressed isoforms for (**C**) IP3R, (**D**) STIM1, and ORAI1. Adjusted p-values from DESeq2. (**E**) Immunofluorescence of ORAI1 in WT and TREM2 KO iPSC-microglia. n=3 images per well from 4 independent wells; students t-test.

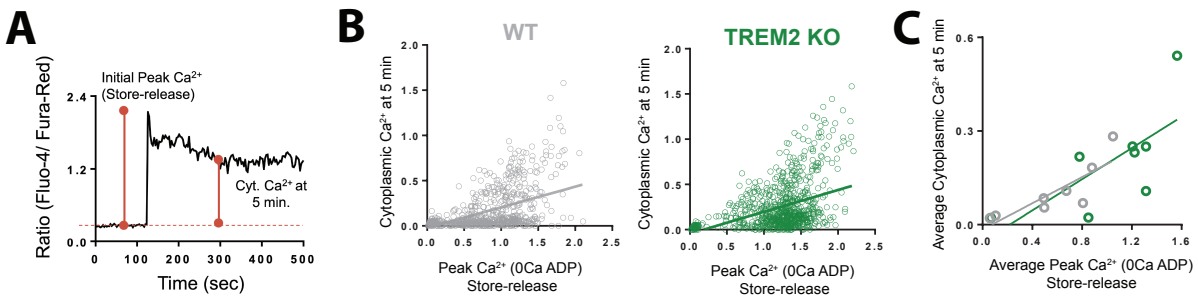

Figure 3.1- figure supplement 3. SOCE engagement is not altered in TREM2 KO. (**A**) Representative single-cell trace of Ca^{2+} signal in response to ADP in 1mM extracellular Ca^{2+} buffer showing the scheme for measuring ER store-release as the initial Ca^{2+} peak and SOCE as cytosolic Ca^{2+} level 5 min after ADP application. (**B**) Scatter-plot showing correlation of initial ADP-induced Ca^{2+} response (store-release) and cytoplasmic Ca^{2+} 5 minutes (SOCE) in WT (grey) and KO (green) cells (N= 866-935 cells from multiple imaging runs with a range of ADP doses). (**C**) Correlation between ADP-induced store-release and SOCE using the same data-set in B but with each data-point representing average Ca^{2+} response to the following doses of ADP in 1 mM Ca^{2+} (in mM: 0.001, 0.1, 0.5, 1, 2, 2.5, 5, 10). WT and TREM2 KO data are overlaid in the same scatter-plot. (Comparison of slopes between WT and TREM2 KO: p-value = 0.7631; Extra sum of squares F test).

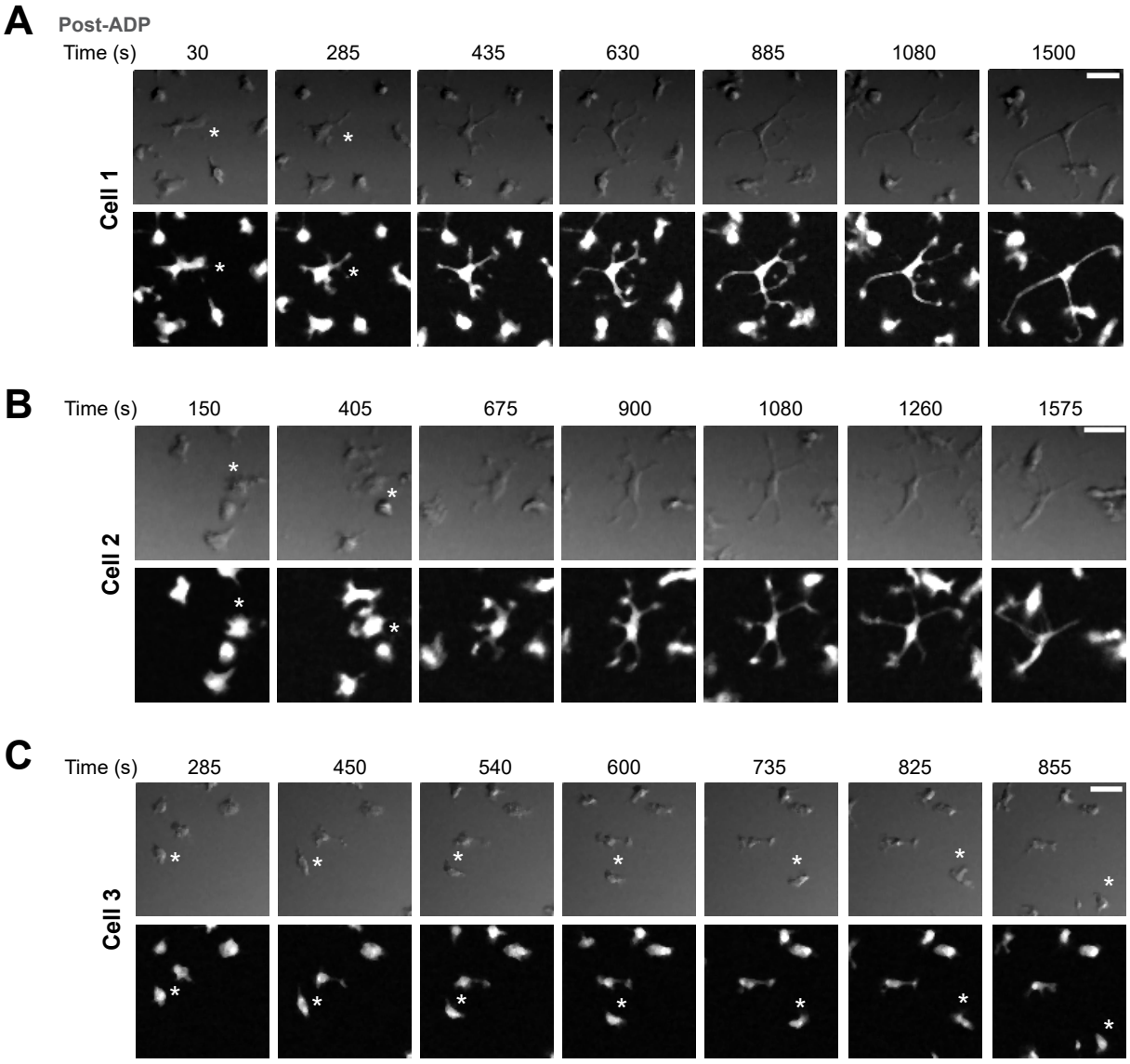

Figure 3.3- figure supplement 1. ADP-mediated process extension in WT iPSC-microglia. (A) Representative images of a cell (Cell 1) from a time-lapse experiment showing increased branching and extension of processes in WT iPSC-microglia, at times indicated following addition of 2.5 μM ADP. Bright field DIC images (top row) and GFP images (bottom row) are shown. (**B**) Another example of a cell (Cell 2) showing process extension in the same imaging field. (**C**) A motile cell (Cell 3) in the same imaging field is shown for comparison. Note the lack of displacement in cells that extend their process, and lack of significant process extension in a highly motile cell. Scale bar: 15 μM.

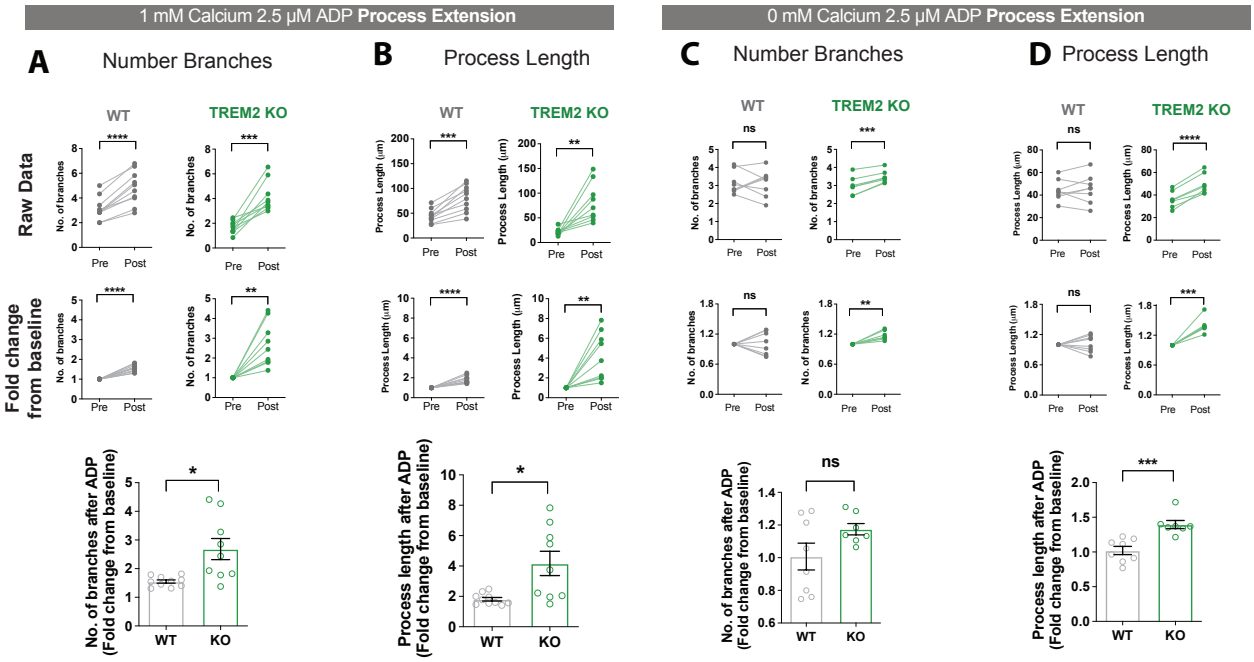

Figure 3.4- figure supplement 1. Comparison of process extension in WT and TREM2 KO Microglia. Branching and process extension in WT and TREM2 KO iPSC-microglia 30 min after addition of ADP in (**A-B**) 1 mM or (**C-D**) 0 mM extracellular Ca^{2+} buffer. (**A**) Data is displayed as paired-plots showing average branch number per cell in an imaging field (top row) and normalized to pre-ADP values for each imaging field (middle row). Bottom row shows fold change of branching after ADP treatment for WT (grey) and KO (green) iPSC-microglia. (**B**) Summary of change in process length in the same dataset as A (n=151-158 cells, WT; 133-167 cells, KO; 9-10 imaging fields, 3-4 experiments). (**C-D**) Same analysis as A, B but with ADP in Ca^{2+} free buffer (n=137-143 cells, 8 imaging fields, 2-3 experiments). (**A-D**) p-value calculated by two-tailed paired Students t-test for the paired-plots, and by unpaired t-test when comparing fold-change in WT and KO cells.

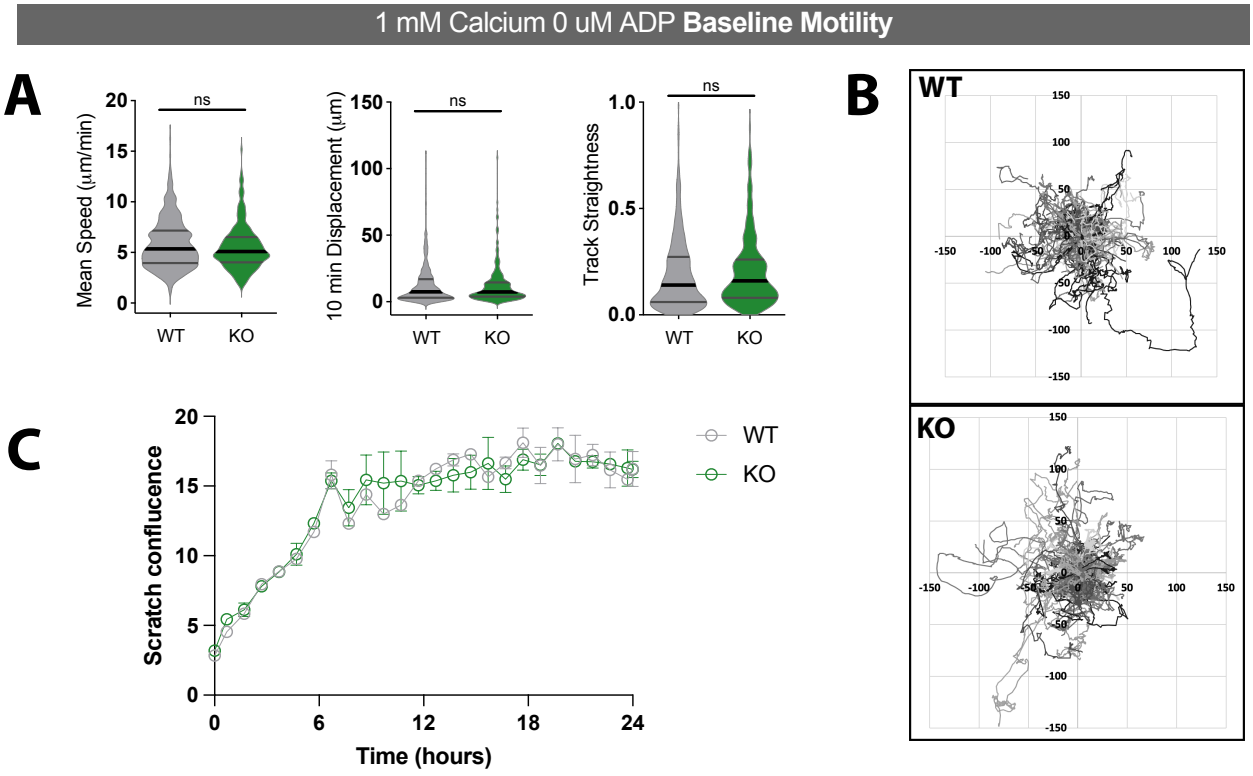

Figure 3.4- figure supplement 2. Baseline motility is equivalent in WT and TREM2 KO iPSC-microglia. Motility tested with no stimulation in Ca^{2+} containing medium. (**A**) Mean Speed, Displacement over 10 min, and track straightness are unchanged (student's t-test). (**B**) Flower plots show similar displacement from origin for WT (top) and TREM2 KO (bottom) cells. (**C**) Scratch Wound performed via IncuCyte S3 WoundMaker shows no difference in migration into the scratch wound area. (Two-way ANOVA with multiple comparisons showed no significant difference. n=2 images per well over 3 independent wells.)

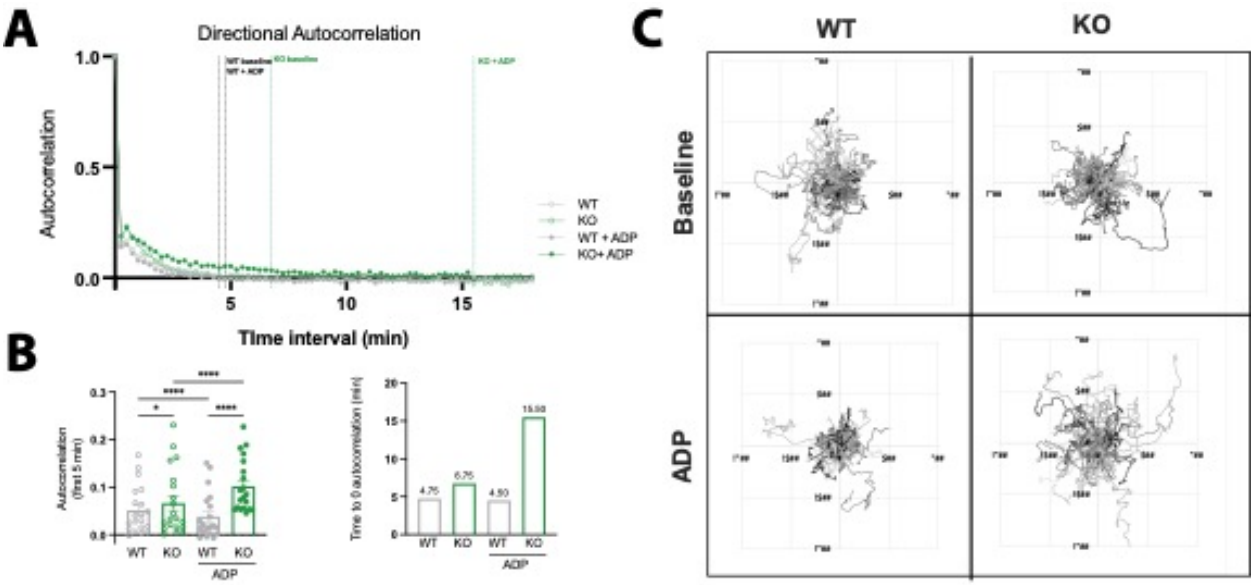

Figure 3.4- figure supplement 3. Increased Directional Persistence in TREM2 KO cells. Directional Autocorrelation calculated via DiPer excel macro. Due to lack of directional gradient, directional autocorrelation of motility vectors is expected to drop quickly (**A**) Directional autocorrelation of WT (grey) and KO (green) iPSC-microglia at baseline (open circles) or after ADP addition (filled circles). Lines denote where each condition shows directional persistence of 0 (no correlation between previous vectors). Data is graphed below plot as mean autocorrelation values in the first 5 minutes (one-way ANOVA) and time (min) until autocorrelation reaches zero. (**B**) Flower plots of all cell tracks over 20 min.

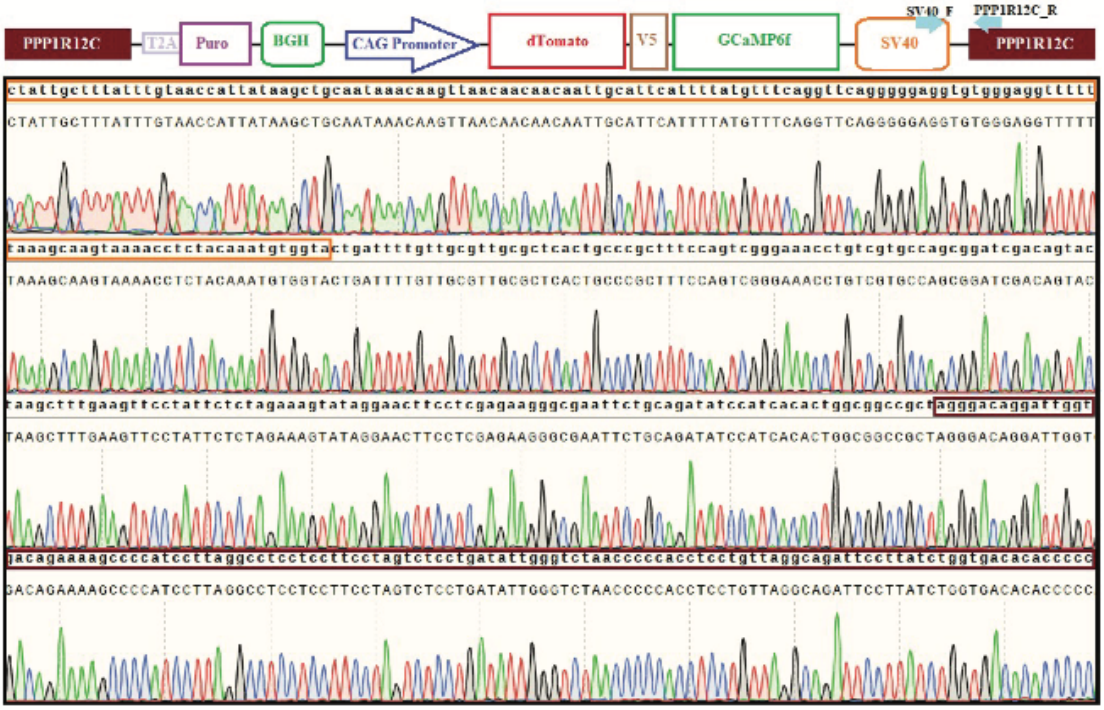

Figure 3.5- figure supplement 1. Generation of Salsa6f iPSC line. Construct design for the Salsa6f knock-in template (top) Primers for sequence validation marked with blue arrows. Sanger sequencing to confirm proper integration of Salsa6f cassette into AAVS1 Safe Harbor Locus (bottom).

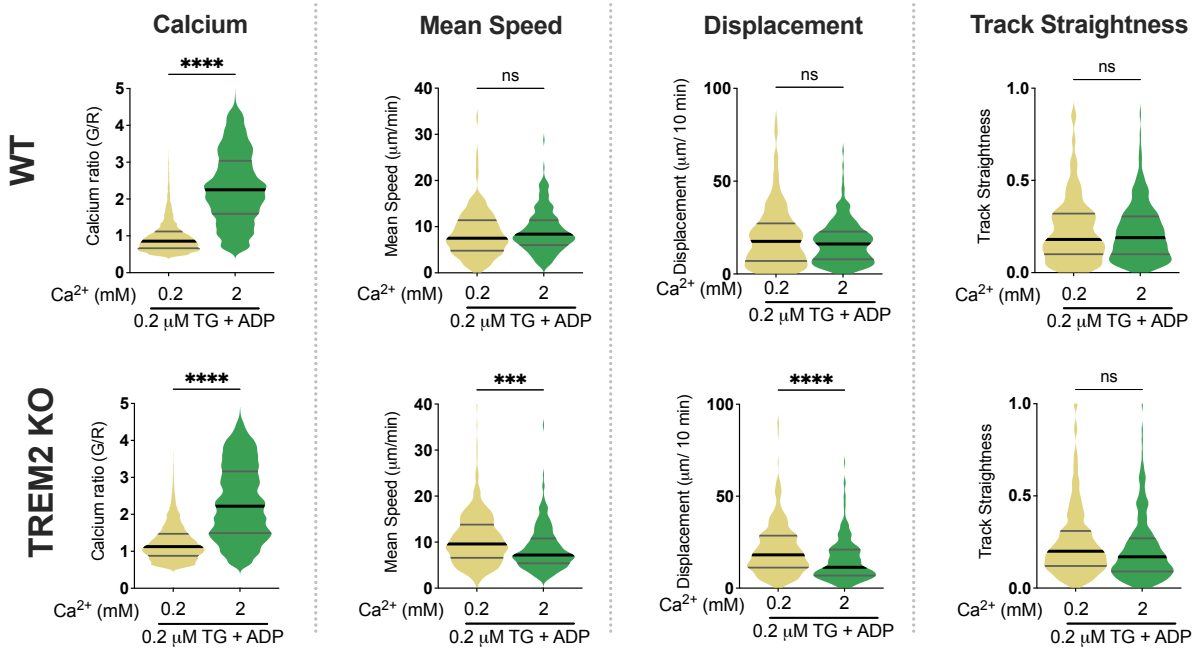

Figure 3.6- figure supplement 1. Cell motility after ADP and Ca^{2+} "clamp". Ca^{2+} ratios and microglia motility in WT (top) and KO (bottom) microglia. Ca^{2+} clamp experiments with ADP added: yellow (0.2 mM Ca^{2+}, TG + ADP), green (2 mM Ca^{2+}, TG + ADP). Students t-test **** $p < 0.0001$; *** $p = 0.0001$. n=164-393 cells.

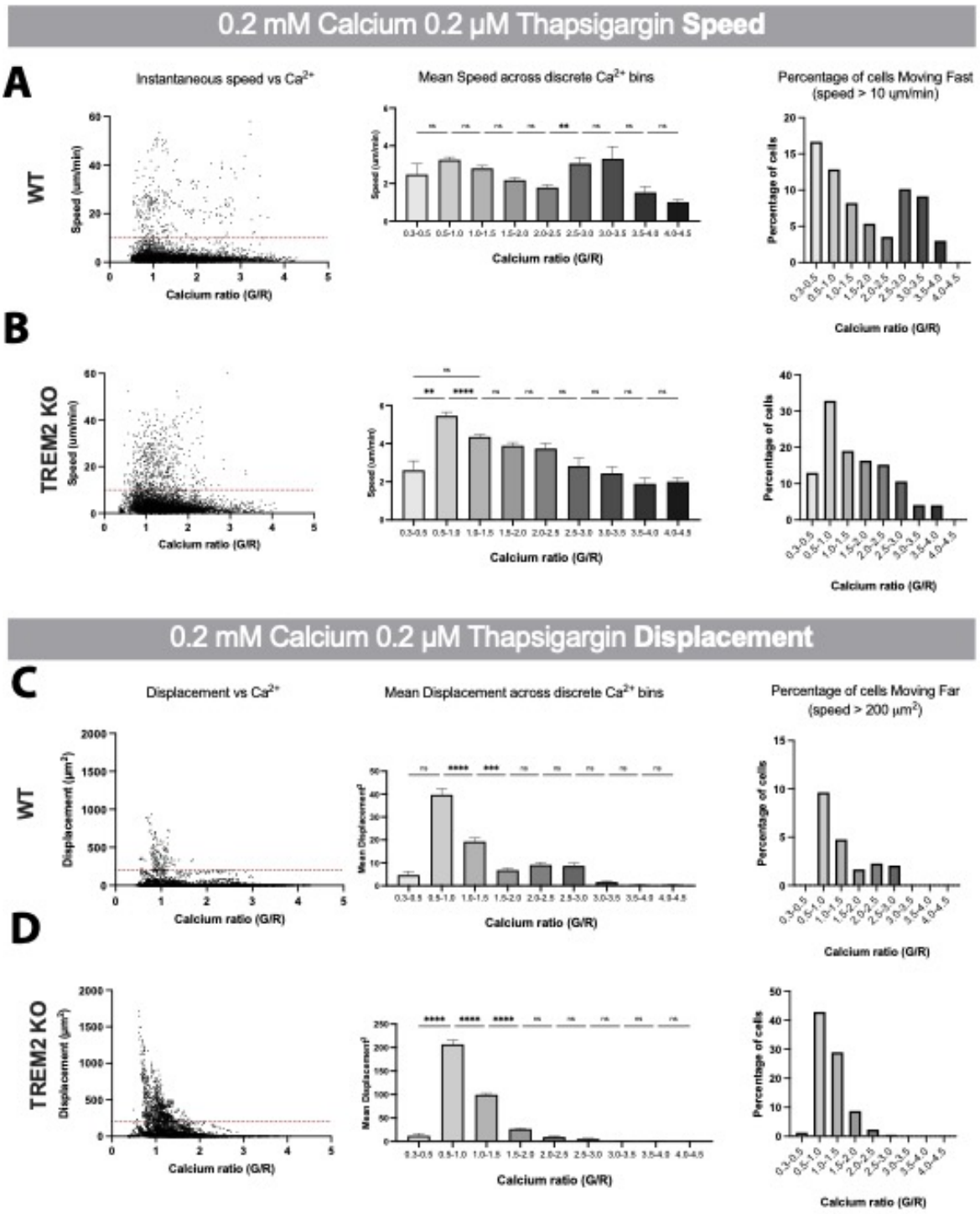

Figure 3.6- figure supplement 2. Ca^{2+} tuning of mean speed and track displacement length. Correlation between instantaneous Ca^{2+} and (**A,B**) mean speed or (**C,D**) cumulative displacement. Each dot represents an individual cell for an individual frame. Dotted red line represents (**A,C**) mean speed 10 µm/min) or (**B,D**) displacement of 200 um^2. WT cells (**C**) displace less than KO cells (**D**). For each cell type, farther displacement is correlated with lower G/R Ca^{2+} ratios. Cells which maintain elevated cytoplasmic Ca^{2+} do not displace as far.

CHAPTER 4

CONCLUSION AND FUTURE DIRECTIONS

In order to develop functional therapeutics for Alzheimer's disease, we need to better understand the processes which underlie this neurodegenerative disease. Investing in comprehensive studies of the molecular pathways which influence neuroinflammation, brain homeostasis, and aging will no doubt better our chances of finding functional biomarkers or even therapies for patients across neurodegenerative diseases.

The studies presented here represent a critical step forward in our understanding of human microglial biology and AD-risk. As better and better model systems for human microglia become available, we will be able to confidently delineate the differences between model organisms and gain insight as to which models are appropriate to answer the many outstanding biological questions. Adapting models such as chimeric transplantation of iPS-microglia will also allow us gain an understanding of what microglial functions are cell intrinsic or environmentally controlled. Additionally, studies using chimeric systems to study the differences between microglial gene expression or function *in vitro* versus *in vivo* will provide recursive feedback to improve future iterations of *in vitro* culture methods (Hasselmann et al., 2019).

Because *in vitro* models such as iPS-Microglia are currently being used as gatekeepers for translational therapeutic studies, it is critically important that these models accurately recapitulate human biology. These research avenues are also being supported by generation of metadata repositories comparing RNA sequencing of most available microglial models in order to delineate where improvements are needed in *in vitro* culturing systems. A recent analysis by Stemformatics highlighted specific shortcomings in cultured microglial systems showing that many of these models are more

similar to peripheral monocytes than human microglia. However, this group also found that the iPS-Microglia protocol presented here stands out as one of the best in replicating human microglial transcription. This was exemplified by up-regulation of CIITA, a transcription factor found in only one other iPS-derived microglial model but all primary microglial cells (Abud et al., 2017; McQuade et al., 2018; Rajab et al., 2021).

While the model system presented here may be one of the best currently available, there still remain caveats to using stem cell derived models. One caveat of all iPS-derived cellular models is the developmental age of cultured cells. Through the reprogramming process, donor cells go through some rejuvenation and lose molecular markers of age. While *in vivo* models can be maintained until old age, *in vitro* cells are comparatively quite young. However, recent data does suggest that induced pluripotent stem cells developed from aged donors do have some epigenetic memory and show age-dependent changes in function (Lee et al., 2020; Mertens et al., 2021). The extent of aging in iPS-cells remains under debate. Moving forward, there are ongoing efforts to “age” induced pluripotent stem cell lines. Dr. Studer’s group has had some success by inducing mutations normally found in progeria patients in order to create accelerated cellular aging (Miller et al., 2013). As these fields become more advanced, we will be able to develop more accurate cellular models of aging and adapt iPS-Microglia to better represent aged immune responses. These future directions will support our basic understanding of human microglial aging and inform therapeutic strategies.

Despite these challenges, the model system described here and subsequent functional studies have successfully uncovered novel phenotypes which occur as a consequence of loss of TREM2 function. We have been able to demonstrate differences

in survival with TREM2 deficient cells showing higher susceptibility to caspase 3/7 apoptotic signaling. This was true in baseline “healthy” culture as well as after aggravation by a CSF1R cytokine starvation paradigm. This priming also seems present *in vivo* as evidenced by specific up-regulation of a p53 driven apoptotic cluster within transcriptomes isolated from TREM2-knockout microglia from a 5x-MITRG Alzheimer’s model. It remains unclear how this phenotype effects pathogenesis *in vivo*, though it is likely that regulation of ERK signaling will be relevant.

Following evidence from RNA-sequencing, we also highlighted a deficit in SYK-dependent phagocytosis which will likely be informative to understanding microglial interactions with neurons and pathological protein accumulations. Lastly, by combining classic *in vitro* migration studies and chimeric transplantation, we profiled a stark migratory deficit in TREM2 knockout microglia. Our *in vitro* mechanistic studies show a deficit in migration to beta-amyloid alone as well as beta-amyloid expressing neuron and astrocyte mixed cultures. With the more complex mixed culture system, we find that migration is reliant on CXCR4-CXCL12 (SDF1a) signaling.

These studies sparked further interest in using iPS-microglia to study motility and migration. Focusing in on the classic purinergic chemoattractants (ATP, ADP, UTP) we characterized hyperactive calcium signaling in TREM2-knockout microglia across many doses of ADP. These responses are resultant of increased receptor expression and not ER store content, SOCE engagement, or IP3R expression. Furthermore, we show that the increased calcium responses to ADP lead to functional differences in TREM2 knockout cells including increased process extension and displacement (decreased klinokinesis).

Although these nondirectional motility assays would suggest TREM2 knockout cells may be better at migration, we find TREM2 knockout microglia unable to perform directed chemotaxis. Potentially this is due to an inability to sense gradients of ADP. At the calcium flux level, TREM2 knockout cells show similar responses across several fold change concentrations of ADP. For the same concentrations, WT cells show a dose response curve suggesting differential encoding of calcium concentrations. More studies will be needed to investigate how concentration gradients are recognized and encoded in microglia, however, we do show preliminary studies in TREM2 knockout cells suggesting calcium flux is able to tune microglial motility with maximal calcium responses resulting in lowered speed and displacement.

While the studies presented here have answered key questions concerning microglial function and TREM2-specific alterations of these processes, this work has also provided insight on how little is known about microglial function. Current studies in the field draw from similar functions in monocytes, tissue resident macrophages, or even other immune cells such as T-cells. While these other cell systems do provide a foundational knowledge of cellular functions, it is imperative that we treat microglia as a distinct cell type and not over generalize from related cells. Several findings from these studies presented here (MCSF mediated survival, differences between SYK dependent and independent phagocytosis, unique SOCE engagement for ADP, lack of calcium tuning of migration in WT cells) seem to be unique to microglia and have not been described in studies of peripheral immune cells. It will be interesting to understand how these smaller pathway level changes lead to overall functional differences in microglia.

As microglia or microglial receptors advance as a therapeutic strategies, deeper understanding of these differences will be required.

Currently there are several ongoing clinical trials investigating the possibility of immunotherapies for Alzheimer's disease. AL002 is a phase 2 clinical trial which began from a partnership between AbbVie and Alector (Alector Inc., 2021a). This trial aims to use a TREM2 activating antibody in order to promote TREM2 signaling and clearance of beta-amyloid (Wang et al., 2020b). In a Phase 1 trial, INVOKE (Alector Inc., 2020), this antibody was found to be well tolerated with no serious side effects. Furthermore, soluble TREM2 was decreased after treatment suggesting proper targeting of the antibody. Denali Therapeutics is also beginning IND-enabling studies on a TREM2 modulating antibody: DNL919 (ATV:TREM2) (Inc, 2021). These clinical trials will be informed by the research conducted in this thesis. As the field moves towards targeting TREM2 in human patients, a well-defined understanding of the downstream effects this manipulation will have is critical in determining not only safety but efficacy of the target engagement.

Anti-TREM2 antibodies are also in development as tools for biomarker identification. This field has recently shown some efficacy in murine models of AD with PET radioligands, however the model still requires better perfusion approaches to be translated for human use (Meier et al., 2021). Furthermore, to support use of this diagnostic tool, there will need to be more comprehensive studies of the dynamics of TREM2 throughout the course of AD pathogenesis as these trends are still not fully understood (Ewers et al., 2020; Knapskog et al., 2020; Ma et al., 2020; Suárez-Calvet et al., 2019). However, these antibodies will certainly be useful to perform the necessary

studies of TREM2 dynamics. Human studies will likely be supported by murine models including the chimeric iPS-Microglia model described in this dissertation.

Beyond TREM2, several other Alzheimer's risk genes are also under investigation for clinical application. Alector is currently undergoing a phase 1 trial on AL003 to determine safety of inhibitory anti-CD33 antibody (Alector Inc., 2021b). David Holtzmann's group has also shown preliminary benefit with an antibody targeted to aggregated APOE4 (HAE-4) (Liao et al., 2018). As we begin to understand the molecular mechanisms of how immune-specific AD risk loci impact microglial activation states, it is likely that more diverse classes of AD immunotherapies will be developed. I expect important mechanistic and efficacy studies will be performed with iPS-microglia models or chimeric adaptations of these models in order to show target engagement in human cells.

Together, the data presented in this dissertation describes the development and use of a novel iPS-microglia model to examine the function of human microglia *in vitro* and through xenotransplantation. Using this model, we have been able to directly interrogate the function of an Alzheimer's risk gene, Triggering Receptor Expressed on Myeloid Cells 2. These studies have uncovered several functions of TREM2 in human microglia and suggests a mechanism by which mutations in TREM2 inhibit microglial activation states and drive disease onset. Manipulation of these microglial states should be investigated further and may lead to therapeutic strategies that will benefit patients suffering from diverse neurodegenerative diseases wherein microglial activation has been implicated including Parkinson's disease, ALS, and Alzheimer's disease.

REFERENCES

Abud, E.M., Ramirez, R.N., Martinez, E.S., Healy, L.M., Nguyen, C.H.H., Newman, S.A., Yeromin, A.V., Scarfone, V.M., Marsh, S.E., Fimbres, C., et al. (2017). iPSC-Derived Human Microglia-like Cells to Study Neurological Diseases. Neuron *94*, 278-293.e9.

Abutbul, S., Shapiro, J., Szaingurten-Solodkin, I., Levy, N., Carmy, Y., Baron, R., Jung, S., and Monsonego, A. (2012). TGF-β signaling through SMAD2/3 induces the quiescent microglial phenotype within the CNS environment. Glia *60*, 1160–1171.

Alector Inc. (2020). A Phase I Study Evaluating the Safety, Tolerability, Pharmacokinetics, Pharmacodynamics, and Immunogenicity of Single and Multiple Doses of AL002 in Healthy Participants and in Participants With Mild to Moderate Alzheimer's Disease (clinicaltrials.gov).

Alector Inc. (2021a). A Phase 2 Randomized, Double-Blind, Placebo-Controlled, Multicenter Study to Evaluate the Efficacy and Safety of AL002 in Participants With Early Alzheimer's Disease (clinicaltrials.gov).

Alector Inc. (2021b). A Phase I Study Evaluating the Safety, Tolerability, Pharmacokinetics, Pharmacodynamics, and Immunogenicity of Single and Multiple Doses of AL003 in Healthy Participants and in Participants With Mild to Moderate Alzheimer's Disease. (clinicaltrials.gov).

Allen, M., Zou, F., Chai, H.S., Younkin, C.S., Crook, J., Pankratz, V.S., Carrasquillo, M.M., Rowley, C.N., Nair, A.A., Middha, S., et al. (2012). Novel late-onset Alzheimer disease loci variants associate with brain gene expression. Neurology *79*, 221–228.

Alzheimer, A., Stelzmann, R.A., Schnitzlein, H.N., and Murtagh, F.R. (1995). An English translation of Alzheimer's 1907 paper, "Uber eine eigenartige Erkankung der Hirnrinde." Clin Anat *8*, 429–431.

Andersen, M.S., Bandres-Ciga, S., Reynolds, R.H., Hardy, J., Ryten, M., Krohn, L., Gan-Or, Z., Holtman, I.R., and Pihlstrøm, L. (2021). Heritability Enrichment Implicates Microglia in Parkinson's Disease Pathogenesis. Annals of Neurology *89*, 942–951.

Andreone, B.J., Przybyla, L., Llapashtica, C., Rana, A., Davis, S.S., Lengerich, B. van, Lin, K., Shi, J., Mei, Y., Astarita, G., et al. (2020). Alzheimer's-associated PLCγ2 is a signaling node required for both TREM2 function and the inflammatory response in human microglia. Nature Neuroscience 1–12.

Andrews, S.J., Fulton-Howard, B., and Goate, A. (2020). Interpretation of risk loci from genome-wide association studies of Alzheimer's disease. Lancet Neurol.

Asai, H., Ikezu, S., Tsunoda, S., Medalla, M., Luebke, J., Haydar, T., Wolozin, B., Butovsky, O., Kügler, S., and Ikezu, T. (2015). Depletion of microglia and inhibition of exosome synthesis halt tau propagation. Nat. Neurosci. *18*, 1584–1593.

Atagi, Y., Liu, C.-C., Painter, M.M., Chen, X.-F., Verbeeck, C., Zheng, H., Li, X., Rademakers, R., Kang, S.S., Xu, H., et al. (2015). Apolipoprotein E Is a Ligand for Triggering Receptor Expressed on Myeloid Cells 2 (TREM2). J. Biol. Chem. *290*, 26043–26050.

Bailey, C.C., DeVaux, L.B., and Farzan, M. (2015). The Triggering Receptor Expressed on Myeloid Cells 2 Binds Apolipoprotein E. J. Biol. Chem. *290*, 26033–26042.

Balasingam, V., Tejada-Berges, T., Wright, E., Bouckova, R., and Yong, V.W. (1994). Reactive astrogliosis in the neonatal mouse brain and its modulation by cytokines. J. Neurosci. *14*, 846–856.

Bemiller, S.M., McCray, T.J., Allan, K., Formica, S.V., Xu, G., Wilson, G., Kokiko-Cochran, O.N., Crish, S.D., Lasagna-Reeves, C.A., Ransohoff, R.M., et al. (2017). TREM2 deficiency exacerbates tau pathology through dysregulated kinase signaling in a mouse model of tauopathy. Molecular Neurodegeneration *12*, 74.

Bennett, M.L., Bennett, F.C., Liddelow, S.A., Ajami, B., Zamanian, J.L., Fernhoff, N.B., Mulinyawe, S.B., Bohlen, C.J., Adil, A., Tucker, A., et al. (2016). New tools for studying microglia in the mouse and human CNS. Proc. Natl. Acad. Sci. U.S.A. *113*, E1738-1746.

Benveniste, E.N., and Benos, D.J. (1995). TNF-alpha- and IFN-gamma-mediated signal transduction pathways: effects on glial cell gene expression and function. FASEB J. *9*, 1577–1584.

Bhaskar, K., Konerth, M., Kokiko-Cochran, O.N., Cardona, A., Ransohoff, R.M., and Lamb, B.T. (2010). Regulation of tau pathology by the microglial fractalkine receptor. Neuron *68*, 19–31.

Bhaskar, K., Maphis, N., Xu, G., Varvel, N.H., Kokiko-Cochran, O.N., Weick, J.P., Staugaitis, S.M., Cardona, A., Ransohoff, R.M., Herrup, K., et al. (2014). Microglial Derived Tumor Necrosis Factor-α Drives Alzheimer's Disease-Related Neuronal Cell Cycle Events. Neurobiol Dis *62*.

Borges, P.A., Waclawiak, I., Georgii, J.L., Fraga-Junior, V. da S., Barros, J.F., Lemos, F.S., Russo-Abrahão, T., Saraiva, E.M., Takiya, C.M., Coutinho-Silva, R., et al. (2021). Adenosine Diphosphate Improves Wound Healing in Diabetic Mice Through P2Y12 Receptor Activation. Front. Immunol. *12*.

Borowiak, M., Maehr, R., Chen, S., Chen, A.E., Tang, W., Fox, J.L., Schreiber, S.L., and Melton, D.A. (2009). Small molecules efficiently direct endodermal differentiation of mouse and human embryonic stem cells. Cell Stem Cell *4*, 348–358.

Borroni, B., Ferrari, F., Galimberti, D., Nacmias, B., Barone, C., Bagnoli, S., Fenoglio, C., Piaceri, I., Archetti, S., Bonvicini, C., et al. (2014). Heterozygous TREM2 mutations in frontotemporal dementia. Neurobiol. Aging *35*, 934.e7-10.

Bouchon, A., Hernández-Munain, C., Cella, M., and Colonna, M. (2001). A Dap12-Mediated Pathway Regulates Expression of Cc Chemokine Receptor 7 and Maturation of Human Dendritic Cells. Journal of Experimental Medicine *194*, 1111–1122.

Boza-Serrano, A., Yang, Y., Paulus, A., and Deierborg, T. (2018). Innate immune alterations are elicited in microglial cells before plaque deposition in the Alzheimer's disease mouse model 5xFAD. Sci Rep *8*.

Brawek, B., Schwendele, B., Riester, K., Kohsaka, S., Lerdkrai, C., Liang, Y., and Garaschuk, O. (2014). Impairment of in vivo calcium signaling in amyloid plaque-associated microglia. Acta Neuropathol *127*, 495–505.

Bray, N.L., Pimentel, H., Melsted, P., and Pachter, L. (2016a). Near-optimal probabilistic RNA-seq quantification. Nature Biotechnology *34*, 525–527.

Bray, N.L., Pimentel, H., Melsted, P., and Pachter, L. (2016b). Erratum: Near-optimal probabilistic RNA-seq quantification. Nat. Biotechnol. *34*, 888.

Brelstaff, J., Tolkovsky, A.M., Ghetti, B., Goedert, M., and Spillantini, M.G. (2018). Living Neurons with Tau Filaments Aberrantly Expose Phosphatidylserine and Are Phagocytosed by Microglia. Cell Rep *24*, 1939-1948.e4.

Brown, G.C., and Neher, J.J. (2014). Microglial phagocytosis of live neurons. Nature Reviews Neuroscience *15*, 209–216.

Burns, A., Jacoby, R., Luthert, P., and Levy, R. (1990). Cause of death in Alzheimer's disease. Age Ageing *19*, 341–344.

Butovsky, O., Jedrychowski, M.P., Moore, C.S., Cialic, R., Lanser, A.J., Gabriely, G., Koeglsperger, T., Dake, B., Wu, P.M., Doykan, C.E., et al. (2014). Identification of a unique TGF-β-dependent molecular and functional signature in microglia. Nat. Neurosci. *17*, 131–143.

Cf, Y., Sp, L., Cp, C., Yh, W., Ws, H., Cp, C., Yt, C., and Jy, W. (2018). Loss of GPNMB Causes Autosomal-Recessive Amyloidosis Cutis Dyschromica in Humans (Am J Hum Genet).

Chen, P., Zhao, W., Guo, Y., Xu, J., and Yin, M. (2016). CX3CL1/CX3CR1 in Alzheimer's Disease: A Target for Neuroprotection. Biomed Res Int *2016*.

Chen, S., Luo, D., Streit, W.J., and Harrison, J.K. (2002). TGF-beta1 upregulates CX3CR1 expression and inhibits fractalkine-stimulated signaling in rat microglia. J. Neuroimmunol. *133*, 46–55.

Cheng, Q., Danao, J., Talreja, S., Wen, P., Yin, J., Sun, N., Li, C.-M., Chui, D., Tran, D., Koirala, S., et al. (2018). TREM2-activating antibodies abrogate the negative pleiotropic effects of the Alzheimer's disease variant Trem2R47H on murine myeloid cell function. J. Biol. Chem. *293*, 12620–12633.

Cheng-Hathaway, P.J., Reed-Geaghan, E.G., Jay, T.R., Casali, B.T., Bemiller, S.M., Puntambekar, S.S., von Saucken, V.E., Williams, R.Y., Karlo, J.C., Moutinho, M., et al. (2018). The Trem2 R47H variant confers loss-of-function-like phenotypes in Alzheimer's disease. Mol Neurodegener *13*, 29.

Choi, S.H., Kim, Y.H., Hebisch, M., Sliwinski, C., Lee, S., D'Avanzo, C., Chen, H., Hooli, B., Asselin, C., Muffat, J., et al. (2014). A three-dimensional human neural cell culture model of Alzheimer's disease. Nature *515*, 274–278.

Condello, C., Yuan, P., Schain, A., and Grutzendler, J. (2015). Microglia constitute a barrier that prevents neurotoxic protofibrillar Aβ42 hotspots around plaques. Nat Commun *6*, 6176.

Corriden, R., and Insel, P.A. (2012). New insights regarding the regulation of chemotaxis by nucleotides, adenosine, and their receptors. Purinergic Signal. *8*, 587–598.

Cosker, K., Mallach, A., Limaye, J., Piers, T.M., Staddon, J., Neame, S.J., Hardy, J., and Pocock, J.M. (2021). Microglial signalling pathway deficits associated with the patient derived R47H TREM2 variants linked to AD indicate inability to activate inflammasome. Sci Rep *11*, 13316.

Crotti, A., Benner, C., Kerman, B.E., Gosselin, D., Lagier-Tourenne, C., Zuccato, C., Cattaneo, E., Gage, F.H., Cleveland, D.W., and Glass, C.K. (2014). Mutant Huntingtin promotes autonomous microglia activation via myeloid lineage-determining factors. Nat Neurosci *17*, 513–521.

Cserép, C., Pósfai, B., Lénárt, N., Fekete, R., László, Z.I., Lele, Z., Orsolits, B., Molnár, G., Heindl, S., Schwarcz, A.D., et al. (2020). Microglia monitor and protect neuronal function through specialized somatic purinergic junctions. Science *367*, 528–537.

Cunningham, F., Achuthan, P., Akanni, W., Allen, J., Amode, M.R., Armean, I.M., Bennett, R., Bhai, J., Billis, K., Boddu, S., et al. (2019). Ensembl 2019. Nucleic Acids Res. *47*, D745–D751.

Cuyvers, E., Bettens, K., Philtjens, S., Van Langenhove, T., Gijselinck, I., van der Zee, J., Engelborghs, S., Vandenbulcke, M., Van Dongen, J., Geerts, N., et al. (2014). Investigating the role of rare heterozygous TREM2 variants in Alzheimer's disease and frontotemporal dementia. Neurobiol. Aging *35*, 726.e11-19.

Das, R., and Chinnathambi, S. (2020). Actin-mediated Microglial Chemotaxis via G-Protein Coupled Purinergic Receptor in Alzheimer's Disease. Neuroscience *448*, 325–336.

Davalos, D., Grutzendler, J., Yang, G., Kim, J.V., Zuo, Y., Jung, S., Littman, D.R., Dustin, M.L., and Gan, W.-B. (2005). ATP mediates rapid microglial response to local brain injury in vivo. Nat. Neurosci. *8*, 752–758.

Daws, M.R., Sullam, P.M., Niemi, E.C., Chen, T.T., Tchao, N.K., and Seaman, W.E. (2003). Pattern Recognition by TREM-2: Binding of Anionic Ligands. The Journal of Immunology *171*, 594–599.

De Jager, P.L., Ma, Y., McCabe, C., Xu, J., Vardarajan, B.N., Felsky, D., Klein, H.-U., White, C.C., Peters, M.A., Lodgson, B., et al. (2018). A multi-omic atlas of the human frontal cortex for aging and Alzheimer's disease research. Sci Data *5*, 180142.

De Simone, R., Niturad, C.E., De Nuccio, C., Ajmone-Cat, M.A., Visentin, S., and Minghetti, L. (2010). TGF-β and LPS modulate ADP-induced migration of microglial cells through P2Y1 and P2Y12 receptor expression. J. Neurochem. *115*, 450–459.

Deming, Y., Filipello, F., Cignarella, F., Hsu, S., Mikesell, R., Li, Z., Del-Aguila, J.L., Dube, U., Farias, F.G., Bradley, J., et al. (2018). The MS4A gene cluster is a key regulator of soluble TREM2 and Alzheimer disease risk. BioRxiv.

Demuro, A., Parker, I., and Stutzmann, G.E. (2010). Calcium Signaling and Amyloid Toxicity in Alzheimer Disease. J Biol Chem *285*, 12463–12468.

Desjardins, M., Huber, L.A., Parton, R.G., and Griffiths, G. (1994). Biogenesis of phagolysosomes proceeds through a sequential series of interactions with the endocytic apparatus. J. Cell Biol. *124*, 677–688.

Dissing-Olesen, L., LeDue, J.M., Rungta, R.L., Hefendehl, J.K., Choi, H.B., and MacVicar, B.A. (2014). Activation of neuronal NMDA receptors triggers transient ATP-mediated microglial process outgrowth. J Neurosci *34*, 10511–10527.

Ditadi, A., and Sturgeon, C.M. (2016). Directed differentiation of definitive hemogenic endothelium and hematopoietic progenitors from human pluripotent stem cells. Methods *101*, 65–72.

Dolmetsch, R.E., Lewis, R.S., Goodnow, C.C., and Healy, J.I. (1997). Differential activation of transcription factors induced by Ca2+ response amplitude and duration. Nature *386*, 855–858.

Donat, C.K., Scott, G., Gentleman, S.M., and Sastre, M. (2017). Microglial Activation in Traumatic Brain Injury. Front Aging Neurosci *9*.

Dong, T.X., Othy, S., Jairaman, A., Skupsky, J., Zavala, A., Parker, I., Dynes, J.L., and Cahalan, M.D. (2017). T-cell calcium dynamics visualized in a ratiometric tdTomato-GCaMP6f transgenic reporter mouse. ELife *6*, e32417.

Donzella, G.A., Schols, D., Lin, S.W., Esté, J.A., Nagashima, K.A., Maddon, P.J., Allaway, G.P., Sakmar, T.P., Henson, G., DeClercq, E., et al. (1998). AMD3100, a small molecule inhibitor of HIV-1 entry via the CXCR4 co-receptor. Nature Medicine *4*, 72–77.

Douvaras, P., Sun, B., Wang, M., Kruglikov, I., Lallos, G., Zimmer, M., Terrenoire, C., Zhang, B., Gandy, S., Schadt, E., et al. (2017). Directed Differentiation of Human Pluripotent Stem Cells to Microglia. Stem Cell Reports *8*, 1516–1524.

Durafourt, B.A., Moore, C.S., Zammit, D.A., Johnson, T.A., Zaguia, F., Guiot, M.-C., Bar-Or, A., and Antel, J.P. (2012). Comparison of polarization properties of human adult microglia and blood-derived macrophages. Glia *60*, 717–727.

Eichhoff, G., Brawek, B., and Garaschuk, O. (2011). Microglial calcium signal acts as a rapid sensor of single neuron damage in vivo. Biochim Biophys Acta *1813*, 1014–1024.

Ellefsen, K.L., Settle, B., Parker, I., and Smith, I.F. (2014). An algorithm for automated detection, localization and measurement of local calcium signals from camera-based imaging. Cell Calcium *56*, 147–156.

Elmore, M.R.P., Najafi, A.R., Koike, M.A., Dagher, N.N., Spangenberg, E.E., Rice, R.A., Kitazawa, M., Matusow, B., Nguyen, H., West, B.L., et al. (2014). Colony-stimulating factor 1 receptor signaling is necessary for microglia viability, unmasking a microglia progenitor cell in the adult brain. Neuron *82*, 380–397.

Endo, F., Komine, O., Fujimori-Tonou, N., Katsuno, M., Jin, S., Watanabe, S., Sobue, G., Dezawa, M., Wyss-Coray, T., and Yamanaka, K. (2015). Astrocyte-derived TGF-β1 accelerates disease progression in ALS mice by interfering with the neuroprotective functions of microglia and T cells. Cell Rep *11*, 592–604.

Ewers, M., Biechele, G., Suárez-Calvet, M., Sacher, C., Blume, T., Morenas-Rodriguez, E., Deming, Y., Piccio, L., Cruchaga, C., Kleinberger, G., et al. (2020). Higher CSF sTREM2 and microglia activation are associated with slower rates of beta-amyloid accumulation. EMBO Mol Med *12*, e12308.

Eyo, U.B., Peng, J., Swiatkowski, P., Mukherjee, A., Bispo, A., and Wu, L.-J. (2014). Neuronal hyperactivity recruits microglial processes via neuronal NMDA receptors and microglial P2Y12 receptors after status epilepticus. J Neurosci *34*, 10528–10540.

Eyo, U.B., Mo, M., Yi, M.-H., Murugan, M., Liu, J., Yarlagadda, R., Margolis, D.J., Xu, P., and Wu, L.-J. (2018). P2Y12R-Dependent Translocation Mechanisms Gate the Changing Microglial Landscape. Cell Reports *23*, 959–966.

Fahira, A., Li, Z., Liu, N., and Shi, Y. (2019). Prediction of causal genes and gene expression analysis of attention-deficit hyperactivity disorder in the different brain region, a comprehensive integrative analysis of ADHD. Behav Brain Res *364*, 183–192.

Filipello, F., Morini, R., Corradini, I., Zerbi, V., Canzi, A., Michalski, B., Erreni, M., Markicevic, M., Starvaggi-Cucuzza, C., Otero, K., et al. (2018). The Microglial Innate Immune Receptor TREM2 Is Required for Synapse Elimination and Normal Brain Connectivity. Immunity *48*, 979-991.e8.

Frenkel, D., Wilkinson, K., Zhao, L., Hickman, S.E., Means, T.K., Puckett, L., Farfara, D., Kingery, N.D., Weiner, H.L., and El Khoury, J. (2013). Scara1 deficiency impairs clearance of soluble amyloid-β by mononuclear phagocytes and accelerates Alzheimer's-like disease progression. Nat Commun *4*, 2030.

Friedman, B.A., Srinivasan, K., Ayalon, G., Meilandt, W.J., Lin, H., Huntley, M.A., Cao, Y., Lee, S.-H., Haddick, P.C.G., Ngu, H., et al. (2018). Diverse Brain Myeloid Expression Profiles Reveal Distinct Microglial Activation States and Aspects of Alzheimer's Disease Not Evident in Mouse Models. Cell Rep *22*, 832–847.

Fu, H., Liu, B., Frost, J.L., Hong, S., Jin, M., Ostaszewski, B., Shankar, G.M., Costantino, I.M., Carroll, M.C., Mayadas, T.N., et al. (2012). Complement component C3 and complement receptor type 3 contribute to the phagocytosis and clearance of fibrillar Aβ by microglia. Glia *60*, 993–1003.

Garofalo, S., Porzia, A., Mainiero, F., Di Angelantonio, S., Cortese, B., Basilico, B., Pagani, F., Cignitti, G., Chece, G., Maggio, R., et al. (2017). Environmental stimuli shape microglial plasticity in glioma. Elife *6*.

Gilbert, D.F., Stebbing, M.J., Kuenzel, K., Murphy, R.M., Zacharewicz, E., Buttgereit, A., Stokes, L., Adams, D.J., and Friedrich, O. (2016). Store-Operated Ca2+ Entry (SOCE) and Purinergic Receptor-Mediated Ca2+ Homeostasis in Murine bv2 Microglia Cells: Early Cellular Responses to ATP-Mediated Microglia Activation. Front Mol Neurosci *9*, 111.

Gorelik, R., and Gautreau, A. (2014). Quantitative and unbiased analysis of directional persistence in cell migration. Nature Protocols *9*, 1931–1943.

Gosselin, D., Skola, D., Coufal, N.G., Holtman, I.R., Schlachetzki, J.C.M., Sajti, E., Jaeger, B.N., O'Connor, C., Fitzpatrick, C., Pasillas, M.P., et al. (2017). An environment-dependent transcriptional network specifies human microglia identity. Science *356*.

Gratuze, M., Leyns, C.E.G., Sauerbeck, A.D., St-Pierre, M.-K., Xiong, M., Kim, N., Serrano, J.R., Tremblay, M.-È., Kummer, T.T., Colonna, M., et al. (2020). Impact of TREM2^{R47H} variant on tau pathology–induced gliosis and neurodegeneration. J Clin Invest *130*, 4954–4968.

Griciuc, A., Serrano-Pozo, A., Parrado, A.R., Lesinski, A.N., Asselin, C.N., Mullin, K., Hooli, B., Choi, S.H., Hyman, B.T., and Tanzi, R.E. (2013). Alzheimer's disease risk gene CD33 inhibits microglial uptake of amyloid beta. Neuron *78*, 631–643.

Grom, A.A., Horne, A., and De Benedetti, F. (2016). Macrophage activation syndrome in the era of biologic therapy. Nat Rev Rheumatol *12*, 259–268.

Guedes, J.R., Lao, T., Cardoso, A.L., and El Khoury, J. (2018). Roles of Microglial and Monocyte Chemokines and Their Receptors in Regulating Alzheimer's Disease-Associated Amyloid-β and Tau Pathologies. Front. Neurol. *9*.

Guo, B., Huang, X., Cooper, S., and Broxmeyer, H.E. (2017). Glucocorticoid hormone-induced chromatin remodeling enhances human hematopoietic stem cell homing and engraftment. Nature Medicine *23*, 424–428.

Haenseler, W., Sansom, S.N., Buchrieser, J., Newey, S.E., Moore, C.S., Nicholls, F.J., Chintawar, S., Schnell, C., Antel, J.P., Allen, N.D., et al. (2017). A Highly Efficient Human Pluripotent Stem Cell Microglia Model Displays a Neuronal-Co-culture-Specific Expression Profile and Inflammatory Response. Stem Cell Reports *8*, 1727–1742.

Hafemeister, C. (2019). sctransform: Variance Stabilizing Transformations for Single Cell UMI Data.

Hall-Roberts, H., Agarwal, D., Obst, J., Smith, T.B., Monzón-Sandoval, J., Di Daniel, E., Webber, C., James, W.S., Mead, E., Davis, J.B., et al. (2020). TREM2 Alzheimer's variant R47H causes similar transcriptional dysregulation to knockout, yet only subtle functional phenotypes in human iPSC-derived macrophages. Alzheimers Res Ther *12*, 151.

Hammond, T.R., Robinton, D., and Stevens, B. (2018). Microglia and the Brain: Complementary Partners in Development and Disease. Annu. Rev. Cell Dev. Biol.

Hanisch, U.-K. (2002). Microglia as a source and target of cytokines. Glia *40*, 140–155.

Hardy, J.A., and Higgins, G.A. (1992). Alzheimer's disease: the amyloid cascade hypothesis. Science *256*, 184–185.

Harris, L.D., Jasem, S., and Licchesi, J.D.F. (2020). The Ubiquitin System in Alzheimer's Disease. Adv. Exp. Med. Biol. *1233*, 195–221.

Hasselmann, J., Coburn, M.A., England, W., Figueroa Velez, D.X., Kiani Shabestari, S., Tu, C.H., McQuade, A., Kolahdouzan, M., Echeverria, K., Claes, C., et al. (2019). Development of a Chimeric Model to Study and Manipulate Human Microglia In Vivo. Neuron.

Haynes, S.E., Hollopeter, G., Yang, G., Kurpius, D., Dailey, M.E., Gan, W.-B., and Julius, D. (2006). The P2Y12 receptor regulates microglial activation by extracellular nucleotides. Nat Neurosci *9*, 1512–1519.

Heneka, M.T., Carson, M.J., Khoury, J.E., Landreth, G.E., Brosseron, F., Feinstein, D.L., Jacobs, A.H., Wyss-Coray, T., Vitorica, J., Ransohoff, R.M., et al. (2015). Neuroinflammation in Alzheimer's disease. The Lancet Neurology *14*, 388–405.

Hollingworth, P., Harold, D., Sims, R., Gerrish, A., Lambert, J.-C., Carrasquillo, M.M., Abraham, R., Hamshere, M.L., Pahwa, J.S., Moskvina, V., et al. (2011). Common variants in ABCA7, MS4A6A/MS4A4E, EPHA1, CD33 and CD2AP are associated with Alzheimer's disease. Nat Genet *43*, 429–435.

Honda, S., Sasaki, Y., Ohsawa, K., Imai, Y., Nakamura, Y., Inoue, K., and Kohsaka, S. (2001). Extracellular ATP or ADP Induce Chemotaxis of Cultured Microglia through Gi/o-Coupled P2Y Receptors. J. Neurosci. *21*, 1975–1982.

Hong, S., Beja-Glasser, V.F., Nfonoyim, B.M., Frouin, A., Li, S., Ramakrishnan, S., Merry, K.M., Shi, Q., Rosenthal, A., Barres, B.A., et al. (2016a). Complement and microglia mediate early synapse loss in Alzheimer mouse models. Science *352*, 712–716.

Hong, S., Beja-Glasser, V.F., Nfonoyim, B.M., Frouin, A., Li, S., Ramakrishnan, S., Merry, K.M., Shi, Q., Rosenthal, A., Barres, B.A., et al. (2016b). Complement and microglia mediate early synapse loss in Alzheimer mouse models. Science *352*, 712–716.

Inc, D.T. (2021). Denali Therapeutics Announces Significant Program Progress and Expected Key Milestones in 2021 for Its Broad Therapeutic Portfolio in Neurodegeneration.

Irino, Y., Nakamura, Y., Inoue, K., Kohsaka, S., and Ohsawa, K. (2008). Akt activation is involved in P2Y12 receptor-mediated chemotaxis of microglia. J Neurosci Res *86*, 1511–1519.

Ishikawa, A., Tokunaga, M., Maeda, J., Minamihisamatsu, T., Shimojo, M., Takuwa, H., Ono, M., Ni, R., Hirano, S., Kuwabara, S., et al. (2018). In Vivo Visualization of Tau Accumulation, Microglial Activation, and Brain Atrophy in a Mouse Model of Tauopathy rTg4510. Journal of Alzheimer's Disease *61*, 1037–1052.

Jansen, I.E., Savage, J.E., Watanabe, K., Bryois, J., Williams, D.M., Steinberg, S., Sealock, J., Karlsson, I.K., Hägg, S., Athanasiu, L., et al. (2019). Genome-wide meta-analysis identifies new loci and functional pathways influencing Alzheimer's disease risk. Nat. Genet.

Jay, T.R., von Saucken, V.E., and Landreth, G.E. (2017). TREM2 in Neurodegenerative Diseases. Mol Neurodegener *12*, 56.

Jehle, A.W., Gardai, S.J., Li, S., Linsel-Nitschke, P., Morimoto, K., Janssen, W.J., Vandivier, R.W., Wang, N., Greenberg, S., Dale, B.M., et al. (2006). ATP-binding cassette transporter A7 enhances phagocytosis of apoptotic cells and associated ERK signaling in macrophages. J Cell Biol *174*, 547–556.

Ji, P., Schachtschneider, K.M., Schook, L.B., Walker, F.R., and Johnson, R.W. (2016). Peripheral viral infection induced microglial sensome genes and enhanced microglial cell activity in the hippocampus of neonatal piglets. Brain Behav. Immun. *54*, 243–251.

Jiang, T., Yu, J.-T., Hu, N., Tan, M.-S., Zhu, X.-C., and Tan, L. (2014). CD33 in Alzheimer's disease. Mol. Neurobiol. *49*, 529–535.

Jin, S.C., Carrasquillo, M.M., Benitez, B.A., Skorupa, T., Carrell, D., Patel, D., Lincoln, S., Krishnan, S., Kachadoorian, M., Reitz, C., et al. (2015). TREM2 is associated with increased risk for Alzheimer's disease in African Americans. Mol Neurodegener *10*, 19.

Jonsson, T., Stefansson, H., Steinberg, S., Jonsdottir, I., Jonsson, P.V., Snaedal, J., Bjornsson, S., Huttenlocher, J., Levey, A.I., Lah, J.J., et al. (2013). Variant of TREM2 associated with the risk of Alzheimer's disease. N. Engl. J. Med. *368*, 107–116.

Kamphuis, W., Middeldorp, J., Kooijman, L., Sluijs, J.A., Kooi, E.-J., Moeton, M., Freriks, M., Mizee, M.R., and Hol, E.M. (2014). Glial fibrillary acidic protein isoform expression in plaque related astrogliosis in Alzheimer's disease. Neurobiology of Aging *35*, 492–510.

Kan, A.A., de Jager, W., de Wit, M., Heijnen, C., van Zuiden, M., Ferrier, C., van Rijen, P., Gosselaar, P., Hessel, E., van Nieuwenhuizen, O., et al. (2012). Protein expression profiling of inflammatory mediators in human temporal lobe epilepsy reveals co-activation of multiple chemokines and cytokines. J Neuroinflammation *9*, 207.

Kang, S.S., Ebbert, M.T.W., Baker, K.E., Cook, C., Wang, X., Sens, J.P., Kocher, J.-P., Petrucelli, L., and Fryer, J.D. (2018). Microglial translational profiling reveals a convergent APOE pathway from aging, amyloid, and tau. J. Exp. Med.

Karch, C.M., Jeng, A.T., Nowotny, P., Cady, J., Cruchaga, C., and Goate, A.M. (2012a). Expression of Novel Alzheimer's Disease Risk Genes in Control and Alzheimer's Disease Brains. PLOS ONE *7*, e50976.

Karch, C.M., Jeng, A.T., Nowotny, P., Cady, J., Cruchaga, C., and Goate, A.M. (2012b). Expression of Novel Alzheimer's Disease Risk Genes in Control and Alzheimer's Disease Brains. PLOS ONE *7*, e50976.

Keren-Shaul, H., Spinrad, A., Weiner, A., Matcovitch-Natan, O., Dvir-Szternfeld, R., Ulland, T.K., David, E., Baruch, K., Lara-Astaiso, D., Toth, B., et al. (2017). A Unique Microglia Type Associated with Restricting Development of Alzheimer's Disease. Cell *0*.

Kim, W.S., Li, H., Ruberu, K., Chan, S., Elliott, D.A., Low, J.K., Cheng, D., Karl, T., and Garner, B. (2013). Deletion of Abca7 Increases Cerebral Amyloid-β Accumulation in the J20 Mouse Model of Alzheimer's Disease. J. Neurosci. *33*, 4387–4394.

Kiyota, T., Yamamoto, M., Xiong, H., Lambert, M.P., Klein, W.L., Gendelman, H.E., Ransohoff, R.M., and Ikezu, T. (2009). CCL2 accelerates microglia-mediated Abeta oligomer formation and progression of neurocognitive dysfunction. PLoS ONE *4*, e6197.

Kleinberger, G., Yamanishi, Y., Suárez-Calvet, M., Czirr, E., Lohmann, E., Cuyvers, E., Struyfs, H., Pettkus, N., Wenninger-Weinzierl, A., Mazaheri, F., et al. (2014). TREM2 mutations implicated in neurodegeneration impair cell surface transport and phagocytosis. Sci Transl Med *6*, 243ra86.

Knapskog, A.-B., Henjum, K., Idland, A.-V., Eldholm, R.S., Persson, K., Saltvedt, I., Watne, L.O., Engedal, K., and Nilsson, L.N.G. (2020). Cerebrospinal fluid sTREM2 in Alzheimer's disease: comparisons between clinical presentation and AT classification. Sci Rep *10*, 15886.

Kober, D.L., Alexander-Brett, J.M., Karch, C.M., Cruchaga, C., Colonna, M., Holtzman, M.J., and Brett, T.J. (2016). Neurodegenerative disease mutations in TREM2 reveal a functional surface and distinct loss-of-function mechanisms. ELife Sciences *5*, e20391.

Koenigsknecht, J., and Landreth, G. (2004). Microglial phagocytosis of fibrillar beta-amyloid through a beta1 integrin-dependent mechanism. J. Neurosci. *24*, 9838–9846.

Koizumi, S., Shigemoto-Mogami, Y., Nasu-Tada, K., Shinozaki, Y., Ohsawa, K., Tsuda, M., Joshi, B.V., Jacobson, K.A., Kohsaka, S., and Inoue, K. (2007). UDP acting at P2Y6 receptors is a mediator of microglial phagocytosis. Nature *446*, 1091–1095.

Kolde, R. (2019). pheatmap: Pretty Heatmaps.

Konttinen, H., Cabral-da-Silva, M. e C., Ohtonen, S., Wojciechowski, S., Shakirzyanova, A., Caligola, S., Giugno, R., Ishchenko, Y., Hernández, D., Fazaludeen, M.F., et al. (2019). PSEN1ΔE9, APPswe, and APOE4 Confer Disparate Phenotypes in Human iPSC-Derived Microglia. Stem Cell Reports.

Krasemann, S., Madore, C., Cialic, R., Baufeld, C., Calcagno, N., El Fatimy, R., Beckers, L., O'Loughlin, E., Xu, Y., Fanek, Z., et al. (2017). The TREM2-APOE Pathway Drives the Transcriptional Phenotype of Dysfunctional Microglia in Neurodegenerative Diseases. Immunity *47*, 566-581.e9.

Kukull, W.A., Brenner, D.E., Speck, C.E., Nochlin, D., Bowen, J., McCormick, W., Teri, L., Pfanschmidt, M.L., and Larson, E.B. (1994). Causes of death associated with Alzheimer disease: variation by level of cognitive impairment before death. J Am Geriatr Soc *42*, 723–726.

L, F., Pg, T., Y, T., H, L.-B., Ed, L., Pg, B., P, C., A, Z., Cv, R., A, N., et al. (2016). TAM Receptors Regulate Multiple Features of Microglial Physiology (Nature).

Lambert, J.C., Ibrahim-Verbaas, C.A., Harold, D., Naj, A.C., Sims, R., Bellenguez, C., DeStafano, A.L., Bis, J.C., Beecham, G.W., Grenier-Boley, B., et al. (2013). Meta-analysis of 74,046 individuals identifies 11 new susceptibility loci for Alzheimer's disease. Nat. Genet. *45*, 1452–1458.

Lee, J., Bignone, P.A., Coles, L.S., Liu, Y., Snyder, E., and Larocca, D. (2020). Induced pluripotency and spontaneous reversal of cellular aging in supercentenarian donor cells. Biochem Biophys Res Commun *525*, 563–569.

Lee, S., Varvel, N.H., Konerth, M.E., Xu, G., Cardona, A.E., Ransohoff, R.M., and Lamb, B.T. (2010). CX3CR1 Deficiency Alters Microglial Activation and Reduces Beta-Amyloid Deposition in Two Alzheimer's Disease Mouse Models. The American Journal of Pathology *177*, 2549–2562.

Lee, S., Sato, Y., and Nixon, R.A. (2011). Lysosomal proteolysis inhibition selectively disrupts axonal transport of degradative organelles and causes an Alzheimer's-like axonal dystrophy. J. Neurosci. *31*, 7817–7830.

Leissring, M.A., Akbari, Y., Fanger, C.M., Cahalan, M.D., Mattson, M.P., and LaFerla, F.M. (2000). Capacitative calcium entry deficits and elevated luminal calcium content in mutant presenilin-1 knockin mice. J Cell Biol *149*, 793–798.

Leyns, C.E.G., Ulrich, J.D., Finn, M.B., Stewart, F.R., Koscal, L.J., Serrano, J.R., Robinson, G.O., Anderson, E., Colonna, M., and Holtzman, D.M. (2017). TREM2 deficiency attenuates neuroinflammation and protects against neurodegeneration in a mouse model of tauopathy. PNAS *114*, 11524–11529.

Liao, F., Li, A., Xiong, M., Bien-Ly, N., Jiang, H., Zhang, Y., Finn, M.B., Hoyle, R., Keyser, J., Lefton, K.B., et al. (2018). Targeting of nonlipidated, aggregated apoE with antibodies inhibits amyloid accumulation. J Clin Invest *128*, 2144–2155.

Lill, C.M., Rengmark, A., Pihlstrøm, L., Fogh, I., Shatunov, A., Sleiman, P.M., Wang, L.-S., Liu, T., Lassen, C.F., Meissner, E., et al. (2015). The role of TREM2 R47H as a risk factor for Alzheimer's disease, frontotemporal lobar degeneration, amyotrophic lateral sclerosis, and Parkinson's disease. Alzheimers Dement *11*, 1407–1416.

Lim, H.M., Woon, H., Han, J.W., Baba, Y., Kurosaki, T., Lee, M.G., and Kim, J.Y. (2017). UDP-Induced Phagocytosis and ATP-Stimulated Chemotactic Migration Are Impaired in STIM1-/- Microglia In Vitro and In Vivo. Mediators Inflamm *2017*, 8158514.

Linnartz, B., and Neumann, H. (2013). Microglial activatory (immunoreceptor tyrosine-based activation motif)- and inhibitory (immunoreceptor tyrosine-based inhibition motif)-signaling receptors for recognition of the neuronal glycocalyx. Glia *61*, 37–46.

Liu, Z., Condello, C., Schain, A., Harb, R., and Grutzendler, J. (2010). CX3CR1 in microglia regulates brain amyloid deposition through selective protofibrillar Aβ phagocytosis. J Neurosci *30*, 17091–17101.

Lock, J.T., Parker, I., and Smith, I.F. (2016). Communication of Ca(2+) signals via tunneling membrane nanotubes is mediated by transmission of inositol trisphosphate through gap junctions. Cell Calcium *60*, 266–272.

Lord, S.J., Velle, K.B., Mullins, R.D., and Fritz-Laylin, L.K. (2020). SuperPlots: Communicating reproducibility and variability in cell biology. J Cell Biol *219*.

Lou, N., Takano, T., Pei, Y., Xavier, A.L., Goldman, S.A., and Nedergaard, M. (2016). Purinergic receptor P2RY12-dependent microglial closure of the injured blood–brain barrier. PNAS *113*, 1074–1079.

Love, M.I., Huber, W., and Anders, S. (2014). Moderated estimation of fold change and dispersion for RNA-seq data with DESeq2. Genome Biol *15*.

Lull, M.E., and Block, M.L. (2010). Microglial activation and chronic neurodegeneration. Neurotherapeutics *7*, 354–365.

Luo, Y., Lathia, J., Mughal, M., and Mattson, M.P. (2008). SDF1α/CXCR4 Signaling, via ERKs and the Transcription Factor Egr1, Induces Expression of a 67-kDa Form of Glutamic Acid Decarboxylase in Embryonic Hippocampal Neurons. J Biol Chem *283*, 24789–24800.

M, H., I, O., H, K., M, O., C, S., S, W., J, W., and O, W. (2018). Glycoprotein NMB: A Novel Alzheimer's Disease Associated Marker Expressed in a Subset of Activated Microglia (Acta Neuropathol Commun).

Ma, J., Jiang, T., Tan, L., and Yu, J.-T. (2015). TYROBP in Alzheimer's Disease. Mol Neurobiol *51*, 820–826.

Ma, L.-Z., Tan, L., Bi, Y.-L., Shen, X.-N., Xu, W., Ma, Y.-H., Li, H.-Q., Dong, Q., and Yu, J.-T. (2020). Dynamic changes of CSF sTREM2 in preclinical Alzheimer's disease: the CABLE study. Molecular Neurodegeneration *15*, 25.

Madry, C., and Attwell, D. (2015). Receptors, ion channels, and signaling mechanisms underlying microglial dynamics. J Biol Chem *290*, 12443–12450.

Malik, M., Simpson, J.F., Parikh, I., Wilfred, B.R., Fardo, D.W., Nelson, P.T., and Estus, S. (2013). CD33 Alzheimer's Risk-Altering Polymorphism, CD33 Expression, and Exon 2 Splicing. J Neurosci *33*, 13320–13325.

Mammana, S., Fagone, P., Cavalli, E., Basile, M.S., Petralia, M.C., Nicoletti, F., Bramanti, P., and Mazzon, E. (2018). The Role of Macrophages in Neuroinflammatory and Neurodegenerative Pathways of Alzheimer's Disease, Amyotrophic Lateral Sclerosis, and Multiple Sclerosis: Pathogenetic Cellular Effectors and Potential Therapeutic Targets. International Journal of Molecular Sciences *19*, 831.

Mancuso, R., Van Den Daele, J., Fattorelli, N., Wolfs, L., Balusu, S., Burton, O., Liston, A., Sierksma, A., Fourne, Y., Poovathingal, S., et al. (2019). Stem-cell-derived human microglia transplanted in mouse brain to study human disease. Nat. Neurosci. *22*, 2111–2116.

Marsh, S.E., Abud, E.M., Lakatos, A., Karimzadeh, A., Yeung, S.T., Davtyan, H., Fote, G.M., Lau, L., Weinger, J.G., Lane, T.E., et al. (2016). The adaptive immune system restrains Alzheimer's disease pathogenesis by modulating microglial function. Proc. Natl. Acad. Sci. U.S.A. *113*, E1316-1325.

Mathys, H., Davila-Velderrain, J., Peng, Z., Gao, F., Mohammadi, S., Young, J.Z., Menon, M., He, L., Abdurrob, F., Jiang, X., et al. (2019). Single-cell transcriptomic analysis of Alzheimer's disease. Nature.

McKhann, G.M., Knopman, D.S., Chertkow, H., Hyman, B.T., Jack, C.R., Kawas, C.H., Klunk, W.E., Koroshetz, W.J., Manly, J.J., Mayeux, R., et al. (2011). The diagnosis of dementia due to Alzheimer's disease: Recommendations from the National Institute on Aging-Alzheimer's Association workgroups on diagnostic guidelines for Alzheimer's disease. Alzheimer's & Dementia: The Journal of the Alzheimer's Association *7*, 263–269.

McLarnon, J.G. (2020). Microglial Store-operated Calcium Signaling in Health and in Alzheimer's Disease. Curr Alzheimer Res *17*, 1057–1064.

McQuade, A., and Blurton-Jones, M. (2019). Microglia in Alzheimer's disease: Exploring how genetics and phenotype influence risk. J Mol Biol *431*, 1805–1817.

McQuade, A., Coburn, M., Tu, C.H., Hasselmann, J., Davtyan, H., and Blurton-Jones, M. (2018). Development and validation of a simplified method to generate human microglia from pluripotent stem cells. Molecular Neurodegeneration *13*, 67.

McQuade, A., Kang, Y.J., Hasselmann, J., Jairaman, A., Sotelo, A., Coburn, M., Shabestari, S.K., Chadarevian, J.P., Fote, G., Tu, C.H., et al. (2020). Gene expression and functional deficits underlie TREM2-knockout microglia responses in human models of Alzheimer's disease. Nature Communications *11*, 5370.

Meier, S.R., Sehlin, D., Hultqvist, G., and Syvänen, S. (2021). Pinpointing Brain TREM2 Levels in Two Mouse Models of Alzheimer's Disease. Mol Imaging Biol.

Meilandt, W.J., Ngu, H., Gogineni, A., Lalehzadeh, G., Lee, S.-H., Srinivasan, K., Imperio, J., Wu, T., Weber, M., Kruse, A.J., et al. (2020). Trem2 deletion reduces late-stage amyloid plaque accumulation, elevates the Aβ42:Aβ40 ratio, and exacerbates axonal dystrophy and dendritic spine loss in the PS2APP Alzheimer's mouse model. J. Neurosci.

Mertens, J., Herdy, J.R., Traxler, L., Schafer, S.T., Schlachetzki, J.C.M., Böhnke, L., Reid, D.A., Lee, H., Zangwill, D., Fernandes, D.P., et al. (2021). Age-dependent instability of mature neuronal fate in induced neurons from Alzheimer's patients. Cell Stem Cell.

Michaelis, M., Nieswandt, B., Stegner, D., Eilers, J., and Kraft, R. (2015). STIM1, STIM2, and Orai1 regulate store-operated calcium entry and purinergic activation of microglia. Glia *63*, 652–663.

Milior, G., Morin-Brureau, M., Chali, F., Le Duigou, C., Savary, E., Huberfeld, G., Rouach, N., Pallud, J., Capelle, L., Navarro, V., et al. (2020). Distinct P2Y Receptors Mediate Extension and Retraction of Microglial Processes in Epileptic and Peritumoral Human Tissue. J Neurosci *40*, 1373–1388.

Miller, J.D., Ganat, Y.M., Kishinevsky, S., Bowman, R.L., Liu, B., Tu, E.Y., Mandal, P.K., Vera, E., Shim, J., Kriks, S., et al. (2013). Human iPSC-based modeling of late-onset disease via progerin-induced aging. Cell Stem Cell *13*, 691–705.

Mizuma, A., Kim, J.Y., Kacimi, R., Stauderman, K., Dunn, M., Hebbar, S., and Yenari, M.A. (2019). Microglial Calcium Release-Activated Calcium Channel Inhibition Improves Outcome from Experimental Traumatic Brain Injury and Microglia-Induced Neuronal Death. J Neurotrauma *36*, 996–1007.

Mm, V., Ka, C., A, Y.-K., G, Y., L, K., S, I., and T, I. (2017). A Split-Luciferase Complementation, Real-Time Reporting Assay Enables Monitoring of the Disease-Associated Transmembrane Protein TREM2 in Live Cells (J Biol Chem).

Moore, C.S., Ase, A.R., Kinsara, A., Rao, V.T.S., Michell-Robinson, M., Leong, S.Y., Butovsky, O., Ludwin, S.K., Séguéla, P., Bar-Or, A., et al. (2015). P2Y12 expression and function in alternatively activated human microglia. Neurol Neuroimmunol Neuroinflamm *2*, e80.

Morrison, H., Young, K., Qureshi, M., Rowe, R.K., and Lifshitz, J. (2017). Quantitative microglia analyses reveal diverse morphologic responses in the rat cortex after diffuse brain injury. Sci Rep *7*, 13211.

Muffat, J., Li, Y., Yuan, B., Mitalipova, M., Omer, A., Corcoran, S., Bakiasi, G., Tsai, L.-H., Aubourg, P., Ransohoff, R.M., et al. (2016). Efficient derivation of microglia-like cells from human pluripotent stem cells. Nat. Med. *22*, 1358–1367.

Mustaly, S., Littlefield, A., and Stutzmann, G.E. (2018). Calcium Signaling Deficits in Glia and Autophagic Pathways Contributing to Neurodegenerative Disease. Antioxid. Redox Signal.

N'Diaye, E.-N., Branda, C.S., Branda, S.S., Nevarez, L., Colonna, M., Lowell, C., Hamerman, J.A., and Seaman, W.E. (2009). TREM-2 (triggering receptor expressed on myeloid cells 2) is a phagocytic receptor for bacteria. J. Cell Biol. *184*, 215–223.

Negulescu, P.A., Krasieva, T.B., Khan, A., Kerschbaum, H.H., and Cahalan, M.D. (1996). Polarity of T cell shape, motility, and sensitivity to antigen. Immunity *4*, 421–430.

Olah, M., Patrick, E., Villani, A.-C., Xu, J., White, C.C., Ryan, K.J., Piehowski, P., Kapasi, A., Nejad, P., Cimpean, M., et al. (2018). A transcriptomic atlas of aged human microglia. Nat Commun *9*, 539.

Olah, M., Menon, V., Habib, N., Taga, M.F., Ma, Y., Yung, C.J., Cimpean, M., Khairallah, A., Coronas-Samano, G., Sankowski, R., et al. (2020). Single cell RNA sequencing of human microglia uncovers a subset associated with Alzheimer's disease. Nature Communications *11*, 6129.

Olmos-Alonso, A., Schetters, S.T.T., Sri, S., Askew, K., Mancuso, R., Vargas-Caballero, M., Holscher, C., Perry, V.H., and Gomez-Nicola, D. (2016). Pharmacological targeting of CSF1R inhibits microglial proliferation and prevents the progression of Alzheimer's-like pathology. Brain *139*, 891–907.

Ormel, P.R., Sá, R.V. de, Bodegraven, E.J. van, Karst, H., Harschnitz, O., Sneeboer, M.A.M., Johansen, L.E., Dijk, R.E. van, Scheefhals, N., Berlekom, A.B. van, et al. (2018). Microglia innately develop within cerebral organoids. Nature Communications *9*, 4167.

Osborn, L.M., Kamphuis, W., Wadman, W.J., and Hol, E.M. (2016). Astrogliosis: An integral player in the pathogenesis of Alzheimer's disease. Progress in Neurobiology *144*, 121–141.

Otero, K., Turnbull, I.R., Poliani, P.L., Vermi, W., Cerutti, E., Aoshi, T., Tassi, I., Takai, T., Stanley, S.L., Miller, M., et al. (2009). Macrophage colony-stimulating factor induces the proliferation

and survival of macrophages via a pathway involving DAP12 and β-catenin. Nature Immunology *10*, 734–743.

Otero, K., Shinohara, M., Zhao, H., Cella, M., Gilfillan, S., Colucci, A., Faccio, R., Ross, F.P., Teitelbaum, S.L., Takayanagi, H., et al. (2012). TREM2 and β-Catenin Regulate Bone Homeostasis by Controlling the Rate of Osteoclastogenesis. The Journal of Immunology *188*, 2612–2621.

Pandya, H., Shen, M.J., Ichikawa, D.M., Sedlock, A.B., Choi, Y., Johnson, K.R., Kim, G., Brown, M.A., Elkahloun, A.G., Maric, D., et al. (2017). Differentiation of human and murine induced pluripotent stem cells to microglia-like cells. Nat. Neurosci. *20*, 753–759.

Parhizkar, S., Arzberger, T., Brendel, M., Kleinberger, G., Deussing, M., Focke, C., Nuscher, B., Xiong, M., Ghasemigharagoz, A., Katzmarski, N., et al. (2019). Loss of TREM2 function increases amyloid seeding but reduces plaque-associated ApoE. Nature Neuroscience 1.

Park, J., Wetzel, I., Marriott, I., Dréau, D., D'Avanzo, C., Kim, D.Y., Tanzi, R.E., and Cho, H. (2018). A 3D human triculture system modeling neurodegeneration and neuroinflammation in Alzheimer's disease. Nat. Neurosci. *21*, 941–951.

Piers, T.M., Cosker, K., Mallach, A., Johnson, G.T., Guerreiro, R., Hardy, J., and Pocock, J.M. (2019). A locked immunometabolic switch underlies TREM2 R47H loss of function in human iPSC-derived microglia. FASEB J.

Pimenova, A.A., Herbinet, M., Gupta, I., Machlovi, S.I., Bowles, K.R., Marcora, E., and Goate, A.M. (2020). Alzheimer's-associated PU.1 expression levels regulate microglial inflammatory response. Neurobiol Dis 105217.

Prakriya, M., and Lewis, R.S. (2015). Store-Operated Calcium Channels. Physiol Rev *95*, 1383–1436.

Proitsi, P., Lee, S.H., Lunnon, K., Keohane, A., Powell, J., Troakes, C., Al-Sarraj, S., Furney, S., Soininen, H., Kłoszewska, I., et al. (2014). Alzheimer's disease susceptibility variants in the MS4A6A gene are associated with altered levels of MS4A6A expression in blood. Neurobiology of Aging *35*, 279–290.

Radford, R.A., Morsch, M., Rayner, S.L., Cole, N.J., Pountney, D.L., and Chung, R.S. (2015). The established and emerging roles of astrocytes and microglia in amyotrophic lateral sclerosis and frontotemporal dementia. Front Cell Neurosci *9*, 414.

Rajab, N., Angel, P.W., Deng, Y., Gu, J., Jameson, V., Kurowska-Stolarska, M., Milling, S., Pacheco, C.M., Rutar, M., Laslett, A.L., et al. (2021). An integrated analysis of human myeloid cells identifies gaps in in vitro models of in vivo biology. Stem Cell Reports.

Ramirez, L.M., Goukasian, N., Porat, S., Hwang, K.S., Eastman, J.A., Hurtz, S., Wang, B., Vang, N., Sears, R., Klein, E., et al. (2016). Common variants in ABCA7 and MS4A6A are associated with cortical and hippocampal atrophy. Neurobiology of Aging *39*, 82–89.

Reich, M., Paris, I., Ebeling, M., Dahm, N., Schweitzer, C., Reinhardt, D., Schmucki, R., Prasad, M., Köchl, F., Leist, M., et al. (2021). Alzheimer's Risk Gene TREM2 Determines Functional Properties of New Type of Human iPSC-Derived Microglia. Front. Immunol. *11*.

Ryan, K.J., White, C.C., Patel, K., Xu, J., Olah, M., Replogle, J.M., Frangieh, M., Cimpean, M., Winn, P., McHenry, A., et al. (2017). A human microglia-like cellular model for assessing the effects of neurodegenerative disease gene variants. Sci Transl Med *9*.

Saini, V., Marchese, A., and Majetschak, M. (2010). CXC chemokine receptor 4 is a cell surface receptor for extracellular ubiquitin. J. Biol. Chem. *285*, 15566–15576.

Sala Frigerio, C., Wolfs, L., Fattorelli, N., Thrupp, N., Voytyuk, I., Schmidt, I., Mancuso, R., Chen, W.-T., Woodbury, M.E., Srivastava, G., et al. (2019). The Major Risk Factors for Alzheimer's Disease: Age, Sex, and Genes Modulate the Microglia Response to Aβ Plaques. Cell Rep *27*, 1293-1306.e6.

Schapansky, J., Nardozzi, J.D., and LaVoie, M.J. (2015). The complex relationships between microglia, alpha-synuclein, and LRRK2 in Parkinson's disease. Neuroscience *302*, 74–88.

Schorey, J.S., and Lawrence, C. (2008). The pattern recognition receptor Dectin-1: from fungi to mycobacteria. Curr Drug Targets *9*, 123–129.

Selmaj, K.W., Farooq, M., Norton, W.T., Raine, C.S., and Brosnan, C.F. (1990). Proliferation of astrocytes in vitro in response to cytokines. A primary role for tumor necrosis factor. J. Immunol. *144*, 129–135.

Shi, Y., and Holtzman, D.M. (2018). Interplay between innate immunity and Alzheimer disease: APOE and TREM2 in the spotlight. Nature Reviews Immunology 1.

Song, W., Hooli, B., Mullin, K., Jin, S.C., Cella, M., Ulland, T.K., Wang, Y., Tanzi, R.E., and Colonna, M. (2017). Alzheimer's disease-associated TREM2 variants exhibit either decreased or increased ligand-dependent activation. Alzheimer's & Dementia *13*, 381–387.

Sosna, J., Philipp, S., Albay, R., Reyes-Ruiz, J.M., Baglietto-Vargas, D., LaFerla, F.M., and Glabe, C.G. (2018). Early long-term administration of the CSF1R inhibitor PLX3397 ablates microglia and reduces accumulation of intraneuronal amyloid, neuritic plaque deposition and pre-fibrillar oligomers in 5XFAD mouse model of Alzheimer's disease. Mol Neurodegener *13*.

Stuart, T., Butler, A., Hoffman, P., Hafemeister, C., Papalexi, E., Mauck, W.M., Hao, Y., Stoeckius, M., Smibert, P., and Satija, R. (2019). Comprehensive Integration of Single-Cell Data. Cell *177*, 1888-1902.e21.

Suárez-Calvet, M., Araque Caballero, M.Á., Kleinberger, G., Bateman, R.J., Fagan, A.M., Morris, J.C., Levin, J., Danek, A., Ewers, M., Haass, C., et al. (2016a). Early changes in CSF sTREM2 in dominantly inherited Alzheimer's disease occur after amyloid deposition and neuronal injury. Sci Transl Med *8*, 369ra178.

Suárez-Calvet, M., Kleinberger, G., Araque Caballero, M.Á., Brendel, M., Rominger, A., Alcolea, D., Fortea, J., Lleó, A., Blesa, R., Gispert, J.D., et al. (2016b). sTREM2 cerebrospinal fluid levels are a potential biomarker for microglia activity in early-stage Alzheimer's disease and associate with neuronal injury markers. EMBO Mol Med *8*, 466–476.

Suárez-Calvet, M., Morenas-Rodríguez, E., Kleinberger, G., Schlepckow, K., Araque Caballero, M.Á., Franzmeier, N., Capell, A., Fellerer, K., Nuscher, B., Eren, E., et al. (2019). Early increase of CSF sTREM2 in Alzheimer's disease is associated with tau related-neurodegeneration but not with amyloid-β pathology. Mol Neurodegener *14*, 1.

Suzuki, J., Fujii, T., Imao, T., Ishihara, K., Kuba, H., and Nagata, S. (2013). Calcium-dependent phospholipid scramblase activity of TMEM16 protein family members. J. Biol. Chem. *288*, 13305–13316.

Suzuki, T., Kohyama, K., Moriyama, K., Ozaki, M., Hasegawa, S., Ueno, T., Saitoe, M., Morio, T., Hayashi, M., and Sakuma, H. (2020). Extracellular ADP augments microglial inflammasome and NF-κB activation via the P2Y12 receptor. European Journal of Immunology *50*, 205–219.

Takata, K., Kozaki, T., Lee, C.Z.W., Thion, M.S., Otsuka, M., Lim, S., Utami, K.H., Fidan, K., Park, D.S., Malleret, B., et al. (2017). Induced-Pluripotent-Stem-Cell-Derived Primitive Macrophages Provide a Platform for Modeling Tissue-Resident Macrophage Differentiation and Function. Immunity *47*, 183-198.e6.

Tam, J.H., Seah, C., and Pasternak, S.H. (2014). The Amyloid Precursor Protein is rapidly transported from the Golgi apparatus to the lysosome and where it is processed into beta-amyloid. Mol Brain *7*, 54.

Tam, J.H.K., Cobb, M.R., Seah, C., and Pasternak, S.H. (2016). Tyrosine Binding Protein Sites Regulate the Intracellular Trafficking and Processing of Amyloid Precursor Protein through a Novel Lysosome-Directed Pathway. PLoS One *11*.

Tan, L., Yu, J.-T., Zhang, W., Wu, Z.-C., Zhang, Q., Liu, Q.-Y., Wang, W., Wang, H.-F., Ma, X.-Y., and Cui, W.-Z. (2013). Association of GWAS-linked loci with late-onset Alzheimer's disease in a northern Han Chinese population. Alzheimers Dement *9*, 546–553.

Tanaka, N., Abe-Dohmae, S., Iwamoto, N., and Yokoyama, S. (2011). Roles of ATP-Binding Cassette Transporter A7 in Cholesterol Homeostasis and Host Defense System. JAT *18*, 274–281.

Turk, B., and Turk, V. (2009). Lysosomes as "Suicide Bags" in Cell Death: Myth or Reality? J Biol Chem *284*, 21783–21787.

Tyurina, Y.Y., Basova, L.V., Konduru, N.V., Tyurin, V.A., Potapovich, A.I., Cai, P., Bayir, H., Stoyanovsky, D., Pitt, B.R., Shvedova, A.A., et al. (2007). Nitrosative stress inhibits the aminophospholipid translocase resulting in phosphatidylserine externalization and macrophage engulfment: implications for the resolution of inflammation. J. Biol. Chem. *282*, 8498–8509.

Ueda, Y., Gullipalli, D., and Song, W.-C. (2016). Modeling complement-driven diseases in transgenic mice: Values and limitations. Immunobiology *221*, 1080–1090.

Ulrich, J.D., Finn, M.B., Wang, Y., Shen, A., Mahan, T.E., Jiang, H., Stewart, F.R., Piccio, L., Colonna, M., and Holtzman, D.M. (2014). Altered microglial response to Aβ plaques in APPPS1-21 mice heterozygous for TREM2. Mol Neurodegener *9*, 20.

Underhill, D.M., Rossnagle, E., Lowell, C.A., and Simmons, R.M. (2005). Dectin-1 activates Syk tyrosine kinase in a dynamic subset of macrophages for reactive oxygen production. Blood *106*, 2543–2550.

Visentin, S., Nuccio, C.D., and Bellenchi, G.C. (2006). Different patterns of Ca^{2+} signals are induced by low compared to high concentrations of P2Y agonists in microglia. Purinergic Signal *2*, 605–617.

Wang, H., Blackall, M., Sominsky, L., Spencer, S.J., Vlahos, R., Churchill, M., and Bozinovski, S. (2018). Increased hypothalamic microglial activation after viral-induced pneumococcal lung infection is associated with excess serum amyloid A production. J Neuroinflammation *15*, 200.

Wang, Q., Xu, Y., Chen, J.-C., Qin, Y.-Y., Liu, M., Liu, Y., Xie, M.-J., Yu, Z.-Y., Zhu, Z., and Wang, W. (2012). Stromal cell-derived factor 1α decreases β-amyloid deposition in Alzheimer's disease mouse model. Brain Res. *1459*, 15–26.

Wang, S., Mustafa, M., Yuede, C.M., Salazar, S.V., Kong, P., Long, H., Ward, M., Siddiqui, O., Paul, R., Gilfillan, S., et al. (2020a). Anti-human TREM2 induces microglia proliferation and reduces pathology in an Alzheimer's disease model. J. Exp. Med. *217*.

Wang, S., Mustafa, M., Yuede, C.M., Salazar, S.V., Kong, P., Long, H., Ward, M., Siddiqui, O., Paul, R., Gilfillan, S., et al. (2020b). Anti-human TREM2 induces microglia proliferation and reduces pathology in an Alzheimer's disease model. J Exp Med *217*.

Wang, Y., Cella, M., Mallinson, K., Ulrich, J.D., Young, K.L., Robinette, M.L., Gilfillan, S., Krishnan, G.M., Sudhakar, S., Zinselmeyer, B.H., et al. (2015). TREM2 lipid sensing sustains the microglial response in an Alzheimer's disease model. Cell *160*, 1061–1071.

Wang, Y., Ulland, T.K., Ulrich, J.D., Song, W., Tzaferis, J.A., Hole, J.T., Yuan, P., Mahan, T.E., Shi, Y., Gilfillan, S., et al. (2016). TREM2-mediated early microglial response limits diffusion and toxicity of amyloid plaques. J. Exp. Med. *213*, 667–675.

Weisman, G.A., Woods, L.T., Erb, L., and Seye, C.I. (2012). P2Y receptors in the mammalian nervous system: pharmacology, ligands and therapeutic potential. CNS Neurol Disord Drug Targets *11*, 722–738.

Westin, K., Buchhave, P., Nielsen, H., Minthon, L., Janciauskiene, S., and Hansson, O. (2012). CCL2 is associated with a faster rate of cognitive decline during early stages of Alzheimer's disease. PLoS ONE *7*, e30525.

Wickham, H. (2009). ggplot2: Elegant Graphics for Data Analysis (New York: Springer-Verlag).

Wisniewski, H.M., Moretz, R.C., and Lossinsky, A.S. (1981). Evidence for induction of localized amyloid deposits and neuritic plaques by an infectious agent. Annals of Neurology *10*, 517–522.

Wu, Y., Zhang, Z., Ren, S., Li, K., Ning, Q., and Jiang, X. (2019). Aberrant expression of long noncoding RNAs in the serum and myocardium of spontaneous hypertensive rats. Mol Biol Rep *46*, 6399–6404.

Xiang, X., Piers, T.M., Wefers, B., Zhu, K., Mallach, A., Brunner, B., Kleinberger, G., Song, W., Colonna, M., Herms, J., et al. (2018). The Trem2 R47H Alzheimer's risk variant impairs splicing and reduces Trem2 mRNA and protein in mice but not in humans. Mol Neurodegener *13*, 49.

Yeh, F.L., Wang, Y., Tom, I., Gonzalez, L.C., and Sheng, M. (2016). TREM2 Binds to Apolipoproteins, Including APOE and CLU/APOJ, and Thereby Facilitates Uptake of Amyloid-Beta by Microglia. Neuron *91*, 328–340.

Yuan, P., Condello, C., Keene, C.D., Wang, Y., Bird, T.D., Paul, S.M., Luo, W., Colonna, M., Baddeley, D., and Grutzendler, J. (2016). TREM2 Haplodeficiency in Mice and Humans Impairs the Microglia Barrier Function Leading to Decreased Amyloid Compaction and Severe Axonal Dystrophy. Neuron *90*, 724–739.

Zhang, S., Zhao, J., Zhang, Y., Zhang, Y., Cai, F., Wang, L., and Song, W. (2019). Upregulation of MIF as a defense mechanism and a biomarker of Alzheimer's disease. Alzheimer's Research & Therapy *11*, 54.

Zhang, Y., Chen, K., Sloan, S.A., Bennett, M.L., Scholze, A.R., O'Keeffe, S., Phatnani, H.P., Guarnieri, P., Caneda, C., Ruderisch, N., et al. (2014). An RNA-Sequencing Transcriptome and Splicing Database of Glia, Neurons, and Vascular Cells of the Cerebral Cortex. J. Neurosci. *34*, 11929–11947.

Zhao, Y., Wu, X., Li, X., Jiang, L.-L., Gui, X., Liu, Y., Sun, Y., Zhu, B., Piña-Crespo, J.C., Zhang, M., et al. (2018). TREM2 Is a Receptor for β-Amyloid that Mediates Microglial Function. Neuron *97*, 1023-1031.e7.

Zheng, H., Liu, C.-C., Atagi, Y., Chen, X.-F., Jia, L., Yang, L., He, W., Zhang, X., Kang, S.S., Rosenberry, T.L., et al. (2016). Opposing roles of the triggering receptor expressed on myeloid

cells 2 and triggering receptor expressed on myeloid cells-like transcript 2 in microglia activation. Neurobiol. Aging *42*, 132–141.

Zheng, H., Jia, L., Liu, C.-C., Rong, Z., Zhong, L., Yang, L., Chen, X.-F., Fryer, J.D., Wang, X., Zhang, Y., et al. (2017). TREM2 Promotes Microglial Survival by Activating Wnt/β-Catenin Pathway. J Neurosci *37*, 1772–1784.

Zhong, L., Chen, X.-F., Wang, T., Wang, Z., Liao, C., Wang, Z., Huang, R., Wang, D., Li, X., Wu, L., et al. (2017). Soluble TREM2 induces inflammatory responses and enhances microglial survival. J. Exp. Med. *214*, 597–607.

Zhou, Z., and Yu, X. (2008). Phagosome maturation during the removal of apoptotic cells: receptors lead the way. Trends Cell Biol *18*, 474–485.

Zhou, J., Yu, W., Zhang, M., Tian, X., Li, Y., and Lü, Y. (2019). Imbalance of Microglial TLR4/TREM2 in LPS-Treated APP/PS1 Transgenic Mice: A Potential Link Between Alzheimer's Disease and Systemic Inflammation. Neurochem. Res. *44*, 1138–1151.

Zuroff, L., Daley, D., Black, K.L., and Koronyo-Hamaoui, M. (2017). Clearance of cerebral Aβ in Alzheimer's disease: reassessing the role of microglia and monocytes. Cell Mol Life Sci *74*, 2167–2201.

(2015). Alzheimers Association update. Alzheimers Dement *11*, 104–105.

BBDuk Guide.

Genialis.